

Encl ✓

NUMERICAL SIMULATION OF TIDES AND STORM SURGES IN THE BAY OF BENGAL

By

VADLAMANI BALAKRISHNA KUMAR

MATH

1983

D

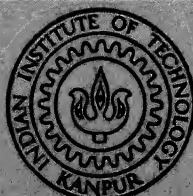
Kum

Num

TH

MATHS/1983/D

K 967



DEPARTMENT OF MATHEMATICS

INDIAN INSTITUTE OF TECHNOLOGY KANPUR

SEPTEMBER, 1983

NUMERICAL SIMULATION OF TIDES AND STORM SURGES IN THE BAY OF BENGAL

A Thesis Submitted
in Partial Fulfilment of the Requirements
for the Degree of

DOCTOR OF PHILOSOPHY

By

VADLAMANI BALAKRISHNA KUMAR

11658

to the

DEPARTMENT OF MATHEMATICS
INDIAN INSTITUTE OF TECHNOLOGY KANPUR

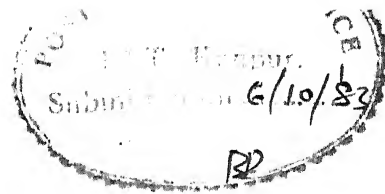
SEPTEMBER, 1983

To

My Alma Mater IIT/K

14 JUN 1985
FBI KANPUR
GENERAL INVESTIGATIVE
DIVISION
SERIAL NO. 87516

MATH-1983-D-KUM- NUM



CERTIFICATE

This is to certify that the work embodied in the thesis "NUMERICAL SIMULATION OF TIDES AND STORM SURGES IN THE BAY OF BENGAL" by V.B.K. Kumar has been carried out under my supervision and has not been submitted elsewhere for a degree or diploma.

September - 1983

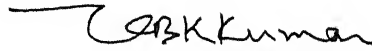
R. K. Jain
(R. K. JAIN)
Professor of Mathematics
Indian Institute of Technology
Kanpur-208016
(INDIA)

ACKNOWLEDGEMENTS

I express, with a sense of profound gratitude, my indebtedness to my supervisor, Prof. R.K. Jain for having bestowed upon me his valuable guidance and inspiration throughout the course of this work. My association with him has been the most rewarding in my academic life.

I wish to record my heartfelt thanks to Prof. J.N. Kapur for his inspiration and encouragement.

September - 1983


V.B.K. KUMAR

CONTENTS

| | | | Page |
|---------|-----|--|------|
| CHAPTER | 0 | INTRODUCTION | |
| | 0.1 | General Introduction | 1 |
| | 0.2 | A Brief Historical Account | 7 |
| | 0.3 | Hydrodynamical Equations and Formulation of Two- Dimensional Surge | 12 |
| | 0.4 | Formulation of the Problem for Three-Dimensional Surge | 21 |
| | 0.5 | Layout and Contribution of the Present Work | 37 |
| CHAPTER | 1 | M_2 -TIDE IN THE BAY OF BENGAL | |
| | 1.1 | Introduction | 44 |
| | 1.2 | Tidal Theorem | 47 |
| | 1.3 | Auxiliary Functions | 51 |
| | 1.4 | Integral Formulation | 54 |
| | 1.5 | Elevation due to the Constituent M_2 | 58 |
| | 1.6 | Computations and Results | 67 |
| CHAPTER | 2 | DEPTH-INTEGRATED MODEL OF TIDES AND STORM SURGES IN BAY OF BENGAL | |
| | 2.1 | Introduction | 85 |
| | 2.2 | Numerical Scheme and Model Area | 88 |
| | 2.3 | Surge without the Tide | 97 |
| | 2.4 | Establishing the Tidal Regime | 110 |
| | 2.5 | Tide-Surge Interaction | 113 |
| | 2.6 | Concluding Remarks | 116 |

| | | | |
|--------------|-----|---|-----|
| CHAPTER | 3 | NUMERICAL SIMULATION OF THREE-DIMENSIONAL SURGES USING A SPECTRAL MODEL | |
| | 3.1 | Introduction | 170 |
| | 3.2 | Numerical Scheme | 172 |
| | 3.3 | Numerical Experiments | 180 |
| | 3.4 | Results and Conclusions | 184 |
| CHAPTER | 4 | A CRITICAL REVIEW AND SOME SUGGESTIONS | 252 |
| APPENDIX | | | 258 |
| BIBLIOGRAPHY | | | 259 |

LIST OF FIGURES

| CHAPTER | 1 | Page |
|---------|---|---------|
| Fig. | 1 (a)-(c) Model region for the tidal theorem | 76 |
| | 2 Model area of Bay of Bengal | 77 |
| | 3 Auxiliary functions independent of | 78 |
| | 4-7 Auxiliary functions of containing factor e^{ipx} | 79-82 |
| | 8 M_2 -tide distribution along the four selected parallels | 83 |
| | 9 Co-tidal map for the region of Bay of Bengal | 84 |
| CHAPTER | 2 | |
| Fig. | 1 (a,b,c) Model area and the grid | 119-120 |
| | 2 Bathymetry contours and the depth values | 121 |
| | 3 (a,b,c) Storm tracks and the selected locations | 122 |
| | 4 (a,b) Elevation contours due to stationary symmetric-storm | 123 |
| | 5-7 (a-f) Elevation contours due to asymmetric and symmetric storms for tracks I, II and III | 124-129 |
| | 8 (a-f) Elevations at selected locations for asymmetric and symmetric storms for tracks I, II and III | 130-132 |

| | | | |
|-------|-------|---|---------|
| 12 | (a-d) | Elevation contours of the tidal cycle at hourly intervals | 144-147 |
| 13 | (a-d) | Depth-mean currents of the tidal cycle at hourly intervals | 148-151 |
| 14 | (a-h) | Tidal profiles at selected locations | 152-155 |
| 15 | (a-h) | Depth-mean current ellipses at selected locations | 156-157 |
| 16-18 | (a-d) | Relative magnitudes of tide, surge, tide surge and tide+surge interaction-corresponding to 4 phases for tracks I,II and III | 158-169 |

CHAPTER 3

| | | | |
|-------|-----------|---|---------|
| 1-3 | (a,b,c) | Comparison of elevations for the 2-D and 3-D models at the three selected locations for tracks I,II and III | 191-193 |
| 4-6 | (a,b,c) | Elevation contours at the three selected instants of time for tracks I,II and III | 194-202 |
| 7 | | Elevation at the point of landfall for tracks I and II | 203 |
| 8 | (a,b,c) | Elevations at the three selected locations for tracks I,II and III | 204 |
| 9-17 | (a,b,c) | Surface, Bottom and Depth-mean currents at the three selected instants of time for tracks I, II and III | 205-213 |
| 18 | | The selected 10 locations of the region for studying the vertical current structure | 214 |
| 19-24 | (a,b,c,d) | Vertical profiles of u,v and their corresponding modes for tracks I and II | 215-226 |

| | | |
|-------|--|---------|
| 25-28 | (a,b,c) Vertical profiles of u,v and their corresponding modes for track III | 227-234 |
| 29-31 | (a,b,c,d) Evolution of the U,v-modes in time at selected locations for tracks I,II and III | 235-240 |
| 32-39 | (a,b,c,d) Current vectors at 5 levels at the selected locations and instants for tracks I and II | 241-248 |
| 40-42 | (a,b,c,d) Current vectors at 5 levels at the selected locations and instants for track III | 249-251 |

LIST OF TABLES

| CHAPTER 1 | | Page |
|-----------|--|------|
| Table 1.1 | Stations of the region at which the harmonic constants are available | 60 |
| Table 1.2 | Linear interpolated values of the harmonic constants | 64 |
| Table 1.3 | Interpolated values after 1st adjustment | 65 |
| Table 1.4 | Values of integrals and ζ_o | 69 |
| Table 1.5 | Values of integrals and ζ_m | 70 |
| Table 1.6 | Interpolated values of harmonic constants after 2nd adjustment | 71 |
| Table 1.7 | Tables of values ζ_o, ζ_m for the selected parallels | 72 |
| | | |
| CHAPTER 2 | | |
| Table 2.1 | Values of the Meteorological forcing parameters | 100 |
| Table 2.2 | Location, time and magnitudes of elevations due to asymmetric storm | 106 |
| Table 2.3 | Location, time and magnitudes of elevations due to symmetric storm | 107 |
| | | |
| CHAPTER 3 | | |
| Table 3.1 | Coordinates of the selected locations | 182 |

SYNOPSIS

NUMERICAL SIMULATION OF TIDES AND STORM SURGES IN THE BAY OF BENGAL

V. B. K. KUMAR

Department of Mathematics
Indian Institute of Technology, Kanpur, INDIA

September, 1983

The Bay of Bengal, which accounts for nearly 15% of the tropical cyclones of the Globe, is well known for the devastating storm surges. The recent examples are the surges of 1971 (Frank and Hussain, 1971) and of 1977 (Johns et al., 1981). With the funnel shape of its coast-line and the vast extent of the continental-shelf at its head, the Bay of Bengal is a potential region for huge tidal ranges and inundating surges. In spite of this fact, there are relatively few studies on the subject of tides and storm surges for this region as compared to the studies for the other regions such as the North Sea. Motivated by this fact, an attempt has been made to investigate the dynamical aspects of the tides and storm surges, in a detailed form, for the region of the Bay of Bengal through numerical simulation. The present dissertation is presented in five chapters.

Chapter 0 contains five sections. Sections 1 and 2 present general introduction and a brief historical account on the study of storm surges in general and for the Bay of Bengal region in particular. Formulation of hydrodynamical equations required for the two-dimensional surges and tides is presented in section 3 and the corresponding formulation required for the three-dimensional surge is presented in section 4. But the main hydrodynamical formulation required for the simulation of M_2 -tide in the Bay of Bengal is presented in Chapter 1. The layout and contribution of the present dissertation are given in section 5.

In Chapter 1, the M_2 -tide has been simulated using the well-known Proudman's Tidal Theorem (Proudman 1925). Owing to its practical limitations (Doodson 1958, Hendershott and Munk 1970, Cartwright 1978, 1980) only one major application of the theorem has appeared in the literature - after a long gap of 28 years (Fairbairn, 1954). Fairbairn applied the tidal theorem to determine the K_2 -constituent along the equator in the Indian Ocean. His selection of the constituent K_2 , owing to its frequency coinciding with the frequency of the earth's rotation, made the mathematical treatment of the problem simple. In the present study, however, the M_2 -constituent is considered, as it is the major tide-producing constituent. Because of this, and also due to the dimensions of the Bay of Bengal which has a relatively large meridional

extent as compared to the extent along the parallels, the auxiliary functions have shown a relatively complex behaviour, requiring a good deal of effort in the computation of the M_2 -tide distribution. The present formulation has allowed a depth variation in the meridional direction in contrast to the Fairbairn's selection of constant depth throughout. The distribution of the constituent M_2 is determined for each of the spaced parallels ($\frac{1}{4}^\circ$ apart) and a co-tidal map is presented for the region of the Bay of Bengal from 10°N to 20°N , which excludes the shelf region at its head.

Surges, tides and their interaction are studied in Chapter 2 using the vertically averaged model given by Flather and Heaps (1975). In the first section the numerical scheme is described and surges without the tidal forcing are simulated. The selected features include the incorporation of non-linear advection terms, fairly realistic bathymetry, storms with asymmetric wind field, three types of tracks striking the coast normally and obliquely - all having typical features representative of the Bay of Bengal region. The model has shown different response features to different meteorological forcing features, particularly the tracks. Two unexpected features observed from the results of the numerical experiments are the swift, local oscillation, fall-rise-fall, of the elevation during hours of land-fall along the track III and the maximum surge peak to the left of the

storm track 1. Both these factors have been attributed to the possible combination of the coastal geometry, bottom and the moving wind-stress field.

In the second section a tidal regime has been established by forcing a sinusoidal tidal oscillation of 1 meter amplitude, in phase, along the open boundary. The established tidal regime, after 28 cycles of integration, is fairly in close agreement with the observed tides and is intended for the simulation of tide-surge interaction in section 3.

In section 3, tide-surge interaction, with an imposed initial tidal distribution of the established tidal regime of the previous section, is studied. Four phases corresponding to maximum-falling zero-minimum-rising zero along the open boundary, of the tidal cycle have been chosen for this purpose and the obtained results are discussed.

In Chapter 3 a spectral method given by Heaps (1975) is chosen to simulate the three-dimensional features of the storm surge. A selected number of numerical experiments have been performed with the kind of meteorological forcing as has been taken in Chapter 2. Regarding elevations, to a large extent, the major features of the two-dimensional surge of the previous chapter are reproduced. However, some interesting features of the residual circulation which can not be realized in a two-dimensional model are presented.

The present dissertation concludes with Chapter 4, giving a comprehensive review of the results obtained and the models used in the earlier chapters. A future program to improve upon the present work has been suggested.

CHAPTER 0

INTRODUCTION

Roll on, thou deep and dark-blue Ocean, roll!
Ten thousand fleets sweep over thee in vain;
Man marks the earth with ruin, his control
Stops with the shore;

-BYRON, Childe Harold, (iv).

Perhaps ocean is one of the most fascinating features of the nature that mankind has experienced. His experience has progressed through mere curiosity and helplessness towards understanding and harnessing the ocean phenomena for the benefit of mankind and forewarning the calamities to save life and property.

Among the destructive phenomena of the sea, storm surge is one of the most devastating. The fury of the hurricane wind causes devastating surges inundating the low-lying coastal areas. Bay of Bengal, which accounts for nearly 15% of the world crop of tropical cyclones, is an excellent example of this phenomenon. The following are the known events of the destruction caused by storm surges.

Table 0.1

| Year | Place | Destruction caused by surge |
|------|---------------------------------------|--------------------------------------|
| 1737 | Mouths of Hoogly River, near Calcutta | Forty-foot storm wave killed 300,000 |
| 1864 | Mouths of Hoogly River near Calcutta | 50,000 were drowned |
| 1876 | Backer Gunge, India | Storm tide killed more than 100,000 |
| 1960 | Bala sore, India | About 5,000 people were killed |
| 1970 | Chittagong, Bangladesh | More than 300,000 were killed |
| 1977 | Divi Point, India | More than 9,000 were killed |

The destruction is so appalling and the facts are so appealing that one feels the immediate need of studying and forewarning the devastation for the region of Bay of Bengal. On this endeavor recently some progress has been made in the study of storm surges, with the help of numerical models, in India and Bangladesh. We describe some of these works in the next section. In the following paragraphs we briefly describe the important factors involved in the surge dynamics.

Definition of Storm Surge

There can be several ways of defining the storm surge phenomena. Here we state the definition given by Heaps (1967).

It is defined as 'a raising or a lowering of sea level by wind and by changes in atmospheric pressure over the sea associated with a storm'.

The forcing due to storm is the principal cause for storm surges. There are other factors as well, which influence the surge dynamics significantly. Thus, the main factors involved in the surge generation are the intensity, size, speed (vector motion) of the cyclone; the track of the storm; the bottom topography and the coastal geometry of the sea basin, and the phase of the astronomical tide. These are well documented by Dunn and Miller (1964). Other factors include the presence of river mouths and Islands. Local effects such as short-period waves, swell and resonance are also important factors in surge amplification. As an introduction of the subject we briefly describe these aspects in the following paragraphs.

Forcing due to Storm

Cyclone impinging on a coast provides two forcing components, namely, the winds and the pressure drop. Wind stresses (due to winds) acting over the sea surface cause a gradual piling up of the sea surface towards the coast, while the inverted barometer effect (due to pressure drop with respect normal sea level pressure) can cause an almost instantaneous elevation of the sea surface - usually

1 cm per 1 mb (millibar) drop of pressure. However, the elevation due to inverted barometer effect seldom exceeds one meter. The size and intensity of the storm have a direct impact on the extent and magnitude of the piling up action by the associated winds. The vector motion of the storm, on the other hand, determines the duration of the storm forcing.

Storm Track and Coastal Geometry

Storm track is an important factor in the prediction of storm surges. In the normal circumstances the peak surge occurs to the right of the direction of the storm movement, because of the stronger winds there. However occasionally the surges also occur to the left of the storm track. There can be several possibilities leading to this type of unusual behaviour. One of them is presence of an enclosed type of coast facing the off-shore winds. The angle of attack of the storm, which is determined by the track is an essential parameter in the storm surge dynamics. Coastal geometry affects the surge propagation in many ways. A converging bay causes surge amplification through funneling effect. Estuaries and river mouths are such regions where the surge amplification leads to devastation in the adjoining low-lying areas.

Bottom Topography

Bottom topography is also a governing factor in the surge dynamics. In 2-D models, the hydrodynamical equations imply that the surge height is inversely proportional to the depth of water. This implies amplification of surges in shallow regions. Also, in shallow regions the (surface) flow follows the bottom contours and the geometry of bottom contours plays an important role in the redistribution of the accumulated water by the wind stresses. Consequently the surge prediction may be affected regarding the time of arrival, the magnitude and location of the peak surges.

The Astronomical Tide

The astronomical tide, unlike the storm surge, is a regular phenomenon associated with the periodic rise and fall of the ocean surface due to the presence of relatively moving celestial bodies. In certain coastal areas the amplitude of the tide is substantial. The phase of the astronomical tide determines the surge heights near the coastal areas. If the peak surge near any coastal location coincides with the high tide at the location, the surge can be more devastating.

Rivers and Islands

River discharge tends to raise the mean sea level near the mouths and the adjoining estuary regions. Also, the

rainfall associated with the striking storm may aggravate the situation - leading to excessive river discharge. On the other hand the presence of Islands may produce local changes in the surge propagation.

It is very interesting to note that the Bay of Bengal has all the above mentioned features and provides a dwelling place for the storm surges. The extensive shelf area towards the north and the bottom topography with the presence of a large canyon, the enclosed type of coasts, the mouths of Gangetic river system and the Islands are the remarkable features.

The evolution process of surge can be divided into 4 different stages. They are (i) the swell (ii) the fore-runner (iii) the surge and (iv) the resurgence. Swell corresponds to the rough sea conditions in the core-wind region of a cyclone and on the other hand 'fore-runner' is a slowly accumulated elevation ahead of the core-wind region. As the storm approaches the landfall point, the elevation takes place at a rapid rate and this stage is known as the 'surge'. When the storm crosses the coast, it weakens and the direct action of the storm on the sea surface is absent. However, in the process of returning to normal sea-level state, some kind of seiches take place and this stage is known as 'resurgence'.

In the following section we present a brief historical account on the subject of surges. Regarding tides we present the historical account in chapter 1.

0.2 A Brief Historical Account

The bulk of the literature on storm surges has appeared after the year 1950. However, the contributions prior to the World War II are quite significant and paved the way for greater understanding of the surge dynamics. The theoretical aspects of tides and waves were given in an article by Airy (1845) which marks a beginning towards the study of storm surges. A definite demarcation between the early publications and the more recent publications on the subject is given by Bretschneider (1967). There is a limited literature prior to the year 1900. Between the years 1900 and 1930 some important contributions towards the theory have come up from the authors like Abbot, Taylor, Cline, Pettersson, Jeffreys, Marmer, Proudman, Doodson, Yamaguti and perhaps a few others. The literature upto 1930 accounts for only 10% of the bulk of the literature until the present time. From 1930 to 1945 only a limited number of publications have appeared, perhaps due to second World War. The notable authors during this period are Montgomery, Rossby, Arakawa and Yoshitake. An extensive bibliography on storm surges upto 1954 is given by Kramer (1955).

1950s

Perhaps more than 80% of the bulk of the literature has appeared since 1950. With the advent of large, high-speed computers the literature began to expand at an increasing rate. Three particular regions in which extensive studies have been made are the coastal regions of United States, the North Sea and Japan. The works of Goldsbrough (1952), Proudman (1953, 1955), Lauwerier (1955), Crease (1956), Doodson (1956), Hansen (1956), Reid (1956, 1957), Harris (1957, 1959), Platzman (1958), Weenink (1958), Kajiura (1959), Rossiter (1959) and Wilson (1959) are some of the notable contributions that have appeared during the decade of 1950s.

1960s

An excellent article on the numerical prediction of storm surges is given by Welander (1961). A summary of all the available, pertinent information on the state of the art of the subject on storm surge (upto 1965) is given by Bretschneider et al. (1966). This is followed by an extensive bibliography on storm surges by Bretschneider and Pick (1966) and a review by Bretschneider (1967). Modeling is one of the dimensions acquired by the storm surge studies during this period. Theoretical models have been given by Heaps (1965) to investigate the surge on a continental shelf and by Heaps and Ramsbottom (1966) to study the wind effects in a long narrow lake. With the development large-memory, fast-computing machines of later generations, numerical models have been developed to include more complex problems. A two-

dimensional numerical model has been developed by Heaps (1969), incorporating the general sea boundaries within the basic grid system. A brief review of some of the numerical schemes can be found in this work. Many of the numerical schemes used by them in solving the governing equations by the explicit finite-difference methods. Some implicit schemes are given by Leendertse (1967). Other important works during this decade are the numerical models by Jelesnianski (1965, 1966), Miyazaki (1965). A general descriptive article on surges is given by Groen and Groves (1962).

1970s

A further leap in the early seventies is the development of three-dimensional models. Some of the models which belong to this class are multi-layer and multi-level models which are discussed in a review by Liu and Leendertse (1978). Three-dimensional models have also been reviewed by Davies (1981).

A new approach to the three-dimensional modeling for the study of storm surges is given by Heaps (1971). This is a spectral method in which the horizontal components of current are expanded in terms of eigen functions developed through the depth coordinate. Coefficients of the expansion, varying in the horizontal and with time are determined from a two-dimensional numerical scheme. The developing three-dimensional current structure, and the elevation patterns are

determined by means of converging series involving these coefficients and the depth coordinate. With the development of this model, a number of applications are given by Heaps and his colleagues. A three-dimensional numerical model of the Irish Sea is given by Heaps (1973, 1974) and Heaps and Jones (1975). As a further development, a formulation of the three-dimensional model, to include nonlinear terms, is given by Heaps (1976). The spectral model has also been used to determine the density currents in the Irish Sea by Heaps and Jones (1977), and to determine tides and storm surges with vertical eddy viscosity prescribed in two layers by Heaps and Jones (1981). During this period three-dimensional numerical models have also been developed by Forristall (1974), Durance (1976), Davies (1977(a), (b)) and Nihoul (1977), and others. Some important two-dimensional models have also been developed during the decade. Among them are the works by Banks (1974), Prandle (1975), Prandle and Wolf (1978) regarding tide-surge interaction; Jelesnianski (1970, 1972, 1976), Reid et al. (1977). In 1978 World Meteorological Organization has published a report on tropical storm surge prediction which gives the present day art in surge prediction. A comparative assessment of the numerical models for the North Sea has been given by Nihoul and Ronday (1976). Besides these works there are several other important works which have made significant contributions to the understanding of the storm surge dynamics.

Study of Storm Surges for the Region of the Bay of Bengal

Storm surge studies for the region of the Bay of Bengal are quite recent as compared to the studies for the coasts of United States and the North Sea. The initiation has come from the articles by Frank and Hussain (1971), Das (1972) and Fleirl and Robinson (1972). Das et al. (1974) have investigated the surge effects due to the storm that struck Chittagong (Bangladesh) in 1971. A two-dimensional formulation is given by Johns (1981) regarding the simulation of surges in the Bay of Bengal. This formulation has been used in a subsequent study by Johns and Ali (1981) for the coasts of Bangladesh. A multi-level model with σ -coordinate approach is also given by Johns (1981). Recently Das (1981) has studied the temporal response of wind stresses and has shown that in the initial stages of the surge the divergence of the wind stress is more important than the curl of the wind stress, while in the later stages the curl becomes more important. This response has been related to the storm speed (vector motion) and it has been shown that the response is inversely proportional to the square-root of the basin depth. An application of this model has been given by Sinha (1981) for the Gulf of Thailand. For the east coast of India, surges are studied by Johns et al. (1981). Besides these works a few other works have appeared regarding some individual aspects of the surge for the region of Bay of Bengal. Of these, the

studies by Ali (1980), Dube et al. (1981), Johns et al. (1982) are notable.

In the next section we proceed to describe the hydrodynamical formulation for the study of surges and tides.

0.3 Hydrodynamical Equations and formulation of Two-Dimensional Surge

We start with a more general form of hydrodynamical equations of Reynolds type to represent an ocean on the rotating earth. We consider the right handed system of coordinates with the z-axis upwards and the xy plane coinciding with the mean sea level, x-axis directed towards the east and y-axis directed towards the north.

With these considerations, the hydrodynamical equations under the action of a tidal potential q' are

$$\begin{aligned} \frac{\partial u}{\partial t} + u \frac{\partial u}{\partial x} + v \frac{\partial u}{\partial y} + w \frac{\partial u}{\partial z} - fv = -\frac{1}{\rho} \frac{\partial p}{\partial x} - \frac{\partial q'}{\partial x} + \\ + \frac{1}{\rho} \left[\frac{\partial}{\partial x} \tau_{xx} + \frac{\partial}{\partial y} \tau_{yx} + \frac{\partial}{\partial z} \tau_{zx} \right] \end{aligned} \quad (0.3.1)$$

$$\begin{aligned} \frac{\partial v}{\partial t} + u \frac{\partial v}{\partial x} + v \frac{\partial v}{\partial y} + w \frac{\partial v}{\partial z} + fu = -\frac{1}{\rho} \frac{\partial p}{\partial y} - \frac{\partial q'}{\partial y} \\ + \frac{1}{\rho} \left[\frac{\partial}{\partial x} \tau_{xy} + \frac{\partial}{\partial y} \tau_{yy} + \frac{\partial}{\partial z} \tau_{zy} \right] \end{aligned} \quad (0.3.2)$$

$$\frac{\partial w}{\partial t} + u \frac{\partial w}{\partial x} + v \frac{\partial w}{\partial y} + w \frac{\partial w}{\partial z} = - \frac{1}{\rho} \frac{\partial p}{\partial z} - g$$

$$+ \frac{1}{\rho} \left[\frac{\partial}{\partial x} \tau_{xz} + \frac{\partial}{\partial y} \tau_{yz} + \frac{\partial}{\partial z} \tau_{zz} \right] \quad (0.3.3)$$

and the equation of continuity is given by

$$\frac{\partial u}{\partial x} + \frac{\partial v}{\partial y} + \frac{\partial w}{\partial z} = 0 . \quad (0.3.4)$$

Based on the scales of motion we have to simplify the above equations to allow a solution of them for a given set of initial and boundary conditions.

In the study of tides and surges it is usual practice to approximate the equations (0.3.1) to (0.3.4) by means of long ocean waves for which it is assumed that the free surface elevation is small and the horizontal scales of motion are large as compared to the depth. With the help of dimensional analysis (Welander 1961) one can neglect vertical accelerations and vertical convection terms, justifying the hydrostatic approximation in the vertical. Under these assumptions equation (0.3.3) becomes

$$\frac{\partial p}{\partial z} = - g \rho$$

or

$$p = p_a - g \rho (z - \zeta). \quad (0.3.5)$$

We also assume that the lateral stresses τ_{xx} , τ_{xy} and τ_{yy} to be insignificant for the present investigation as we are not considering narrow regions for the adjacent currents to be important (Groen and Groves 1962). Under these assumptions, equation (0.3.3) can be eliminated by incorporating its reduced form (0.3.5) in the equations (0.3.1) and (0.3.2). Thus we have

$$\frac{\partial u}{\partial t} + u \frac{\partial u}{\partial x} + v \frac{\partial u}{\partial y} + w \frac{\partial u}{\partial z} - fv = -g \frac{\partial}{\partial x} (\zeta - \zeta') + \frac{1}{\rho} \frac{\partial}{\partial z} \tau_{zx} \quad (0.3.6)$$

$$\frac{\partial v}{\partial t} + u \frac{\partial v}{\partial x} + v \frac{\partial v}{\partial y} + w \frac{\partial v}{\partial z} + fu = -g \frac{\partial}{\partial y} (\zeta - \zeta') + \frac{1}{\rho} \frac{\partial}{\partial z} \tau_{zy} \quad (0.3.7)$$

$$\frac{\partial u}{\partial x} + \frac{\partial v}{\partial y} + \frac{\partial w}{\partial z} = 0 \quad (0.3.8)$$

where we have replaced the tidal potential q' by the instantaneous response $-g\bar{\zeta}$ (called the equilibrium elevation) and for convenience it is written

$$\left. \begin{aligned} \frac{\partial \zeta'}{\partial x} &= \frac{\partial \bar{\zeta}}{\partial x} - \frac{1}{\rho g} \frac{\partial p_a}{\partial x} \\ \frac{\partial \zeta'}{\partial y} &= \frac{\partial \bar{\zeta}}{\partial y} - \frac{1}{\rho g} \frac{\partial p_a}{\partial y} \end{aligned} \right\} \quad (0.3.9)$$

The common type of boundary conditions associated with the above hydrodynamical system of equations (Welander 1961) are

$$\left. \begin{aligned} u = v = w = 0 \\ \tau_{zx} = F_b, \quad \tau_{zy} = G_b \end{aligned} \right\} \text{ at the bottom } z = -h \quad (0.3.10)$$

and

$$\left. \begin{aligned} w = \frac{d\zeta}{dt} = \frac{\partial \zeta}{\partial t} + u \frac{\partial \zeta}{\partial x} + v \frac{\partial \zeta}{\partial y} \\ \tau_{zx} = F_s, \quad \tau_{zy} = G_s \end{aligned} \right\} \begin{aligned} &\text{at the free surface (0.3.11)} \\ &z = \zeta \end{aligned}$$

In the actual problem solving, the hydrodynamical equations are subjected to appropriate initial and lateral boundary conditions, in addition to the boundary conditions (0.3.10) and (0.3.11).

For convenience in the later stages of our study we depart from the present system of equations in two different directions. In the first instance we derive a system of equations that is amenable to the study of two-dimensional surge. In the second instance we derive a system of equations leading to the study of three-dimensional surge.

Formulation of the Problem for the Study of Two-Dimensional Surge

In an attempt to simplify further the system (0.3.6) to (0.3.11) it is usual to introduce the vertical averaging defined by

$$\bar{u}(x, y, t) = \frac{1}{\zeta + h} \int_{-h(x, y)}^{\zeta(x, y, t)} u(x, y, z, t) dz. \quad (0.3.12)$$

With this vertical averaging and the use of boundary conditions (0.3.10) and (0.3.11) the system (0.3.6) to (0.3.8) becomes

$$\begin{aligned}
 \frac{\partial \bar{u}}{\partial t} + \bar{u} \frac{\partial \bar{u}}{\partial x} + \bar{v} \frac{\partial \bar{u}}{\partial y} + \frac{1}{\zeta+h} \left[\frac{\partial}{\partial x} \{ (\zeta+h) (\bar{u}^2 - \bar{u}^2) \} \right. \\
 \left. + \frac{\partial}{\partial y} \{ (\zeta+h) (\bar{u}\bar{v} - \bar{u}\bar{v}) \} \right] - f\bar{v} \\
 = -g \frac{\partial}{\partial x} (\zeta - \zeta') + \frac{1}{\rho(\zeta+h)} (F_s - F_b) \quad (0.3.13)
 \end{aligned}$$

$$\begin{aligned}
 \frac{\partial \bar{v}}{\partial t} + \bar{u} \frac{\partial \bar{v}}{\partial x} + \bar{v} \frac{\partial \bar{v}}{\partial y} + \frac{1}{\zeta+h} \left[\frac{\partial}{\partial x} \{ (\zeta+h) (\bar{u}\bar{v} - \bar{u}\bar{v}) \} \right. \\
 \left. + \frac{\partial}{\partial y} \{ (\zeta+h) (\bar{v}^2 - \bar{v}^2) \} \right] + f\bar{u} \\
 = -g \frac{\partial}{\partial y} (\zeta - \zeta') + \frac{1}{\rho(\zeta+h)} (G_s - G_b) \quad (0.3.14)
 \end{aligned}$$

$$\frac{\partial \zeta}{\partial t} + \frac{\partial}{\partial x} \{ (\zeta+h) \bar{u} \} + \frac{\partial}{\partial y} \{ (\zeta+h) \bar{v} \} = 0 \quad (0.3.15)$$

where

$$\left. \begin{aligned}
 F_s &= \tau_{zx}|_{z=\zeta}, \quad F_b = \tau_{zx}|_{z=-h} \\
 G_s &= \tau_{zy}|_{z=\zeta}, \quad G_b = \tau_{zy}|_{z=-h}
 \end{aligned} \right\} \quad (0.3.16)$$

Though the above equations are vertically averaged, some form of vertical structure still prevails in the sense that the square of the mean (product of the mean) and the mean of the square (mean of the product) for the variables u and v need not be the same. In the absence of extremely shallow water this vertical structure can be neglected with the assumption that $\overline{u^2} = \overline{u}^2$, $\overline{v^2} = \overline{v}^2$ and $\overline{uv} = \overline{u} \overline{v}$. Also, in the expressions for $\frac{\partial \zeta'}{\partial x}$ and $\frac{\partial \zeta'}{\partial y}$ we do not consider the equilibrium tide and instead we enforce the tide as an input from the adjacent oceans through the lateral open boundaries. Thus, in the present case we have

$$\left. \begin{aligned} \frac{\partial \zeta'}{\partial x} &= -\frac{1}{\rho g} \frac{\partial p_a}{\partial x} \\ \frac{\partial \zeta'}{\partial y} &= -\frac{1}{\rho g} \frac{\partial p_a}{\partial y} \end{aligned} \right\} \quad (0.3.17)$$

Taking the above arguments into consideration the equations (0.3.13) to (0.3.15) with the over-bars removed can be written as

$$\frac{\partial u}{\partial t} + u \frac{\partial u}{\partial x} + v \frac{\partial u}{\partial y} - fv = -g \frac{\partial \zeta}{\partial x} - \frac{1}{\rho} \frac{\partial p_a}{\partial x} + \frac{F_s - F_b}{\rho(\zeta+h)} \quad (0.3.18)$$

$$\frac{\partial v}{\partial t} + u \frac{\partial v}{\partial x} + v \frac{\partial v}{\partial y} + fu = -g \frac{\partial \zeta}{\partial y} - \frac{1}{\rho} \frac{\partial p_a}{\partial y} + \frac{G_s - G_b}{\rho(\zeta+h)} \quad (0.3.19)$$

$$\frac{\partial \zeta}{\partial t} + \frac{\partial}{\partial x} \{(\zeta+h)u\} + \frac{\partial}{\partial y} \{(\zeta+h)v\} = 0. \quad (0.3.20)$$

The closure of the above system requires the characterization of the bottom-stress components F_b , G_b in terms of the mean flow variables u, v . Depending upon the type of flow in the model we can have relations between the bottom stresses and the mean flow quantities. A good account on the subject can be found in Welander (1961). In the present work we adopt the widely used quadratic law for bottom stress characterization. Thus

$$\left. \begin{aligned} F_b &= k \rho u (u^2 + v^2)^{1/2} = \lambda u \\ G_b &= k \rho v (u^2 + v^2)^{1/2} = \lambda v \end{aligned} \right\} \quad (0.3.21)$$

where $\lambda = k \rho (u^2 + v^2)^{1/2}$.

In addition to the parameterization of the bottom stresses the problem requires the specification of stresses near the free surface as an input from the meteorological forcing. This is provided in terms of wind stresses near the free surface. Though not directly concerned with the ocean dynamics (the present problem) we have a two-stage problem in the specification of the wind stresses. In the first stage one should have a good observed values of the surface winds and in the second stage one should choose a good parameterization of the wind stresses (at the sea surface) in terms of the observed wind velocities. Here too,

we can have a variety of relations in practice depending on the type of the approximations made for the surface winds from the observed winds, usually 10 meters above the sea-level. A good account of these aspects can be found in the review by Lick (1975). As in the case of bottom stresses we adopt the commonly used quadratic law for surface stresses given by

$$\left. \begin{aligned} F_s &= C_D^w \rho^w u_w (u_w^2 + v_w^2)^{1/2} \\ G_s &= C_D^w \rho^w v_w (u_w^2 + v_w^2)^{1/2} \end{aligned} \right\} \quad (0.3.22)$$

where w refers to the wind condition.

Other boundaries to be included in the model are the lateral boundaries of closed and open type. For obtaining a solution of the equations we have to prescribe conditions across these boundaries. In the present formulation we consider the fixed wall-type closed boundaries across which the water transport is set to zero. In real situations incorporation of moving coastal boundaries would be proper. But in the absence of reliable data regarding the coastal topography one can consider the wall-type coastal boundaries in which case, the obtained elevation magnitudes, for obvious reason, tend to be higher. Regarding open lateral boundaries we can prescribe various types of the conditions. In the present case we prescribe the following conditions for the lateral boundaries.

For coastal boundaries : $\underline{u} \cdot \underline{n} = 0$ (0.3.23)

For open boundaries : $\zeta = 0$ in the case of
no-tide
or $\zeta = A \cos \sigma t$ in the
case of tide with
amplitude A and
frequency σ (0.3.24)

To avoid the reflection of long waves from the model's interior special procedure has to be used at the model's open boundary. In an analytical investigation of coastal tides Proudman (1940) applied the admittance type of radiative boundary condition. The condition has also been considered by Reid and Bodine (1968). Masch et al. (1971) converted the forcing tide at the model's open boundary into a tidal flow according to the relation

$$\bar{q}_n = C |\zeta_g - \zeta| \quad (0.3.25)$$

where C is an admittance coefficient taken as the gravity wave velocity, ζ_g represents the specified water level at the boundary (eg. observed time history of water levels) and ζ is the previously computed water level at the boundary.

In view of the characterization of bottom stresses we rewrite the equations (0.3.18) to (0.3.20), with the continuity equation appearing first.

Thus

$$\frac{\partial \zeta}{\partial t} + \frac{\partial}{\partial x} \{ (\zeta+h)u \} + \frac{\partial}{\partial y} \{ (\zeta+h)v \} = 0 \quad (0.3.26)$$

$$\frac{\partial u}{\partial t} + u \frac{\partial u}{\partial x} + v \frac{\partial u}{\partial y} - fv = -g \frac{\partial \zeta}{\partial x} - \frac{1}{\rho} \frac{\partial p_a}{\partial x} - \frac{\lambda u}{\rho(\zeta+h)} + \frac{F_s}{\rho(\zeta+h)} \quad (0.3.27)$$

$$\frac{\partial v}{\partial t} + u \frac{\partial v}{\partial x} + v \frac{\partial v}{\partial y} + fu = -g \frac{\partial \zeta}{\partial y} - \frac{1}{\rho} \frac{\partial p_a}{\partial y} - \frac{\lambda v}{\rho(\zeta+h)} + \frac{G_s}{\rho(\zeta+h)} \quad (0.3.28)$$

In chapter 2 we directly incorporate these equations for the numerical treatment along with the appropriate initial and boundary conditions.

0.4 Formulation of the Problem for Three Dimensional Surge

Three-dimensional models for tides and storm surges are physically more realistic as compared to the two-dimensional models. Vertically averaged models are simple for numerical treatment and a good number of experimentations can be performed at a reasonable effort but forgo some of the physical processes required for better understanding of the surge mechanism. For example, in a two-dimensional (vertically averaged) model the characterization of the bottom friction, for conceiving the 'closure', is done in terms of the averaged velocity components, instead of actual velocity components near the bottom. The three-

dimensional model can closely represent the current structure whereas it is not possible in the case of two-dimensional models. However, the three-dimensional models are much more tedious and require enormous computer budget as well as human effort as compared to their two-dimensional counterparts. Perhaps a better way is to have a compromise between the two-dimensional and the three-dimensional models by splitting the complex problem in terms of tasks moulded into either of these models, complementing each other, in achieving the required objective.

Some notable three-dimensional models have been developed in recent years. Heaps (1972, 1973, 1974, 1976) has developed a spectral method for the numerical solution of the three-dimensional hydrodynamical equations for tides and storm surges. In this method, the horizontal components of current are expanded through the vertical from the sea-surface to the sea-bed in terms of a set of eigen functions, taking into consideration, the dynamical boundary conditions at the free surface and at the sea-bed. Coefficients in the expansion, varying in the horizontal and with time are determined following which the current structure and the elevation pattern can be determined. Application of this method is given by Heaps and Jones (1975, 1977). In all these models, however, a constant eddy viscosity through the vertical is assumed with a slip condition at the bed

representing, albeit crudely, the special circumstances hold in the bottom layer. Nihoul (1977) has developed a three-dimensional spectral model, some what similar to that of Heaps' model but incorporating a variable eddy viscosity in the vertical. In the later models, however, Heaps (Heaps and Jones (1981) have considered linearly varying vertical eddy viscosity in their two-layer model. In this model they have resolved a bottom boundary layer in which a linearly varying eddy viscosity in the vertical (logarithmic velocity profile) is taken with the assumption of no-slip at the sea-bed. In the upper layer a constant vertical eddy viscosity is assumed making the distribution continuous at the interface. Johns (1977) has developed a three-dimensional multi-layer model with σ -coordinate approach. An application of this is given by Johns et al. (1982). Other notable models are given by Davies (1977 a,b), Forristall (1974), and Durand (1976). Despite these works, the development of three-dimensional numerical models of water movements in the continental-shelf sea is in its early stages and much has to be done in developing the models with vertical density stratification so that thermocline movements and the associated currents may be taken into account and predicted (Heaps 1981a). In the following paragraphs we describe the spectral model given by Heaps (1976).

Rewriting equations (0.2.6) to (0.2.8) in a convenient form, we have

$$\frac{\partial u}{\partial t} + u \frac{\partial u}{\partial x} + v \frac{\partial u}{\partial y} + w \frac{\partial u}{\partial z} - fv = -g \frac{\partial}{\partial x} (\zeta - \zeta') + \frac{\partial}{\partial z} (N \frac{\partial u}{\partial z}) \quad (0.4.1)$$

$$\frac{\partial v}{\partial t} + u \frac{\partial v}{\partial x} + v \frac{\partial v}{\partial y} + w \frac{\partial v}{\partial z} + fu = -g \frac{\partial}{\partial y} (\zeta - \zeta') + \frac{\partial}{\partial z} (N \frac{\partial v}{\partial z}) \quad (0.4.2)$$

$$\frac{\partial \zeta}{\partial t} + \frac{\partial}{\partial x} \int_{-h}^{\zeta} u dz + \frac{\partial}{\partial y} \int_{-h}^{\zeta} v dz = 0 \quad (0.4.3)$$

in which the continuity equation is retained in the vertically integrated form. In writing the above equations we have assumed the eddy-viscosity model with N as the coefficient of vertical eddy viscosity. These equations are to be solved for u, v and ζ subject to

$$u = v = w = 0 \quad \text{at the bottom } z = -h(x, y) \quad (0.4.4)$$

and

$$w = \frac{d\zeta}{dt} = \frac{\partial \zeta}{\partial t} + u \frac{\partial \zeta}{\partial x} + v \frac{\partial \zeta}{\partial y} \quad \text{at the free surface} \\ z = \zeta(x, y, t) \quad (0.4.5)$$

and also subject to appropriate initial conditions and lateral boundary conditions.

The vertical velocity component is given by

$$w = \frac{\partial}{\partial x} \int_{-h}^z u dz + \frac{\partial}{\partial y} \int_{-h}^z v dz . \quad (0.4.6)$$

By the choice of the coordinate system the free surface of the ocean is at $z = \zeta(x, y, t)$ and the bottom is at $z = -h(x, y)$. If F_s, G_s denote the x, y components of the wind stress on the sea surface, then

$$F_s = -\rho \left(N \frac{\partial u}{\partial z} \right)_{\zeta}, \quad G_s = -\rho \left(N \frac{\partial v}{\partial z} \right)_{\zeta} \quad (0.4.7)$$

Correspondingly, if F_b, G_b denote the x, y components of the frictional stress of the water on the sea bed, then

$$F_b = -\rho \left(N \frac{\partial u}{\partial z} \right)_{-h}, \quad G_b = -\rho \left(N \frac{\partial v}{\partial z} \right)_{-h}. \quad (0.4.8)$$

Assuming the quadratic law for the bottom friction

$$\left. \begin{aligned} F_b &= k \rho u_{-h} (u_{-h}^2 + v_{-h}^2)^{\frac{1}{2}} \\ G_b &= k \rho v_{-h} (u_{-h}^2 + v_{-h}^2)^{\frac{1}{2}} \end{aligned} \right\} \quad (0.4.9)$$

in which k is a constant. Thus, equation (0.4.8) may be expressed in the form

$$\left(N \frac{\partial u}{\partial z} \right)_{-h} = -K u_{-h}, \quad \left(N \frac{\partial v}{\partial z} \right)_{-h} = -K v_{-h} \quad (0.4.10)$$

where

$$K = k (u_{-h}^2 + v_{-h}^2)^{\frac{1}{2}}. \quad (0.4.11)$$

In addition to these conditions we consider the problem in a more physically realistic sense. For example, the non-linearities result from the occurrence of ζ as the lower limit in the integrals of equation (0.4.3); due to the presence of the convective terms in equations (0.4.1) and (0.4.2); because of the evaluation at $z = \zeta$ in the equation (0.4.7); and because K is a function of the motion in equation (0.4.10). We include all these facts in the formulation and any modification would be mentioned instantly when such an occasion arises.

Transformation

In the present method (Heaps 1976) we introduce a function $\varphi(x, y, z, t)$ defined within the depth range $\zeta \geq z \geq -h$ for each x, y, t . Thus

$$\varphi = \varphi(x, y, z, t) \quad -h \leq z \leq \zeta \quad (0.4.12)$$

where

$$\zeta = \zeta(x, y, t), \quad h = h(x, y). \quad (0.4.13)$$

Multiplying the equations (0.4.1) and (0.4.2) by $\varphi(x, y, z, t)$, integrating from $-h$ to ζ and then dividing by $\zeta + h$, yields

$$\frac{\partial \hat{u}}{\partial t} - f\bar{v} = -ga \frac{\partial}{\partial x} (\zeta - \zeta') + \frac{1}{h+\zeta} \int_{-h}^{\zeta} \varphi \frac{\partial}{\partial z} (N \frac{\partial u}{\partial z}) dz + R_u - S_u \quad (0.4.14)$$

$$\frac{\partial \hat{v}}{\partial t} + f \hat{u} = -ga \frac{\partial}{\partial y} (\zeta - \zeta') + \frac{1}{h+\zeta} \int_{-h}^{\zeta} \varphi \frac{\partial}{\partial z} (N \frac{\partial v}{\partial z}) dz + R_v - S_v \quad (0.4.15)$$

where

$$\hat{u} = \frac{1}{h+\zeta} \int_{-h}^{\zeta} u \varphi dz, \quad \hat{v} = \frac{1}{h+\zeta} \int_{-h}^{\zeta} v \varphi dz, \quad a = \frac{1}{h+\zeta} \int_{-h}^{\zeta} \varphi dz \quad (0.4.16)$$

and

$$R_u = \frac{1}{h+\zeta} \left\{ \frac{\partial \zeta}{\partial t} (u \varphi)_{\zeta} - \hat{u} \frac{\partial \zeta}{\partial t} + \int_{-h}^{\zeta} u \frac{\partial \varphi}{\partial t} dz \right\} \quad (0.4.17)$$

$$R_v = \frac{1}{h+\zeta} \left\{ \frac{\partial \zeta}{\partial t} (v \varphi)_{\zeta} - \hat{v} \frac{\partial \zeta}{\partial t} + \int_{-h}^{\zeta} v \frac{\partial \varphi}{\partial t} dz \right\} \quad (0.4.18)$$

$$S_u = \frac{1}{h+\zeta} \int_{-h}^{\zeta} \left(u \frac{\partial u}{\partial x} + v \frac{\partial u}{\partial y} + w \frac{\partial u}{\partial z} \right) \varphi dz \quad (0.4.19)$$

$$S_v = \frac{1}{h+\zeta} \int_{-h}^{\zeta} \left(u \frac{\partial v}{\partial x} + v \frac{\partial v}{\partial y} + w \frac{\partial v}{\partial z} \right) \varphi dz \quad (0.4.20)$$

The terms R_u and R_v arise from the following operation on $\frac{\partial u}{\partial t}$ and $\frac{\partial v}{\partial t}$.

$$\frac{1}{h+\zeta} \int_{-h}^{\zeta} \varphi \frac{\partial u}{\partial t} dz = \frac{\partial \hat{u}}{\partial t} - R_u \quad (0.4.21)$$

$$\frac{1}{h+\zeta} \int_{-h}^{\zeta} \varphi \frac{\partial v}{\partial t} dz = \frac{\partial \hat{v}}{\partial t} - R_v \quad (0.4.22)$$

The terms S_u and S_v arise from the convective accelerations. The vertical structure is retained and is represented by means

of a complete orthonormal set of functions appropriate to the present problem.

We observe that the equations (0.4.14) and (0.4.15) have some comparable similarities with the equations (0.3.5) and (0.3.6) respectively. In this perspective, it is natural to look forward for the characterization of the integrals

$$\int_{-h}^{\zeta} \varphi \frac{\partial}{\partial z} \left(N \frac{\partial u}{\partial z} \right) dz \quad \text{and} \quad \int_{-h}^{\zeta} \varphi \frac{\partial}{\partial z} \left(N \frac{\partial v}{\partial z} \right) dz$$

to make the equations (0.4.14) and (0.4.15) into the familiar solvable form of the two-dimensional model.

In this endeavor let us consider the integral

$\int_{-h}^{\zeta} \varphi \frac{\partial}{\partial z} \left(N \frac{\partial u}{\partial z} \right) dz$. Integrating by parts, twice in succession, we get

$$\int_{-h}^{\zeta} \varphi \frac{\partial}{\partial z} \left(N \frac{\partial u}{\partial z} \right) dz = \left[\varphi N \frac{\partial u}{\partial z} \right]_{-h}^{\zeta} - \left[u N \frac{\partial \varphi}{\partial z} \right]_{-h}^{\zeta} + \int_{-h}^{\zeta} u \frac{\partial}{\partial z} \left(N \frac{\partial \varphi}{\partial z} \right) dz$$

$$\begin{aligned} \text{or } \int_{-h}^{\zeta} \varphi \frac{\partial}{\partial z} \left(N \frac{\partial u}{\partial z} \right) dz &= \frac{F_s}{\rho} (\varphi)_{\zeta} - K(u\varphi)_{-h} - \left[Nu \frac{\partial \varphi}{\partial z} \right]_{-h} \\ &\quad + \int_{-h}^{\zeta} u \frac{\partial}{\partial z} \left(N \frac{\partial \varphi}{\partial z} \right) dz . \quad (0.4.23) \end{aligned}$$

Similarly for the integral $\int_{-h}^{\zeta} \varphi \frac{\partial}{\partial z} \left(N \frac{\partial v}{\partial z} \right) dz$, we have

$$\begin{aligned} \int_{-h}^{\zeta} \varphi \frac{\partial}{\partial z} \left(N \frac{\partial v}{\partial z} \right) dz &= \frac{G_s}{\rho} (\varphi)_{\zeta} - K(v\varphi)_{-h} - \left[Nv \frac{\partial \varphi}{\partial z} \right]_{-h} \\ &\quad + \int_{-h}^{\zeta} v \frac{\partial}{\partial z} \left(N \frac{\partial \varphi}{\partial z} \right) dz . \quad (0.4.24) \end{aligned}$$

Thus if we require

$$\frac{1}{h+\zeta} \int_{-h}^{\zeta} \varphi \frac{\partial}{\partial z} \left(N \frac{\partial u}{\partial z} \right) dz = \frac{F_s}{\rho(\zeta+h)} - \lambda \hat{u} \quad (0.4.25)$$

$$\text{and } \frac{1}{h+\zeta} \int_{-h}^{\zeta} \varphi \frac{\partial}{\partial z} \left(N \frac{\partial v}{\partial z} \right) dz = \frac{G_s}{\rho(\zeta+h)} - \lambda \hat{v} \quad (0.4.26)$$

(where λ is intended to play a similar role as in the two-dimensional problem) we shall have to encounter, for each (x, y, t) , the eigen value problem

$$\frac{\partial}{\partial z} \left(N \frac{\partial \varphi}{\partial z} \right) = -\lambda \varphi \quad -h \leq z \leq \zeta \quad (0.4.27)$$

where λ is independent of z , and

$$\left. \begin{array}{l} \varphi = 1 \\ \frac{\partial \varphi}{\partial z} = 0 \end{array} \right\} \text{ at } z = \zeta \quad (0.4.28)$$

$$\text{and } \frac{\partial \varphi}{\partial z} = \frac{K}{N} \varphi \quad \text{at } z = -h. \quad (0.4.29)$$

The above eigen value problem is the familiar problem of Sturm-Liouville type. The operator $\frac{\partial}{\partial z} \left(N \frac{\partial}{\partial z} \right)$ for the above eigen value problem is self-adjoint and consequently the eigen functions φ_n , corresponding to the unboundedly increasing eigen values λ_n form a complete orthonormal set, with the normalizing factor

$$\Psi = \left[\frac{-(h+\zeta)}{N(\frac{\partial \varphi}{\partial z} \frac{\partial \varphi}{\partial \lambda} - \varphi \frac{\partial}{\partial \lambda} \frac{\partial \varphi}{\partial z})_{\lambda=\lambda_r}} \right]_{z=-h}^{z=\zeta} \quad (0.4.30)$$

For each (x, y, t) , let the ascending eigen values and the corresponding eigen functions derived from the equations (0.4.27) to (0.4.29) be denoted by λ_r and φ_r ($r = 1, 2, 3, \dots, \infty$) respectively. Thus for each pair (λ_r, φ_r) we have from (0.4.14) and (0.4.15)

$$\frac{\partial \hat{u}_r}{\partial t} + \lambda_r \hat{u}_r - f \hat{v}_r = -g a_r \frac{\partial}{\partial x} (\zeta - \zeta') + \frac{F_s}{\rho(\zeta+h)} + R_{u,r} - S_{u,r} \quad (0.4.31)$$

$$\frac{\partial \hat{v}_r}{\partial t} + \lambda_r \hat{v}_r + f \hat{u}_r = -g a_r \frac{\partial}{\partial y} (\zeta - \zeta') + \frac{G_s}{\rho(\zeta+h)} + R_{v,r} - S_{v,r} \quad (0.4.32)$$

where $\hat{u}_r, \hat{v}_r, a_r$ etc. have the previously defined meaning with the subscript r . Solving for \hat{u}_r, \hat{v}_r ($r = 1, 2, 3, \dots, \infty$) we can write

$$u = \sum_{r=1}^{\infty} \Psi_r \hat{u}_r \varphi_r, \quad v = \sum_{r=1}^{\infty} \Psi_r \hat{v}_r \varphi_r \quad (0.4.33)$$

Substituting (0.4.33) in (0.4.3) we get

$$\frac{\partial \Psi}{\partial t} + \sum_{r=1}^{\infty} \left[\frac{\partial}{\partial x} \{ (h+\zeta) a_r \Psi_r \hat{u}_r \} + \frac{\partial}{\partial y} \{ (h+\zeta) a_r \Psi_r \hat{v}_r \} \right] = 0 \quad (0.4.34)$$

Similarly (0.4.33) in (0.4.4) yields

$$w = \sum_{r=1}^{\infty} \left[\frac{\partial}{\partial x} \{ (h+\zeta) q_r \Psi_r \hat{u}_r \} + \frac{\partial}{\partial y} \{ (h+\zeta) q_r \Psi_r \hat{v}_r \} \right] \quad (0.4.35)$$

where

$$q_r = \frac{1}{h+\zeta} \int_{-h}^z \phi_r dz \quad (0.4.36)$$

The depth mean values for u and v are given by

$$\bar{u} = \sum_{r=1}^{\infty} \Psi_r \hat{u}_r a_r, \quad \bar{v} = \sum_{r=1}^{\infty} \Psi_r \hat{v}_r a_r \quad (0.4.37)$$

In the equations (0.4.31) and (0.4.32) the terms $R_{u,r}$, $R_{v,r}$, $S_{u,r}$, $S_{v,r}$ take the following form

$$R_{u,r} = \frac{1}{h+\zeta} \frac{\partial \zeta}{\partial t} (-\hat{u}_r + \sum_j \Psi_j \hat{u}_j) + \sum_j \Psi_j \hat{u}_j B_{r,j} \quad (0.4.38)$$

$$R_{v,r} = \frac{1}{h+\zeta} \frac{\partial \zeta}{\partial t} (-\hat{v}_r + \sum_j \Psi_j \hat{v}_j) + \sum_j \Psi_j \hat{v}_j B_{r,j} \quad (0.4.39)$$

$$\begin{aligned} S_{u,r} = & \sum_j \sum_m \Psi_j \Psi_m \hat{u}_m \left[\hat{u}_j (P_{r,j,m}^{(1)} + P_{r,j,m}^{(2)}) + \hat{v}_j (Q_{r,j,m}^{(1)} + Q_{r,j,m}^{(2)}) \right] \\ & + \sum_j \sum_m \Psi_j \Psi_m \left(\hat{u}_j \frac{\partial \hat{u}_m}{\partial x} + \hat{v}_j \frac{\partial \hat{u}_m}{\partial y} \right) D_{r,j,m} \\ & + \sum_j \sum_m \Psi_j \Psi_m \hat{u}_m \left[\frac{\partial}{\partial x} \{ (h+\zeta) \hat{u}_j \} + \frac{\partial}{\partial y} \{ (h+\zeta) \hat{v}_j \} \right] E_{r,j,m} \end{aligned} \quad (0.4.40)$$

$$\begin{aligned}
S_{v,r} = & \sum_j \sum_m \Psi_j \Psi_m \hat{v}_m [\hat{u}_j (P_{r,j,m}^{(1)} + P_{r,j,m}^{(2)}) + \hat{v}_j (Q_{r,j,m}^{(1)} + Q_{r,j,m}^{(2)})] \\
& + \sum_j \sum_m \Psi_j \Psi_m (\hat{u}_j \frac{\partial \hat{v}_m}{\partial x} + \hat{v}_j \frac{\partial \hat{u}_m}{\partial y}) D_{r,j,m} \\
& + \sum_j \sum_m \Psi_j \Psi_m \hat{v}_m [\frac{\partial}{\partial x} \{(h+\zeta) \hat{u}_j\} + \frac{\partial}{\partial y} \{(h+\zeta) \hat{v}_j\}] E_{r,j,m}
\end{aligned}
\tag{O.4.41}$$

where

$$B_{r,j} = \frac{1}{h+\zeta} \int_{-h}^{\zeta} \frac{\partial \varphi_r}{\partial t} \varphi_j dz \tag{O.4.42}$$

$$P_{r,j,m}^{(1)} = \frac{1}{h+\zeta} \int_{-h}^{\zeta} \varphi_r \varphi_j \frac{\partial \varphi_m}{\partial x} dz \tag{O.4.43}$$

$$P_{r,j,m}^{(2)} = \frac{1}{h+\zeta} \int_{-h}^{\zeta} \varphi_r \frac{\partial \varphi_r}{\partial x} \frac{\partial \varphi_m}{\partial z} dz \tag{O.4.44}$$

$$Q_{r,j,m}^{(1)} = \frac{1}{h+\zeta} \int_{-h}^{\zeta} \varphi_r \varphi_j \frac{\partial \varphi_m}{\partial y} dz \tag{O.4.45}$$

$$Q_{r,j,m}^{(2)} = \frac{1}{h+\zeta} \int_{-h}^{\zeta} \varphi_r \frac{\partial \varphi_j}{\partial y} \frac{\partial \varphi_m}{\partial z} dz \tag{O.4.46}$$

$$D_{r,j,m} = \frac{1}{h+\zeta} \int_{-h}^{\zeta} \varphi_r \varphi_j \varphi_m dz \tag{O.4.47}$$

$$E_{r,j,m} = \frac{1}{h+\zeta} \int_{-h}^{\zeta} \varphi_r \varphi_j \frac{\partial \varphi_m}{\partial z} dz \tag{O.4.48}$$

A particular Formulation:

For mathematical simplicity we assume the eddy viscosity N to be uniform with respect to the depth coordinate z . Thus if we use the normalized form of depth coordinate, given by

$$\xi = \frac{z - \zeta}{h + \zeta} \quad (0.4.49)$$

the eigen value problem (0.4.27) to (0.4.29) can be written as

$$\varphi'' = - (h + \zeta)^2 \frac{\lambda}{N} \varphi \quad (0.4.50)$$

$$\varphi = 1, \quad \varphi' = 0 \quad \text{at} \quad \xi = 0 \quad (0.4.51)$$

$$\text{and} \quad \varphi' = \frac{K}{N} (h + \zeta) \varphi \quad \text{at} \quad \xi = -1. \quad (0.4.52)$$

Conditions at $\xi = 0$ lead to the solution

$$\varphi = \cos (\alpha \xi) \quad (0.4.53)$$

$$\text{where} \quad \alpha = \sqrt{\frac{\lambda}{N}} (h + \zeta)$$

Condition at $\xi = -1$ implies

$$\alpha \tan \alpha - c = 0 \quad (0.4.54)$$

$$\text{where} \quad c = \frac{K}{N} (h + \zeta) \quad (0.4.55)$$

Let $\alpha_r, r = 1, 2, 3, \dots$ be the positive roots of the equation (0.4.54) in the ascending order. Then the

corresponding Sturm-Liouville problem leads to

$$\lambda_r = \frac{N\alpha_r^2}{(h+\xi)^2} \quad (\text{eigen values}) \quad (0.4.56)$$

$$\varphi_r = \cos(\alpha_r \xi) \quad (\text{eigen functions}) \quad (0.4.57)$$

$$\Psi_r = \frac{2}{(1 + a_r \cos \alpha_r)} \quad (\text{Normalizing factors}) \quad (0.4.58)$$

$$a_r = \frac{\sin \alpha_r}{\alpha_r} \quad (0.4.59)$$

$$q_r = \frac{\sin \alpha_r + \sin \alpha_r \xi}{\alpha_r} \quad (0.4.60)$$

In practice, the series for u and v in (0.4.33) have to be terminated at some point, say, at the M^{th} term.

Similarly all the summations are to be truncated after the first M terms. In this particular formulation all the terms $P_{r,j,m}^{(1)}$, $P_{r,j,m}^{(2)}$, $Q_{r,j,m}^{(1)}$, $Q_{r,j,m}^{(2)}$ vanish. Making use of the equations (0.4.56) to (0.4.60) the expressions of (0.4.38) to (0.4.41) reduce to

$$R_{u,r} = \frac{1}{h+\xi} \frac{\partial \xi}{\partial t} \left[-\hat{u}_r + \sum_{j=1}^M (1 + \alpha_r B_{r,j}) \Psi_j \hat{u}_j \right] \quad (0.4.61)$$

$$R_{v,r} = \frac{1}{h+\xi} \frac{\partial \xi}{\partial t} \left[-\hat{v}_r + \sum_{j=1}^M (1 + \alpha_r B_{r,j}) \Psi_j \hat{v}_j \right] \quad (0.4.62)$$

$$\begin{aligned}
S_{u,r} = & \sum_{j=1}^M \sum_{n=1}^M \Psi_j \Psi_n \left(\hat{u}_j \frac{\partial u_n}{\partial x} + \hat{v}_j \frac{\partial u_n}{\partial y} \right) D_{r,j,n}^{(1)} \\
& + \frac{1}{h+\xi} \sum_{j=1}^M \sum_{n=1}^M \Psi_j \Psi_n \hat{u}_j \left[\frac{\partial}{\partial x} \{ (h+\xi) \hat{u}_n \} + \frac{\partial}{\partial y} \{ (h+\xi) \hat{v}_n \} \right] \frac{\alpha_j}{\alpha_n} E_{r,j,n}^{(1)}
\end{aligned}
\tag{0.4.63}$$

$$\begin{aligned}
S_{v,r} = & \sum_{j=1}^M \sum_{n=1}^M \Psi_j \Psi_n \left(\hat{u}_j \frac{\partial \hat{v}_n}{\partial x} + \hat{v}_j \frac{\partial \hat{v}_n}{\partial y} \right) D_{r,j,n}^{(1)} \\
& + \frac{1}{h+\xi} \sum_{j=1}^M \sum_{n=1}^M \Psi_j \Psi_n \hat{v}_j \left[\frac{\partial}{\partial x} \{ (h+\xi) \hat{u}_n \} + \frac{\partial}{\partial y} \{ (h+\xi) \hat{v}_n \} \right] \frac{\alpha_j}{\alpha_n} E_{r,j,n}^{(1)}
\end{aligned}
\tag{0.4.64}$$

where

$$\begin{aligned}
B_{r,j} = & \int_{-1}^0 (1+\xi) \sin(\alpha_r \xi) \cos(\alpha_j \xi) d\xi \\
= & \frac{\alpha_r}{(\alpha_r + \alpha_j)(\alpha_r - \alpha_j)} + \frac{1}{2} \left\{ \frac{\sin(\alpha_r + \alpha_j)}{(\alpha_r + \alpha_j)^2} + \frac{\sin(\alpha_r - \alpha_j)}{(\alpha_r - \alpha_j)} \right\}
\end{aligned}
\tag{0.4.65}$$

$$\begin{aligned}
D_{r,j,n}^{(1)} = & \int_{-1}^0 \cos(\alpha_r \xi) \cos(\alpha_j \xi) \cos(\alpha_n \xi) d\xi \\
= & \frac{1}{4} \left[\frac{\sin(\beta_1 - \alpha_n)}{\beta_1 - \alpha_n} - \frac{\sin(\beta_1 + \alpha_n)}{\beta_1 + \alpha_n} + \frac{\sin(\beta_2 + \alpha_n)}{\beta_2 + \alpha_n} \right. \\
& \left. - \frac{\sin(\beta_2 - \alpha_n)}{\beta_2 - \alpha_n} \right]
\end{aligned}
\tag{0.4.66}$$

$$\begin{aligned}
E_{r,j,n}^{(1)} &= \int_{-1}^0 \cos(\alpha_r \xi) \sin(\alpha_j \xi) \{ \sin(\alpha_n \xi) + \sin \alpha_n \} d\xi \\
&= \frac{1}{4} \left[\frac{\sin(\beta_1 - \alpha_n)}{\beta_1 - \alpha_n} - \frac{\sin(\beta_1 + \alpha_n)}{\beta_2 + \alpha_n} + \frac{\sin(\beta_2 + \alpha_n)}{\beta_2 + \alpha_n} - \frac{\sin(\beta_2 - \alpha_n)}{\beta_2 - \alpha_n} \right] \\
&\quad + \frac{\sin \alpha_n}{2} \left\{ \frac{\cos \beta_1}{\beta_1} - \frac{\cos \beta_2}{\beta_2} + \frac{2\alpha_j}{\beta_1 \beta_2} \right\}, \quad (\beta_2 \neq 0) \quad (0.4.67)
\end{aligned}$$

where

$$\beta_1 = \alpha_r + \alpha_j, \quad \beta_2 = \alpha_r - \alpha_j \quad (0.4.68)$$

when $r = j$ ($\beta_2 = 0$),

$$E_{r,j,n}^{(1)} = \int_{-1}^0 \cos(\alpha_r \xi) \sin(\alpha_j \xi) \{ \sin(\alpha_n \xi) + \sin \alpha_n \} d\xi$$

$$\begin{aligned}
\text{or } E_{r,j,n}^{(1)} &= \frac{1}{4} \left[\frac{\sin(2\alpha_r + \alpha_n)}{2\alpha_r + \alpha_n} - \frac{\sin(2\alpha_r - \alpha_n)}{2\alpha_r - \alpha_n} \right] \\
&\quad + \frac{\sin \alpha_n}{4\alpha_r} (1 + \cos 2\alpha_r) \quad (0.4.69)
\end{aligned}$$

Using the equations (0.4.56) to (0.4.69) and with the properly specified boundary and initial conditions we carry out the computations regarding the study of three-dimensional surge. This will be presented in chapter 3. The vertical velocity component can be determined from (0.4.35) and the depth-mean values for u and v can be obtained from (0.4.37).

0.5 Layout and contribution of the present work

In the following paragraphs we give the layout and the contribution of the present work.

Chapter 1 deals with the study of determining the distribution of M_2 -tide in the region of the Bay of Bengal by means of the well known Tidal Theorem given by Proudman (1925). The Bay depth is allowed to vary in the latitudinal coordinate. Amplitude and phase distributions are determined on each of the equally spaced parallels ($\frac{1}{4}^\circ$ apart) from 10°N to 18°N . A co-tidal chart is drawn and is found to be in reasonable agreement with that given by Pekeris and Accad (1969).

In chapter 2 we have taken up the study of two-dimensional (vertically averaged) surge, tide and their interaction for the region of the Bay of Bengal. A shelf-area at the head Bay of Bengal is considered for the numerical experiments with the tidal and meteorological forcings. Asymmetric storm forcing is considered to study the difference in the surge behaviour as compared to the surge behaviour due to the symmetric storm (from which the asymmetry is derived). Other features included are the geostrophic terms, nonlinear advective terms, the atmospheric pressure gradient, quadratic formulation for the surface and bottom stresses and the fixed wall-type coastal boundaries. In all the numerical

experiments a severe cyclonic storm typical in strength and character for the region of the Bay of Bengal is considered. Three types of tracks are chosen for the numerical experiments, making different angles of incidence with the coast line. Track I is chosen to represent the nearly normal incidence and track II is chosen to represent the nearly parallel incidence at the point of landfall near Chittagong. Track III is chosen to represent the normal incidence at the point of landfall at a location to the right of Hoogly estuary. From the numerical experiments with the storm forcing along tracks I and II (with the same point of landfall), it is shown that the location of maximum peak surge occurs to the right in the case of track II and to the left in the case of track I. It is also observed that the asymmetry of the wind field (with the stronger winds to the right of the track) can produce a maximum peak surge in excess of 2 meteres as compared to the predicted surge with the symmetric storm forcing. In the case of track III some local, short lived oscillations are obtained during the landfall hours. Tidal regime has been established with a sinusoidal forcing of 1 meter amplitude (in phase) along the open boundary of the model area. The obtained tidal amplitude (2.1 meters near Chittagong) as well as the phase is shown to be in close agreement with the observed values. Tide-surge interaction has been studied with the forcing of the established tidal regime and the asymmetric

storm forcing. The interaction produced by the present model is shown to be weak and it is felt that the further refinement of the mesh in the shallow areas and the inclusion of further river-shallow systems are necessary for the proper representation of the non-linear interaction of tide and surge. Owing to the incorporation of fixed wall-type coastal boundaries, the obtained values of elevation are found to be higher in magnitude (upto 20%) as compared to the available observations, particularly near the concave corner points. However, the qualitative features are in reasonable agreement with the available observations.

In chapter 3 a spectral three-dimensional model (Heaps 1975) has been considered for the simulation of the three-dimensional surge. Same features regarding the storm forcing as taken in chapter 2 are considered for the numerical experiments. Three numerical experiments, with the asymmetric storm forcing along tracks I, II and III have been carried out. The obtained elevation patterns of the spectral model have shown marked similarity with the corresponding elevation patterns of the two-dimensional model. The elevations obtained in the spectral model have shown slightly higher magnitudes (upto 10%) as compared to the corresponding elevations of the two-dimensional model. The local oscillation near the point of land fall for the track III numerical experiment in both the models are quite similar. A better explanation of

this behaviour has been given with the help of the spectral model. Also, it is verified that this behaviour is due to a very particular combination of the storm, coast line and the bottom contours. For this purpose the two-dimensional model has been run with the tracks passing through the same point of landfall (of track III) but with different (obliquely opposite) angles of incidence. No such local, swift oscillations have been observed from these runs.

Regarding the current patterns, few interesting results are obtained. During the intensification period (the first ten hours after the initialization) of the storm to the mature stage, the surface currents (just at the free surface) in some regions have attained the magnitudes (over 6 meters/sec !?) in excess of the so far observed values upto 3% of the speeds of the prevailing surface winds. In the absence of data regarding the currents in the severe storm conditions a comparison could not be made. Even for moderate wind conditions the current meter readings, to the best of the author's knowledge, are usually available at a level 4 meters (or more) below the free surface. Excepting these local excessive magnitudes, for which no field observations are available, the over-all current structure is in reasonable agreement with the normal observed values. Other interesting feature is the horizontal circulation of the water mass across the open boundary owing to the wide extent of the open

boundary, and the smaller depth as compared to the 'Ekman Depth' for the region under study (see Appendix at the end of chapter 4). The inflow across the open boundary near the central portion is compensated by the outflow through the side ways across the open boundary and is in consistence with the horizontal circulation pattern described by Welander (1961). This region of inflow is observed to occur to the south-west of the storm centre in a region outside the maximum wind core.

In chapter 4, an over view of the present study has been given by making comparisons of the models used and the results obtained. Vast scope for the future work for the region of the Bay of Bengal has been suggested.

NOMENCLATURE (Chapter 0)

(Symbols not explained in Chapter 0)

| | |
|-----------------|--|
| u, v, w | the velocity components taken in the directions of increasing x, y, z respectively |
| p | the pressure |
| ρ | the density of sea water, assumed constant (1025 kg/Mtr ³) |
| ζ | elevation of the sea-surface above the undisturbed sea-level |
| h | the depth of the undisturbed sea |
| f | the Coriolis parameter |
| t | time |
| g | the acceleration due to gravity |
| p_a | the sea-level atmospheric pressure |
| F_s, G_s | the horizontal forcing stress components (due to wind) at the sea surface |
| F_b, G_b | the horizontal stress components near the sea-bed |
| c_d^w | coefficient of wind drag |
| ρ^w | the density of air |
| u_w, v_w | the horizontal components of the wind velocity at the sea surface |
| \underline{u} | the vector with components u, v, w |
| \underline{n} | the unit outward-normal vector |
| k | drag coefficient (for the flow at the sea-bed) |

$()_{\zeta}$, $()_{-h}$ refer to evaluations at $z = \zeta$ and
at $z = -h$ respectively

τ_{xx} , τ_{yx} etc. are the components of the Reynolds'
stresses of the fluid motion

Units M.K.S.

CHAPTER 1

M_2 -TIDE IN THE BAY OF BENGAL

1.1 Introduction

Oceanic tides, which we observe as periodic rise and fall of the ocean surface in synchronization with the motions of the sun and the moon, are due to the gravitational attraction between the earth and the relatively moving celestial bodies. The subject of tidal phenomenon is an old one, with a vast literature, mostly Victorian (Hendershott and Munk 1970). Newton was the first to give a physical explanation of ocean tides. Later Bernoulli, Laplace, Hough, Airy, Kelvin, Darwin and Poincaré set up a classical theory of tides, the aim of which was to understand qualitatively and quantitatively this natural phenomenon. The discussions on this subject for the past three centuries have passed through myths, paradoxes and heated controversies (Schwiderski 1980). Despite its age and its vast literature, the research on this subject is flourishing in new directions from time to time. In this respect, Doodson's review (1958) has stimulated work on numerical models. At present, the stress regarding the development of the subject is laid on the observational aspects to understand the pitfalls of the hitherto developed work which had led to some controversies (Cartwright 1977).

The theory of oceanic tides is of special importance since the observations are only available from coastal areas. In this regard, late Prof. Proudman (1925) had enunciated a theorem in tidal dynamics as an integral formulation involving certain auxiliary functions. This formulation envisages that, the tidal distribution can be determined in the interior of an ocean region bounded by a coast line (which can have openings to the other adjacent ocean basins), when the tidal data in the form of harmonic constants is available along the coast line. Proudman has provided some illustrations for simple land-locked basins as well as for basins having openings to other ocean regions.

It was after many years, a detailed application of the tidal theorem has been given by Fairbairn (1954) in which the distribution of the semi-diurnal constituent K_2 along the equator in the Indian Ocean has been determined. Consideration of the harmonic constituent K_2 was natural because theoretical investigations prefer K_2 in the case of semi-diurnal tides and K_1 in the case of diurnal tides - in order to avoid mathematical difficulties. Fairbairn in his work has assumed constant depth for the Indian ocean. Based on the obtained tidal distribution along the equator, a co-tidal map has been presented. However, it is more proper to find the tidal distribution along the other parallels of the region for presenting a co-tidal map. In fact, this

has been mentioned by Fairbairn himself and also by Doodson (1958). From the review articles by Doodson (1958), Hendershott and Munk (1970), Hendershott (1972, 1973, 1977), Wunsch (1967, 1972, 1975), Cartwright (1977), Leblond and Mysak (1979), Schwiderski (1980) and from a survey of the recent literature available on ocean tides, it is felt that Fairbairn's work still stands alone regarding the major application of the Proudman's tidal theorem-perhaps owing to its practical limitations (Cartwright 1977).

In the present investigation, the distribution of the harmonic constituent M_2 (which is the principal harmonic constituent for the Bay of Bengal) is determined for the region of Bay of Bengal. In contrast to the constituent K_2 , the consideration of the constituent M_2 requires a different development of the auxiliary functions. Depth is allowed to vary with the latitude coordinate. This is fairly reasonable in the case of Bay of Bengal which has narrow shelves to the east and west. The distribution of M_2 is determined along the parallels of latitude, spaced $\frac{1}{4}^\circ$ apart, ranging from 10°N to 20°N . The relatively shallow area is excluded because it requires the inclusion of frictional terms in the formulation and the problem becomes difficult to tackle. Based on the obtained distribution along the various parallels running through the bay, a co-tidal chart is drawn.

1.2 Tidal Theorem

Hydrodynamical Equations

With the assumption of linearized shallow-water equations on a rotating spherical earth, the hydrodynamical equations are given by (Proudman 1953)

$$\frac{\partial u}{\partial t} - fv = -\frac{g}{a \cos \varphi} \frac{\partial \zeta'}{\partial \lambda} - \frac{F}{h} \quad , \quad (1.2.1)$$

$$\frac{\partial v}{\partial t} + fu = -\frac{g}{a} \frac{\partial \zeta'}{\partial \varphi} - \frac{G}{h} \quad , \quad (1.2.2)$$

and the continuity equation is given by

$$\frac{\partial \zeta}{\partial t} + \frac{1}{a \cos \varphi} \left\{ \frac{\partial}{\partial \lambda} (hu) + \frac{\partial}{\partial \varphi} (hv \cos \varphi) \right\} = 0. \quad (1.2.3)$$

On the other hand the elevation ζ and the current components u, v are also set up by the harmonic constituents. Thus

$$\zeta_{M_2} = \zeta_0 \cos (\sigma t - \kappa) = \zeta_1 \cos \sigma t - \zeta_2 \sin \sigma t = \operatorname{Re} [\zeta e^{i\sigma t}] ,$$

$$u_{M_2} = u_0 \cos (\sigma t - \kappa_u) = u_1 \cos \sigma t - u_2 \sin \sigma t = \operatorname{Re} [u e^{i\sigma t}] ,$$

$$v_{M_2} = v_0 \cos (\sigma t - \kappa_v) = v_1 \cos \sigma t - v_2 \sin \sigma t = \operatorname{Re} [v e^{i\sigma t}] ,$$

(1.2.4)

where Re stands for real part. Amplitudes and phases, for instance ζ_0 and κ , are called harmonic constants; normally they are derived from long-term records of the sea-level. These records are also used in the derivation of tidal currents. The introduction of these kinds of harmonic constituents simplifies the mathematical treatment of tidal problems by means of the hydrodynamical equations. Thus, with the introduction of time dependence in the form $e^{i\sigma t}$ for the variables u, v and ζ' we can write the equations (1.2.1) to (1.2.3) as

$$i\sigma u - fv = -\frac{g}{a \cos \varphi} \frac{\partial \zeta'}{\partial \lambda} - \frac{F}{h} \quad (1.2.5)$$

$$i\sigma v + fu = -\frac{g}{a} \frac{\partial \zeta'}{\partial \varphi} - \frac{G}{h} \quad (1.2.6)$$

$$\text{and } i\sigma \zeta + \frac{1}{a \cos \varphi} \left\{ \frac{\partial}{\partial \lambda} (hu) + \frac{\partial}{\partial \varphi} (hv \cos \varphi) \right\} = 0 \quad (1.2.7)$$

We introduce the auxiliary functions U, V, Z which are analogous to the elements in a free type of motion, but for the rotation of the earth (taken in reverse direction) and require them to satisfy the following corresponding equations

$$i\sigma U + fV = -\frac{g}{a \cos \varphi} \frac{\partial Z}{\partial \lambda} \quad (1.2.8)$$

$$i\sigma V - fU = -\frac{g}{a} \frac{\partial Z}{\partial \varphi} \quad (1.2.9)$$

$$\text{and } i\sigma Z + \frac{1}{a \cos \varphi} \left\{ \frac{\partial}{\partial X} (hU) + \frac{\partial}{\partial \varphi} (hV \cos \varphi) \right\} = 0. \quad (1.2.10)$$

For a region of the ocean, Stokes' theorem reduces to

$$\int h \nu \, ds = \iint \frac{1}{a \cos \varphi} \left\{ \frac{\partial}{\partial X} (hu) + \frac{\partial}{\partial \varphi} (hV \cos \varphi) \right\} dS \quad (1.2.11)$$

Replacing u, v, ν by $\zeta'U, \zeta'V, \zeta'N$ respectively in the equation (1.2.11) and using the equations (1.2.5), (1.2.6) and (1.2.10), we get

$$\begin{aligned} \int h \zeta'N \, ds &= i\sigma \iint \zeta'Z \, dS - \frac{1}{g} \iint h \{ i\sigma(Uu+Vv) - f(Uv-Vu) \} dS \\ &\quad - \frac{1}{g} \iint (FU+GV) dS \end{aligned} \quad (1.2.12)$$

Similarly, replacing u, v, ν by $Zu, Zv, Z\nu$ respectively in the equation (1.2.11) and using the equations (1.2.8), (1.2.9) and (1.2.7), we get

$$\int hZ\nu \, ds = -i\sigma \iint Z\zeta \, dS - \frac{1}{g} \iint h \{ i\sigma(uU+vV) + f(uV-vU) \} dS \quad (1.2.13)$$

Subtracting equation (1.2.13) from equation (1.2.12), we get

$$\int h \zeta'N \, ds - \int hZ\nu \, ds = i\sigma \iint \bar{\zeta}Z \, dS - \frac{1}{g} \iint_S (FU + GV) dS$$

$$\text{or } \int h(\zeta - \bar{\zeta})N \, ds - \int hZ\nu \, ds = i\sigma \iint \bar{\zeta}Z \, dS - \frac{1}{g} \iint (FU+GV) dS. \quad (1.2.14)$$

This is the tidal theorem which was enunciated by Proudman in 1925. The elevation ζ can be determined in the interior of an ocean region S , bounded by the coast line C , with an opening L (which we specify at a later stage), if the equilibrium elevation $\bar{\zeta}$ and the external friction terms F, G are known over the entire area S and the value of ζ over the boundary. The equilibrium elevation can be determined from the following relation (Proudman 1953)

$$\bar{\zeta} = \bar{H} \exp \left\{ 2i \left(\chi + \omega t - \frac{4}{9} \pi \right) \right\} \cos^2 \varphi .$$

If the standard meridian is set to coincide with the meridian of Indian Standard Time (i.e., 82.5°E), this relation becomes

$$\bar{\zeta} = \bar{H} \exp \left\{ 2i \left(\chi - \frac{4}{9} \pi \right) \right\} \cos^2 \varphi \quad (1.2.15)$$

where the value of the amplitude \bar{H} for the present case is taken as 0.267 meters.

The region of Bay of Bengal is considered as a region bounded by the coastline and open boundaries as shown in Fig. 1a. We exclude the relatively shallow region above 20°N whose study requires a separate investigation because of the involvement of the frictional terms F and G . For

an ocean region such as this, the tidal theorem (1.2.14) can be stated as (Fairbairn 1954),

$$\begin{aligned}
 \int_{\Phi} (hV \cos \varphi) \zeta \, dX &= \int_{\Phi} (hV \cos \varphi) \bar{\zeta} \, dX + \int_C (\zeta - \bar{\zeta}) hV \cos \varphi \, dX \\
 &+ \int_C (\zeta - \bar{\zeta}) hU \, d\varphi - \int_L hZ \nu \, ds - i\sigma a \iint_S \bar{\zeta} Z \cos \varphi \, d\varphi \, dX \\
 &+ \frac{a}{g} \iint_S (FU + GV) \cos \varphi \, d\varphi \, dX \quad (1.2.16)
 \end{aligned}$$

Note: We are carrying the frictional terms as far as we can even though our intention is not to retain them. This is done for the sake of a general formulation, and we drop their role at a convenient stage.

In its (tidal theorem) more practical form, if a certain family of free waves can be defined in the ocean area ACB but unrestricted by the boundaries, then the elevations and currents of forced tides along the parallel of latitude Φ can be determined by a series of explicit integrals involving the family of free waves, the tide generating potential, and the tidal elevations round the coast ACB (Cartwright 1977).

1.3 Auxiliary Functions

For the sake of convenience we subdivide this section into two parts. The first part involves the auxiliary

functions which are independent of the longitude coordinate x . We call these auxiliary functions as auxiliary functions I. The second part involves the auxiliary functions containing the factor e^{ipx} , where $p = \frac{\pi}{x_2 - x_1}$, x_1 and x_2 being the bounding longitudes of the region under consideration. We call them as auxiliary functions II.

Auxiliary Functions I

In this case the equations (1.2.8), (1.2.9) and (1.2.10) are written as

$$\left. \begin{aligned} i\sigma U + fV &= 0 \\ i\sigma V - fU &= -\frac{g}{a} \frac{dz}{d\varphi} \\ i\sigma Z + \frac{1}{a \cos \varphi} \frac{d}{d\varphi} (hV \cos \varphi) &= 0 \end{aligned} \right\} \quad (1.3.1)$$

Elimination of U leads to the system

$$\left. \begin{aligned} \frac{dz_1}{d\varphi} &= \frac{a^2 (\sigma^2 - f^2)}{gh \cos \varphi} v_1 \\ \frac{dv_1}{d\varphi} &= -\cos \varphi z_1 \end{aligned} \right\} \quad (1.3.2)$$

where U_1 , V_1 and Z_1 are dimensionless and are given by

$$\left. \begin{aligned} U_1 &= \frac{h}{\sigma a^2} U \\ V_1 &= \frac{h \cos \varphi}{i \sigma a^2} V \\ \text{and } Z_1 &= \frac{Z}{a} \end{aligned} \right\} \quad (1.3.3)$$

U_1 can be determined from the relation

$$U_1 = - \frac{f}{\sigma \cos \varphi} V_1 \quad (1.3.4)$$

Auxiliary Functions II (containing a factor e^{ipX})

Taking U, V, Z in the form given by

$$\left. \begin{aligned} U &= \frac{a^2 \sigma}{h} U_p e^{ipX} \\ V &= \frac{ia^2 \sigma}{h} \frac{V_p}{\cos \varphi} e^{ipX} \\ Z &= a Z_p e^{ipX} \end{aligned} \right\} \quad (1.3.5)$$

where U_p , V_p and Z_p are dimensionless and functions of φ , we can write the equations (1.2.8), (1.2.9) and (1.2.10) in the form

$$\left. \begin{aligned}
 \frac{\sigma a}{h} U_p + \frac{af}{h} \frac{V_p}{\cos \varphi} &= - \frac{gp}{a \sigma \cos \varphi} Z_p \\
 \frac{\sigma a}{h} \frac{V_p}{\cos \varphi} + \frac{af}{h} U_p &= \frac{g}{a \sigma} \frac{dZ_p}{d\varphi} \\
 Z_p + \frac{p}{\cos \varphi} U_p &= - \frac{1}{\cos \varphi} \frac{dV_p}{d\varphi}
 \end{aligned} \right\} \quad (1.3.6)$$

Elimination of U_p leads to the system

$$\left. \begin{aligned}
 \frac{dZ_p}{d\varphi} &= A_1 V_p - B_1 Z_p \\
 \frac{dV_p}{d\varphi} &= B_1 V_p - C_1 Z_p
 \end{aligned} \right\} \quad (1.3.7)$$

where

$$A_1 = \frac{a^2(\sigma^2 - f^2)}{gh \cos \varphi}, \quad B_1 = \frac{fp}{\sigma \cos \varphi} \quad \text{and} \quad C_1 = \cos \varphi - \frac{hg p^2}{a^2 \sigma^2 \cos \varphi} \quad (1.3.8)$$

1.4 Integral Formulation

In the case of auxiliary functions I the integral formulation of the tidal theorem (1.2.14) becomes

$$\begin{aligned}
 \int_{\Phi} \zeta dX &= \int_{\Phi} \bar{\zeta} dX + \int_{C_1} (\zeta - \bar{\zeta}) V_1 d\varphi - i \int_{C_1} (\zeta - \bar{\zeta}) U_1 d\varphi + G_1 \int Z_1 \cos^3 \varphi d\varphi \\
 &+ \frac{i}{\sigma a} \int_L h Z_1 \nu ds + \frac{a}{g} \iint_S \frac{V_1 G}{h} d\varphi dX - \frac{ia}{g} \iint_S \frac{U_1 F}{h} \cos \varphi d\varphi dX
 \end{aligned} \quad (1.4.1)$$

where $G_1 = \frac{i}{2} e^{-\frac{8\pi i}{9}} \bar{H} \{e^{2iX_2} - e^{2iX_1}\}$, X_1 and X_2 being the bounding latitudes for the region. Since the initial values for U_1 , V_1 and Z_1 are at our disposal, we choose $U_1(\Phi) = Z_1(\Phi) = 0$ and $V_1(\Phi) = 1$. The last of the conditions is used in deriving equation (1.4.1).

Similarly, for the auxiliary functions II with index p , the integral formulation of the tidal theorem (1.2.14) becomes

$$\begin{aligned}
 \int_{\Phi} \zeta e^{ipX} dX &= \int_{\Phi} \bar{\zeta} e^{ipX} dX + \frac{1}{V_p(\Phi)} \int_c (\zeta - \bar{\zeta}) V_p e^{ipX} dX \\
 &\quad - \frac{i}{V_p(\Phi)} \int_c (\zeta - \bar{\zeta}) U_p e^{ipX} dX \\
 &\quad - \frac{1}{V_p(\Phi)} \iint_S \bar{\zeta} Z_p \cos \varphi e^{ipX} d\varphi dX + c_p \\
 &\quad + \frac{a}{V_p(\Phi)g} \iint_S \frac{GV_p}{h} e^{ipX} d\varphi dX - \\
 &\quad - \frac{ia}{V_p(\Phi)g} \iint_S \frac{FU_p}{h} \cos \varphi e^{ipX} d\varphi dX \quad (1.4.2)
 \end{aligned}$$

Likewise for the index $-p$ we have

$$\begin{aligned}
 \int_{\Phi} \zeta e^{-ipX} dX &= \int_{\Phi} \bar{\zeta} e^{-ipX} dX + \frac{1}{V_{-p}(\Phi)} \int_c (\zeta - \bar{\zeta}) V_{-p} e^{-ipX} dX \\
 &\quad - \frac{i}{V_{-p}(\Phi)} \int_c (\zeta - \bar{\zeta}) U_{-p} e^{-ipX} dX \\
 &\quad - \frac{1}{V_{-p}(\Phi)} \iint_S \bar{\zeta} Z_{-p} \cos \varphi e^{-ipX} d\varphi dX
 \end{aligned}$$

where,

$$G_2 = \frac{1}{p+2} e^{-\frac{8}{9}\pi i} \bar{H} \{ e^{i(p+2)X_2} - e^{i(p+2)X_1} \}$$

$$G_3 = \frac{1}{2-p} e^{-\frac{8}{9}\pi i} \bar{H} \{ e^{i(2-p)X_2} - e^{i(2-p)X_1} \}$$

and $C_p = c_p + c_{-p}$.

As the initial conditions are at our disposal we choose $U_{\pm p}(\bar{\phi}) = 0 = Z_{\pm p}(\bar{\phi})$, $V_{\pm p}(\bar{\phi}) = \frac{1}{2}$ as initial values. The last condition is used in deriving the equation (1.4.4).

Note: In the equation (1.4.4) the surface integral containing Z is reduced to an ordinary integral, by carrying out the integration with respect to X . C_p, c_p, c_{-p} are the terms arisen out of the correction term $\int hZ^\nu ds$.

Method of determination of ζ along each successive parallel $\bar{\phi}$.

Regarding the determination of the elevation ζ along the various parallels of the region under study, the computational procedure can be carried out in two different ways. In the first case, for the region ACB (Fig. 1(b)), we compute ζ along AB, knowing the value along the boundary ACB, and then repeat the procedure for the region DABE to determine ζ along DE. Thus we proceed further downwards (Cartwright 1977).

In this method, however, there is a continuous and explicit dependence of ζ of the other parallels on ζ of the initial parallel AB (i.e.; errors are carried).

In the second case, we choose the lower most parallel of the region ACB (Fig. 1(c)) and determine ζ along AB, knowing the boundary values along ACB. We repeat this procedure for the region DCE to determine ζ along DE. Thus we exhaust all the parallels upwards. But this procedure suffers from the disadvantage of large magnitudes of the auxiliary functions due to large meridional extent of the region. We have chosen the second method for our computations taking various difficulties of both the methods into consideration.

1.5 Elevation due to the constituent M_2

Let the extent of the bounding parallel ϕ be from 0 to b . All the integrations in the previous section are carried out from 0 to b . Let $p = \frac{n\pi}{b}$ where n is an integer. Then the integrals are transformed to give the coefficients of the Fourier cosine series for ζ along ϕ . As n is at our disposal, we can calculate the Fourier coefficients $\zeta_0, \zeta_p, \zeta_{2p}$, etc. Thus with the transformation

$$x' = \frac{b(x-x_1)}{x_2-x_1} \quad \text{we have}$$

$$\zeta_0 = \frac{p}{\pi} \int \zeta dx' = \zeta_{1,0} + i\zeta_{2,0} \quad (1.5.1)$$

$$\text{and } \zeta_p = \frac{2p}{\pi} \int \zeta \cos px' dx' = \zeta_{1,p} + i\zeta_{2,p} \quad (1.5.2)$$

where ζ_1 refers to the real part and ζ_2 refers to the imaginary part. Having determined the mean elevation ζ_0 and the coefficients ζ_p , ζ_{2p} , ζ_{3p} etc., the amplitude and the phase of the tidal constituent M_2 can be determined from the equation (1.2.4). That is from

$$\begin{aligned} \zeta_{M_2} = & (\zeta_{1,0} + \zeta_{1,p} \cos px' + \zeta_{1,2p} \cos 2px' + \zeta_{1,3p} \cos 3px' + \dots) \cos \sigma t \\ & - (\zeta_{2,0} + \zeta_{2,p} \cos px' + \zeta_{2,2p} \cos 2px' + \zeta_{2,3p} \cos 3px' + \dots) \sin \sigma t \end{aligned} \quad (1.5.3)$$

Tidal Data

Tidal data, in the form of harmonic constants at various coastal stations are taken from the list of harmonic constants supplied by the Geodetic and Research Branch, Survey of India Department. The phase angles are given in terms of g_2 (given below) and necessary conversions are made to adjust them for a standard meridian and time. This is done using the formulae (Dronkers 1964)

$$g_2 = \kappa + 2L - \sigma T \quad (1.5.4)$$

$$\text{and } g_1 - g_2 = \sigma(T - T_1)$$

where κ is the phase lag of the tidal constituent behind the phase of the corresponding equilibrium constituent at the place; L is the longitude of the station in degrees west of Greenwich;

σ is the angular speed of the constituent M_2 in degrees per mean solar hour ($\sigma = 28.984$ deg/mean solar hour), the time measured in standard time T hours later than Greenwich Mean Time.

The second of the above two equations (1.5.4) allows for a change in the time meridian from T to T_1 . Standard time is taken with $T_1 = -5.5$ hours. That is, 5.5 hours fast with respect to Greenwich Mean Time. The phase lag g_1 is calculated for each station and these values together with the amplitudes are given in the following table.

Table 1.1

| Sl.No. | Station | phase lag in degrees | Amplitude in meters |
|--------|----------------|----------------------------|---------------------------|
| 1 | Nagapatnam | 253.3 | 0.1996 |
| 2 | Madras | 237.3 | 0.3316 |
| 3 | Kakinada | 247.6 | 0.4680 |
| 4 | Visakhapatnam | 239.0 | 0.4752 |
| 5 | Paradeep | 241.4 | 0.6218 |
| 6 | Akyab | 254.0 | 0.7821 |
| 7 | Diamond Island | 254.42 | 0.6712 |
| 8 | Port Blair | 252.8 | 0.6148 |

Use of this standard meridian, and the omission of the time factor gives,

$$\bar{\zeta} = \bar{H} e^{2i(\chi - \frac{4}{9}\pi)} \cos^2 \varphi$$

where \bar{H} is taken to be 0.267 meters. Similarly $\zeta = H e^{-ig_1}$.

As the formalities regarding the formulation are almost complete, we proceed to describe the computational aspects in the following paragraphs.

Computation of Auxiliary Functions

For solving the systems (1.3.2) and (1.3.7) which are representative of the auxiliary functions I and II respectively a Runge-Kutta method based on Verner's fifth and sixth order formulae has been used. In the case of the system (1.3.2) the initial conditions at the bounding parallel ϕ are specified as $U_1(\phi) = Z_1(\phi) = 0$, $V_1(\phi) = 1$; and those for the system (1.3.7) are specified as $U_{\pm p}(\phi) = Z_{\pm p}(\phi) = 0$, $V_{\pm p} = 0.5$. The distribution of depth as a function of φ is fitted with the quadratic

$$h(\varphi) = (a_0 + a_1 \varphi + a_2 \varphi^2) \times 1000.0$$

where $a_0 = 1.360099$, $a_1 = 24.28704$ and $a_2 = -72.42843$.

The data for the bathymetry is taken from the charts provided by the Naval Hydrographic Office.

The extent of the latitude from the bounding parallel to the final parallel (i.e., the open boundary at 20°N) has been partitioned into equally spaced strips of width $\frac{1^{\circ}}{4}$. Solution is advanced through each of these strips (in the direction of increasing ϕ) using the Runge-Kutta-Verner's method. Solutions for $\phi = 10.25^{\circ}\text{N}$ are shown in Figs. 3,4,5,6 and 7.

Interpolation of Harmonic Constants Along the Coast

To evaluate the integrals on the right hand side of the integral formulation (1.2.14) we must know the values of ζ along the coast-line which is available in the form of harmonic constants inferred from tidal observations at selected stations along the coast. It is necessary to interpolate them along the entire coast. For this purpose we have selected the rectangles of the mesh through which the coast-line passes (Fig. 2). There are 121 such rectangles (of size $\frac{1^{\circ}}{4}$ each) and the data is available for 8 rectangles only (Table 1.1). In such a situation as this, it is difficult to obtain proper distribution of the interpolated harmonic constants along the coast-line. From the available data for the harmonic constants for stations along the coast, it is observed that, except for the region at the head Bay of Bengal, the variations in phase lag are relatively small; but there is a continuous variation in amplitude from 20 cms

near Nagapatnam to 75 cms near Akyab and slowly decreasing to 60 cms near Port Blair. The difficulty is further aggravated by the choice of an open boundary along the parallel at 20°N , which has considerable extent, at which the auxiliary functions attain their maximum magnitude and the amplitude of the tide too is quite high. The obtained tide is thus sensitive to the changes in the interpolated harmonic constants. Initially we have taken the linearly interpolated values of the harmonic constants (Table 1.2) in the rectangles along the coast between the coastal stations. However, it became necessary to adjust the linearly interpolated constants to obtain a proper distribution of the tidal constituent along the parallel ϕ . The adjustment is done by means of numerical experimentation - for the computation of the tidal distribution along the first parallel (Table 1.3). This adjustment is supposed to be valid for the computations regarding the tidal distribution for the other parallels as well. However, we had to adjust the interpolated values of the harmonic constants once again for the reasons which will be mentioned in section 1.5.

Correction Terms of the Open Boundaries

If an ocean region has openings to the adjacent basins, one must account for the transport across these open boundaries. In the integral formulation (1.2.14) the transport is

Table 1.2

Linearly Interpolated Values of Harmonic Constants

G1 = PHASE-LAG IN DEGREES, H = AMPLITUDE IN METERS

| S.No. | G1 | H | S.No. | G1 | H | S.No. | G1 | H |
|-------|--------|-------|-------|--------|-------|-------|--------|-------|
| 1 | 258.63 | 0.156 | 41 | 239.00 | 0.475 | 81 | 250.15 | 0.765 |
| 2 | 256.85 | 0.170 | 42 | 239.00 | 0.475 | 82 | 250.50 | 0.771 |
| 3 | 255.08 | 0.185 | 43 | 239.18 | 0.486 | 83 | 260.85 | 0.776 |
| 4 | 253.30 | 0.200 | 44 | 239.37 | 0.498 | 84 | 251.20 | 0.782 |
| 5 | 251.52 | 0.214 | 45 | 239.55 | 0.509 | 85 | 251.20 | 0.782 |
| 6 | 249.74 | 0.229 | 46 | 239.74 | 0.520 | 86 | 251.20 | 0.776 |
| 7 | 247.97 | 0.244 | 47 | 239.92 | 0.532 | 87 | 251.20 | 0.769 |
| 8 | 246.19 | 0.258 | 48 | 240.11 | 0.543 | 88 | 251.20 | 0.763 |
| 9 | 244.41 | 0.273 | 49 | 240.29 | 0.554 | 89 | 251.20 | 0.756 |
| 10 | 242.63 | 0.288 | 50 | 240.48 | 0.565 | 90 | 251.20 | 0.749 |
| 11 | 240.86 | 0.302 | 51 | 240.66 | 0.577 | 91 | 251.20 | 0.743 |
| 12 | 239.08 | 0.317 | 52 | 240.85 | 0.588 | 92 | 251.20 | 0.736 |
| 13 | 237.30 | 0.332 | 53 | 241.03 | 0.599 | 93 | 251.20 | 0.730 |
| 14 | 237.30 | 0.332 | 54 | 241.22 | 0.611 | 94 | 251.20 | 0.723 |
| 15 | 237.79 | 0.338 | 55 | 241.40 | 0.622 | 95 | 251.20 | 0.717 |
| 16 | 238.28 | 0.345 | 56 | 241.40 | 0.622 | 96 | 251.20 | 0.710 |
| 17 | 238.77 | 0.351 | 57 | 241.75 | 0.627 | 97 | 251.20 | 0.704 |
| 18 | 239.26 | 0.358 | 58 | 242.10 | 0.633 | 98 | 251.20 | 0.697 |
| 19 | 239.75 | 0.364 | 59 | 242.45 | 0.639 | 99 | 251.20 | 0.691 |
| 20 | 240.24 | 0.371 | 60 | 242.80 | 0.645 | 100 | 251.20 | 0.684 |
| 21 | 240.78 | 0.377 | 61 | 243.15 | 0.650 | 101 | 251.20 | 0.678 |
| 22 | 241.22 | 0.384 | 62 | 243.50 | 0.656 | 102 | 251.20 | 0.671 |
| 23 | 241.71 | 0.390 | 63 | 243.85 | 0.662 | 103 | 251.20 | 0.671 |
| 24 | 242.20 | 0.397 | 64 | 244.20 | 0.668 | 104 | 251.29 | 0.668 |
| 25 | 242.70 | 0.403 | 65 | 244.55 | 0.673 | 105 | 251.38 | 0.665 |
| 26 | 243.19 | 0.409 | 66 | 244.90 | 0.679 | 106 | 251.47 | 0.662 |
| 27 | 243.68 | 0.416 | 67 | 245.25 | 0.685 | 107 | 251.55 | 0.659 |
| 28 | 244.17 | 0.422 | 68 | 245.60 | 0.690 | 108 | 251.64 | 0.656 |
| 29 | 244.66 | 0.429 | 69 | 245.95 | 0.696 | 109 | 251.73 | 0.652 |
| 30 | 245.45 | 0.435 | 70 | 246.30 | 0.702 | 110 | 251.82 | 0.649 |
| 31 | 245.64 | 0.442 | 71 | 246.65 | 0.708 | 111 | 251.91 | 0.646 |
| 32 | 246.13 | 0.448 | 72 | 247.00 | 0.713 | 112 | 252.00 | 0.643 |
| 33 | 246.62 | 0.455 | 73 | 247.35 | 0.719 | 113 | 252.09 | 0.640 |
| 34 | 247.11 | 0.462 | 74 | 247.70 | 0.725 | 114 | 252.18 | 0.637 |
| 35 | 247.60 | 0.468 | 75 | 248.05 | 0.731 | 115 | 252.27 | 0.634 |
| 36 | 247.60 | 0.468 | 76 | 248.40 | 0.736 | 116 | 252.89 | 0.612 |
| 37 | 245.88 | 0.469 | 77 | 248.75 | 0.742 | 117 | 252.98 | 0.608 |
| 38 | 244.16 | 0.471 | 78 | 249.10 | 0.748 | 118 | 253.07 | 0.605 |
| 39 | 242.44 | 0.472 | 79 | 249.45 | 0.753 | 119 | 253.15 | 0.602 |
| 40 | 240.72 | 0.474 | 80 | 249.80 | 0.759 | 120 | 253.24 | 0.599 |

Table 1.3

Adjustment I of the interpolated harmonic constants

G1 = PHASE-LAG IN DEGREES. H = AMPLITUDE IN METERS

| S. No. | G1 | H | S. No. | G1 | H | S. No. | G1 | H |
|-----------|--------|-------|-----------|--------|-------|-----------|--------|-------|
| 1 | 253.20 | 0.195 | 41 | 239.70 | 0.481 | 81 | 252.20 | 0.735 |
| 2 | 252.80 | 0.196 | 42 | 239.80 | 0.486 | 82 | 252.70 | 0.730 |
| 3 | 252.40 | 0.197 | 43 | 240.00 | 0.492 | 83 | 252.40 | 0.725 |
| 4 | 252.00 | 0.200 | 44 | 240.30 | 0.500 | 84 | 252.00 | 0.720 |
| 5 | 251.50 | 0.215 | 45 | 240.60 | 0.508 | 85 | 251.70 | 0.718 |
| 6 | 249.50 | 0.224 | 45 | 241.00 | 0.516 | 86 | 251.40 | 0.715 |
| 7 | 247.50 | 0.234 | 47 | 241.50 | 0.528 | 87 | 251.50 | 0.712 |
| 8 | 245.50 | 0.248 | 48 | 242.20 | 0.540 | 88 | 251.80 | 0.710 |
| 9 | 243.50 | 0.262 | 49 | 243.00 | 0.550 | 89 | 252.00 | 0.708 |
| 10 | 242.50 | 0.280 | 50 | 243.80 | 0.560 | 90 | 252.00 | 0.705 |
| 11 | 240.50 | 0.295 | 51 | 244.70 | 0.570 | 91 | 252.00 | 0.703 |
| 12 | 238.50 | 0.310 | 52 | 245.10 | 0.576 | 92 | 252.00 | 0.700 |
| 13 | 236.50 | 0.332 | 53 | 245.10 | 0.581 | 93 | 252.20 | 0.697 |
| 14 | 235.50 | 0.335 | 54 | 245.10 | 0.587 | 94 | 252.40 | 0.695 |
| 15 | 236.10 | 0.338 | 55 | 245.10 | 0.592 | 95 | 252.20 | 0.693 |
| 16 | 236.50 | 0.342 | 56 | 245.20 | 0.595 | 96 | 252.20 | 0.690 |
| 17 | 237.00 | 0.346 | 57 | 245.20 | 0.598 | 97 | 252.00 | 0.688 |
| 18 | 237.50 | 0.350 | 58 | 245.20 | 0.601 | 98 | 251.60 | 0.685 |
| 19 | 238.00 | 0.354 | 59 | 245.30 | 0.605 | 99 | 251.20 | 0.682 |
| 20 | 238.40 | 0.358 | 60 | 245.30 | 0.610 | 100 | 251.00 | 0.680 |
| 21 | 238.50 | 0.362 | 61 | 245.40 | 0.615 | 101 | 250.50 | 0.678 |
| 22 | 238.80 | 0.366 | 62 | 245.40 | 0.619 | 102 | 250.00 | 0.675 |
| 23 | 239.10 | 0.370 | 63 | 245.40 | 0.622 | 103 | 249.50 | 0.670 |
| 24 | 240.20 | 0.375 | 64 | 245.40 | 0.625 | 104 | 249.90 | 0.665 |
| 25 | 240.50 | 0.385 | 65 | 245.50 | 0.630 | 105 | 250.10 | 0.660 |
| 26 | 241.30 | 0.395 | 66 | 245.50 | 0.635 | 106 | 250.20 | 0.655 |
| 27 | 241.70 | 0.405 | 67 | 245.50 | 0.640 | 107 | 250.30 | 0.650 |
| 28 | 241.90 | 0.415 | 68 | 245.50 | 0.645 | 108 | 250.40 | 0.645 |
| 29 | 242.30 | 0.425 | 69 | 245.60 | 0.650 | 109 | 250.50 | 0.640 |
| 30 | 242.70 | 0.435 | 70 | 245.70 | 0.655 | 110 | 250.60 | 0.635 |
| 31 | 243.10 | 0.435 | 71 | 246.00 | 0.660 | 111 | 250.60 | 0.630 |
| 32 | 243.80 | 0.440 | 72 | 246.90 | 0.665 | 112 | 250.70 | 0.626 |
| 33 | 244.50 | 0.450 | 73 | 247.70 | 0.670 | 113 | 250.70 | 0.623 |
| 34 | 245.00 | 0.468 | 74 | 248.50 | 0.680 | 114 | 250.80 | 0.620 |
| 35 | 246.00 | 0.460 | 75 | 249.20 | 0.690 | 115 | 250.80 | 0.618 |
| 36 | 247.10 | 0.464 | 76 | 249.50 | 0.700 | 116 | 250.90 | 0.616 |
| 37 | 244.40 | 0.468 | 77 | 249.90 | 0.710 | 117 | 250.90 | 0.615 |
| 38 | 242.10 | 0.472 | 78 | 250.90 | 0.720 | 118 | 251.00 | 0.615 |
| 39 | 240.50 | 0.475 | 79 | 251.00 | 0.730 | 119 | 251.00 | 0.613 |
| 40 | 238.10 | 0.478 | 80 | 251.50 | 0.740 | 120 | 251.40 | 0.611 |

represented by the integral $\int_{OB} hZ \nu ds$ which has to be evaluated along a fictitious line constituting the open boundary. For the evaluation of this integral one should know apriori the transport component ν across the open boundary. For a general ocean it is difficult to obtain data regarding this, and there is no adequate data for the region under consideration. In the absence of such information an alternative representation of this integral is suggested by Fairbairn (1954). That is, when certain mean values for ζ, Z and φ are assumed which are representative of the boundary enclosing the region S, then

$$\int_{OB} h \nu ds = \frac{\partial}{\partial t} \iint \zeta dS$$

and hence
$$\int_{OB} hZ \nu ds = Z_B \frac{\partial \zeta_B}{\partial t} A \quad (1.5.5)$$

where A is the area of the basin adjacent to the open boundary.

With $\zeta_B = H_B e^{i(\sigma t - g_B)}$ we have

$$\frac{\partial \zeta_B}{\partial t} = i\sigma \zeta_B \quad (1.5.6)$$

and
$$A = a^2 \cos \varphi_B \iint_A d\varphi dx \quad (1.5.7)$$

Since we have incorporated two open boundaries, one towards north along the parallel at 20°N and the other along a fictitious line drawn connecting the submerged ridges of the Andaman Islands and the Diamond Island off Burma coast. Hence the correction terms in the integral formulations (1.4.1) and (1.4.4) will have two components which are representative of these open boundaries. Thus, in the integral formulation (1.4.1) we have

$$\begin{aligned} C_N &= -\bar{H}_N e^{-ig_N Z_N} \\ C_E &= -\bar{H}_E e^{-ig_E Z_E} \end{aligned} \quad (1.5.8)$$

Similarly for the integral formulation (1.4.4) with index p we have

$$\begin{aligned} C_{N,p} &= -\bar{H}_N A_N e^{-ig_N \{ (Z_{N,p} + Z_{N,-p}) \cos X_N + (Z_{N,p} - Z_{N,-p}) \sin X_N \}} \\ C_{E,p} &= -\bar{H}_E A_E e^{-ig_E \{ (Z_{E,p} + Z_{E,-p}) \cos X_E + (Z_{E,p} - Z_{E,-p}) \sin X_E \}} \end{aligned} \quad (1.5.9)$$

1.6 Computations and Results

A criterion has been specified in which the matching of the computed value and the observed value of ζ_{M_2} at the extremities (coastal points) of the bounding parallel is required. After the first adjustment of the linearly

interpolated harmonic constants, numerical experiments have been performed with the help of the above specified criterion. The matching of the computed values and the observed values for ζ_{M_2} is achieved by adjusting the correction term $C_{N,p}$. This is because the only course left in the formulation, after the adjustment of the harmonic constants, is the adjustment of the correction terms to a proper level. The adjustment of $C_{N,p}$ is done by choosing a proper combination of the mean values H_B, Z_B, X_B, g_B representative of the open boundary towards the north. It is the adjustment of X_B in most cases, which helped in achieving the required matching. The values of H_B and g_B are kept the same as those for the case of computation for the first bounding parallel and the value of X_B is chosen as $20^\circ N$, at which the values of $Z_{\pm p}$ are taken for computing the integrals. However, the value of X_{BN} has been adjusted in the range between $91^\circ E$ and $93^\circ E$ to achieve the required matching. The values of the integrals and the coefficients of the Fourier cosine series (in the equation (1.5.3)) are given in Tables 1.4 and 1.5 respectively for the bounding parallel ϕ of $10^\circ N$.

Table 1.4

| Integral | Value |
|--|--------------------|
| $\int (\zeta - \bar{\zeta}) v_1 dX$ | $0.013 + 0.003 i$ |
| $-i \int (\zeta - \bar{\zeta}) u_1 d\varphi$ | $-0.005 + 0.096 i$ |
| $\int \bar{\zeta} dX$ | $-0.053 + 0.037 i$ |
| $G_1 \int Z_1 \cos^3 \varphi d\varphi$ | $0.018 + 0.013 i$ |
| C_E | $0.002 - 0.006 i$ |
| C_N | $-0.002 - 0.013 i$ |
| <hr/> | |
| $\zeta_o = -0.1065 + 0.2234i$ | |

Table 1.5

| Integral | m=p | m=2p | m=3p | m=4p |
|---|-----------------|-----------------|-----------------|------------------|
| $\int (\zeta - \bar{\zeta})(V_m + V_{-m}) \cos mX dX$ | 0.1008+0.0032i | -0.3626-0.0326i | 1.0011+0.0562i | -13.7646-0.9973i |
| $\int (\zeta - \bar{\zeta})(V_m - V_{-m}) \sin mX dX$ | 0.0166-0.0696i | 0.0539-0.4618i | -0.3037+0.8628i | 1.3374+4.6271i |
| $-\int (\zeta - \bar{\zeta})(U_m + U_{-m}) \cos mXd\varphi$ | -0.0009+0.0327i | -0.0295+0.583i | 0.1754-1.2907i | 0.2863+0.2496i |
| $\int (\zeta - \bar{\zeta})(U_m - U_{-m}) \sin mXd\varphi$ | -0.0986-0.0084i | 0.3720-0.0541i | -1.0080-0.1323i | 13.2566+0.9425i |
| $\int \bar{\zeta} \cos mXd\varphi$ | -0.0022-0.003i | -0.0014-0.0017i | -0.001-0.0012i | -0.0008-0.0009i |
| $G_2 \int Z_p \cos^3 \varphi d\varphi + G_3 \int \cos^3 \varphi d\varphi$ | 0.0019-0.0028i | -0.0004-0.0003i | 0.0013-0.0020i | -0.0003-0.0002i |
| $C_{E,M}$ | -0.002+0.0064i | 0.0025-0.0081i | -0.0036+0.0113i | 0.0052-0.0159i |
| $C_{N,m}$ | -0.0051+0.0265i | -0.0245-0.1105i | 0.1352+0.4856i | -1.1173-4.8072i |
| ζ_m | 0.1636-0.1178i | 0.0782-0.1738i | -0.0258-0.082i | 0.0192-0.0182i |

Table 1.6

Adjustment II of the Interpolated Harmonic Constants
For $\Phi = 16^\circ \text{N}$.

G1 = Phase-lag in Degrees. H = Amplitude in Meters

| S.NO. | G1 | H | S.NO. | G1 | H | S.NO. | G1 | H |
|-------|-------|-------|-------|-------|-------|-------|-------|-------|
| 1 | 241.7 | 0.405 | 24 | 244.4 | 0.560 | 47 | 248.5 | 0.675 |
| 2 | 241.9 | 0.415 | 25 | 244.7 | 0.570 | 48 | 249.0 | 0.680 |
| 3 | 242.5 | 0.428 | 26 | 245.1 | 0.576 | 49 | 249.5 | 0.695 |
| 4 | 242.7 | 0.438 | 27 | 245.7 | 0.581 | 50 | 249.9 | 0.710 |
| 5 | 243.1 | 0.440 | 28 | 246.1 | 0.587 | 51 | 250.9 | 0.714 |
| 6 | 243.8 | 0.440 | 29 | 245.1 | 0.592 | 52 | 251.0 | 0.720 |
| 7 | 244.5 | 0.450 | 30 | 245.2 | 0.595 | 53 | 251.5 | 0.728 |
| 8 | 245.0 | 0.468 | 31 | 245.2 | 0.598 | 54 | 252.2 | 0.730 |
| 9 | 246.0 | 0.473 | 32 | 245.2 | 0.601 | 55 | 252.7 | 0.730 |
| 10 | 247.1 | 0.484 | 33 | 245.3 | 0.605 | 56 | 252.4 | 0.725 |
| 11 | 244.4 | 0.490 | 34 | 245.3 | 0.610 | 57 | 252.0 | 0.720 |
| 12 | 242.1 | 0.502 | 35 | 245.4 | 0.619 | 58 | 251.7 | 0.718 |
| 13 | 240.5 | 0.500 | 36 | 245.4 | 0.622 | 59 | 251.4 | 0.715 |
| 14 | 238.1 | 0.510 | 37 | 245.4 | 0.625 | 60 | 251.5 | 0.712 |
| 15 | 239.7 | 0.514 | 38 | 245.5 | 0.630 | 61 | 251.8 | 0.710 |
| 16 | 239.8 | 0.520 | 39 | 245.5 | 0.635 | 62 | 252.0 | 0.708 |
| 17 | 240.0 | 0.522 | 40 | 245.5 | 0.640 | 63 | 252.0 | 0.705 |
| 18 | 240.3 | 0.525 | 41 | 245.5 | 0.645 | 64 | 252.0 | 0.703 |
| 19 | 240.6 | 0.528 | 42 | 245.6 | 0.650 | 65 | 252.0 | 0.700 |
| 20 | 241.0 | 0.530 | 43 | 245.7 | 0.655 | 66 | 252.2 | 0.697 |
| 21 | 241.5 | 0.535 | 44 | 246.0 | 0.660 | 67 | 252.4 | 0.695 |
| 22 | 242.2 | 0.540 | 45 | 246.9 | 0.665 | 68 | 252.2 | 0.693 |
| 23 | 243.0 | 0.550 | 46 | 247.7 | 0.670 | 69 | 252.2 | 0.690 |

Matching of the computed tide and the observed tide (harmonic constants) at the extremities of the parallel ϕ became a difficult task for higher parallels, particularly after 16°N . At this stage, a second adjustment of the linearly interpolated harmonic constants became necessary. However, both these adjustments have been made within a tolerable difference. At any coastal rectangle the maximum phase angle difference due to adjustment with respect to the corresponding interpolated value is 10° . The corresponding maximum difference in the case of amplitude is 5 cms. The readjusted values of the harmonic constants are given in Table 1.6. This readjustment of the initially interpolated values of the harmonic constants has produced a reasonable matching of the amplitudes of the obtained and observed tides bringing down the highly excessive amplitudes to an excess of 10 cms above the observed amplitudes. In the following table we provide the values of ζ_0, ζ_m ($m = 1, 2, 3, 4$) for the latitudes 10°N , 12.5°N , 15°N , 16.25°N respectively

Table 1.7

| Parallel | ζ_0 | ζ_1 | ζ_2 | ζ_3 | ζ_4 |
|-----------------------|-------------|-------------|-------------|--------------|--------------|
| 10°N | -0.01, 0.27 | 0.27, -0.16 | 0.02, 0.06 | -0.04, -0.03 | -0.01, -0.01 |
| 12.5°N | -0.15, 0.31 | 0.23, -0.12 | -0.06, 0.03 | 0.04, 0.05 | -0.01, -0.02 |
| 15°N | -0.21, 0.39 | 0.09, -0.18 | 0.03, 0.08 | -0.02, 0.03 | -0.01, -0.01 |
| 16.25°N | -0.22, 0.43 | 0.08, -0.18 | 0.04, 0.09 | -0.03, -0.02 | -0.01, 0.02 |

The longitudinal amplitude distributions for the latitudes 10°N , 12.5°N , 15°N and 16.25°N are shown in Fig. 8.

A cotidal map based on the tidal distribution on each of the parallels, spaced $\frac{1}{4}^{\circ}$ apart, from 10°N to 20°N , is drawn (Fig. 9).

The following concluding remarks are made regarding the obtained results.

Conclusions.

- (i) Towards higher latitudes (above 18°N) the computed amplitude is 10 cm more than the observed amplitude.
- (ii) The computed phase lag is advanced by 45° with respect to the observed phase. This phase lag remained almost the same in both the cases of adjustments of the harmonic constants about the initial interpolated values.
- (iii) In the case of readjusted values of the harmonic constants the amphidromic point (not seen in Fig. 9) is found shifted towards the west.
- (iv) Except for small discrepancies in magnitudes the results have shown the trend similar to that found in the work of Pekeris and Accad (1969).

List of Symbols and their Meaning

- a the radius of the earth = 6.37×10^6 meters
- ω the angular speed of earth's rotation = 15 deg/hour
- g the acceleration due to gravity = $9.8 \times 3600 \times 3600$ meters/hr
- $h(\varphi)$ the depth of water below any point in the mean surface
- φ the colatitude
- X the east longitude
- t the time measured from the instant of high-water of the equilibrium constituent at the meridian 80°E where the parallel of the latitude 10°N intersects the Indian coast of the Bay of Bengal
- $\zeta(X, \varphi, t)$ the elevation of the free surface of the water at any time above any point of the mean surface
- $\bar{\zeta}(X, \varphi, t)$ the equilibrium elevation corresponding to the astronomical disturbing forces
- σ the angular frequency of the tidal constituent. For M_2 , $\sigma = 28.984$ degrees per mean solar hour
- u, v, w the mean values along any vertical, of the velocity components at any time the directions of increasing X and φ and along the outward normal to a section respectively
- U, V, Z mathematical functions satisfying differential equations similar to those for tidal motion

- N the component along the outward normal to a boundary section of the vector whose components in the directions of increasing X and φ are U and V respectively
- g_1 the phase-lag at the place behind the phase of the corresponding equilibrium tide at Greenwich
- \bar{H} the amplitude of the equilibrium harmonic constituent. For M_2 , $\bar{H} = 0.267$ meters
- F, G the components of ~~external~~ frictional force per horizontal area and per density of water
- $p = \frac{\pi}{X_2 - X_1}$ where X_1 and X_2 are the bounding longitudes enclosing the Bay of Bengal with the open parallel under consideration
- $\bar{\varphi}$ is the bounding parallel line in the open ocean along which we determine the distribution of the tidal constituent M_2
- $\zeta' = \zeta - \bar{\zeta}$ is taken for convenience in notation
- M.K.H. system of units is chosen for the entire investigation.

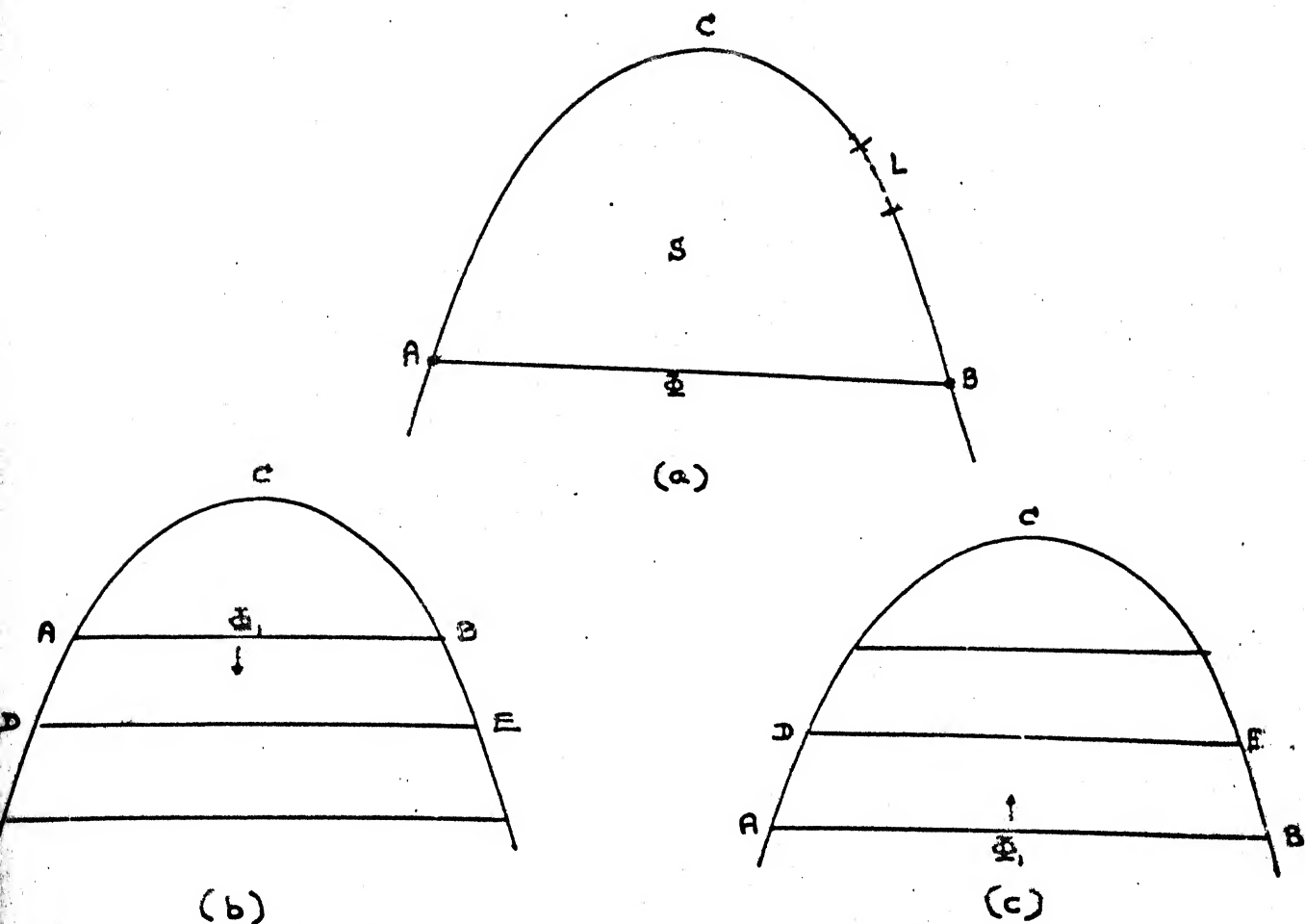


FIG.1. (a), (b), (c).

- (a)..... MODEL REGION FOR THE TIDAL THEOREM.
 (b)..... DOWNWARD COMPUTATION.
 (c)..... UPWARD COMPUTATION.

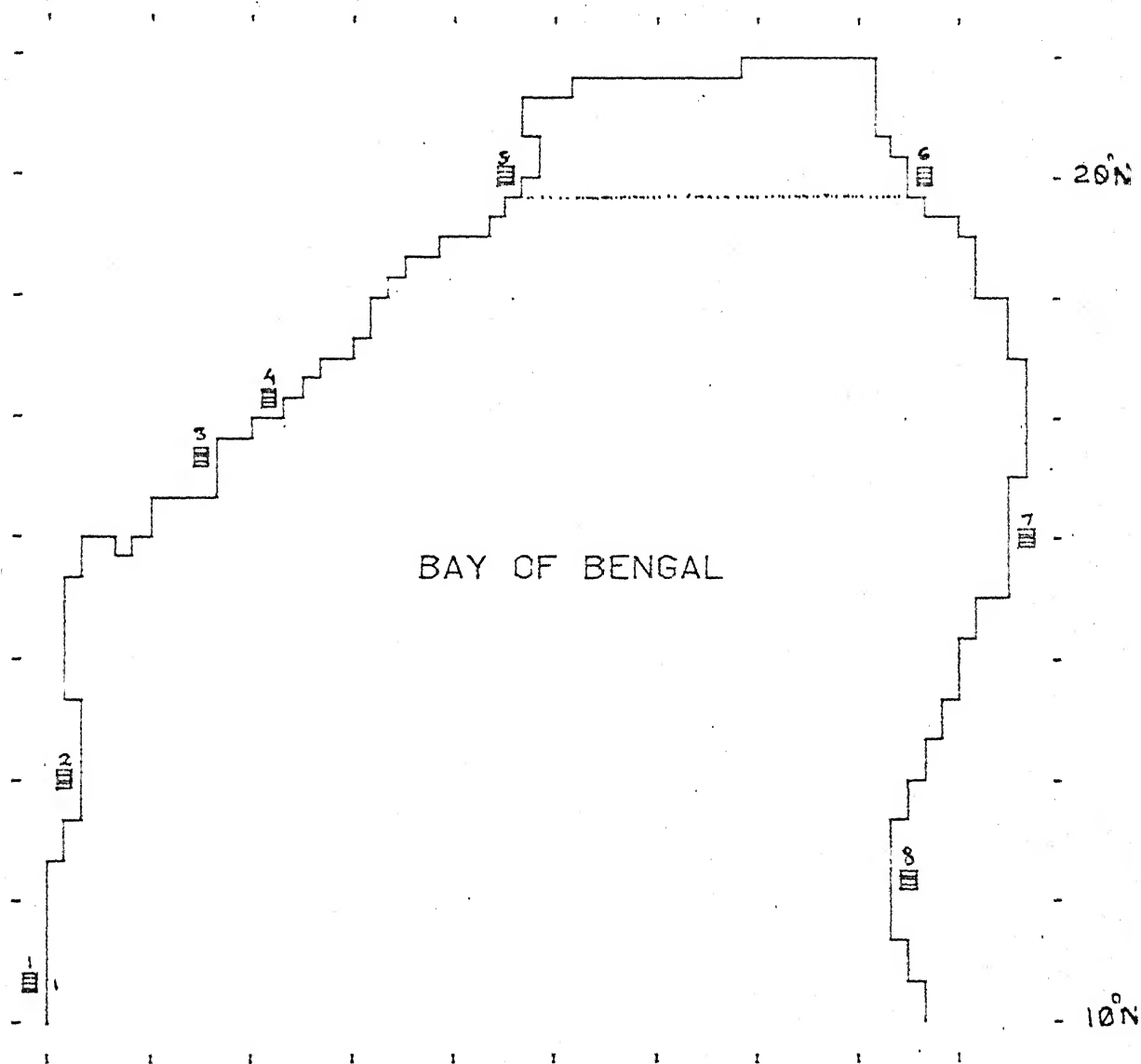


FIG. 2. MODEL AREA OF BAY OF BENGAL.
■ THE COASTAL STATIONS FOR WHICH THE
HARMONIC CONSTANTS ARE AVAILABLE

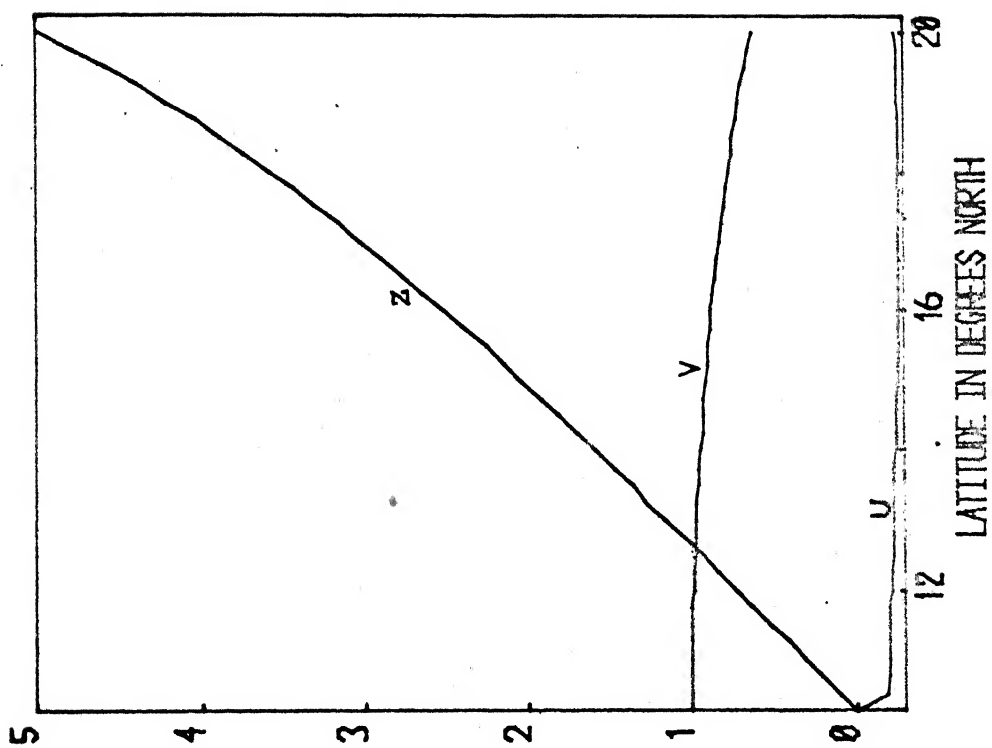


FIG. 3. AUXILIARY FUNCTIONS FOR THE PARALLEL $10^{\circ} 15' N$

AUXILIARY FUNCTIONS WITH FACTOR $\sin^2 \phi$

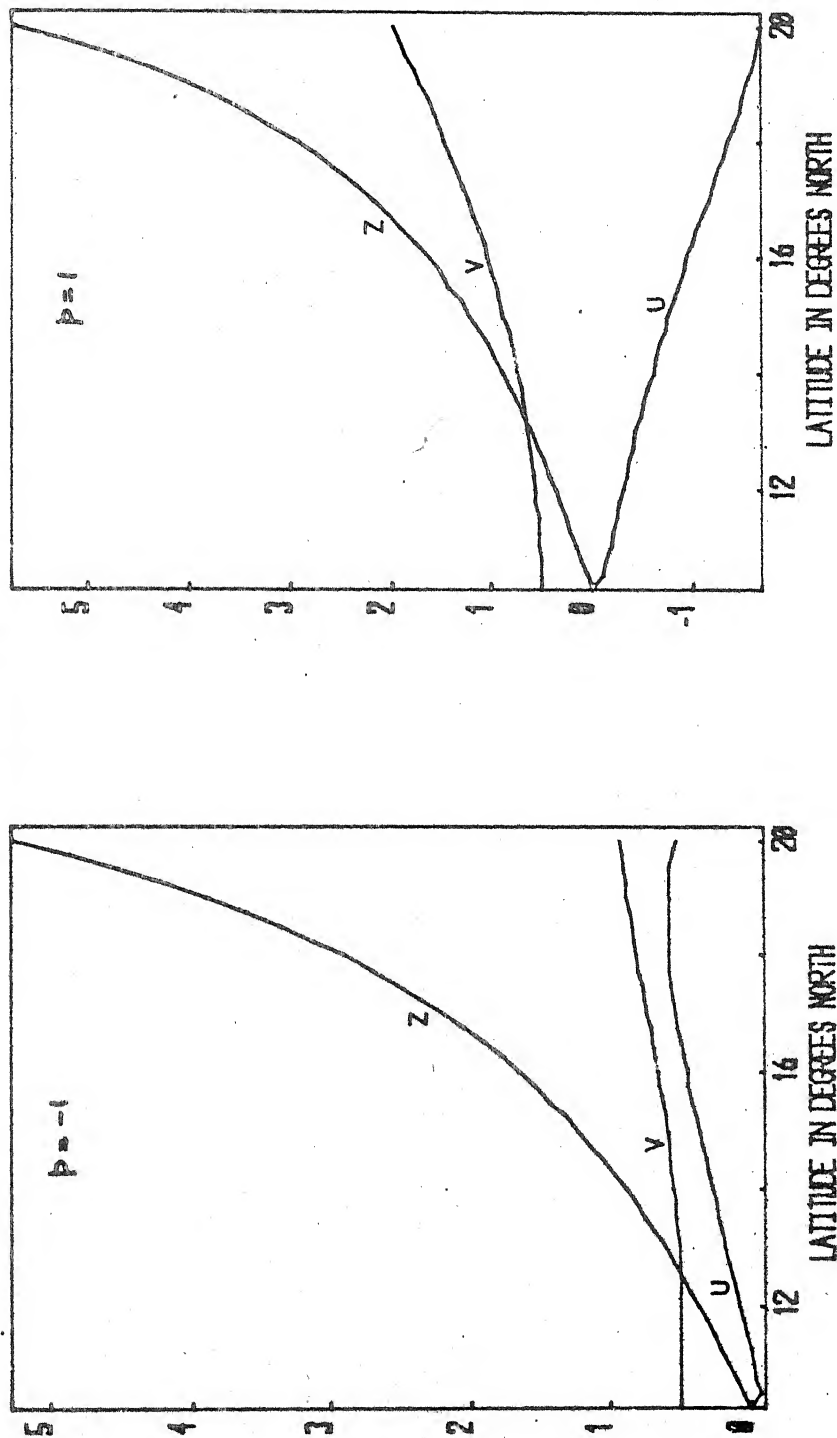


FIG. 4. AUXILIARY FUNCTIONS FOR THE PARALLEL $10^{\circ}15' N$

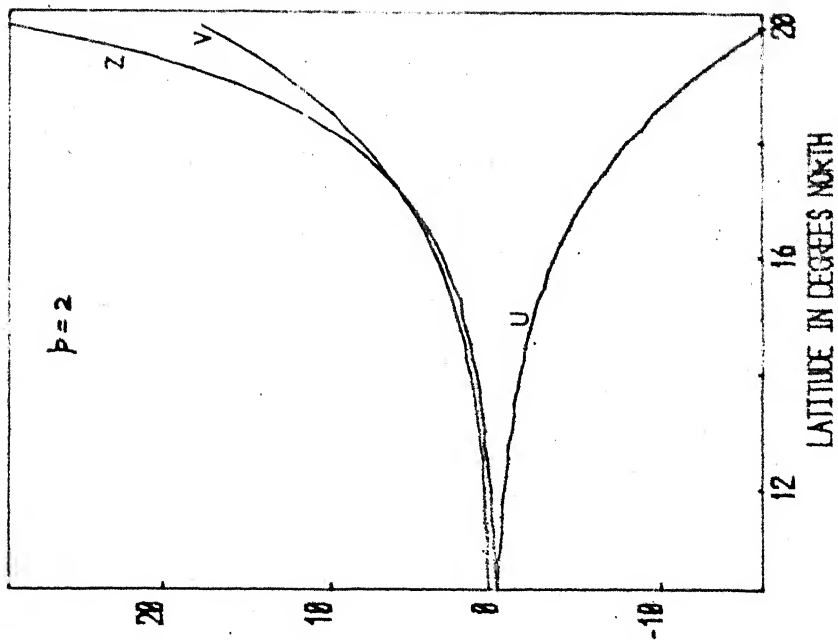
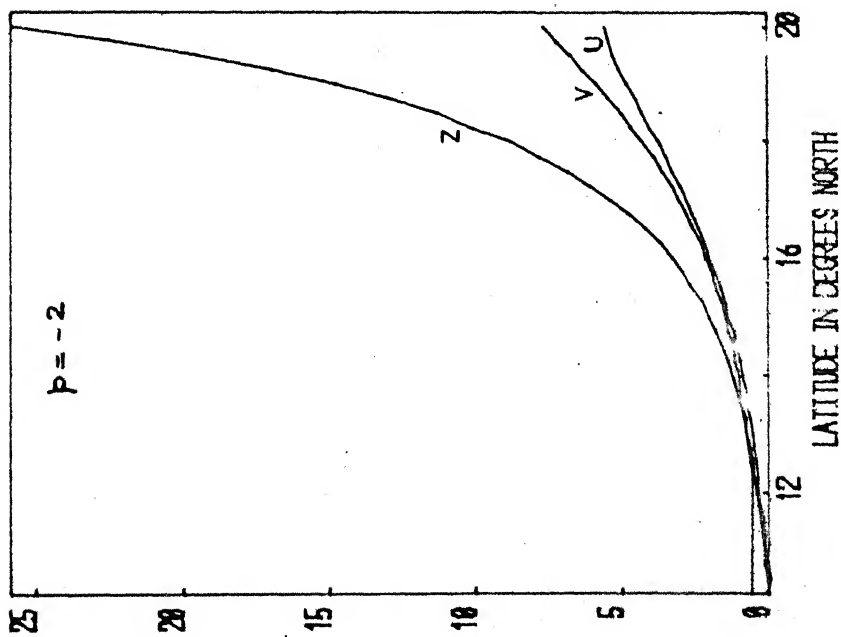


FIG. 5. AUXILIARY FUNCTIONS FOR THE PARALLEL $10^{\circ}15'N$

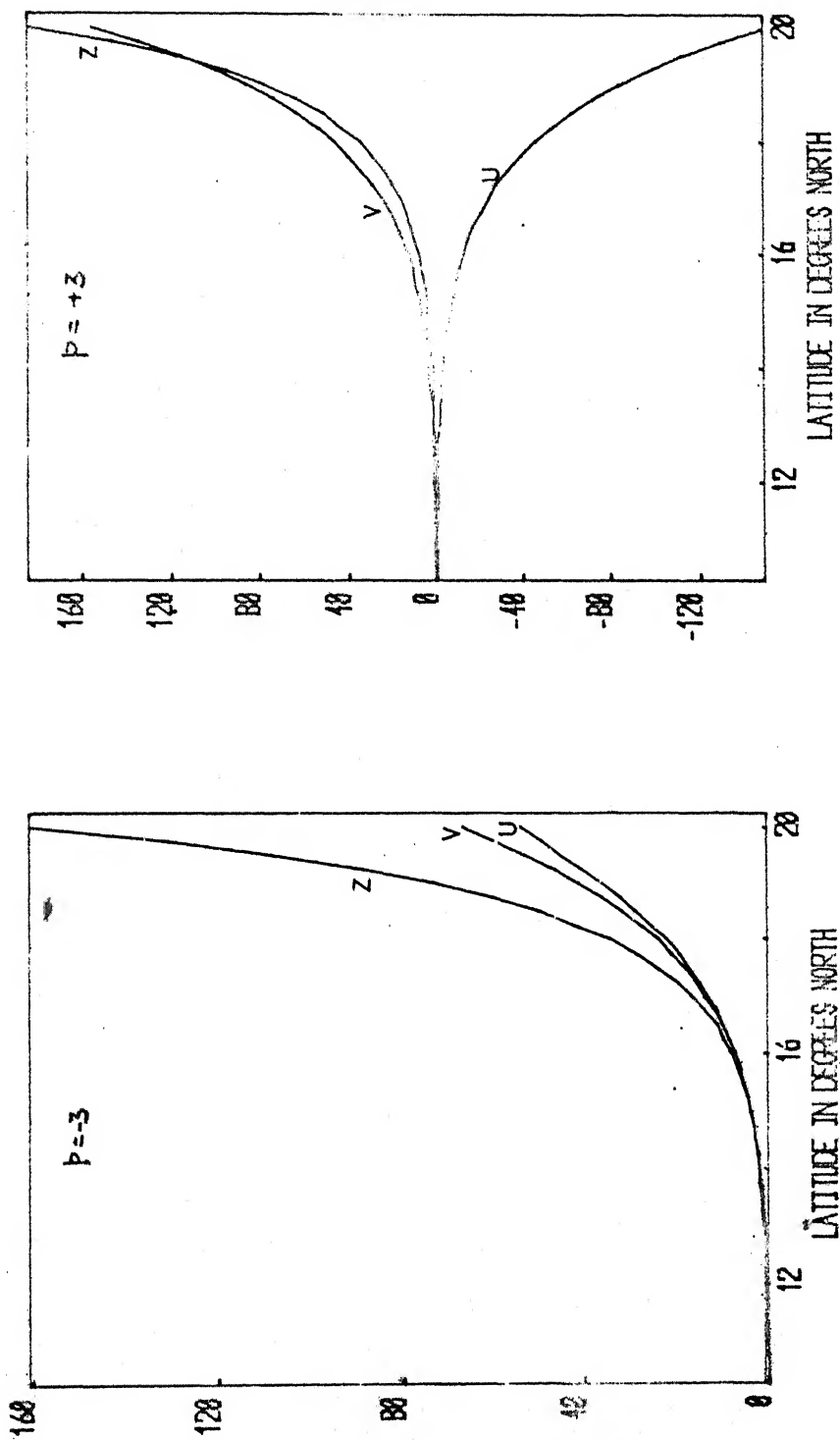


FIG. 6. AUXILIARY FUNCTIONS FOR THE PARALLEL $10^{\circ}15' N$

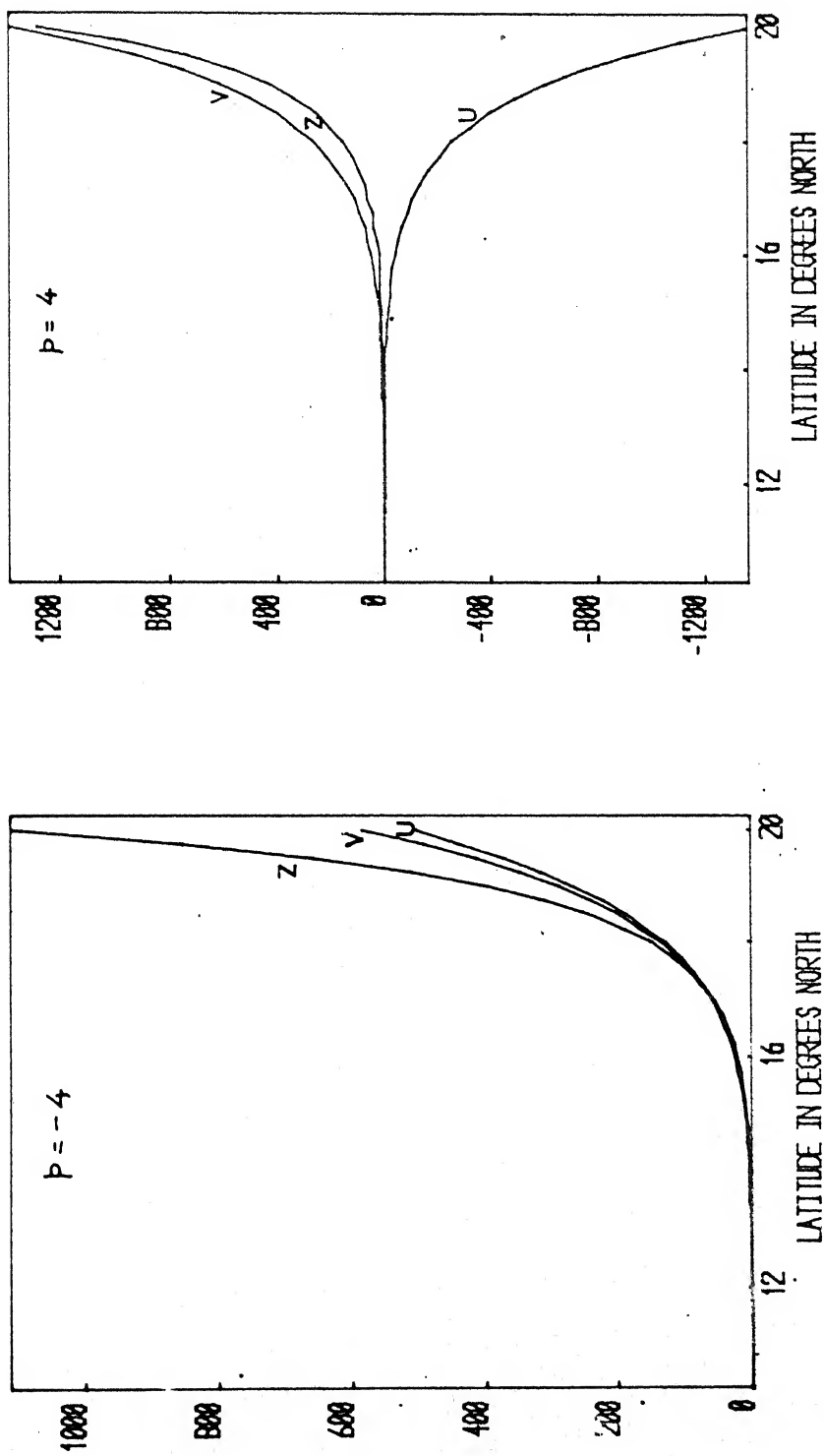


FIG. 7. AUXILIARY FUNCTIONS FOR THE PARALLEL $10^{\circ} 15' N$

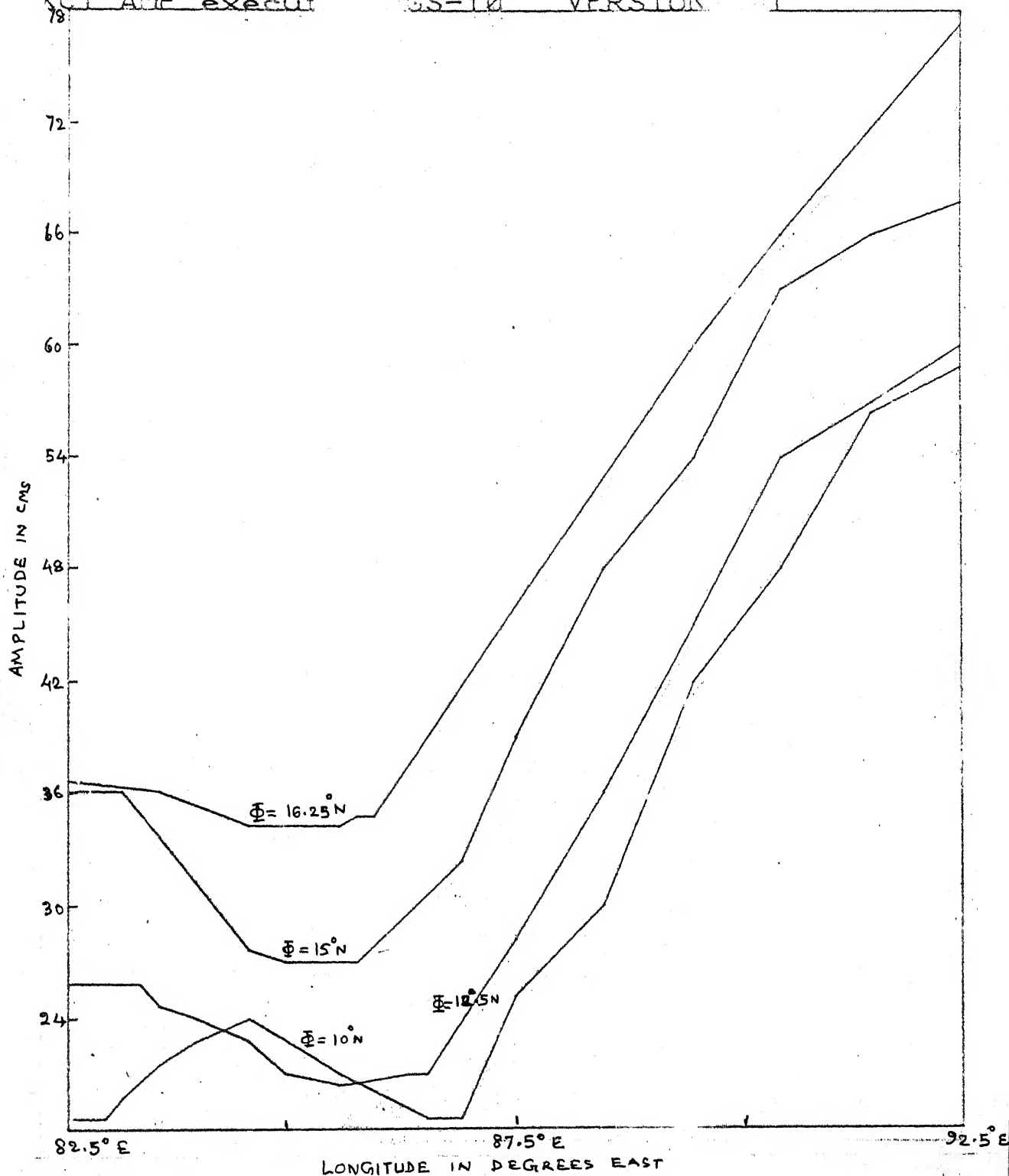
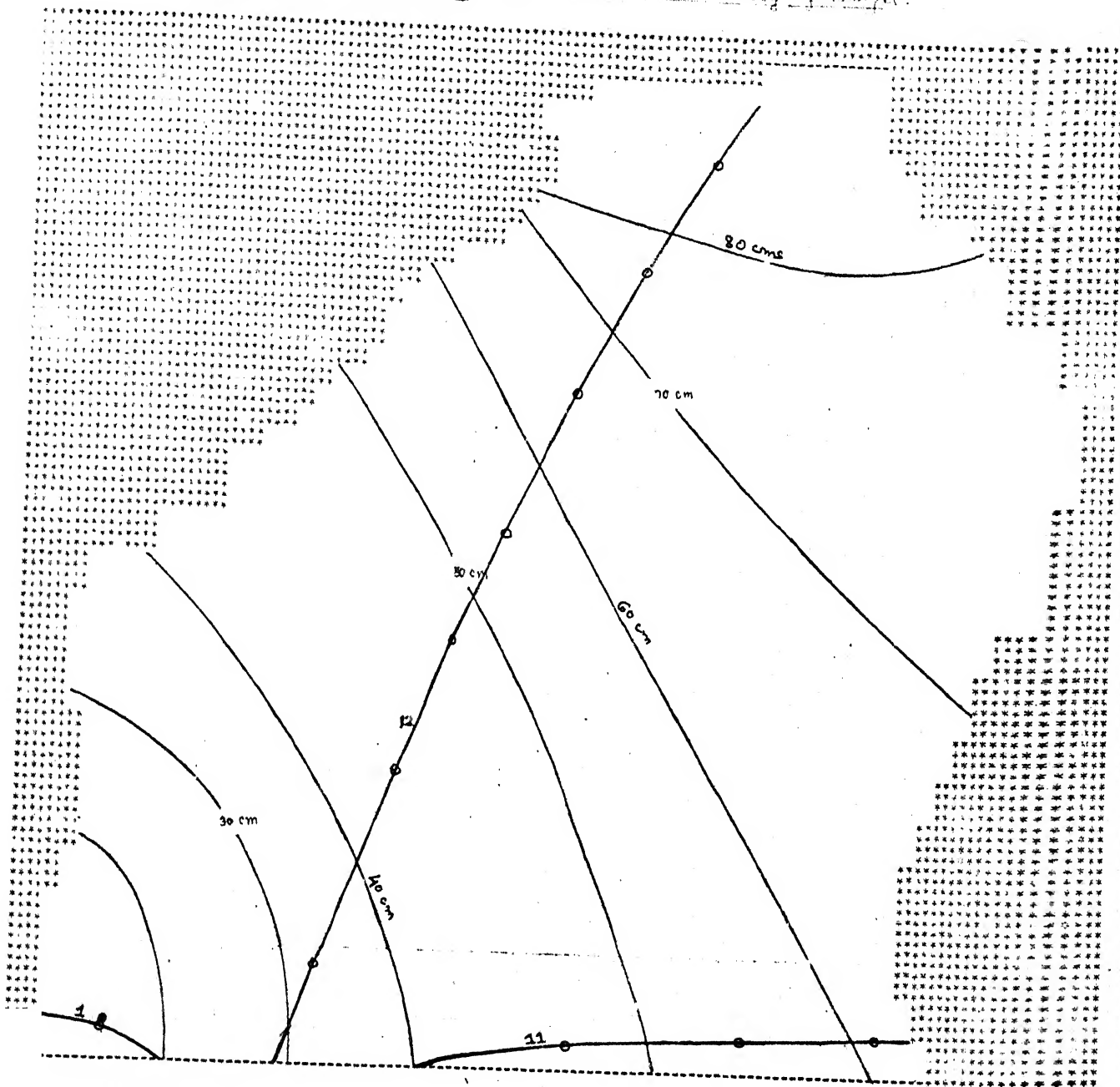


FIG. 8. M2-TIDE DISTRIBUTION ALONG THE FOUR SELECTED PARALLELS

Cotidal lines and Co-range lines of M₂ in the Bay of Bengal.



DATA FILE

FIG. 9. COTIDAL MAP FOR BAY OF BENGAL

— CO-RANGE LINES
 —•— CO-TIDAL LINES

CHAPTER 2

DEPTH-INTEGRATED MODEL OF TIDES AND STORM SURGES IN BAY OF BENGAL

2.1 Introduction

Depth-integrated, two-dimensional models of ocean hydrodynamics are now very well established, in which the basic hydrodynamical equations for the two-dimensional tides and surges are obtained by integrating the equations which are in full three-dimensional form, from the bottom $z = -h(x,y)$ to the free surface $z = \zeta(x,y,t)$. These models are called vertically integrated models. If the integrated equations are divided by the total depth (from $z = -h(x,y)$ to $z = \zeta(x,y,t)$) the models are known as vertically averaged models. These models, in the former or the latter form, have proved to be very useful in understanding the surge dynamics, particularly, for the prediction of sea-levels due to storms and other disturbances. These models are relatively simple in conception and require much less computer budget as compared to the expensive three-dimensional models. The equations, when reduced to complete linear form eliminate the vertical structure (Johns 1981). Some important vertically-Integrated models have been mentioned in section 3, chapter 0.

Though much literature on the subject for the region of North-Sea and elsewhere has appeared, there is not much literature regarding the study of tides and surges for the region of Bay of Bengal. However, there are a few important contributions to the study of surges for this region following the articles by Frank and Hussain (1971), Das (1972) and Flierl and Robinson (1972). Das et al. (1974) have studied storm surges including the interaction with tides and made a first major contribution on the subject for the region of Bay of Bengal. They have used the linearized long-wave equations, dropping the role of advection and using a linear law for bottom friction with an assumed bottom current structure by a steady Ekman Spiral. Surges have been computed for three storm tracks (straightly directed towards North-West, North and North-east), using a Predictor-Corrector method. Johns (1981) has given a formulation for depth-averaged model, and a multi-level model with σ -coordinate approach. In both the cases the atmospheric pressure-gradient is considered unimportant and neglected. Based on his approach Johns and Ali (1981) have studied the storm surges for the region of head Bay of Bengal and Johns et al. (1981) have studied storm surges for the east-coast of India. Recently Das (1981) has studied the temporal response of wind-stress and has shown that in the initial stages of the surge the divergence of the wind stress is more important than the curl of the

wind stress, while in the subsequent stages the curl becomes more important. This response is related to the storm speed (vector motion) and is shown to be inversely proportional to the square-root of the basin depth. An application of this model has been given by Sinha (1981) for the gulf of Thailand. Due to some limitation or the other, many of these models, though made a good start, lack some details needed for the better understanding of the surge mechanism. These models can be improved by incorporating all the needed physical parameters into the problem, as many of these models have ignored one physical parameter or the other with the assumption of their negligible role. However, in particular local situations these physical parameters may be important and can no longer be ignored. For instance, the nonlinear advection may be important in extremely shallow waters and the so called 'Inverted Barometer Effect' may be important in the case of slow moving storms (Dunn and Miller 1964). Also, in the nature, many of the storms are not axi-symmetric and the assumption of an axi-symmetric storm may considerably alter the magnitude, time and location of the peak-surge. On the other hand, the interaction with the tide is very crucial for the accurate surge prediction. A good model of surge requires the incorporation of all these factors. In view of the above factors it is felt that a reinvestigation of the surge problem with many needed details is essential. On the other hand the incorporation of essential features like the

asymmetric wind field, the real bathymetry, the gradual initialization and control of the storm movement etc., enhances our understanding of the surge mechanism paving the way for an accurate surge prediction.

In the present chapter we have used the hydrodynamical equations derived in section 0.3 and incorporate all the essential parameters required for the study. In section 2 of this chapter we have described the numerical model of the region under consideration. In sections 3,4 and 5 we have studied the three aspects of the surge problem, namely, the surge without tidal interaction, establishing of the tidal regime and the simulation of tide-surge interaction. Conclusions based on the results obtained in sections 3,4,5 have been given in section 6.

2.2 Numerical Scheme and Model Area

In the present chapter we consider the numerical scheme described by Flather and Heaps (1975) in which the nonlinear advection is retained and properly represented by a scheme given by Robert and Wiess (1966). In the following paragraphs we describe the discretization procedure for the numerical treatment of the hydrodynamical equations governing the two-dimensional model of tides and surges derived in section 0.3.

An array of grid points in the (x,y) plane is taken, consisting of ζ -points, u -points and v -points. The points of each type form a rectangular network of 1 columns and m rows with a square mesh of size s . Rows run parallel to the x -axis and columns parallel to the y -axis. Point by point, relative to the ζ -points, the u -points are displaced a distance $s/2$ in the positive x -direction and v -points a distance $s/2$ in the negative y -direction (Fig. 1(a)). All these points form a staggered grid system in which the points of each type are numbered

$$i = 1(1) 1, 1+1(1) 21, 21+1(1) 31, \dots, (m-1)1+1(1) m1$$

Counting in the positive x -direction along each row, moving from one row to the next in the negative y -direction. If we are to compute the values of u, v or ζ at the points other than their own type the following averaging is used

$$u \text{ at } v\text{-point } i : \tilde{u}_i = (u_{i-1} + u_i + u_{i+m-1} + u_{i+m})/4$$

$$v \text{ at } u\text{-point } i : \tilde{v}_i = (v_{i-m} + v_{i-m+1} + v_i + v_{i+1})/4$$

where u_i, v_i are the values of u, v at their respective points i . The following notation is used for denoting the values of the variables or parameters at the grid points.

At u-point i : $u = u_i$, $F_s = F_i$, $\lambda^u = \lambda_i^u$;

at v-point i : $v = v_i$, $G_s = G_i$, $\lambda^v = \lambda_i^v$;

at ζ -point i : $\zeta = \zeta_i$, $h = h_i$

where h_i are the depths at ζ -point i . As mentioned earlier a simple averaging is used for the total depth $\zeta + h$ at u and v -points. Thus

at u-point i : $d_i = (h_i + \zeta_i + h_{i+1} + \zeta_{i+1})/2$,

at v-point i : $e_i = (h_i + \zeta_i + h_{i+m} + \zeta_{i+m})/2$.

F, G denote the wind stress components at the sea surface in directions of increasing x, y respectively and λ denotes the bottom stress parameterization as described in section 0.3.

Treatment of Advective Terms

As we have decided to retain the nonlinear advective terms, a numerical treatment of these terms requires special attention. A number of conditionally stable, explicit schemes are given by Lax and Wendroff (1960), Crowley (1970), Sielecki and Wurtele (1970) and others. In the present numerical scheme for the simulation of two-dimensional tides and surges, we make use of the numerical scheme given by Robert and Wiess (1966). In the following paragraphs we briefly describe the scheme. For this purpose we consider

the following expressions

$$\frac{\partial u}{\partial t} + u \frac{\partial u}{\partial x} + v \frac{\partial u}{\partial y} \quad (2.2.1)$$

$$\text{and } \frac{\partial v}{\partial t} + u \frac{\partial v}{\partial x} + v \frac{\partial v}{\partial y} \quad (2.2.2)$$

By the use of the selected staggered grid (Fig. 1(a)) the above expressions can be discretized, for odd time steps with i increasing, as follows

$$\begin{aligned} \frac{u_i(t+\tau) - u_i(t)}{\tau} + \bar{u}_i(t) \left[\frac{1}{2} \left\{ \frac{u_i(t+\tau) - u_{i-1}(t+\tau)}{s} + \frac{u_{i+1}(t) - u_i(t)}{s} \right\} \right] \\ + \frac{1}{2} \left[\frac{v_{i-m}(t) + v_{i-m+1}(t)}{2} \left(\frac{u_{i-m}(t+\tau) - u_i(t+\tau)}{s} \right) \right. \\ \left. + \frac{v_i(t) + v_{i+1}(t)}{2} \left(\frac{u_i(t) - u_{i+m}(t)}{s} \right) \right] \quad (2.2.3) \end{aligned}$$

$$\begin{aligned} \frac{v_i(t+\tau) - v_i(t)}{\tau} + \frac{1}{2} \left[\frac{u_{i-1}(t) + u_{i+m-1}(t)}{2} \left(\frac{v_i(t+\tau) - v_{i-1}(t+\tau)}{s} \right) \right. \\ \left. + \frac{u_i(t) + u_{i+m}(t)}{2} \left(\frac{v_{i+1}(t) - v_i(t)}{s} \right) \right. \\ \left. + \bar{v}_i(t) \left[\frac{1}{2} \left\{ \frac{v_{i-m}(t+\tau) - v_i(t+\tau)}{s} + \frac{v_i(t) - v_{i+m}(t)}{s} \right\} \right] \right] \quad (2.2.4) \end{aligned}$$

Similarly for even time steps with i decreasing we have

$$\begin{aligned}
 & \frac{v_i(t+\tau) - v_i(t)}{\tau} + \frac{1}{2} \left[\frac{u_i(t) + u_{i+m}(t)}{2} \left(\frac{v_{i+1}(t+\tau) - v_i(t+\tau)}{s} \right) \right. \\
 & \quad \left. + \frac{u_{i-1}(t) + u_{i+m-1}(t)}{2} \left(\frac{v_i(t) - v_{i-1}(t)}{s} \right) \right] \\
 & \quad + \bar{v}_i(t) \left[\frac{1}{2} \left\{ \frac{v_i(t+\tau) - v_{i+m}(t+\tau)}{s} + \frac{v_{i-m}(t) - v_i(t)}{s} \right\} \right]
 \end{aligned} \tag{2.2.5}$$

$$\begin{aligned}
 & \frac{u_i(t+\tau) - u_i(t)}{\tau} + \left[\frac{1}{2} \left\{ \frac{u_{i+1}(t+\tau) - u_i(t+\tau)}{s} + \frac{u_i(t) - u_{i-1}(t)}{s} \right\} \right] + \bar{u}_i(t) \\
 & \quad + \frac{1}{2} \left[\frac{v_i(t) + v_{i+1}(t)}{2} \left(\frac{u_i(t+\tau) - u_{i+m}(t+\tau)}{s} \right) \right. \\
 & \quad \left. + \frac{v_{i-m}(t) + v_{i-m+1}(t)}{2} \left(\frac{u_{i-m}(t) - u_i(t)}{s} \right) \right]
 \end{aligned} \tag{2.2.6}$$

For the even time step we calculate v first and then u . The over bar in the above expressions denotes the average values given by

$$\left. \begin{aligned} \bar{u}_i &= (u_{i-1} + 2u_i + u_{i+1})/4 \\ \bar{v}_i &= (v_{i-m} + 2v_i + v_{i+m})/4 \end{aligned} \right\} \tag{2.2.7}$$

With the above representation of the nonlinear advective terms

we write the discretized form of hydrodynamical equations of section 3-chapter 0, from (0.3.26) to (0.3.28), with forward-time and central-space differencing, as follows

$$\frac{\zeta_i(t+\tau) - \zeta_i(t)}{\tau} = - \frac{1}{s} \{ d_i(t) u_i(t) - d_{i-1}(t) u_{i-1}(t) + e_{i-m}(t) v_{i-m}(t) - e_i(t) v_i(t) \} \quad (2.2.8)$$

For odd time-steps with increasing i , the equations of motion are discretized as

$$\begin{aligned} \frac{u_i(t+\tau) - u_i(t)}{\tau} = & - \frac{\bar{u}_i(t)}{2s} [u_i(t+\tau) - u_{i-1}(t+\tau) + u_{i+1}(t) - u_i(t)] \\ & - \frac{1}{4s} [\{ v_{i-m}(t) + v_{i-m+1}(t) \} \{ u_{i-m}(t+\tau) - u_i(t+\tau) \} \\ & + \{ v_i(t) + v_{i+1}(t) \} \{ u_i(t) - u_{i+m}(t) \}] \\ & + f \tilde{v}_i(t) - \frac{k u_i(t+\tau)}{d_i(t)} [u_i^2(t) + v_i^2(t)]^{1/2} \\ & + \frac{F_i(t)}{\rho d_i(t)} - \frac{g}{s} [\zeta_{i+1}(t+\tau) - \zeta_i(t+\tau)] \\ & + \frac{1}{\rho s} [p_{i+1}^u(t+\tau) - p_i^u(t+\tau)] \quad (2.2.9) \end{aligned}$$

$$\begin{aligned}
\frac{v_i(t+\tau) - v_i(t)}{\tau} = & - \frac{1}{4s} [(u_{i-1}(t) + u_{i+m-1}(t))(v_i(t+\tau) - v_{i-1}(t+\tau)) \\
& + (u_i(t) + u_{i+m}(t))(v_{i+1}(t) - v_i(t))] \\
& - \frac{\bar{v}_i(t)}{2s} [v_{i-m}(t+\tau) - v_i(t+\tau) + v_i(t) - v_{i+m}(t)] - \tilde{f}u_i(t+\tau) \\
& - \frac{k v_i(t+\tau)}{e_i(t)} [\tilde{u}_i^2(t) + v_i^2(t)]^{1/2} + \frac{G_i(t)}{\rho e_i(t)} \\
& - \frac{g}{s} [\zeta_i(t+\tau) - \zeta_{i+m}(t+\tau)] + \frac{1}{\rho s} [p_i^v(t+\tau) - p_{i+m}^v(t+\tau)]
\end{aligned}
\tag{2.2.10}$$

and for even time steps, with decreasing i (taking v first)

$$\begin{aligned}
\frac{v_i(t+\tau) - v_i(t)}{\tau} = & - \frac{1}{4s} [(u_i(t) + u_{i+m}(t))(v_{i+1}(t+\tau) - v_i(t+\tau)) \\
& + (u_{i-1}(t) + u_{i+m-1}(t))(v_i(t) - v_{i-1}(t))] \\
& - \frac{\bar{v}_i(t)}{2s} [v_i(t+\tau) - v_{i+m}(t+\tau) + v_{i-m}(t) - v_i(t)] - \tilde{f}u_i(t) \\
& - \frac{k v_i(t+\tau)}{e_i(t)} [\tilde{u}_i^2(t) + v_i^2(t)]^{1/2} + \frac{G_i(t)}{\rho e_i(t)} \\
& - \frac{g}{s} [\zeta_i(t+\tau) - \zeta_{i+m}(t+\tau)] + \frac{1}{\rho s} [p_i^v(t+\tau) - p_{i+m}^v(t+\tau)]
\end{aligned}
\tag{2.2.11}$$

$$\begin{aligned}
\frac{u_i(t+\tau) - u_i(t)}{\tau} = & - \frac{\bar{u}_i(t)}{2s} [u_{i+1}(t+\tau) - u_i(t+\tau) + u_i(t) - u_{i-1}(t)] \\
& - \frac{1}{4s} [(v_i(t) + v_{i+1}(t))(u_i(t+\tau) - u_{i+m}(t+\tau)) \\
& + (v_{i-m}(t) + v_{i-m+1}(t))(u_{i-m}(t) - u_i(t))] \\
& + f\tilde{v}_i(t+\tau) - \frac{ku_i(t+\tau)}{d_i(t)} [u_i^2(t) + \tilde{v}_i^2(t)]^{1/2} + \frac{F_i(t)}{\rho d_i(t)} \\
& - \frac{g}{s} [\zeta_{i+1}(t+\tau) - \zeta_i(t+\tau)] + \frac{1}{\rho s} [p_{i+1}^u(t+\tau) - p_i^u(t+\tau)]
\end{aligned}
\tag{2.2.12}$$

where

$$\left. \begin{aligned}
p_a \text{ at } u\text{-point } i &= p_i^u \\
p_a \text{ at } v\text{-point } i &= p_i^v
\end{aligned} \right\}
\tag{2.2.13}$$

Finally for solving the problem numerically we take the equations (2.2.8) to (2.2.12) with appropriate initial and boundary conditions, which we specify at appropriate stages in the following sections. In the next section we briefly describe the numerical model of Bay of Bengal representing its boundaries and other details such as bathymetry etc.

Model area of Bay of Bengal

Usually one is interested to study the surges in the shallow water regions such as the continental-shelf, estuaries and river outlets, where they are predominant and devastating. However, in storm-surge modeling, it is proper to include a much larger area encompassing the whole extent of the cyclone, consisting of deeper seas outside the continental-shelf as well. With this in view two model areas, a large area (Fig.1(c)) and a shelf-area (Fig. 1(b)), have been considered. Three probe runs have been carried out for both the models, with the storm forcing (other parameters set as in Table 2.1) along the tracks I, II, III of both the models. These probe runs have indicated a maximum-excess of elevation of 0.5 meters of the large area model over the corresponding values of the shelf area model at the same coastal location in the case of positive surge. On the other hand a storm initialization to mature stage with its centre fixed at a point on the open boundary of the shelf-area model provided a reasonable closeness of the elevations with those corresponding to the large-area model. Weighing this fact on one hand and the envisaged extensive investigation with the limited resources for the computation on the other, it has been decided to take up the shelf-area model for the further investigation.

Bathymetry of the Shelf-Area Model

As a compromise between the real and the ideal bathymetries we have chosen the smoothened values of the bathymetry at the elevation points. In this process the Ganges Canyon is fairly smoothed (Figs. 2). The smallest depth near the coast is 10 meters and the greatest depth at the open boundary is 300 meters.

Storm Tracks

Storm tracks for the present investigation have been chosen to represent those of typical severe cyclonic storms which occur in the region of the Bay of Bengal. Three types of tracks, making different angles of attack with the coast, have been chosen. Tracks I and II have the normal and parallel incidence respectively with the coast line at the time of landfall (Figs. 3(a), (b)). The landfall location for the tracks I and II is set near Chittagong. The landfall location for track III is taken right to the Hoogly estuary. Track III makes normal incidence with the coast at the time of land-fall (Fig. 3(c)).

2.3 Surge Without the Tide

In this section, we intend to perform a number of numerical experiments to study the several aspects regarding the effects of atmospheric forcing on the sea surface. Wind stress as well as the sea-level barometric pressure are considered for this purpose.

Boundary Conditions

We prescribe the following boundary conditions which are to be associated with the system of equations (2.2.8) to (2.2.12). In the discretized form they are

$u_i(t)=0$, for the east and west coastal boundary points -

for all $t \geq 0$

$v_i(t)=0$, for the northern boundary points of the coast -

for all $t \geq 0$ (2.3.1)

and $v_i(t) = \frac{1}{e_i(t)} \left[\frac{s}{\tau} \{ \zeta_i(t+\tau) - \zeta_i(t) \} + d_i(t)u_i(t) \right.$

$\left. - d_{i-1}(t)u_{i-1}(t) + e_{i-m}(t)v_{i-m}(t) \right]$ (2.3.2)

for the open boundary towards the south - for all $t \geq 0$.

This condition follows from the continuity equation (2.2.8).

Asymmetric Storm

In many practical situations of surge prediction we require three factors, namely, the magnitude, place and time of surge-event. Most of the studies on the subject deal with ideal storms having surface wind field with circular symmetry. However, in real cases many storms deviate

from this ideal circular-symmetry affecting the above three factors. Taking this fact into account asymmetry in the surface wind field is introduced in the form of deviation from the circular symmetry by using the formula (Chang and Anthes 1978)

$$V_{ASY} = V_{SY} (1 + \alpha \cos \beta), \quad 0 \leq \alpha \leq 1 \quad \text{and} \quad 0 \leq \beta \leq 2\pi$$

(2.3.3)

V_{SY} and V_{ASY} represent the magnitudes of the wind speeds in symmetric and asymmetric storms respectively. The argument β is taken anti-clockwise from the right-hand direction perpendicular to the direction of movement of the storm-centre. As the intensity of storm may change during the course of its motion, the value of α can be specified from time to time during the course of storm movement. The above formula indicates a stronger right-hand side wind field and a weaker left-hand side wind field with respect to the direction of storm movement in comparison with the symmetric storm from which the asymmetry is obtained. This asymmetry is taken from the numerical experiments along with the symmetric storm for providing a comparative study of the response of the bay due to these two types of wind fields. For the present study the value of α is taken equal to 0.3 for the entire course of storm movement.

Time Step for Numerical Computations

The governing inequality for the linear stability

$$\tau < \frac{s}{\sqrt{gh_{\max}}} \quad (2.3.4)$$

for the chosen grid space $s \approx 13$ km yielded a maximum value for time step $\tau = 240$ seconds. For overall stability in the computations a time step $\tau = 120$ seconds has been chosen after a probe run.

Meteorological Forcing

The following meteorological forcing parameters are considered for the numerical experiments

Table 2.1

| Storm parameter | Value |
|--|--|
| Central-pressure drop: Δp | 50 milli bars = 5×10^3 Newtons/ sq. mtr. |
| Radius of maximum winds : R_{mn} | 52 km |
| Radial extent of the storm: R_{\max} | 300 km |
| Radius of the eye : R_{eye} | 13 km |
| Speed of the maximum sustained winds: V_{\max} | 60 meters/sec |
| Average vector motion of the storm | 20 km/hr |
| Angle of inflow in the annular region between R_{mw} and R_{\max} at the matured stage | 20° |

| | |
|------------------------------------|--|
| Cyclostrophic wind profile formula | $v^2 = 4v_{\max}^2 \left[\left(\frac{r}{R} \right)^2 / \{ 1 + \left(\frac{r}{R} \right)^2 \}^2 \right]$ (Das et al., 1974) |
| Wind-pressure relation | $V_{\max} = 0.85 \sqrt{\Delta p}$ |
| Drag coefficient for wind stress | $C_D^W = 0.003 \text{ (Simons 1974)}$ |

Also we consider the following.

| | |
|------------------------------------|--------------------|
| Drag coefficient for bottom stress | $\bar{k} = 0.0025$ |
|------------------------------------|--------------------|

| | |
|---|----------------------|
| Growth time to matured stage of the storm | $= 10 \text{ hours}$ |
|---|----------------------|

Numerical Experiments

We have performed two numerical experiments, with the help of the parameters described in the preceding paragraphs and table 2.1. In the following paragraphs we describe the numerical experiments and discuss the results obtained from these experiments.

Experiment 1.

Experiment though an elementary one, is intended to get a first hand information regarding the steady-state response of the sea basin under study, due to an imposed wind-stress field of a stationary storm whose centre is stationed at $S_1(20,19)$ on the open boundary of the model area. This experiment is repeated by stationing the storm-centre at $S_2(20,32)$ of the model area (Fig. 1(b)). A point near Chittagong is chosen for noting the hourly elevations. Also,

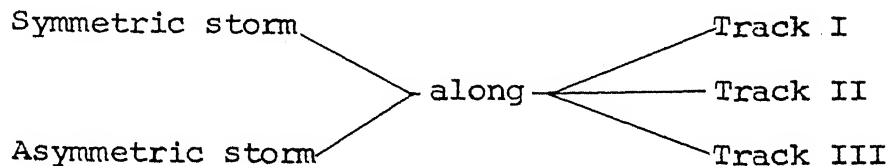
the hourly values of the maximum elevation with respect to the entire shelf (for each hour) have been noted. This has provided a valuable information regarding the shifting of the hourly maximum-surge in space for the region. Finally, the elevations for the entire shelf area are recorded at the end of 35 hours of integration which was enough duration for establishing a steady-state response of the sea due to stationary storm. The experiment has been performed with and without the role of advection.

Results.

This experiment has provided a testing case for the validity of the present model and an insight into the order of magnitude of the elevations due to the prevailing meteorological forcing. The sea-level contours at the end of 35 hours of numerical integration are shown in Figs. 4(a),(b). The positive surge due to on-shore and the negative surge due to off-shore winds are clearly seen. This experiment has also shown the negligible role of advection, owing to the stationary storm with centre situated far away from the coastal boundaries. In all the runs, with storm centres on the open boundary, the peak-surge elevations never exceeded 1 meter. The magnitude of the storm forcing and the magnitudes of elevations are in reasonable agreement with the observations. This justifies the validity of the present model for carrying out further numerical experiments.

Experiment 2.

In the following numerical experiment, unlike the previous experiment, we consider a moving storm along the tracks as shown in Figs. 3(a), (b), (c). Two sets of numerical experiments are chosen corresponding to the symmetric and asymmetric storms. Thus, keeping the other parameters fixed, we consider the following combination of parameters for the present numerical experiments which includes nonlinear advection.



Probe runs have been carried out with the following storm durations.

Period of runs for tracks I, II and III : 60 hours

Hour of landfall for tracks I and II : 35th hour

Hour of landfall for track III : 26th hour

During the first 10 hours of each run the storm is gradually allowed to reach the mature stage and then allowed to move along the chosen track. This has been done in order to avoid any spurious oscillations due to suddenly forced strong winds. For the first three runs of the experiment a symmetric storm moving along the tracks I, II and III respectively is considered. After the landfall the storm

movement is continued further for a period of 10 hours during which time the storm intensity is brought down gradually to a 10 knot wind (1 knot = 0.5144 meters/sec.). This procedure is adopted after carrying out the probe runs to determine the locations of maximum surge-peaks* for each of these runs in which no significant surge peaks have been obtained after the storm intensity has been decreased to a 10 knot wind speed-after the landfall. The three subsequent runs have been repeated with the asymmetric storm as specified in the parameter list (table 2.1).

The results computed for the runs with symmetric and asymmetric storms along tracks I, II, III include the hourly values of the elevation-maximum in space and its corresponding location. Also computed are the hourly values of elevation at the location of landfall, as well as at the location of another potential surge-peak, and the values of the individual terms in the hydrodynamical equations.

The distribution of the sea-level elevations, due to asymmetric storm along track I, at the three selected instants of time (at 29, 35, 40 hours respectively) are shown in Figs. 5(a), (b), (c); while those corresponding to the symmetric storm along track I are shown in 5(d), (e), (f) respectively. The corresponding elevation contours

* Maximum surge peak: Maximum taken for all time steps $\left[\begin{array}{l} \text{Maximum} \\ \text{for all} \\ \text{space points } i \end{array} (\zeta_i) \right]$

(at 29, 35, 40 hours) for track II are shown in Figs. 6(a), (b), (c) and Figs. 6(d), (e), (f) respectively. The elevation contours due to asymmetric storm forcing along track III (at 21, 26, 31 hours respectively) are shown in Figs. 7(a), (b), (c) and those corresponding to symmetric storm forcing (along track III) are shown in Figs. 7(d), (e), (f) respectively.

With asymmetric storm along track I the computed peak-surge of 4.8 meters, at the point of landfall, has occurred 3 hours before landfall while the computed maximum peak-surge of 8.6 meters has occurred at the point (2,36), seven hours before landfall (Fig. 8(a)). The corresponding results with asymmetric storm along track II revealed a sustained negative surge at the point of landfall almost throughout the period of storm movement, and the maximum peak-surge of 6.9 meters at (13,46), ten hours before landfall (Fig. 8(b)). Similarly the corresponding computed results for track III revealed a peak-surge of 2.0 meters at the point of landfall, ten hours before the landfall and the maximum peak-surge of 3.5 meters, three hours before the landfall (Fig. 8(c)). These aspects are summarized in the following table.

Table 2.2

| Asymmetric storm along | Elevation above the Mean Sea Level in meters | | Location coordinates | Time of occurrence with respect to land fall time |
|------------------------|--|------|----------------------|---|
| Track I | MPS | 8.6 | (2,36) | 7 hours before the LFH |
| | SLF | 4.8 | (3,43) | 3 hours before the LFH |
| Track II | MPS | 6.9 | (13,46) | 10 hours before the LFH |
| | SLF | -3.0 | (3,43) | 8 hours before the LFH |
| Track III | MPS | 3.5 | (8,22) | 3 hours before the LFH |
| | SLF | 2.0 | (8,18) | 10 hours before the LFH |

MPS: Maximum Peak-Surge;

SLF: Peak-surge at landfall location;

LFH: Landfall Hour.

The numerical experiments with symmetric storm have shown that the peak-surge elevation can be 2.0 meters less than those corresponding to those with the asymmetric storm (Figs. 8(a), (d)). However the corresponding maximum peak-surge locations, for any track, remained almost the same in both the numerical experiments. The computed results corresponding to the symmetric storm are summarized in the following table.

Table 2.3

| Symmetric storm along | Elevation above the Mean Sea Level in meters | | Location coordinates | Time of occurrence with respect to the landfall hour |
|-----------------------|--|------|----------------------|--|
| Track I | MPS | 6.7 | (2,36) | 8 hours before the LFH |
| | SLF | 3.5 | (3,43) | 3 hours before the LFH |
| Track II | MPS | 4.8 | (13,46) | 8 hours before the LFH |
| | SLF | -3.0 | (3,43) | 7 hours before the LFH |
| Track III | MPS | 2.6 | (8,22) | 4 hours before the LFH |
| | SLF | 1.3 | (8,18) | 14 hours before the LFH |

where the abbreviations are as those given for Table 2.2.

In all the above mentioned numerical experiments the maximum peak-surge as well as the peak-surge at the landfall point have occurred several hours before landfall. An interesting observation from the present numerical experiments is the combined role of the coastline configuration of the bay and the angle of attack of the storm near the coast, giving an interesting behaviour of the surge patterns. The maximum peak-surge to the left of track I (normal to the coast) and the maximum peak-surge to the right of track II are the manifestations of such a track-coastline combination (Figs. 8(a), (b) and 8(d), (e)).

In the case of numerical experiments with track III, however, there are some local, short-lived, abrupt oscillations around the point of landfall (Figs. 8(c) and 8(f)). This has resulted in sharp fall-rise-fall of the elevation with sharp peak at $t = 22$ hours near the location of landfall. This is also evident from the depth-mean current vectors depicted in Figs. 8(g) to (l) from $t = 12$ hours to $t = 22$ hours at two-hour intervals. From these figures we observe the emptying by the westward current and the subsequent swift filling by Northward current at the point of land-fall. The large horizontal extent of the coast and the approach of the storm in the normal direction are presumed for this kind of swift oscillations. This is particularly so because of rapid change in the wind-direction near the point of land-fall as the storm closely approaches the coast. This kind of situation is peculiar to this kind of coast-track combination and is not observed in the case of numerical experiments with track I and track II.

The individual contribution of the terms in the hydrodynamical equations, in the form of vectors (also called stick diagrams) at hourly intervals, at the three selected locations for each of the tracks I, II, III (with asymmetric storm) are shown in Figs. 9(a), (b), (c); 10(a), (b), (c); and 11(a), (b), (c) respectively. In the figures these are termed as CORIOLIS, ADVECTION, ATMOSPHERIC PRESSURE, WIND STRESS, ELEVATION SLOPE, BOTTOM FRICTION respectively. In

each case the vectors are normalized with respect to the maximum of the magnitudes of the vectors of all the terms taken together. From the results we observe that the contribution of the atmospheric pressure (the so called Inverted Barometer Effect) is insignificant in all the cases. We also observe that in most of the cases of peak surge, the elevation slope has played a major role, particularly during the hours before landfall. It is the restoration force of the surface slope following the bottom contours, particularly in shallow areas, which caused the majority of these peak surges. The set up by the wind is rather a gradual accumulative process (except when the storm centre approaching the landfall point) as compared to the local surface slope dynamics (free-wave types). However, during landfall hours the direct action of the atmospheric forcing may be in 'resonance' with the forces due to the surface slope inequalities. In such cases the surges can be more devastating. The swift local oscillation in the case of track III-numerical experiment is, perhaps, due to such manifestation of resonance. However, in shallow areas such a resonance is controlled by the bottom friction, which has comparable magnitude to counter it - bringing such an oscillation confined to local scales in space and time. This can be seen in Fig . 10 (a). On the other hand, for the region under consideration, the nonlinear advective terms played no significant role in the surge dynamics - even in the shallowest

areas upward. This envisages the inclusion of a further shallow-river system in which nonlinear advection can be significant. In all the cases it is observed that the depth-mean currents as well as the elevations decrease rapidly with the decreasing intensity of the meteorological forcing after the landfall.

2.4 Establishing the Tidal Regime

As a first step for the study of tide-surge interaction we establish an appropriate tidal regime giving steady co-oscillations of the tide corresponding to a prescribed sinusoidal oscillation of 1 meter amplitude, in phase, along the open boundary of the region under study. For this purpose we consider the equations (2.2.8) - (2.2.12), with the exception that we drop the meteorological forcing ($p_a^u, p_a^v, FI, GI = 0$) and include the tidal forcing as a boundary condition across the open boundary. Thus the associated boundary conditions for the present problem, in the discretized form are

$$\left. \begin{aligned} u_i(t) &= 0 \text{ for the east, west coastal boundary points for } t \geq 0, \\ v_i(t) &= 0 \text{ for the northern coastal boundary points for } t \geq 0, \\ \zeta_i(t) &= A \cos \sigma t, t \geq 0, \text{ where } \sigma \text{ denotes frequency of the } M_2\text{-tide and } A \text{ denotes the amplitude of the total tide,} \end{aligned} \right\} \quad (2.4.1)$$

$$v_i(t) = \left[\frac{1}{e_i(t)} \frac{\delta}{\tau} \{ \zeta_i(t+\tau) - \zeta_i(t) \} + d_i(t)u_i(t) - d_{i-1}(t)u_{i-1}(t) + e_{i-m}(t)v_{i-m}(t) \right]$$

for the open boundary points for $t \geq 0$.

The last equation follows from the continuity equation. This equation will make use of the elevations prescribed as tidal forcing at the elevation points adjacent and interior to the open boundary. In addition to the above conditions we have

$u_i = v_i = \zeta_i = 0$ at $t = 0$ for all the interior points of the region. In the present case we have taken $A = 1$ at all the points of the open boundary.

Two values for the time-step are chosen satisfying the necessary condition for the stability of the numerical scheme

$$\tau < \frac{s}{\sqrt{gh_{\max}}} \quad (2.4.2)$$

and probe runs are carried out with $\tau = \frac{1}{24}$ Lunar hour and $\tau = \frac{1}{32}$ Lunar hour. It was found $\tau = \frac{1}{32}$ Lunar hour (116 seconds approximately) yielded satisfactory results. With this time step we have performed two runs corresponding to the hydrodynamical equations with and without advective terms. A criterion is set for establishing a satisfactory tidal regime by which the integration process is terminated, if at the end of a cycle the elevation at any point is close to that with respect the corresponding value at the end of the previous cycle, within a tolerable difference of 1 cm. In the case of no advection the tidal regime with the desired accuracy is achieved after 28 cycles of integration. In the run with advection the desired tidal regime is achieved after 30 cycles

of integration. However the tidal regimes achieved in both the cases are very close and nonlinear advection did not play an important role in the tidal dynamics for the region under study.

The elevation contours are given in Figs. 12(a) to 12(1) and the depth-mean currents are given in Figs. 13(a) to 13(1). The computed tidal regime has produced a High Water of amplitude 2.3 meters as compared to the observed amplitude of 2 meters near Chittagong. The computed phase lag of High Water near Chittagong with respect to the High Water near the open boundary is 120 degrees (\approx 4 hours). These computed values are fairly in agreement with the observed values. Depth-mean current ellipses for the eight selected locations are given in Figs. 15 (a) to (h). At shallow area corners the depth-mean tidal currents have shown distorted patterns indicating their complexity at such locations (Fig. 15(g)). This is also evident from the current vector diagrams (figs. 13(e) and 13(j)). For a comparison on time-scale of the elevation and the depth-mean current, tidal profiles are provided in Figs. 14(a), to (h) at the eight selected locations. The model has responded well to the presence of the 'swatch of no land' (Ganges Canyon) making the main crest of the tide to refract and progress in two directions, North-West and North-east (Figs. 12(a) to 12(1)).

2.5 Tide-Surge Interaction

It is well known that surges and tides interact with each other modifying each other's propagation. In shallow areas like an estuary this interaction may be important in view of the nonlinear mass transport, and for a good prediction of surge this factor must be taken into account. In recent years some progress has been made regarding the study of tide-surge interaction and a general account on the development of this subject is presented in section 0.2. For the region of the Bay of Bengal, tide-surge interaction has been studied by Das et al. (1974), Johns (1981) and Johns and Ali (1981). In the present investigation we have incorporated some of the features not considered by these earlier studies. For instance, we have included the nonlinear advection terms which are omitted by Das et al. (1974). The importance of these terms can be seen in the case of surge due to meteorological forcing along track I (Fig. 9(a)). In contrast to the works of Johns (1981) and Johns and Ali (1981) the present study differs in the selection of parameters such as storm tracks, wind-field asymmetry.

Model.

We have chosen the same model as has been described in the section 2.2 regarding the meteorological forcing. An additional feature is the specification of tidal forcing.

as an Initial-Boundary Condition* (IBC). The main feature of the meteorological forcing is the asymmetric storm along tracks I, II and III.

Tidal Forcing.

We have selected the tidal regime established in the previous section for the purpose of astronomical tidal forcing.

* By Initial-Boundary condition we mean the specification of the values of u, v, ζ corresponding to a particular phase of the established tidal cycle over the entire region at time $t = 0$ (initial condition), and the subsequent continuation of the sinusoidal tidal oscillation along the open boundary for further time steps (Boundary condition).

Thus

$$\left. \begin{aligned} u_i &= u_i^{\text{tide}}, \quad v_i = v_i^{\text{tide}}, \quad \zeta_i = \zeta_i^{\text{tide}} \quad \text{At } t = 0 \quad \text{for all } i \\ \text{and } \zeta_i &= 1.0 \times [\cos(\sigma t)]_i \quad \text{for } t > 0 \quad \text{at the open boundary points} \\ \text{and } v_i(t) &= \frac{1}{e_i(t)} \left[\frac{s}{\tau} \{ \zeta_i(t+\tau) - \zeta_i(t) \} + d_i(t)u_i(t) \right. \\ &\quad \left. - d_{i-1}(t)u_{i-1}(t) + e_{i-m}(t)v_{i-m}(t) \right] \\ &\quad \text{for } t > 0 \quad \text{at the open boundary points.} \end{aligned} \right\}$$

(3.5.1)

For each track we have performed 4 numerical experiments with 4 types of initial-boundary conditions representing the four phases of the established tidal cycle corresponding to the Maximum (High-Water of 1 meter) - Falling Zero - Minimum Rising Zero of the elevation along the open boundary.

As in the case of pure-surge problem (sec. 3.2) we have carried out the probe runs and found no significant displacement of the maximum surge-peak locations as those corresponding to the pure-surge problem. Taking this fact into account we have retained the same locations for noting the elevations as those corresponding to the pure-surge problem. The surge computations are carried out with the IBC referring to the phase values along the open boundary and the corresponding phase lag for any coastal location can be found from the figures 12(a) to 12(1). All the numerical experiments are performed through 4 cycles of integration approximately and the obtained results are plotted in Figs. 16(a) to (d), 17(a) to (d), 18(a) to (d) respectively.

In contrast to the pure surge problem where, at any coastal location, we normally have single surge-peak, several surge peaks are obtained, each corresponding to the tidal cycle at the location. In almost all the cases the linear superposition of the tide on the surge produced higher magnitudes of peak surge than the corresponding surge peaks due to tide-surge interaction. The exception is the phase 3-track II

case where the peak surge at the location (8,22) coincided with the Low-Water phase at the location. However, at any instant of time 8 location, the difference between the elevation due to tide-surge interaction and the elevation due to tide+surge is relatively small (≈ 0.5 meters) as compared to the magnitudes of the corresponding elevations themselves. Also, the positive surge-peaks, at a location in most of the cases under investigation have coincided with the High Water at the location. These factors indicate that the tide-surge interaction is rather weak in the present model area and the inclusion of a further shallow area into the river system would have been more proper as the trends of the present results indicated a stronger interaction in the estuary-river system which will be a large enough extent for the propagation and interaction of tide and surge.

2.6 Concluding Remarks

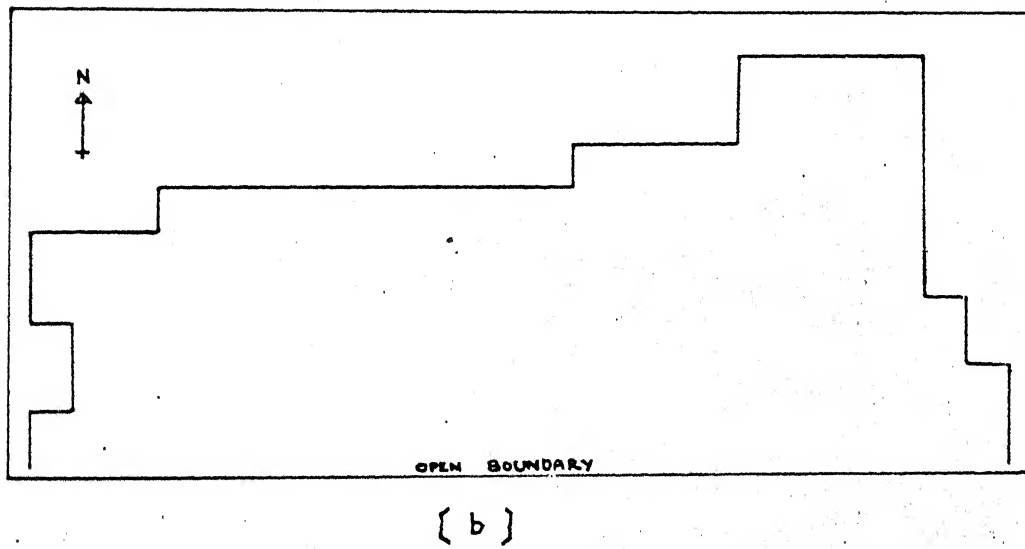
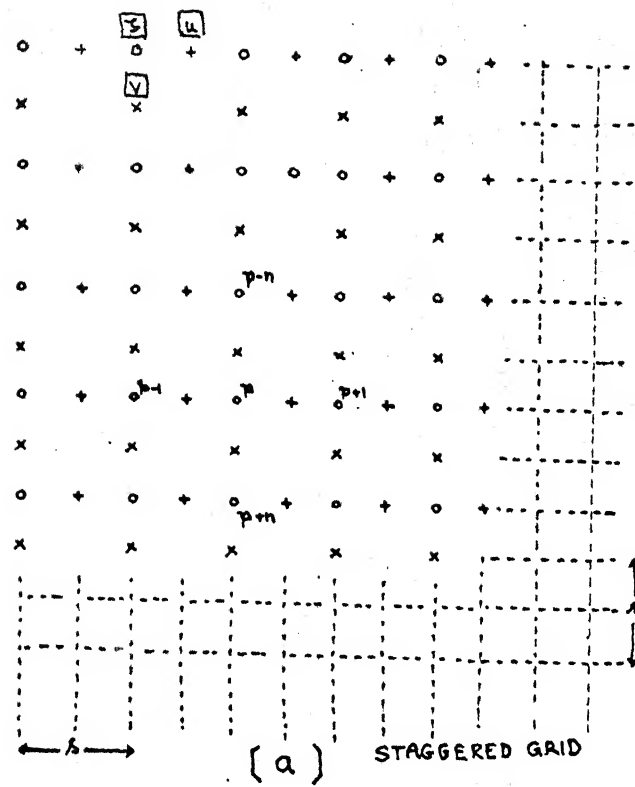
Based on the results of the numerical experiments, we would like to spell out the following concluding remarks.

- 1) The specification of the wind field is necessary rather than an idealization from the given pressure drop. Many of the cyclonic storms possess some kind of asymmetry regarding pressure and wind field distribution. The specification of the pressure-wind relations in terms of the radial distance r (from the centre of the storm) becomes

difficult in such cases, and as a result we have many such relations in practice. We have shown that for a given radial pressure distribution of the symmetric storm the derived asymmetry produced more devastating surges-with the magnitudes differing by as much as 2 meters in some cases. With the present kind of monitoring by satellites and other devices we should be able to specify the surface winds more accurately. Efforts should be concentrated in this regard.

2) Coastal geometry, bottom contours and the storm tracks play a vital role in the surge dynamics. It has been found that the Bay of Bengal has all these features (peculiar to itself) whose combination in surge dynamics are quite interesting. For instance, at the same land fall location, tracks I and II have produced entirely different kinds of surge response with different locations, time and magnitudes of maximum peak surge. On the other hand, track III has produced a different kind of surge response with local, short-lived, swift oscillations near the point of land fall-during the land fall hours. All these are attributed to the track-coastline-bottom contour combination. In the case of the numerical experiment with track III, the obtained unusual behaviour is believed to have been caused by some kind of near resonance due to local effects. On the other hand it is also believed that this oscillation is confined to the

surface layer of that local region (owing the quick damping). Perhaps the current structure through the depth may provide a better answer for this problem. In the next chapter we explore this aspect.



SHELF AREA OF THE
BAY OF BENGAL

FIG.1.(a),(b).

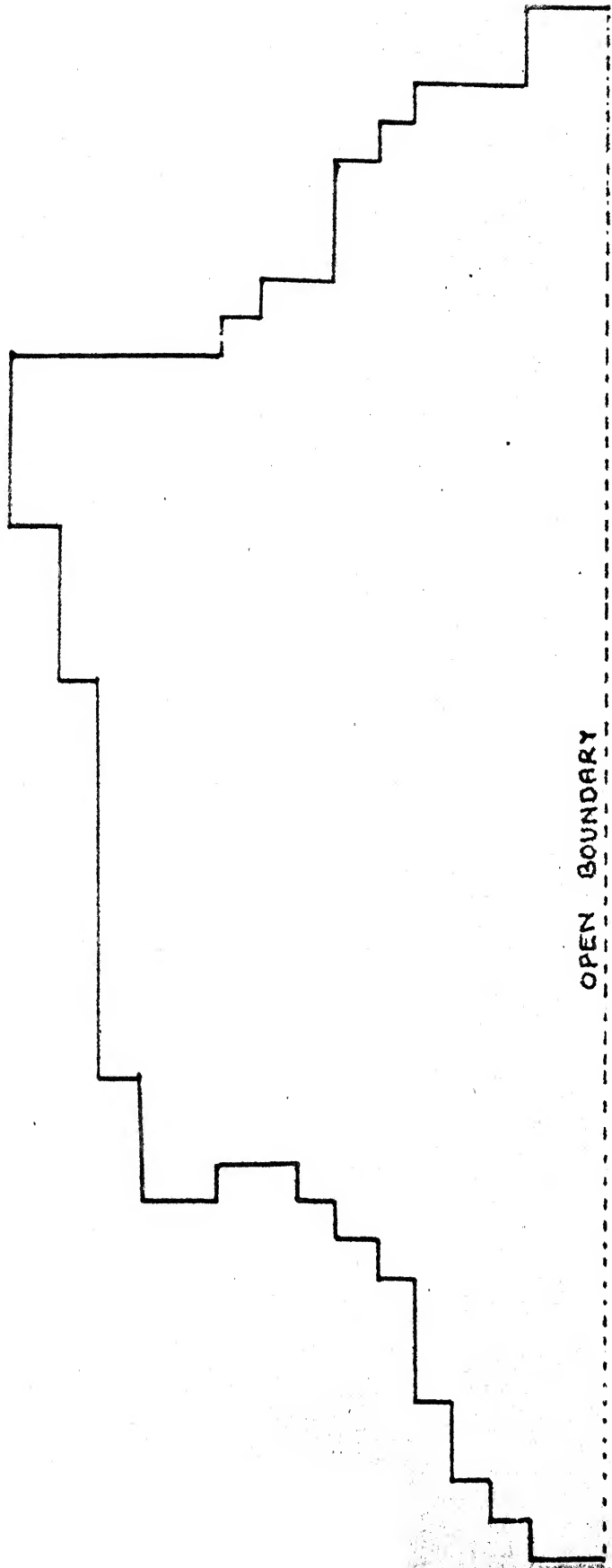


FIG.1 (c).

BAY OF BENGAL (FULL AREA MODEL)

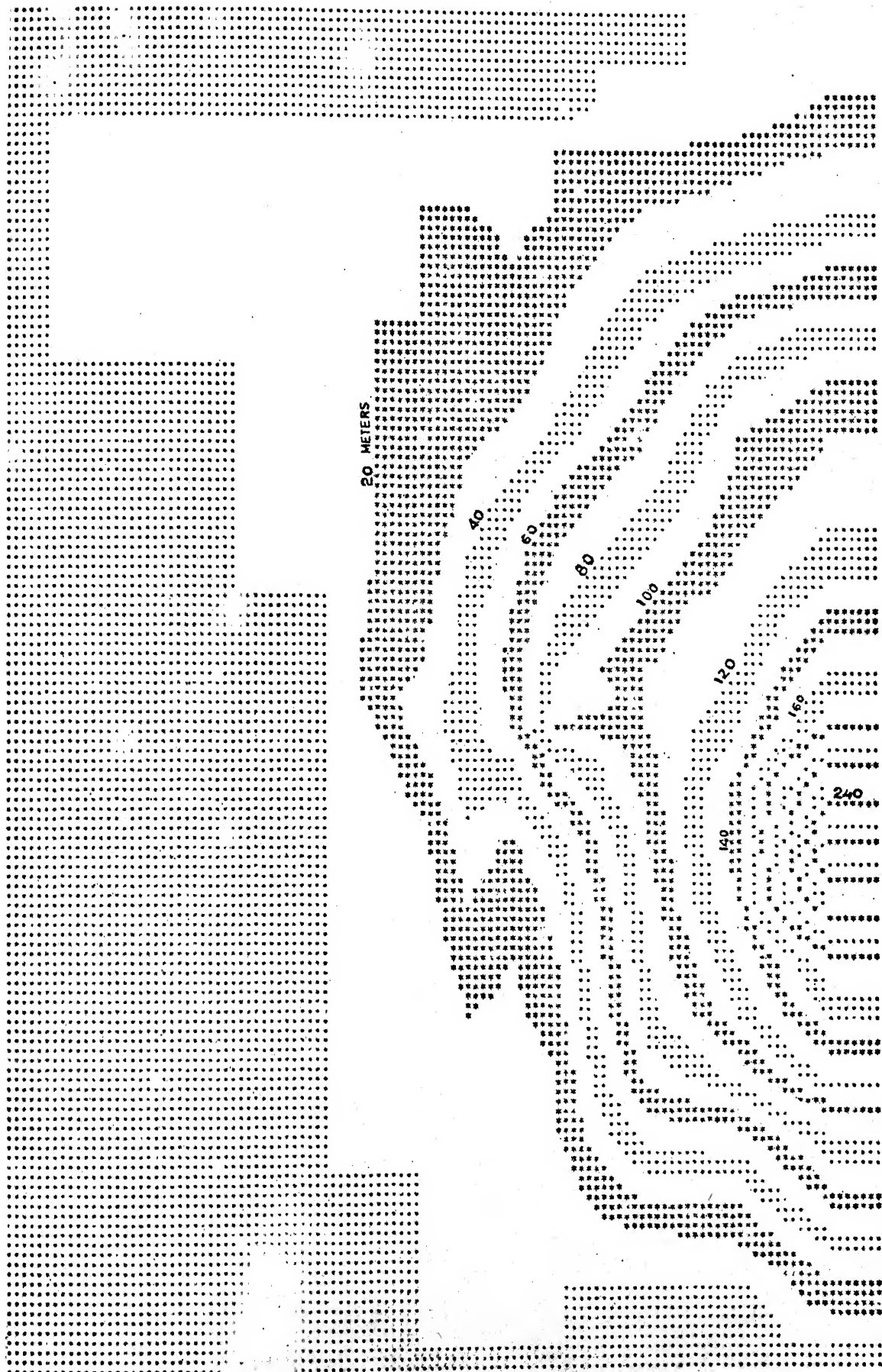
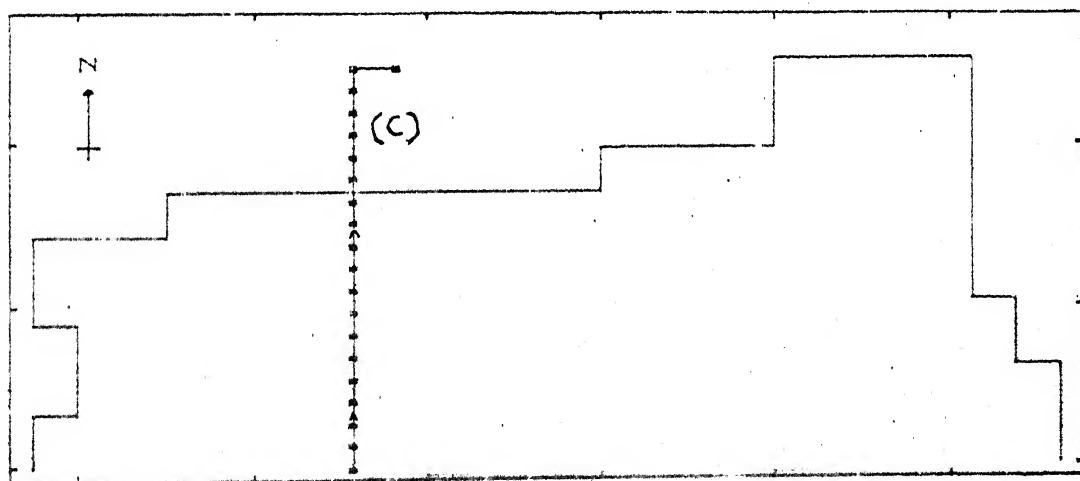
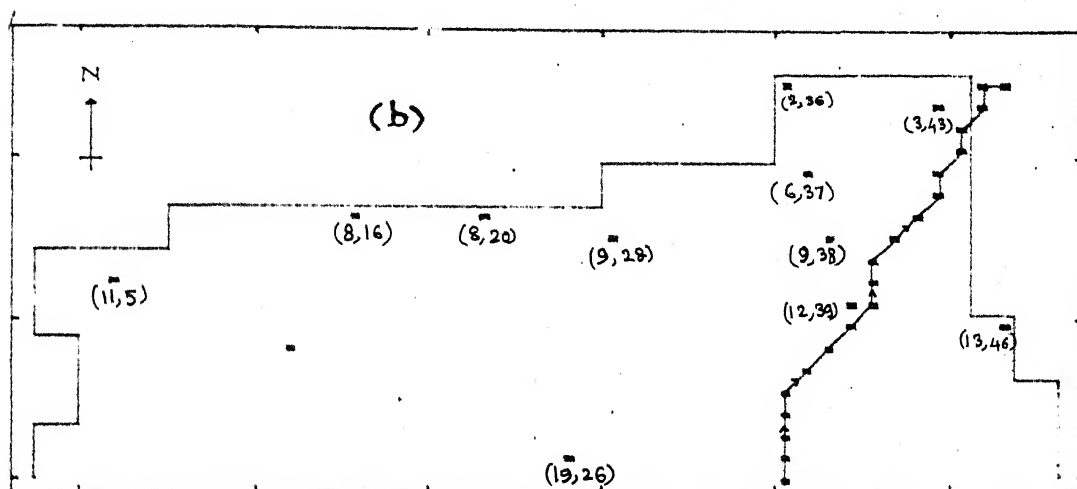
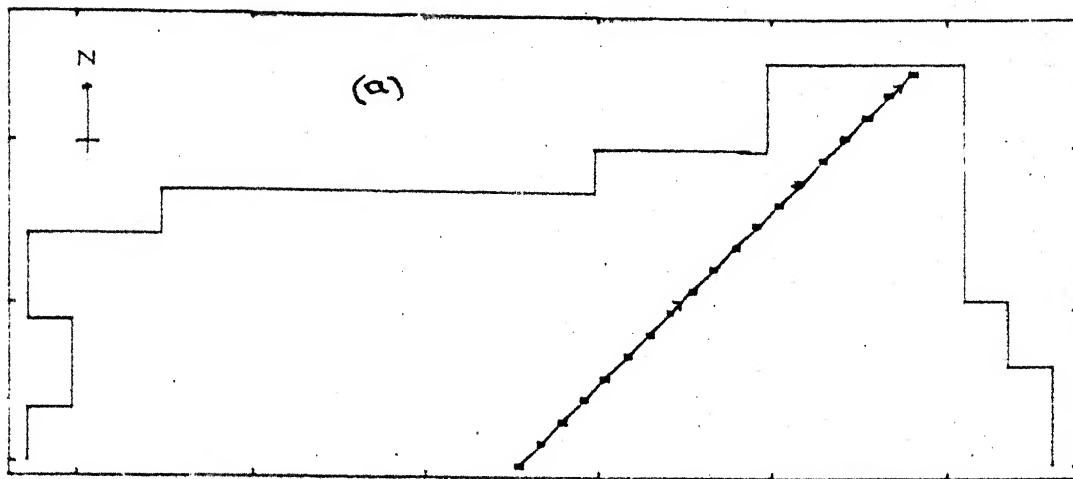
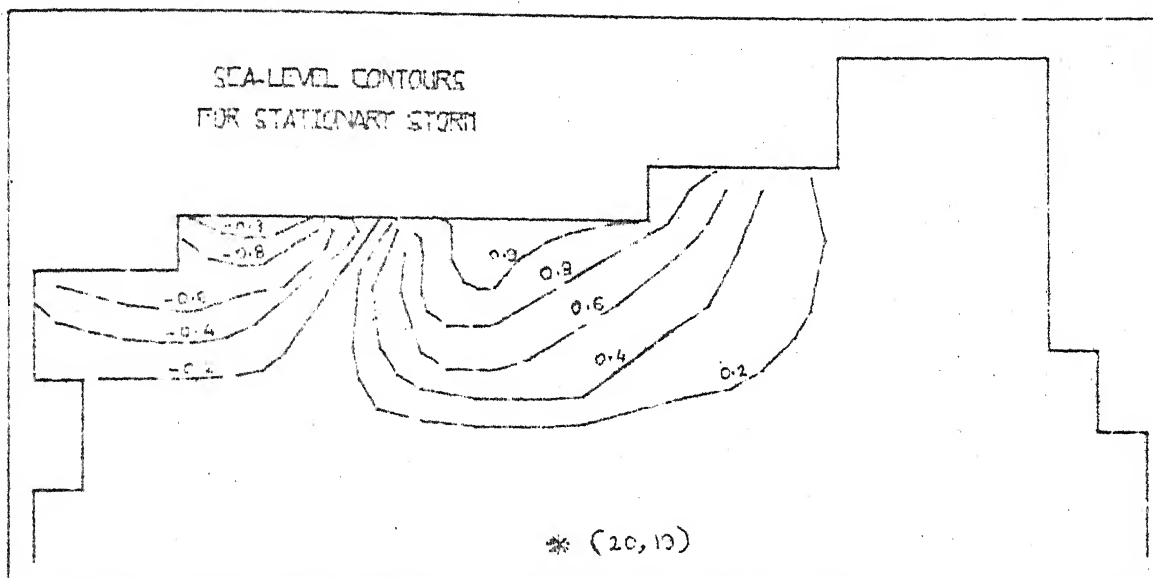


FIG. 2. BATHYMETRY CONTOUR BANDS (IN METERS)

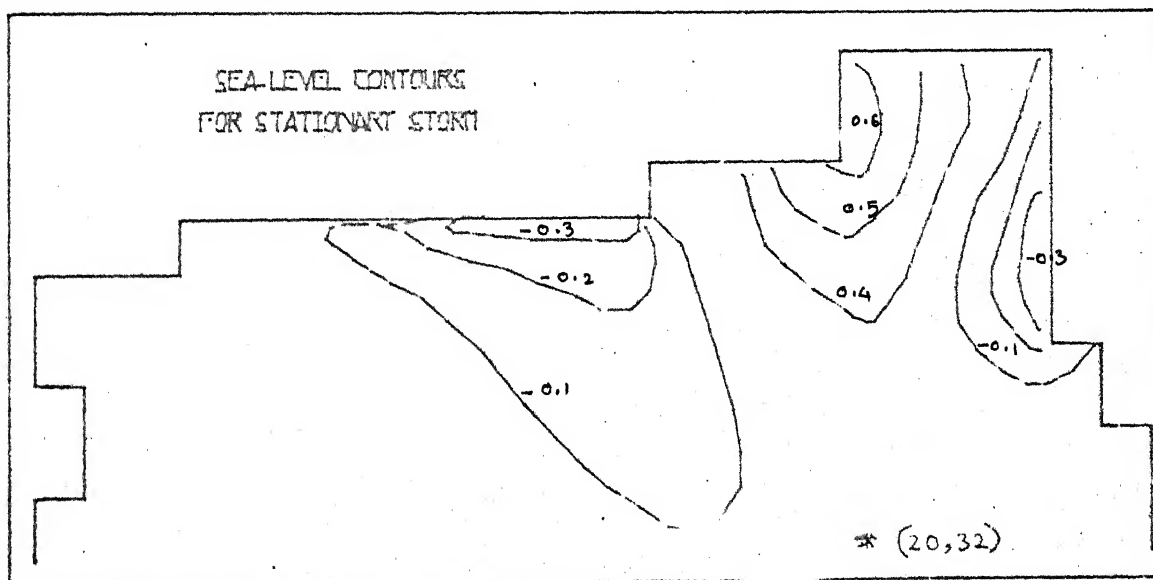


— hourly shifting of the storm centre

FIG. 3. (a), (b), (c), STORM TRACKS AND THE SELECTED LOCATIONS.



(a)



(b)

FIG. 4 .a, b. SEA LEVEL CONTOURS (IN METERS)
STATIONARY STORM (Steady State Response)
CENTRE AT : (a) (20,19) , (b) (20,32)

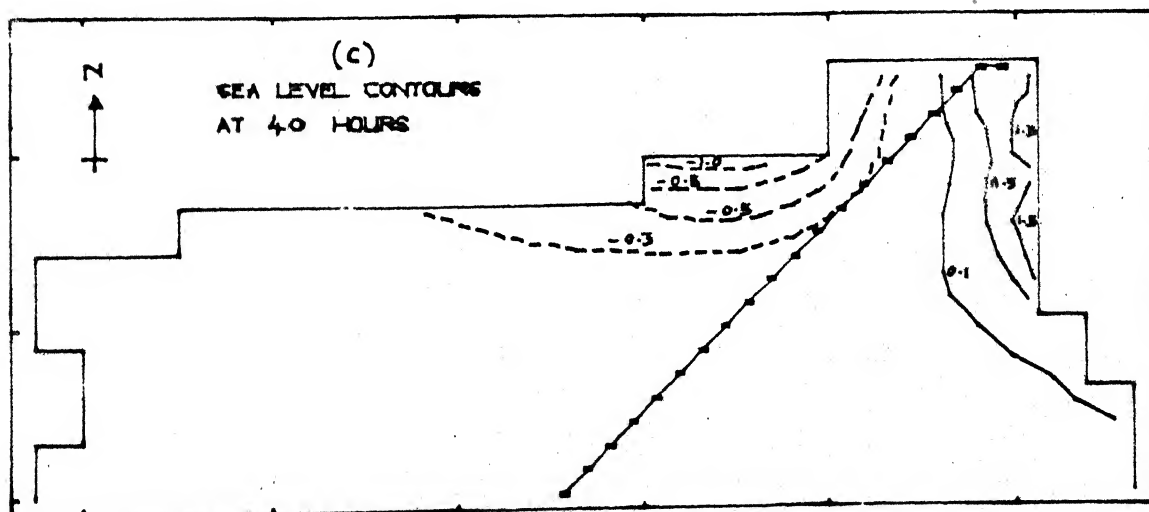
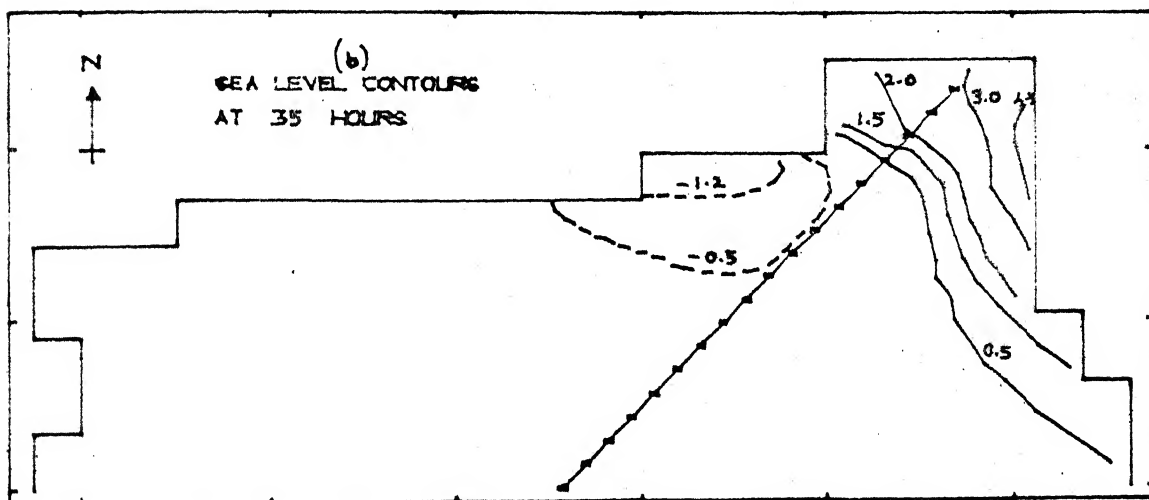
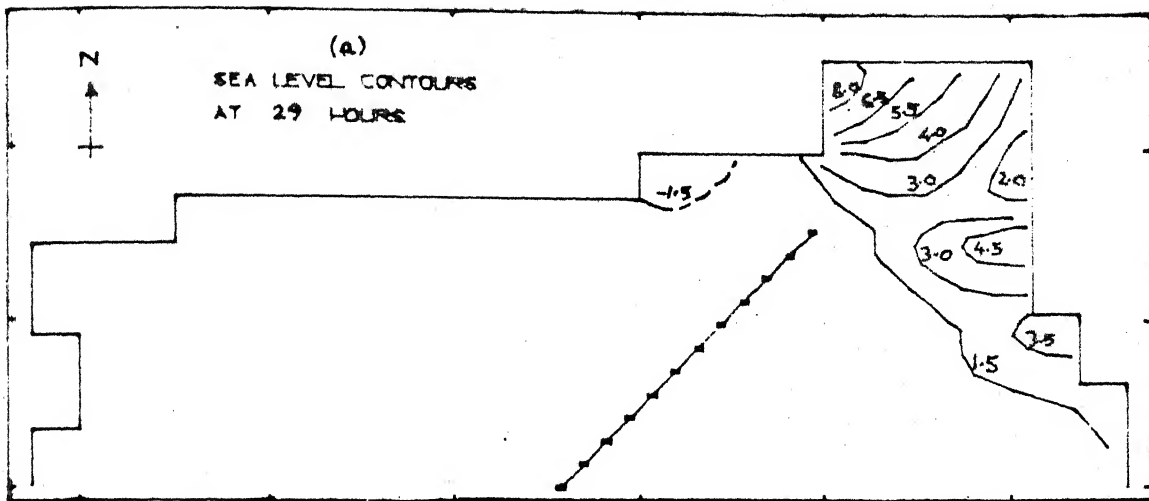


FIG. 5 a, b, c. ELEVATION CONTOURS IN METERS
DUE TO ASYMMETRIC STORM ALONG TRACK 1

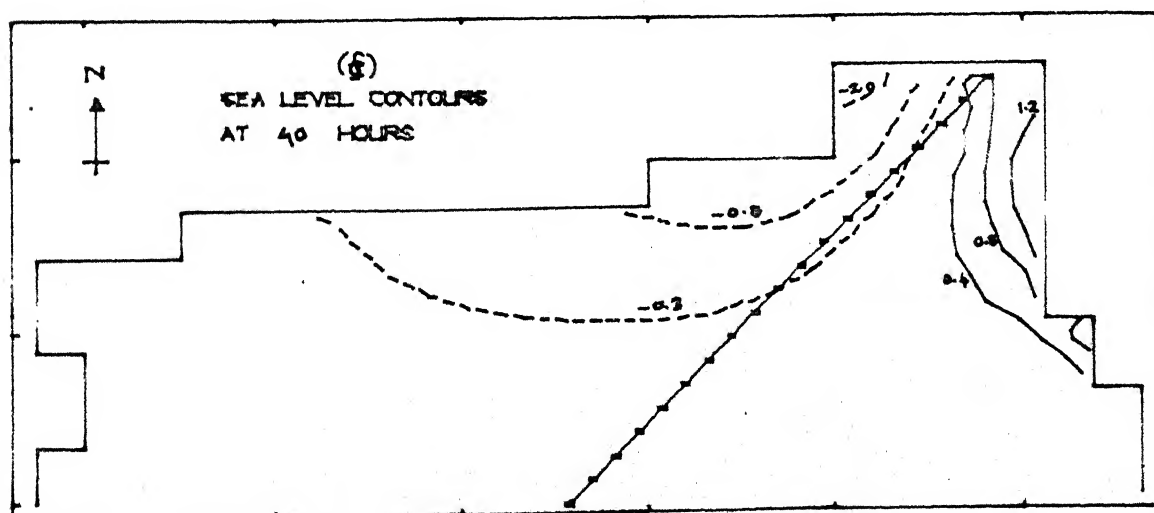
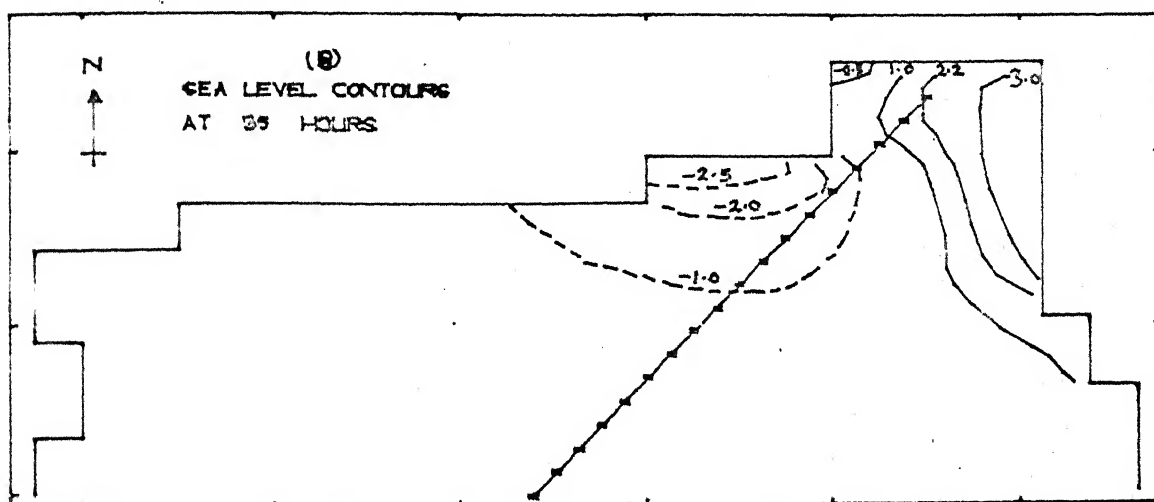
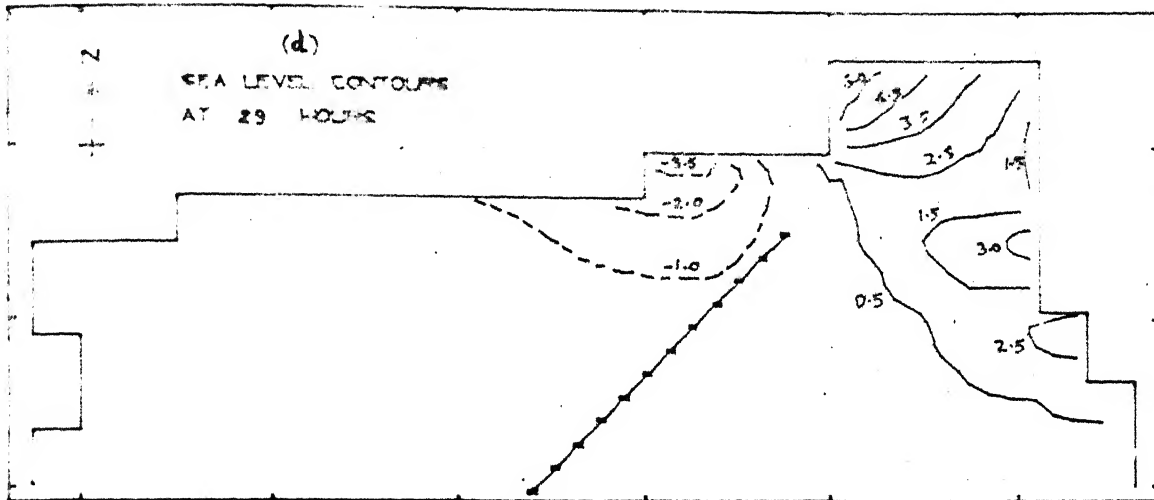


FIG. 5. d, e, f. ELEVATION CONTOURS IN METERS
DUE TO SYMMETRIC STORM ALONG TRACK 1

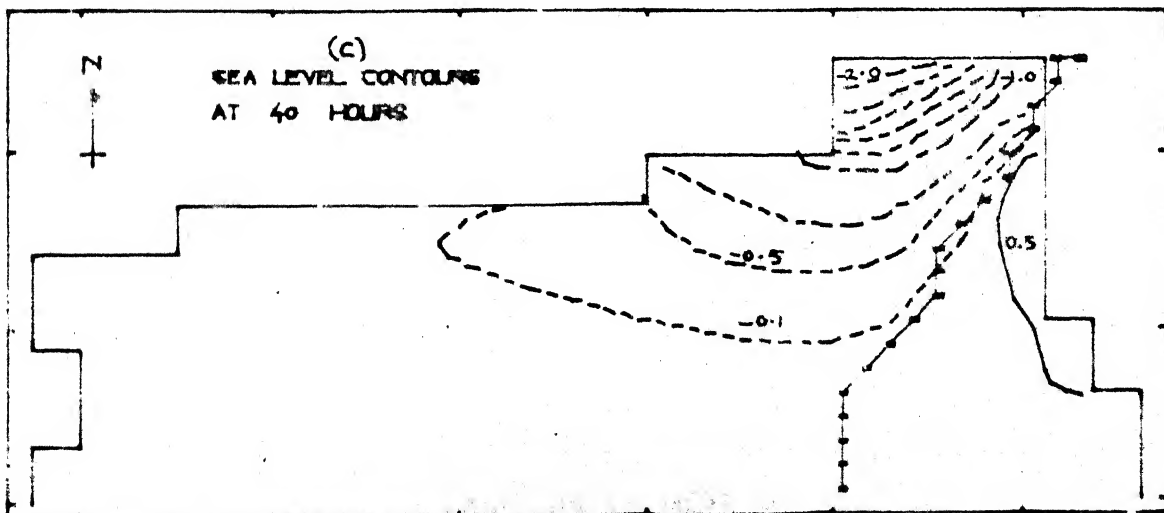
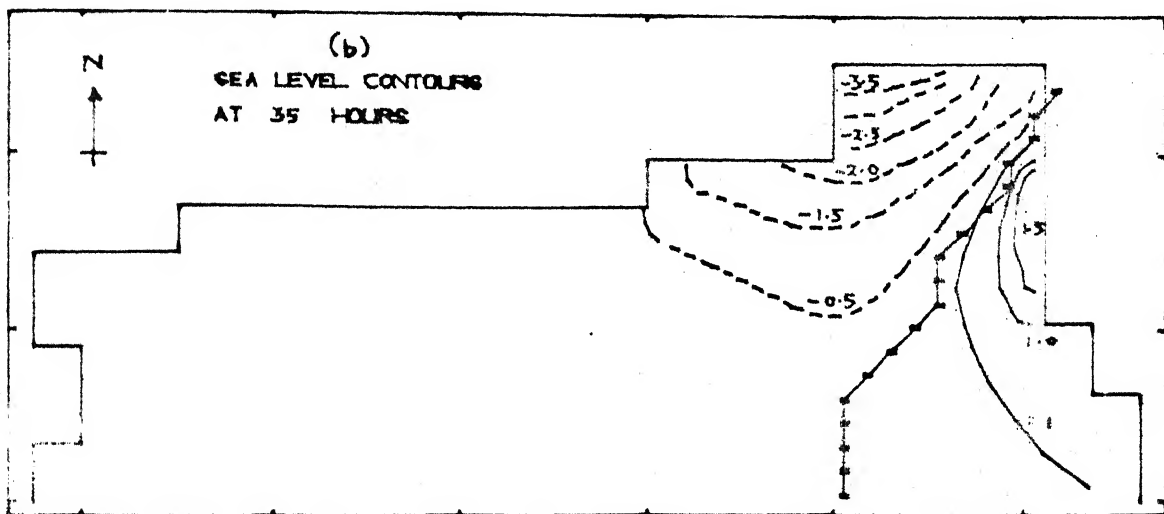
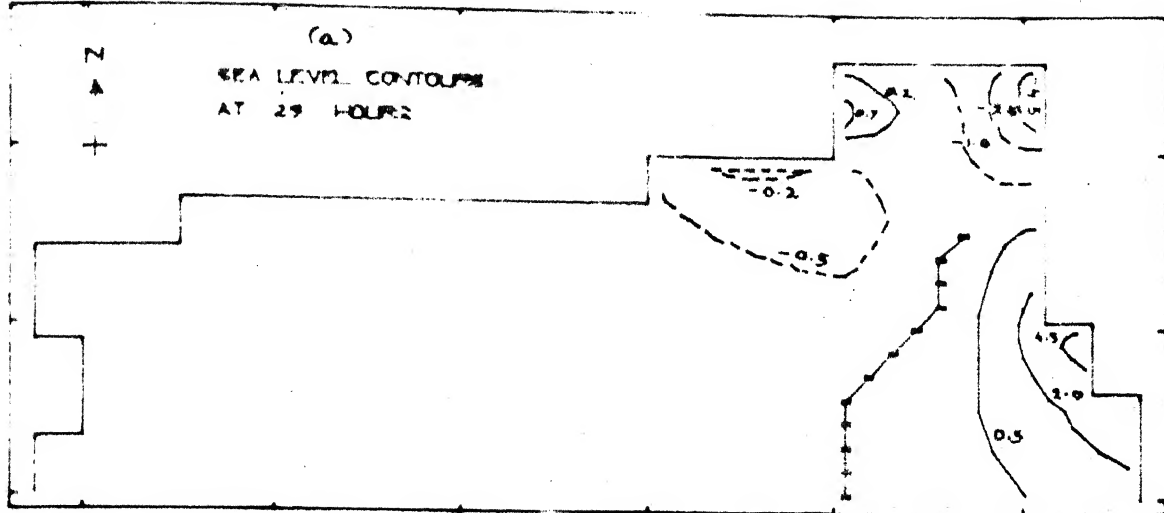


FIG. 6 a, b, c. ELEVATION CONTOURS IN METERS
DUE TO ASYMMETRIC STORM ALONG TRACK II

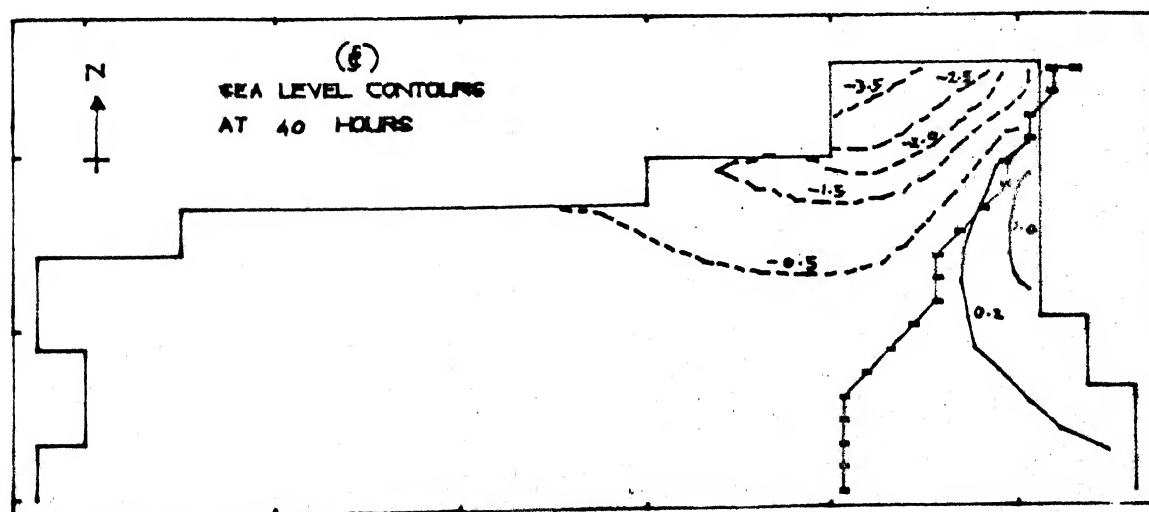
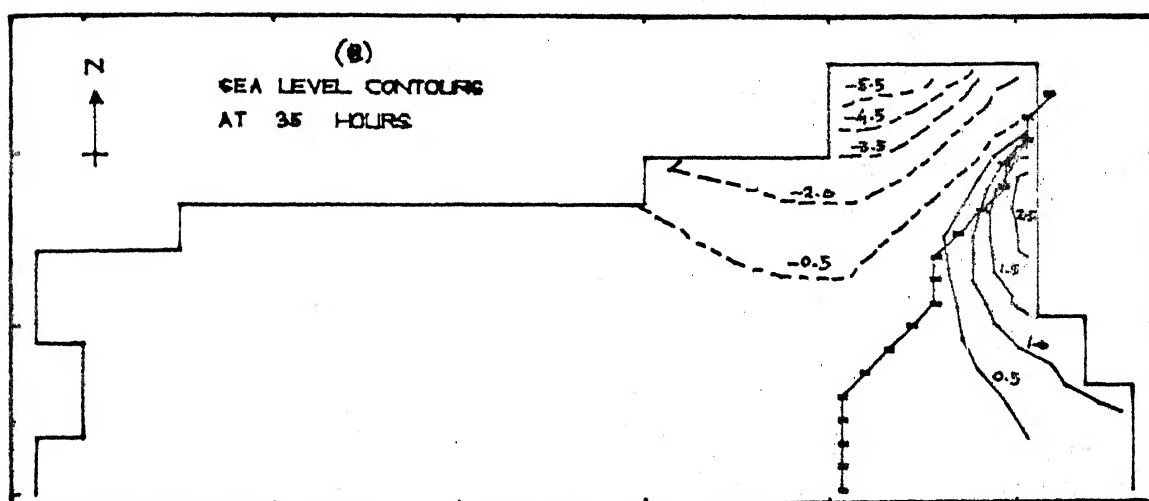
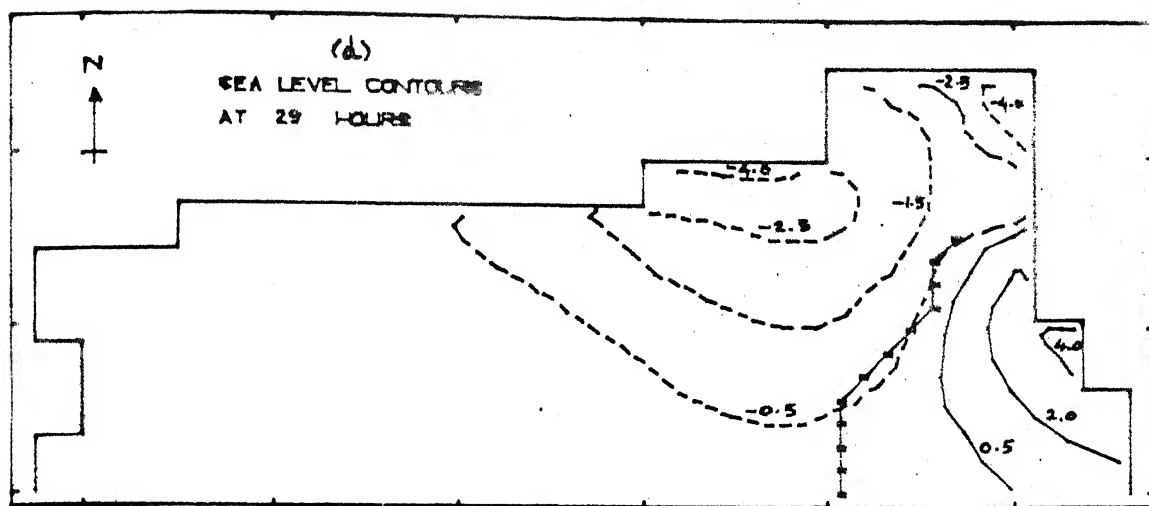


FIG. 6. d, e, f ELEVATION CONTOURS IN METERS
DUE TO SYMMETRIC STORM ALONG TRACK II

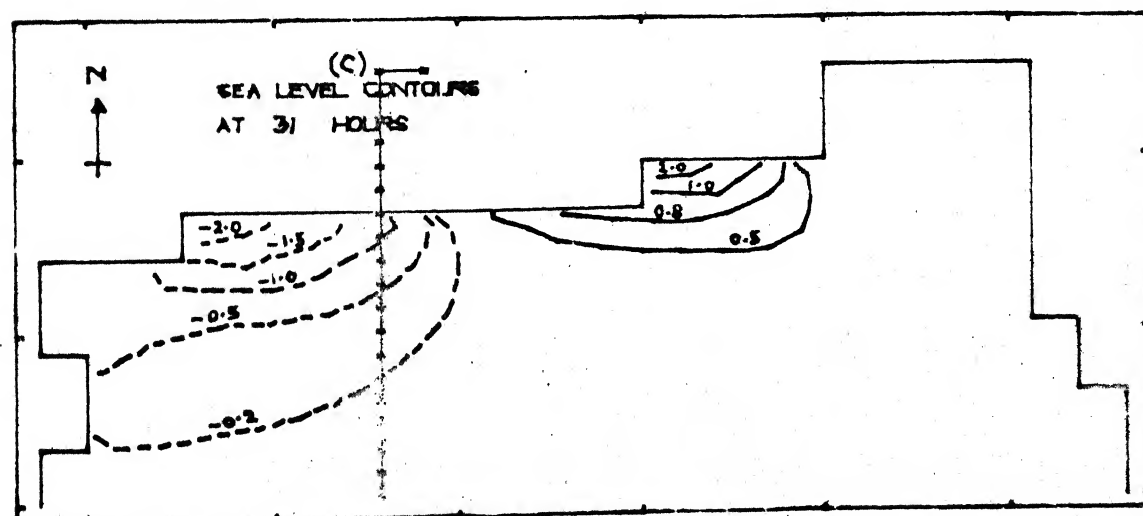
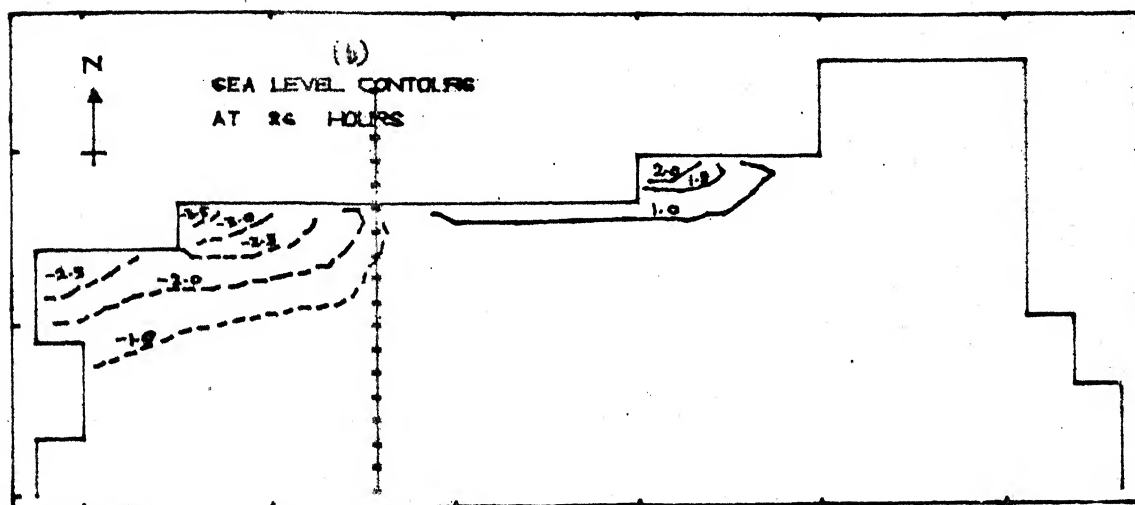
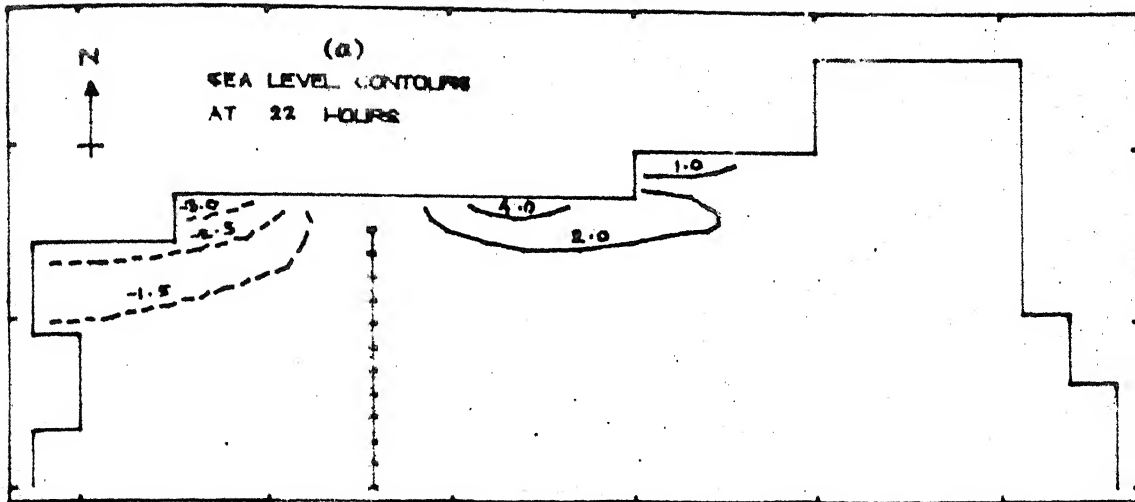


FIG. 7. a, b, c. ELEVATION CONTOURS IN METERS
DUE TO ASYMMETRIC STORM ALONG TRACK III

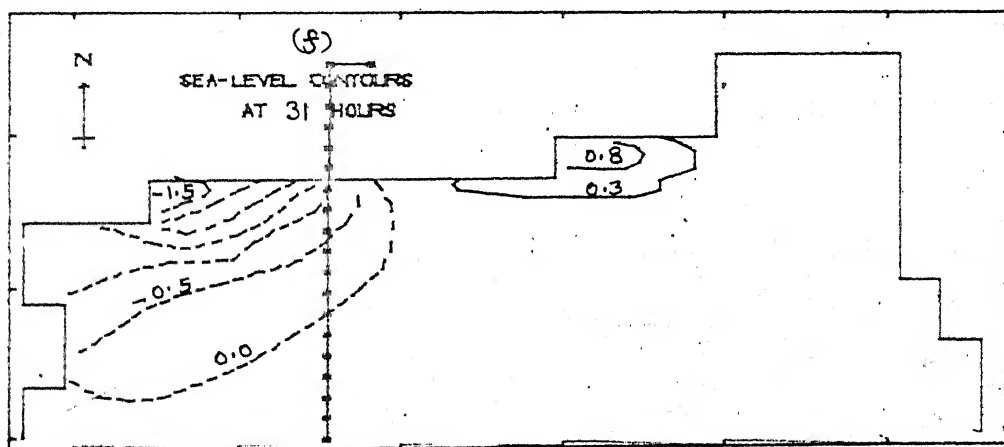
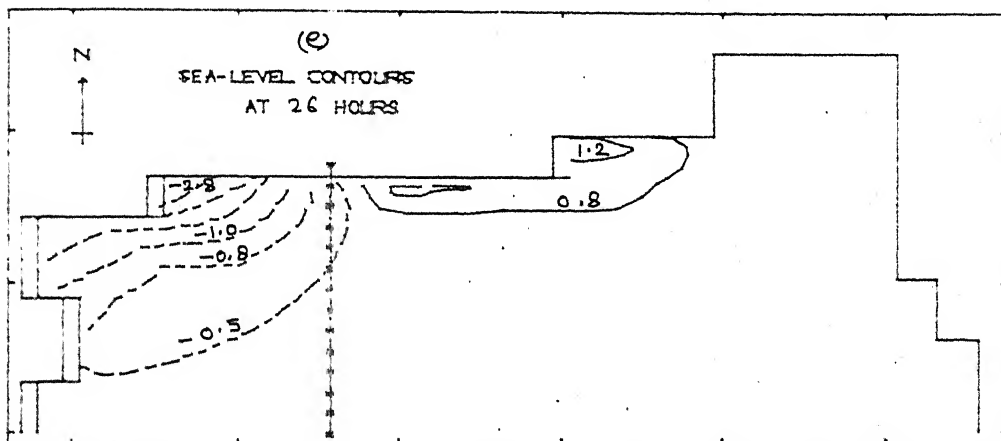
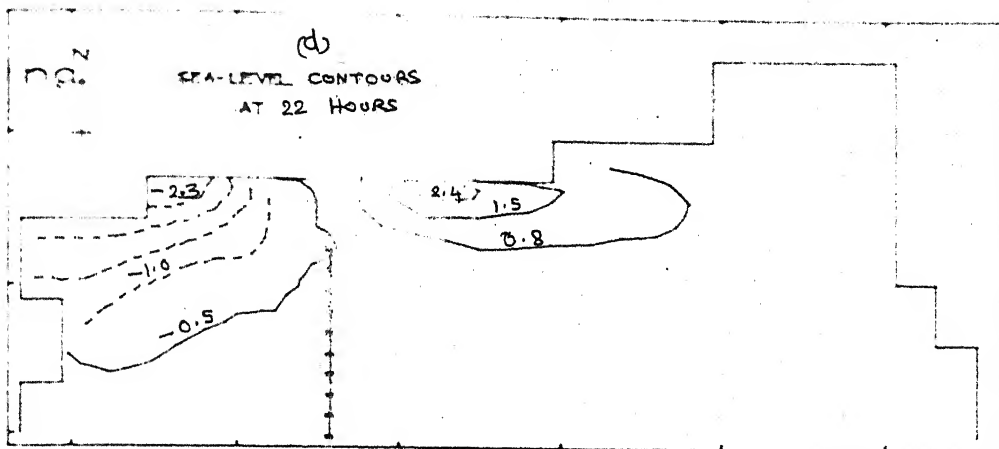
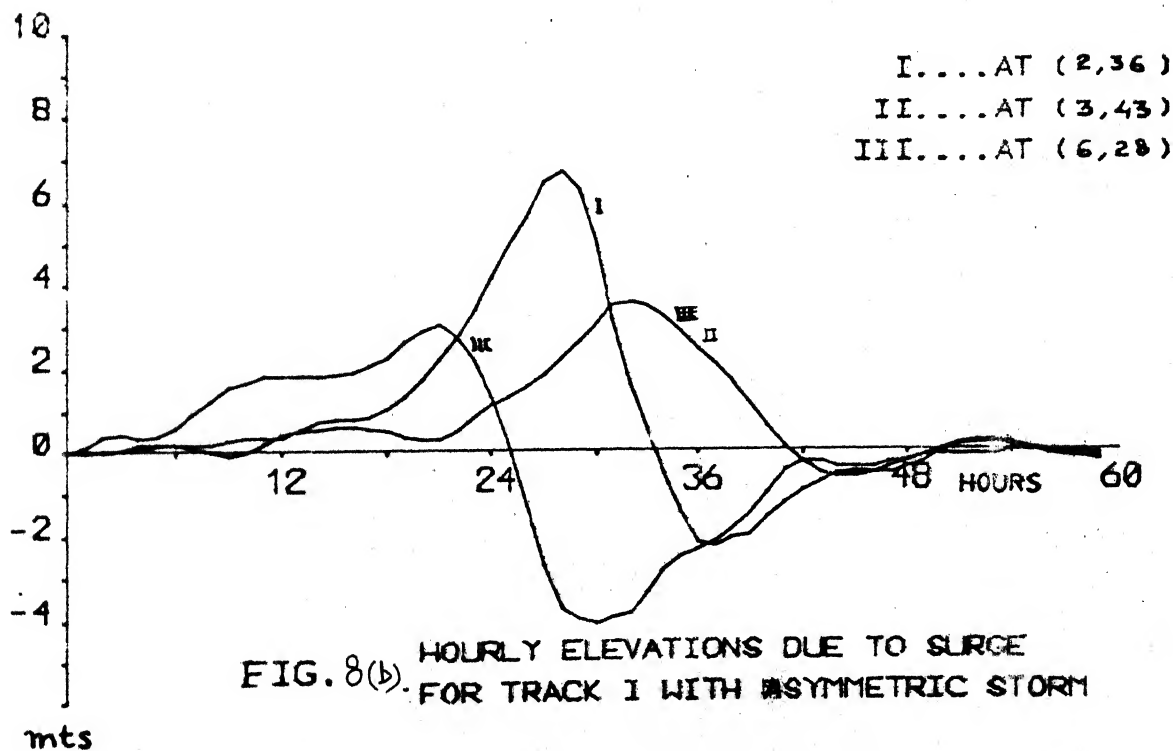
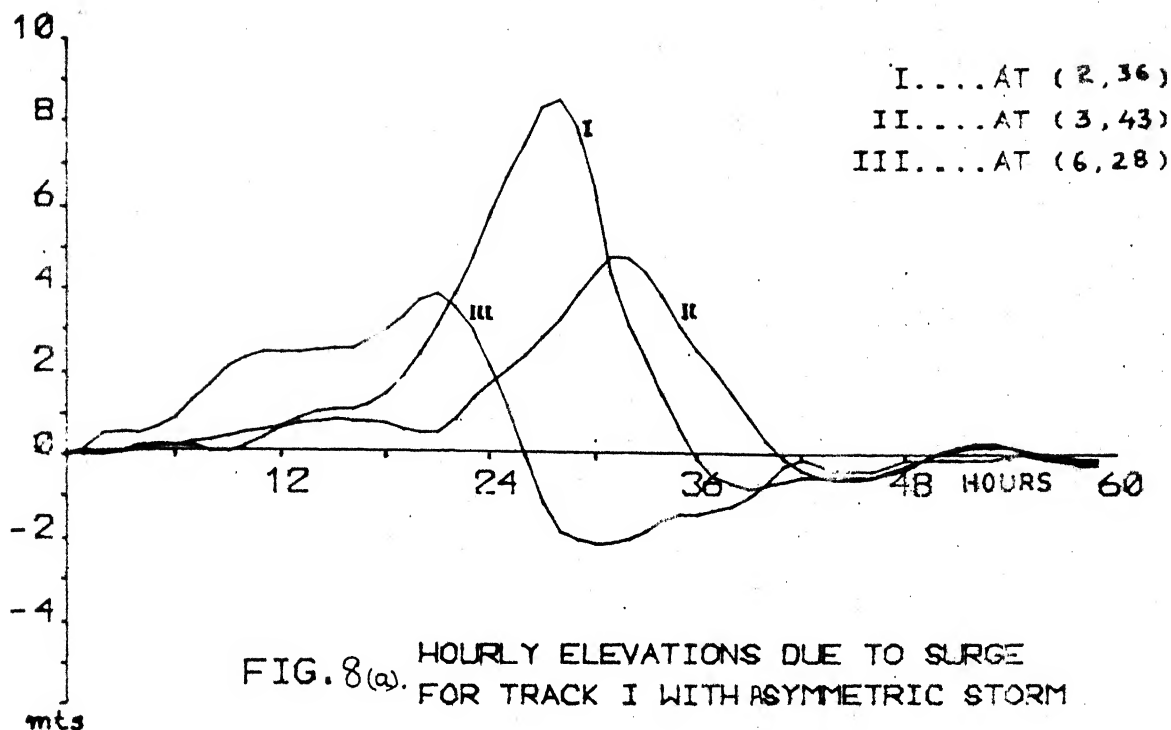
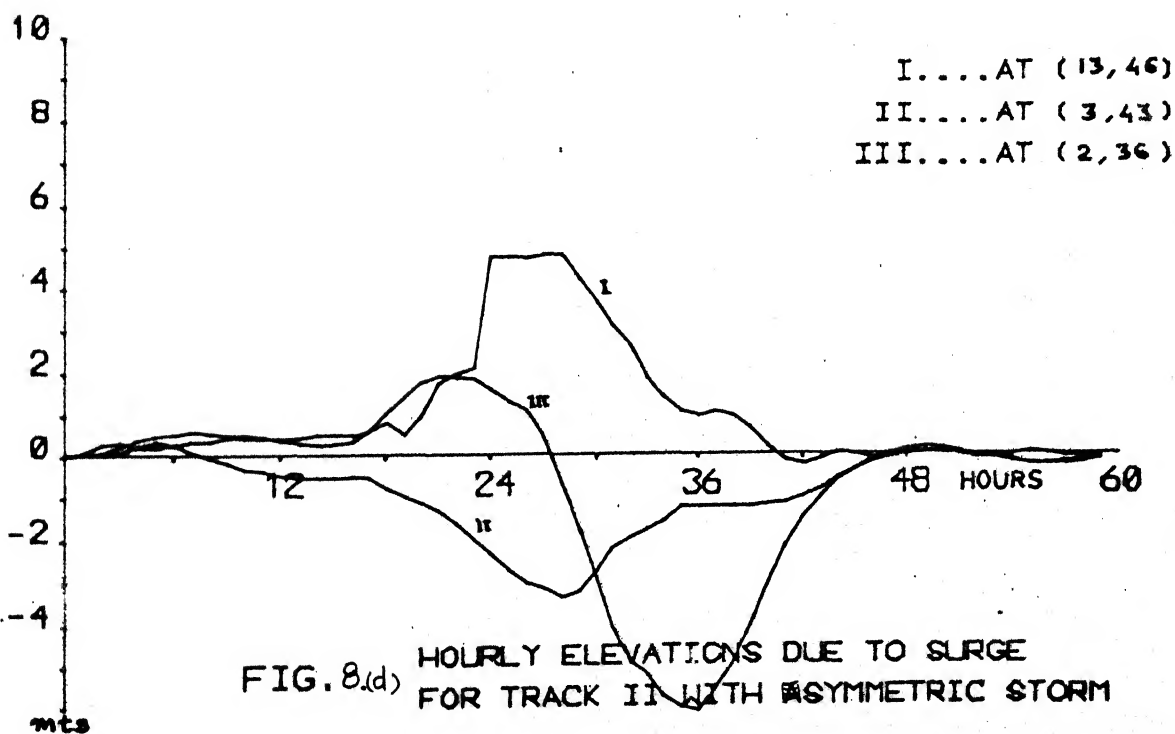
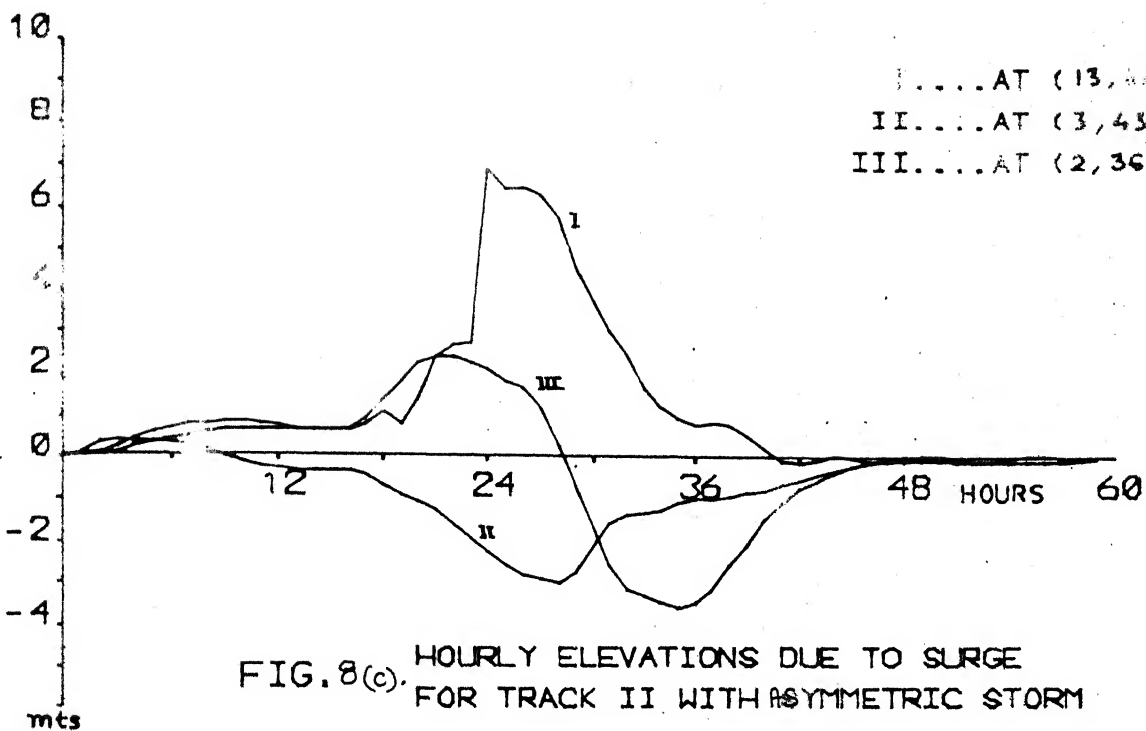
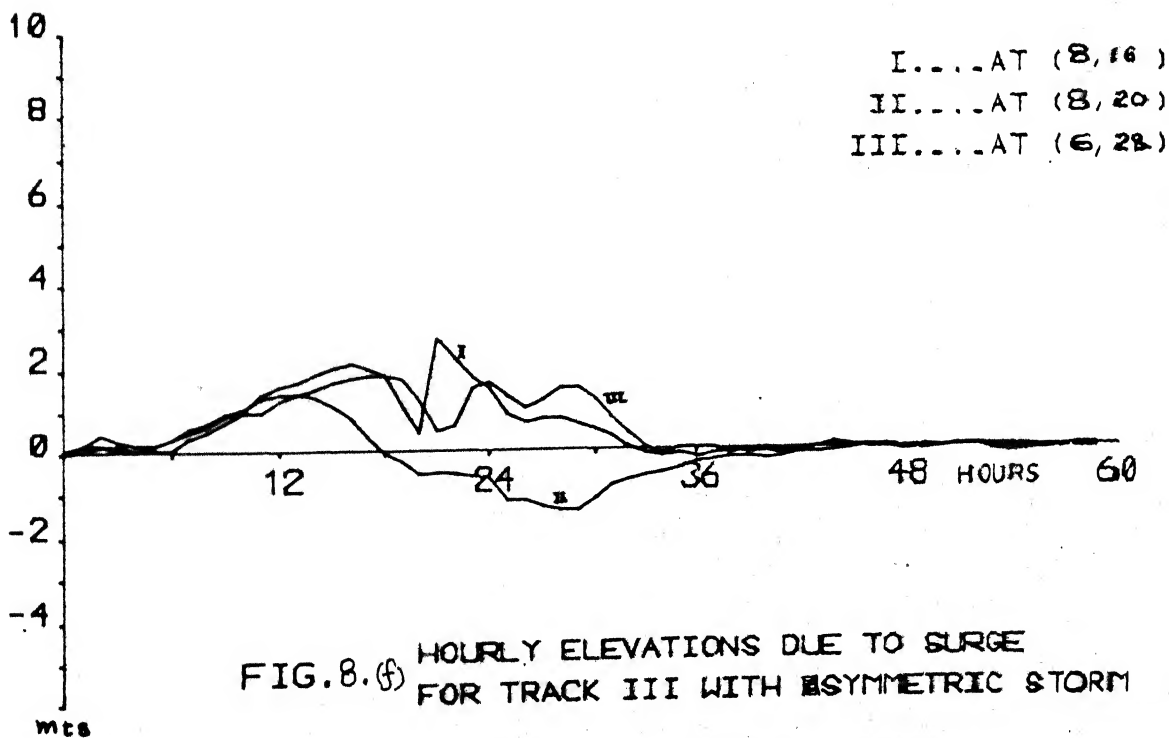
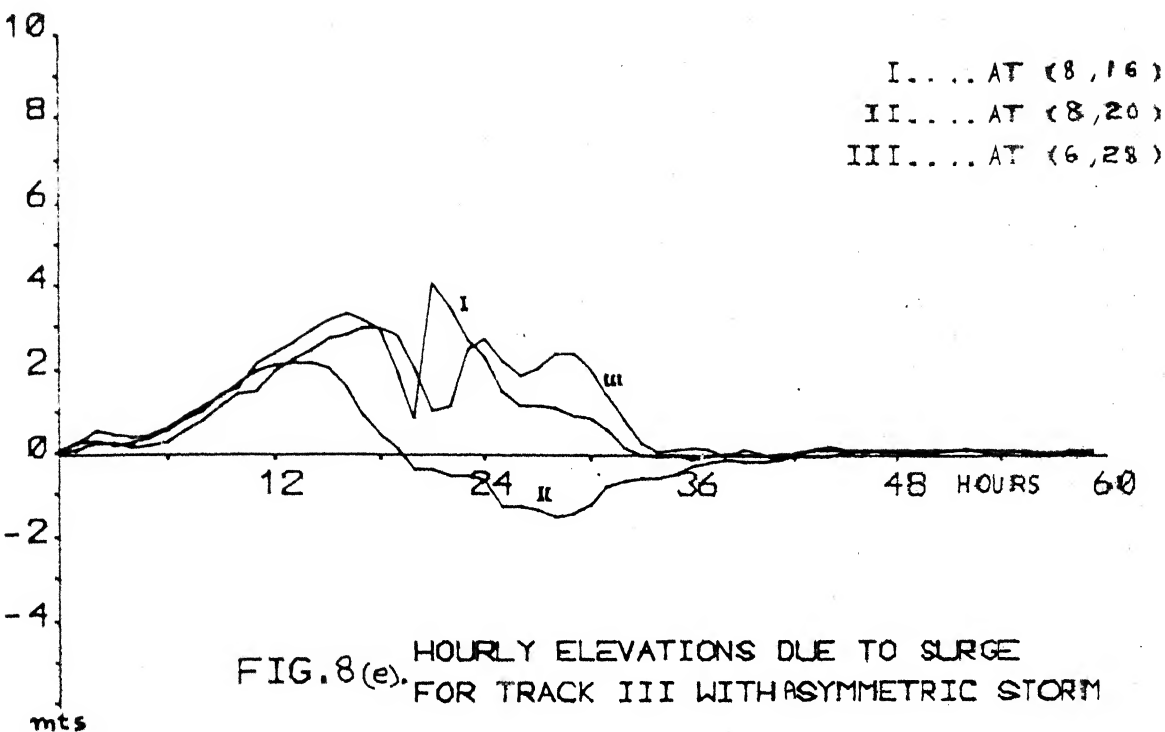
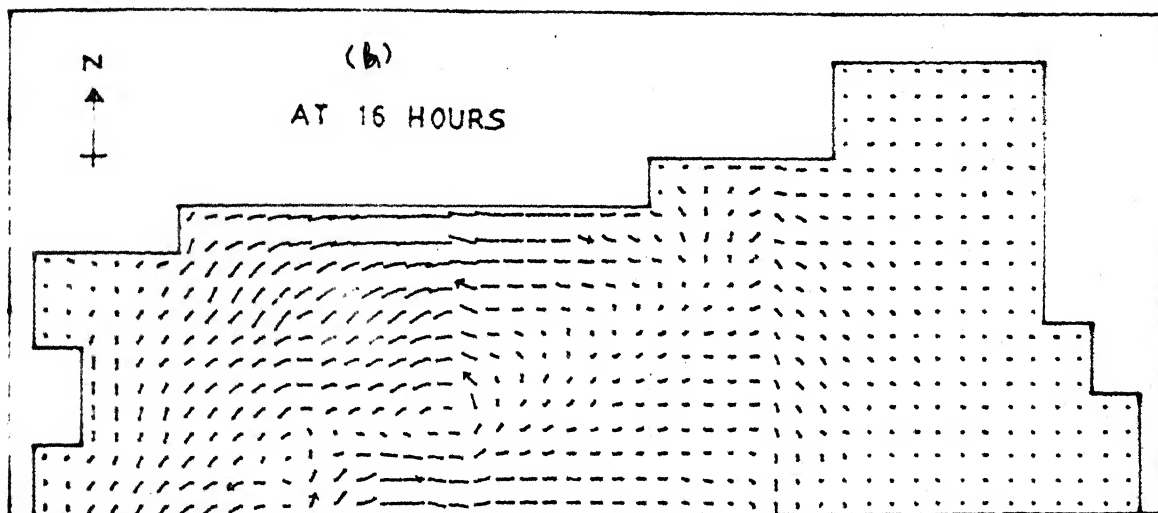
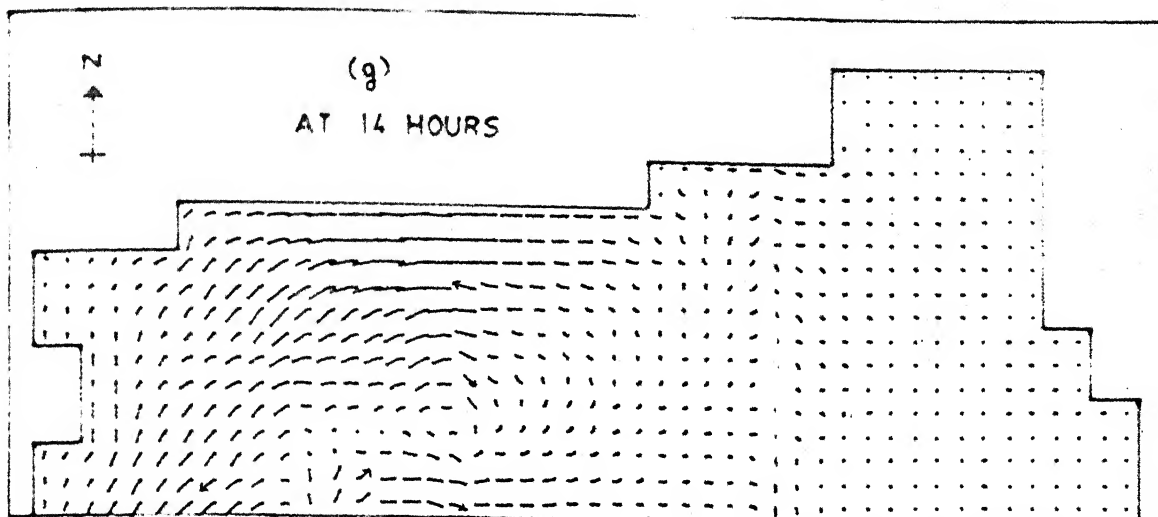


FIG. 7 d,e,f: ELEVATION CONTOURS IN METERS.
SYMMETRIC STORM ALONG TRACK III









CURRENT STRENGTH — 200. CMS/SEC

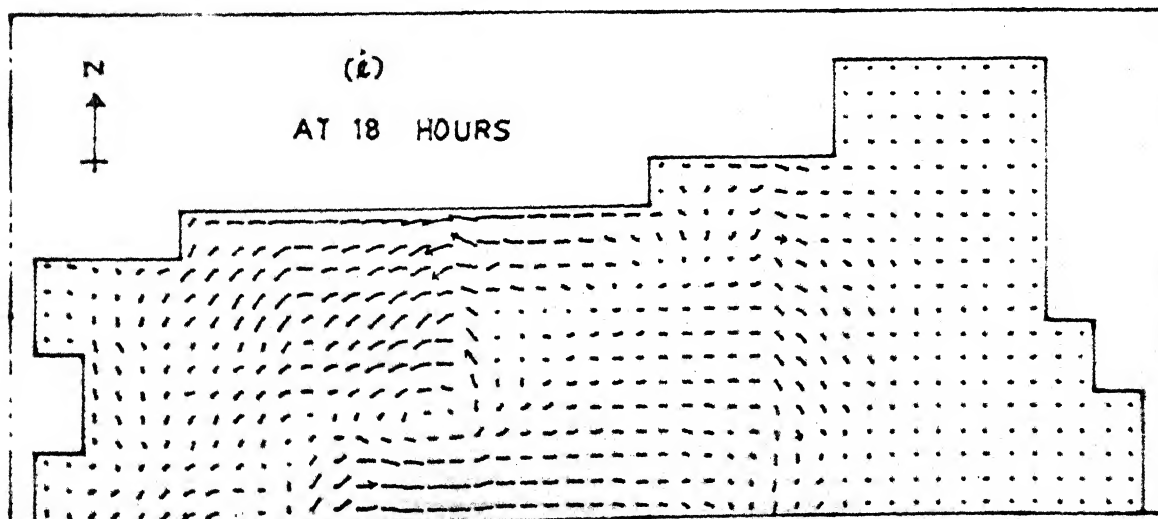
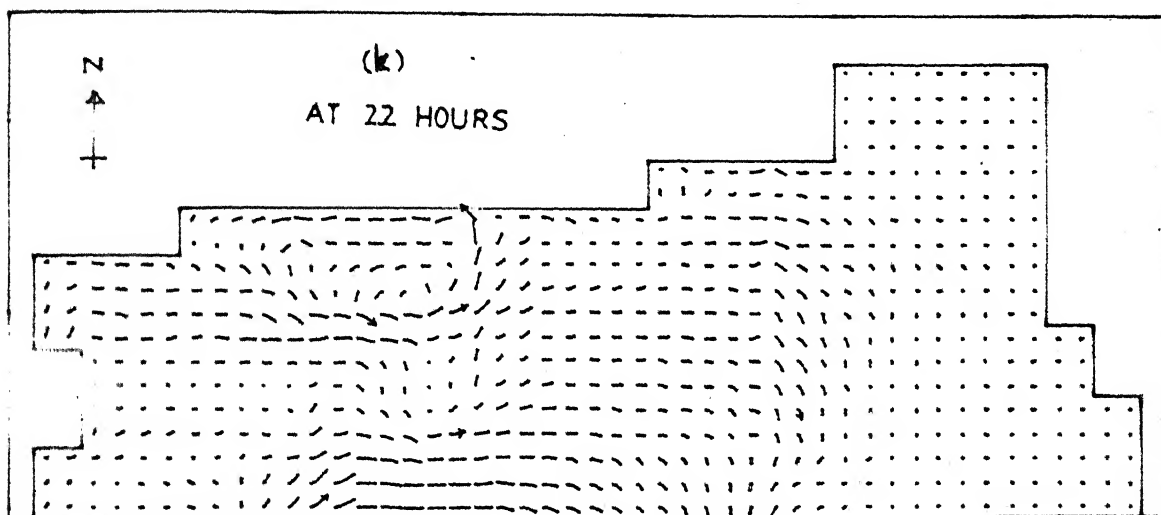
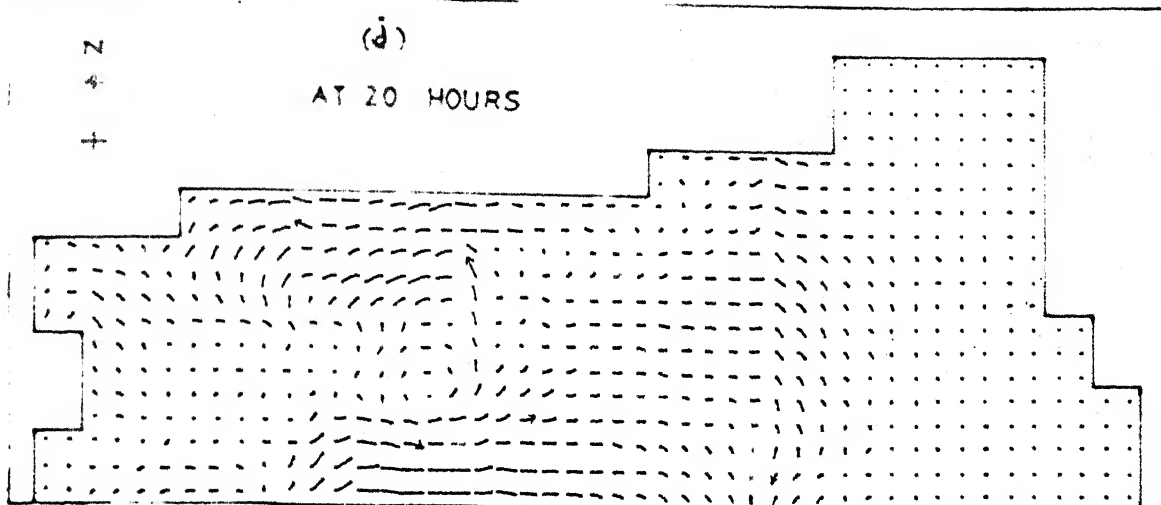


FIG. 8. g, h, i

DEPTH-MEAN CURRENT VECTORS
DUE TO ASYMMETRIC STORM ALONG TRACK III



CURRENT STRENGTH \rightarrow 200 CMS/SEC

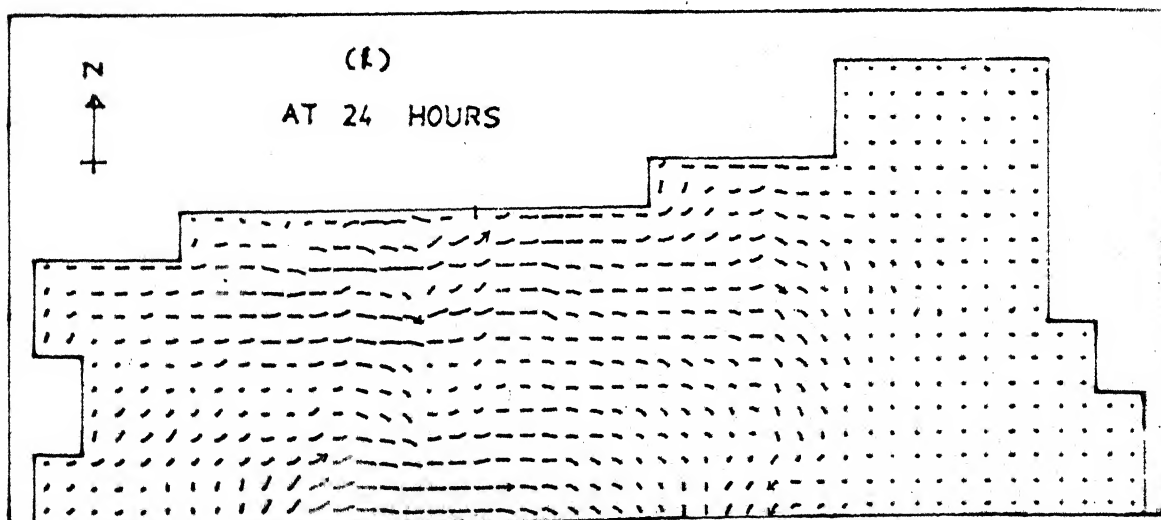


FIG. 8 d, k, l

DEPTH-MEAN CURRENT VECTORS
DUE TO ASYMMETRIC STORM ALONG TRACK III

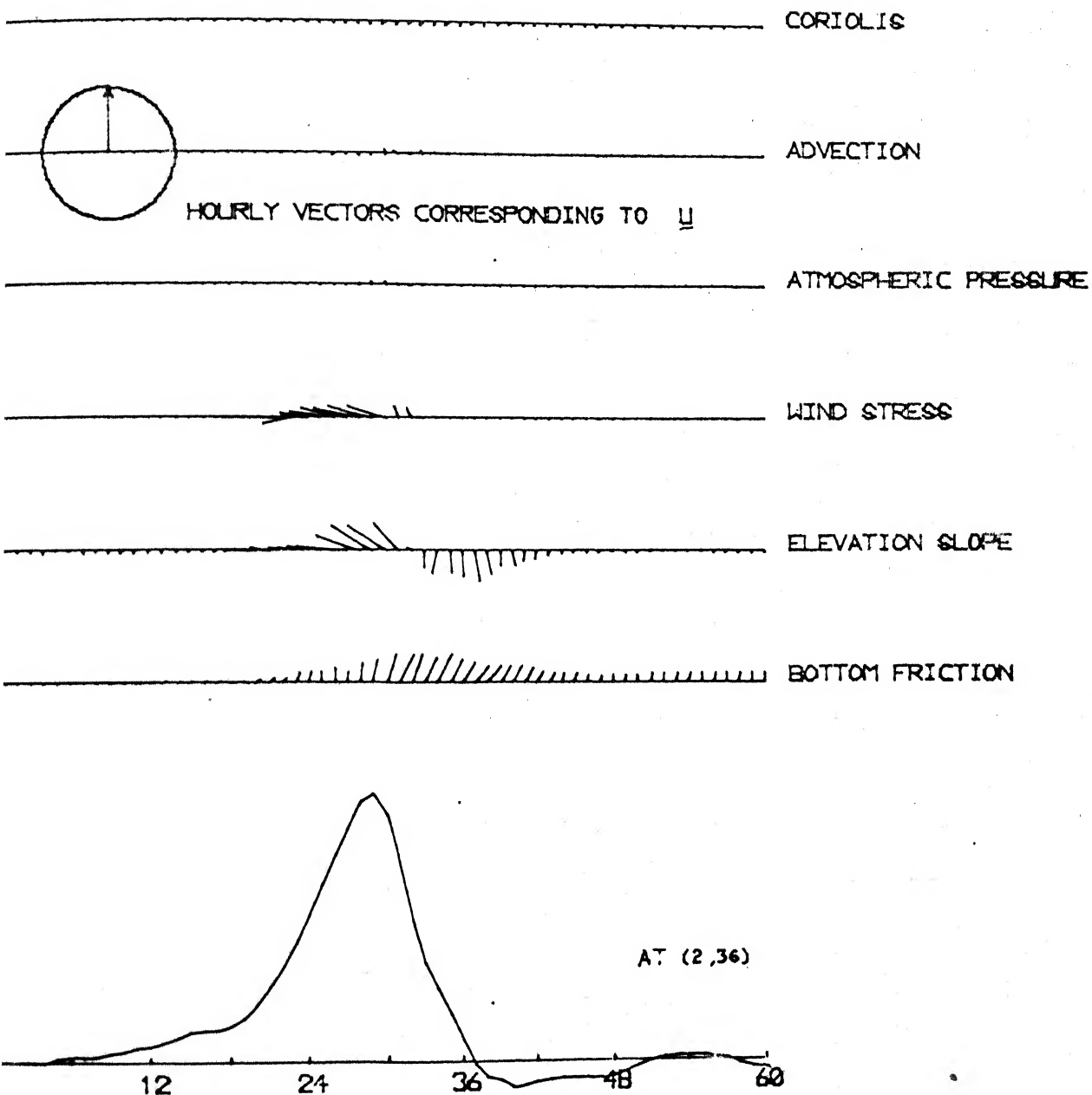


FIG. 9(a) HOURLY ELEVATIONS DUE TO SURGE
FOR TRACK I WITH ASYMMETRIC STORM

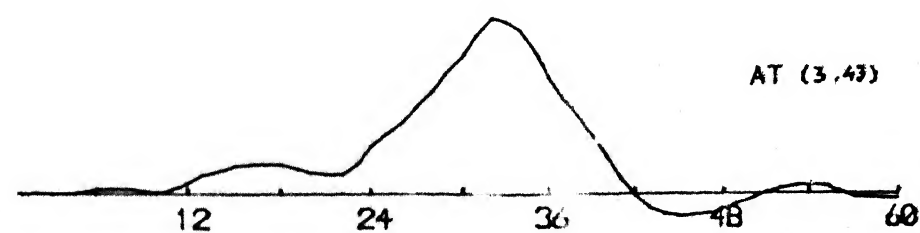
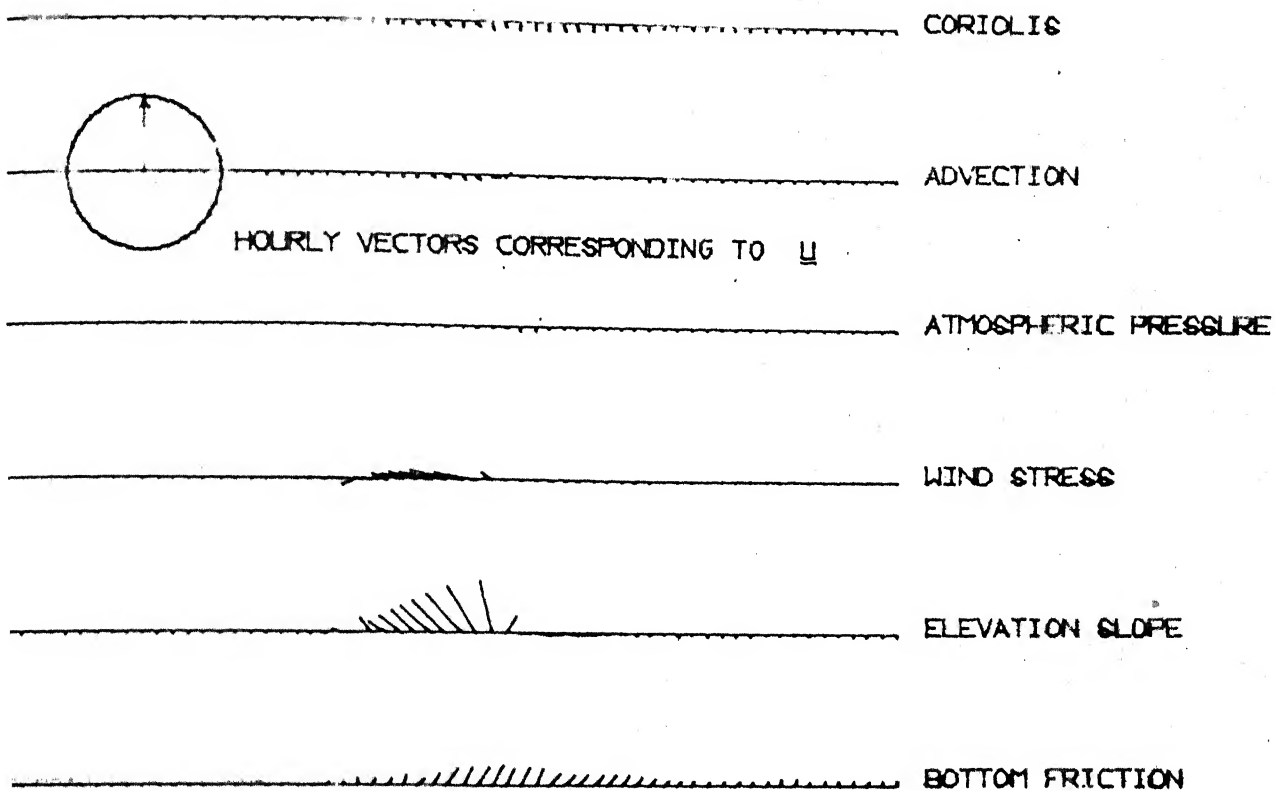
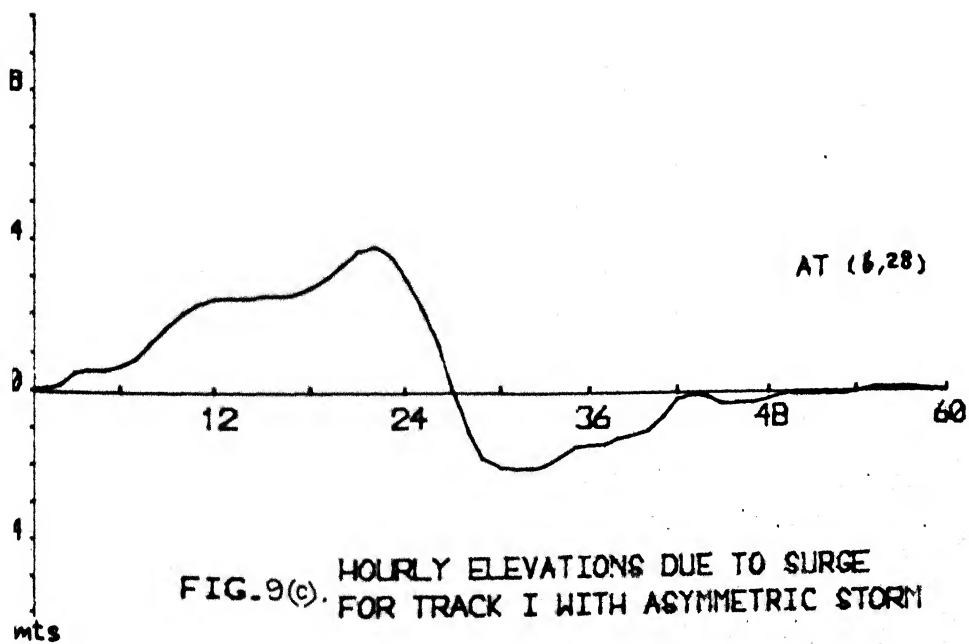
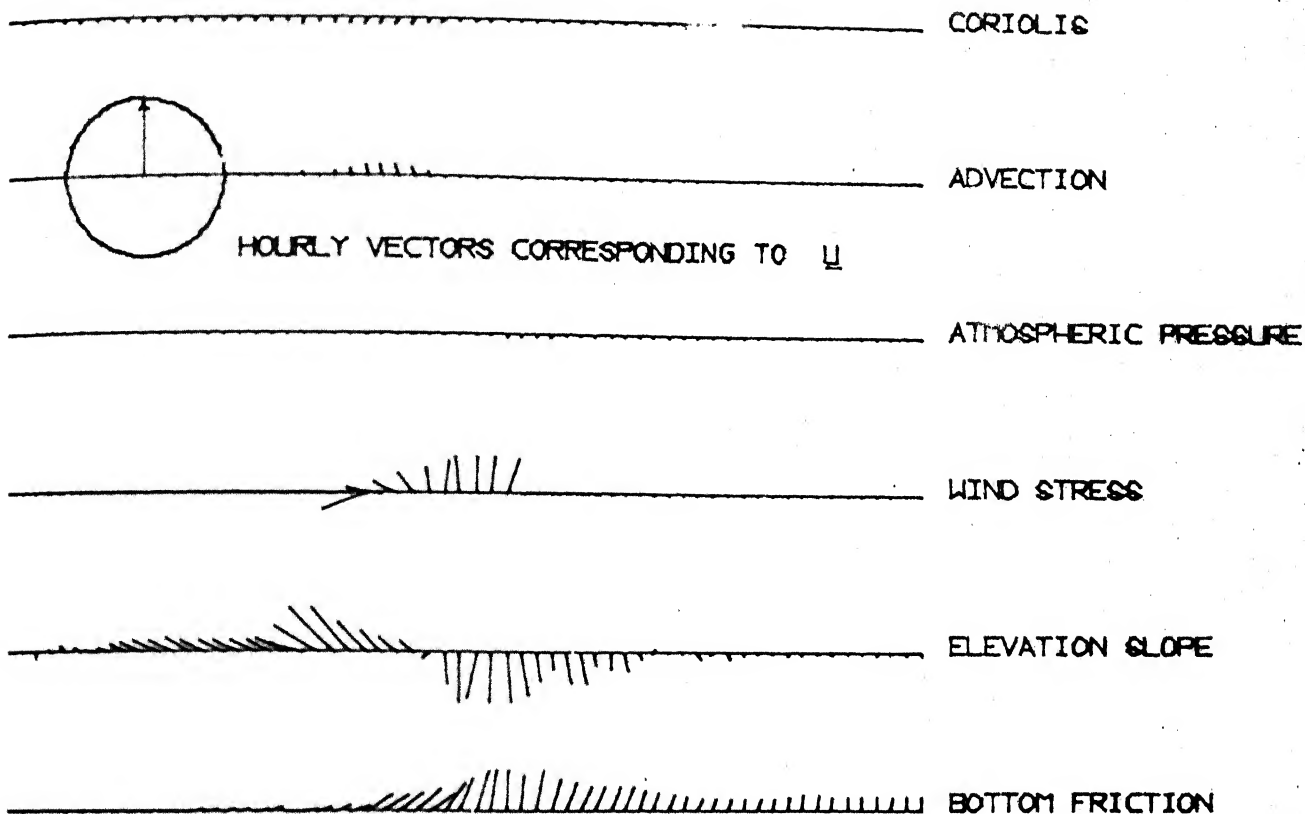


FIG. 9(b). HOURLY ELEVATIONS DUE TO SURGE
FOR TRACK I WITH ASYMMETRIC STORM



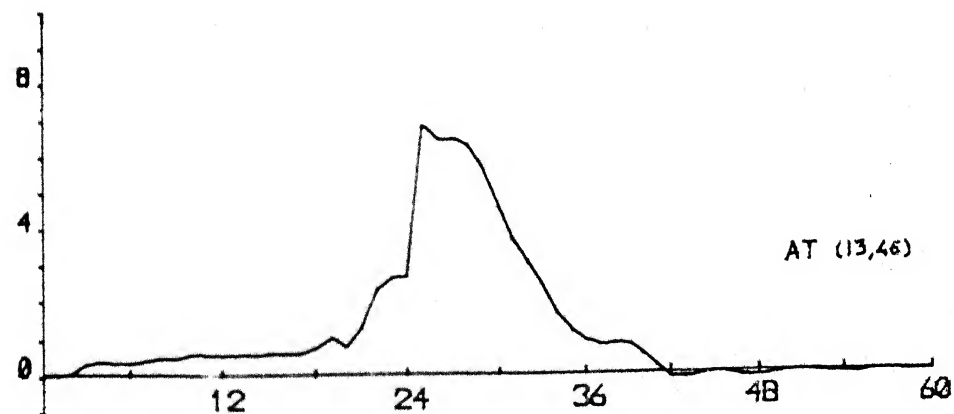
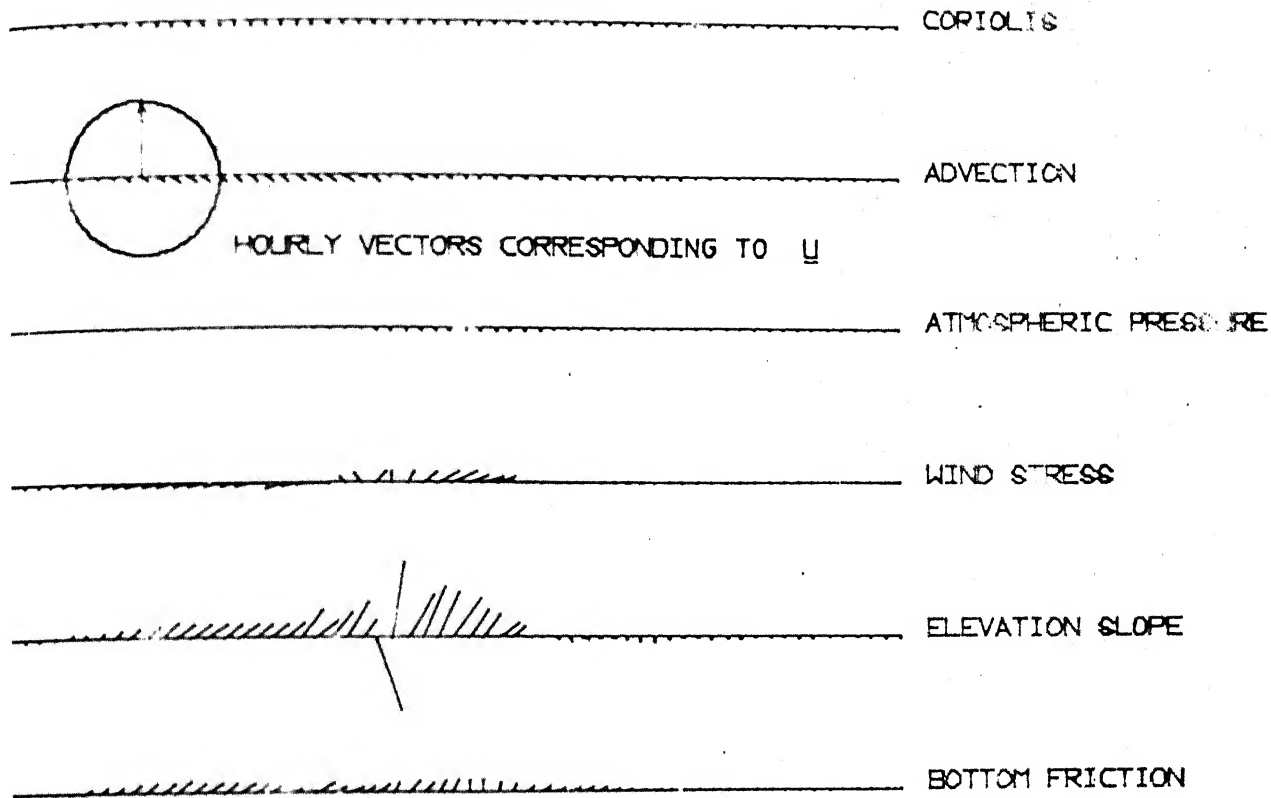
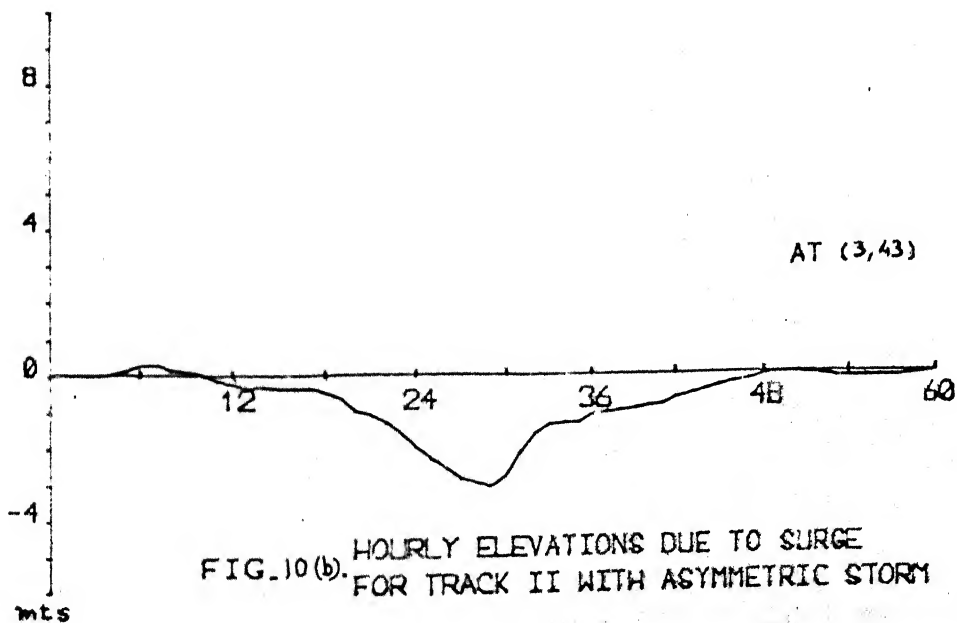
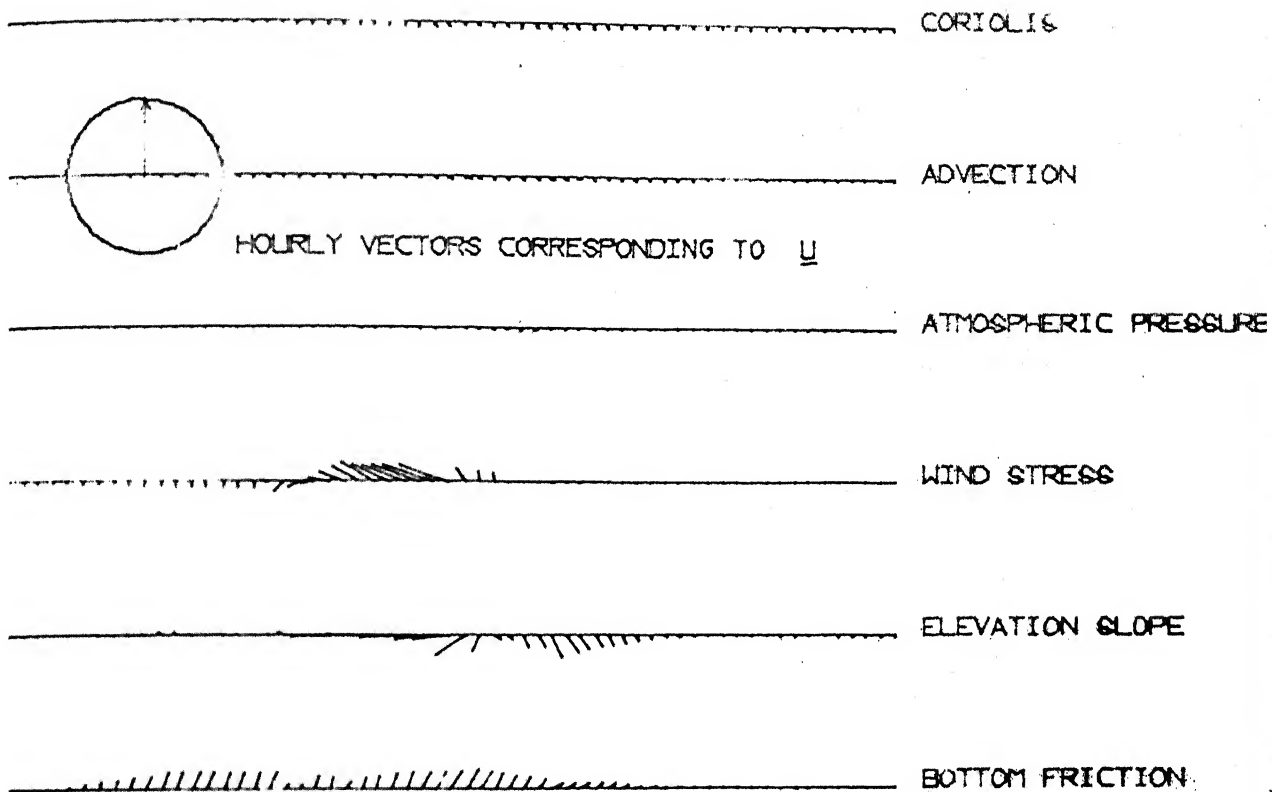


FIG. 10a. HOURLY ELEVATIONS DUE TO SURGE
FOR TRACK II WITH ASYMMETRIC STORM



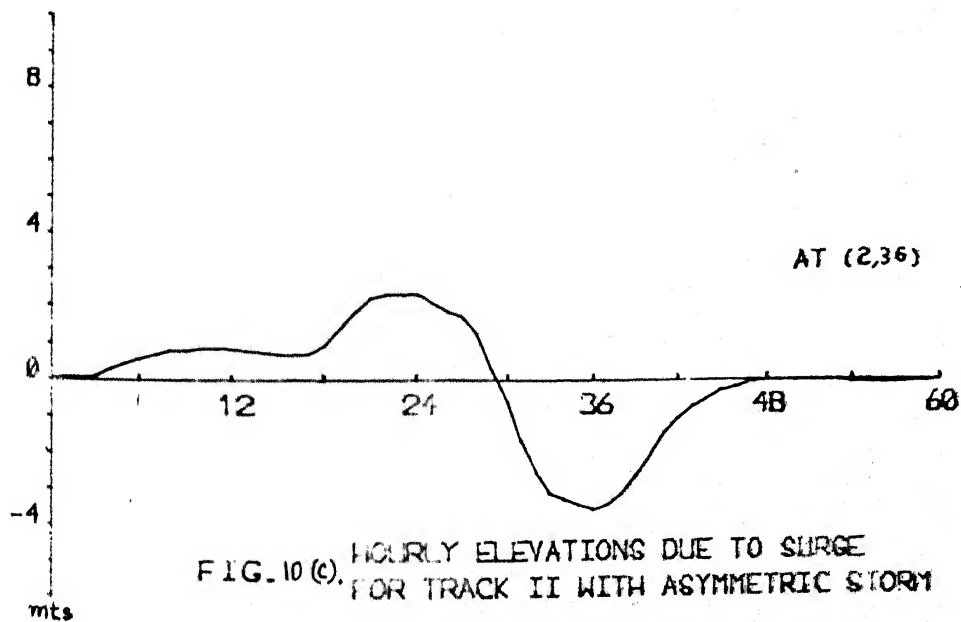
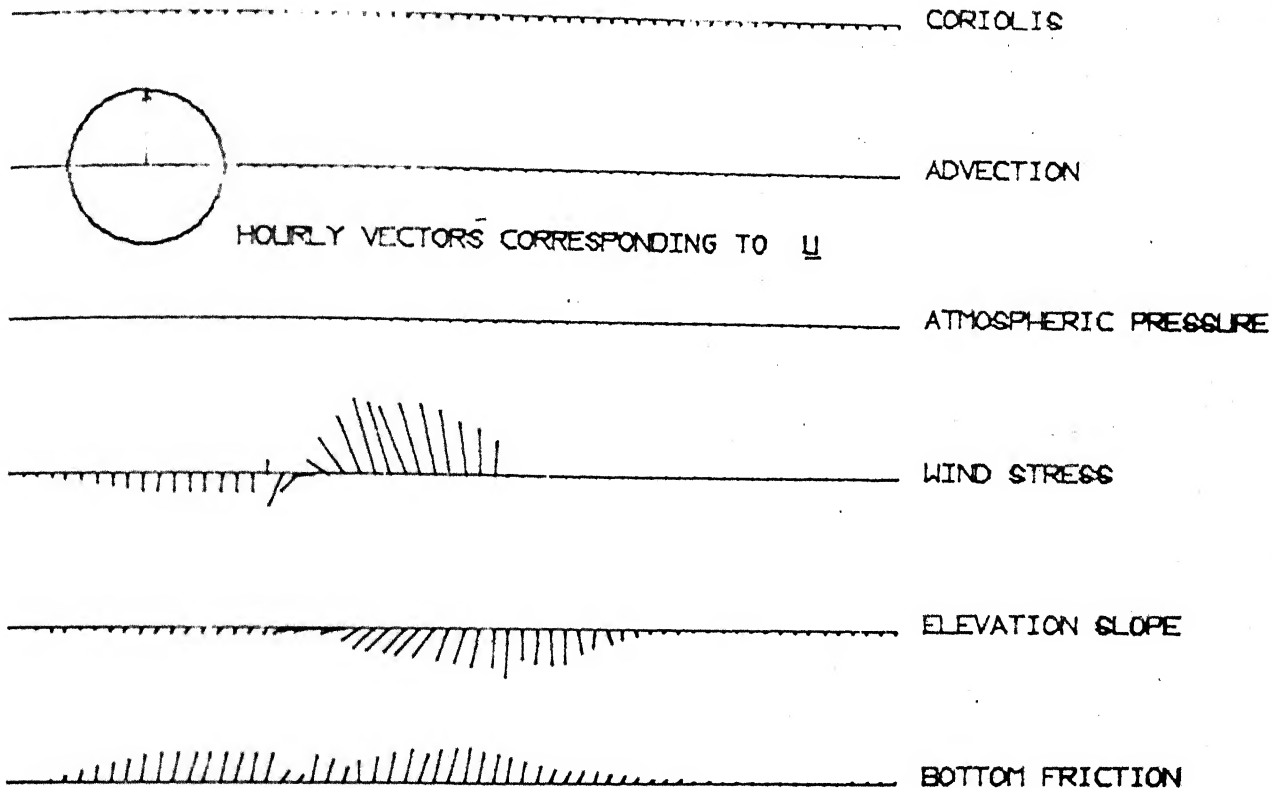


FIG. 10 (C). HOURLY ELEVATIONS DUE TO SURGE
FOR TRACK II WITH ASYMMETRIC STORM

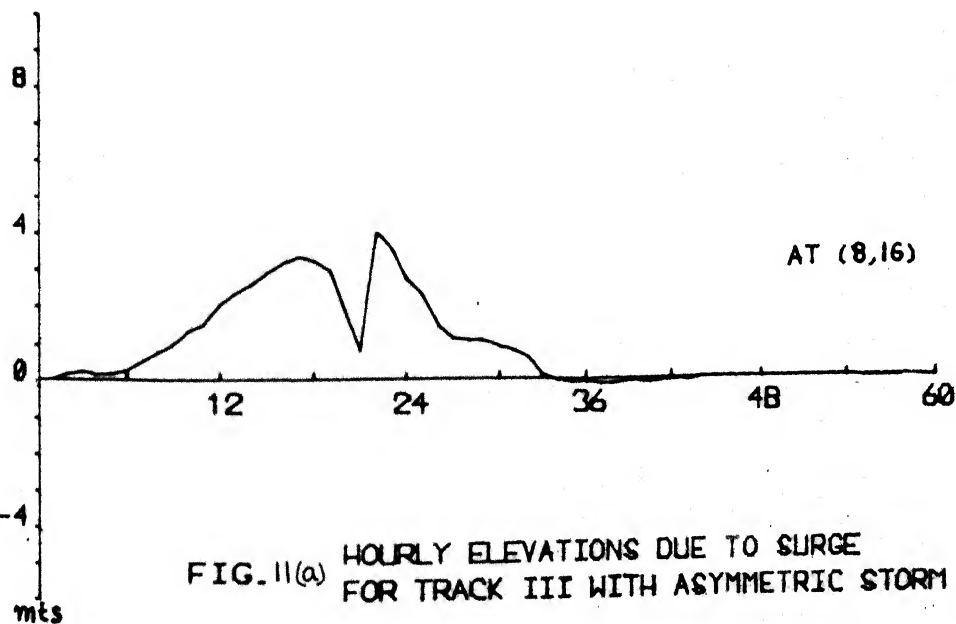
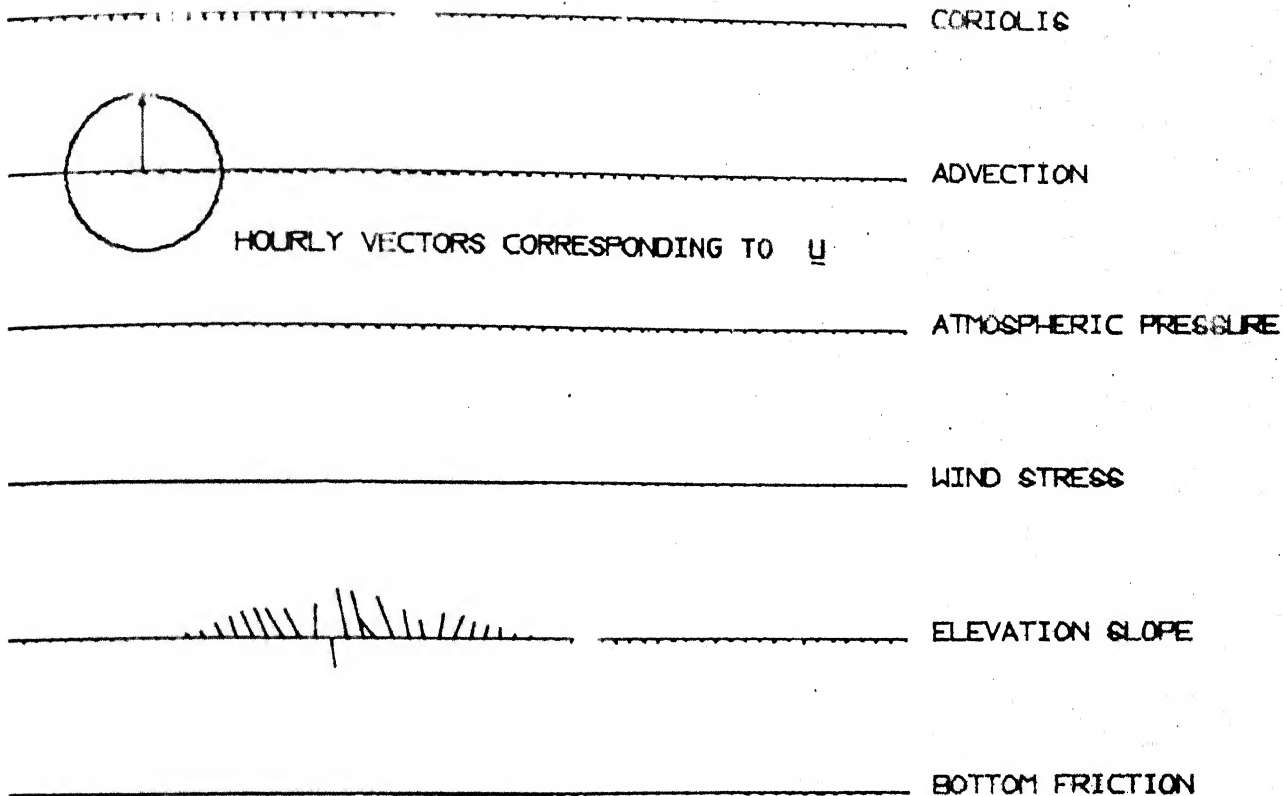
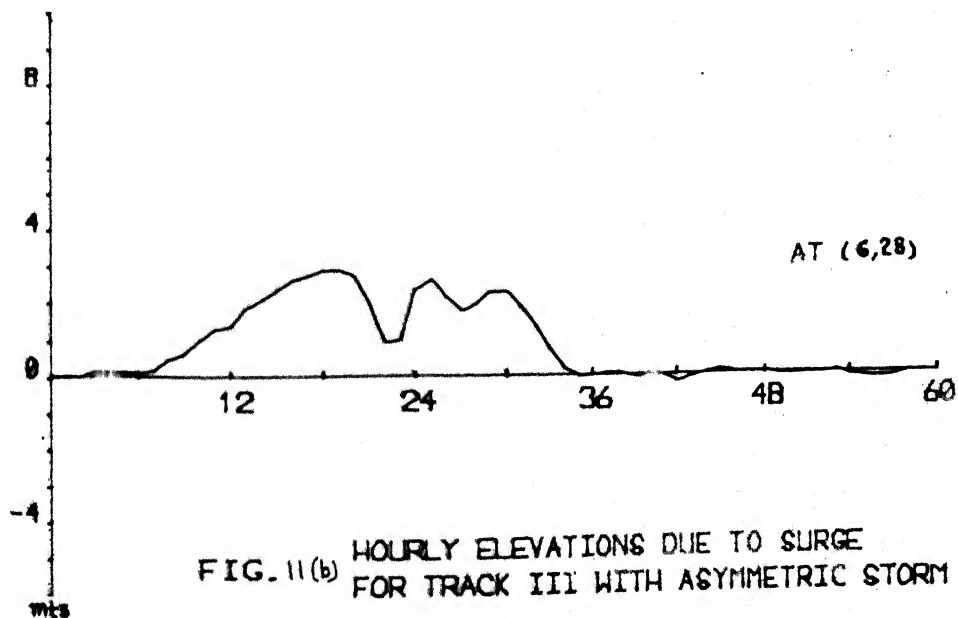
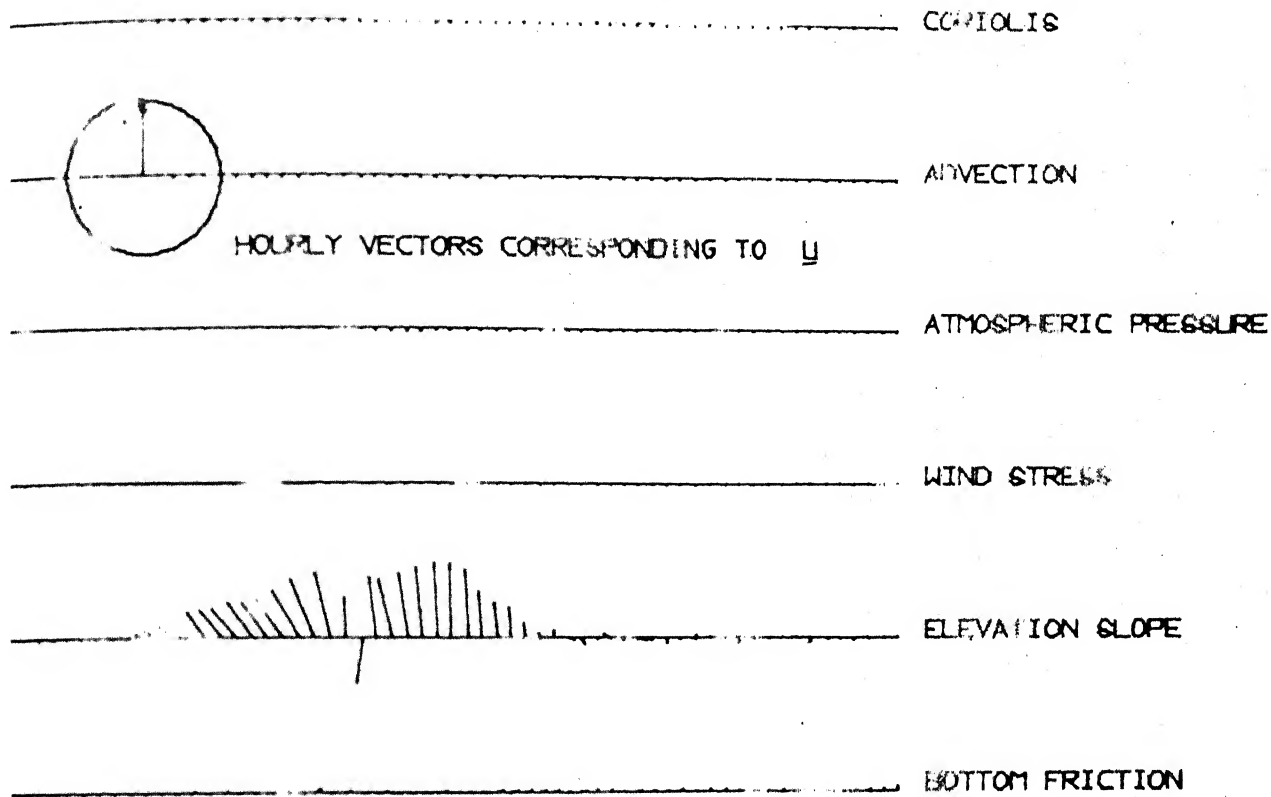


FIG. 11(a) HOURLY ELEVATIONS DUE TO SURGE
FOR TRACK III WITH ASYMMETRIC STORM



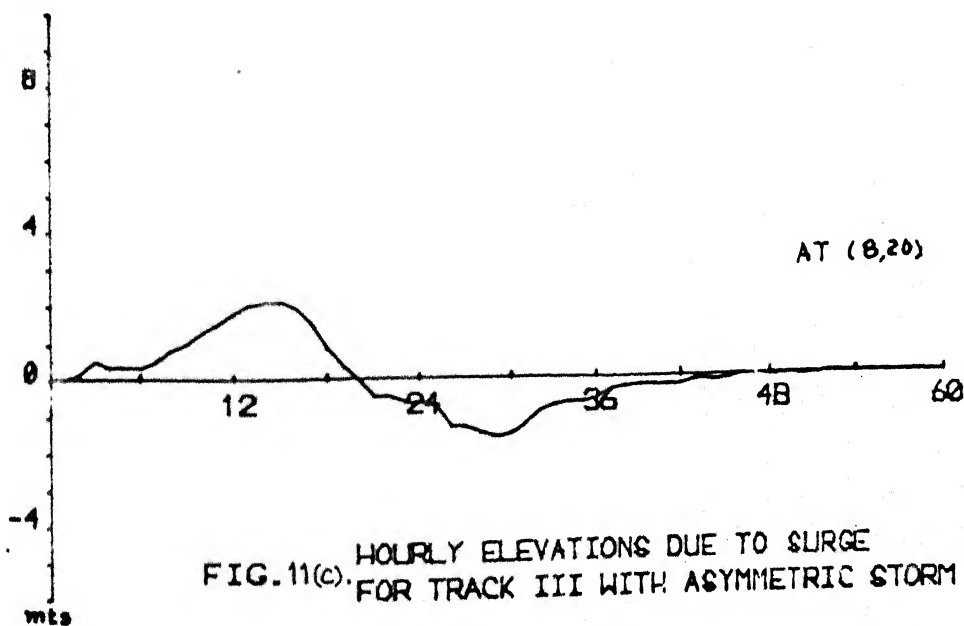
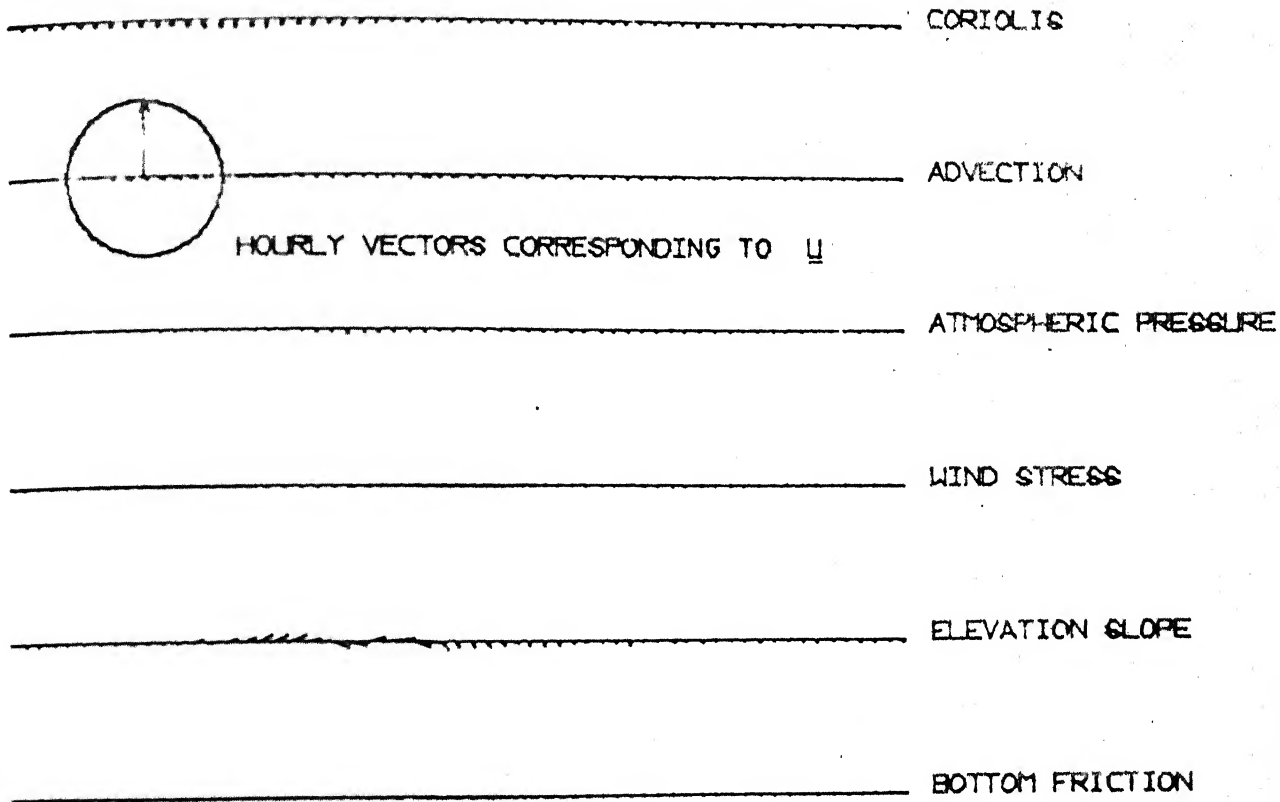


FIG. 11(c) HOURLY ELEVATIONS DUE TO SURGE
FOR TRACK III WITH ASYMMETRIC STORM

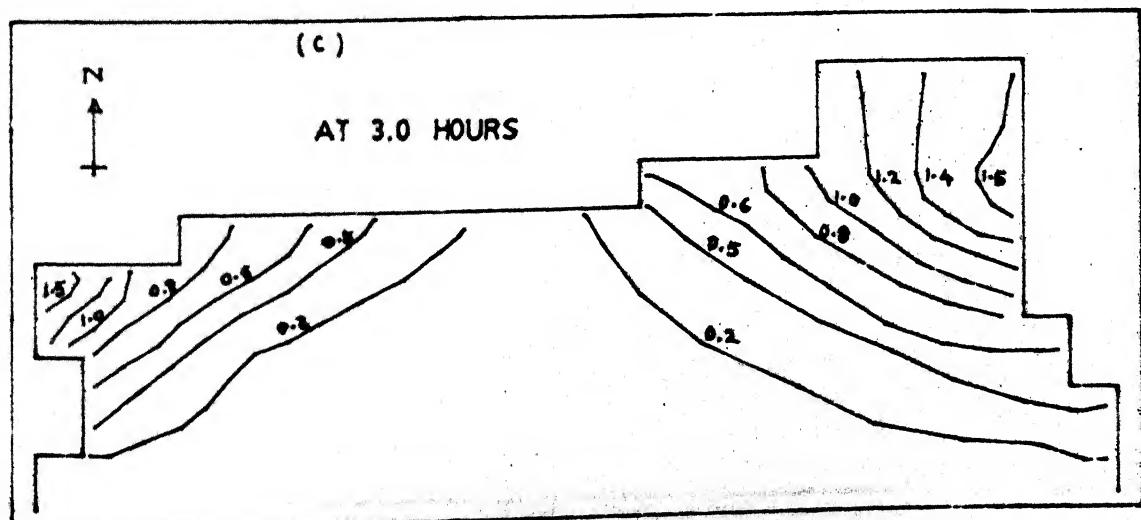
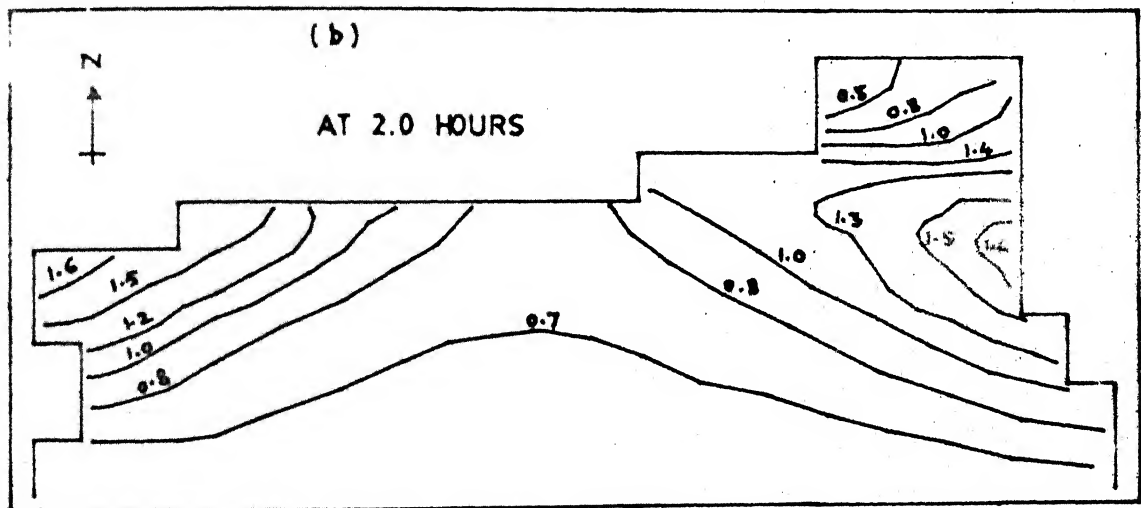
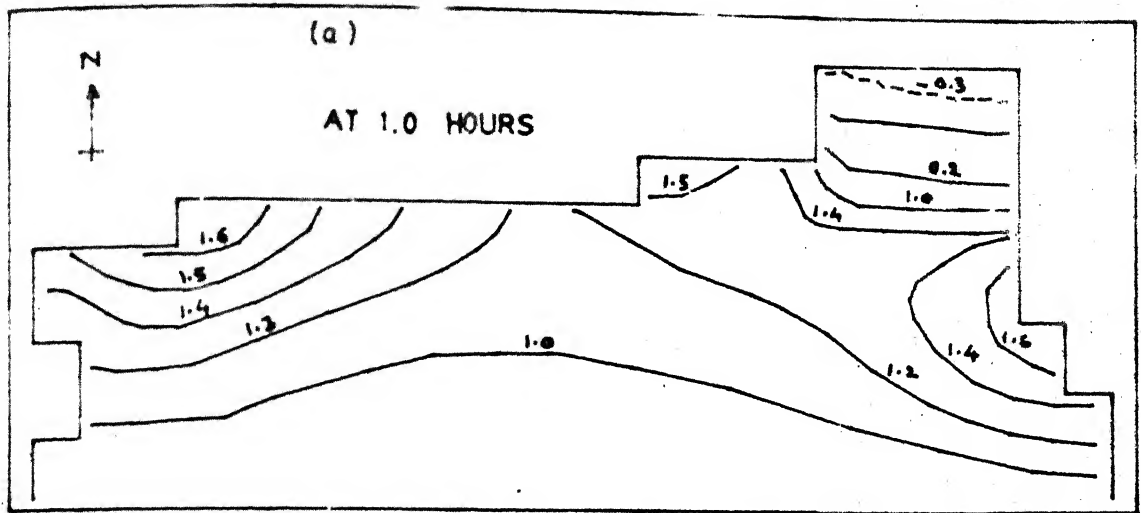


FIG.12.a,b,c

ELEVATION CONTOURS IN METERS
(AT LUNAR HOURS)

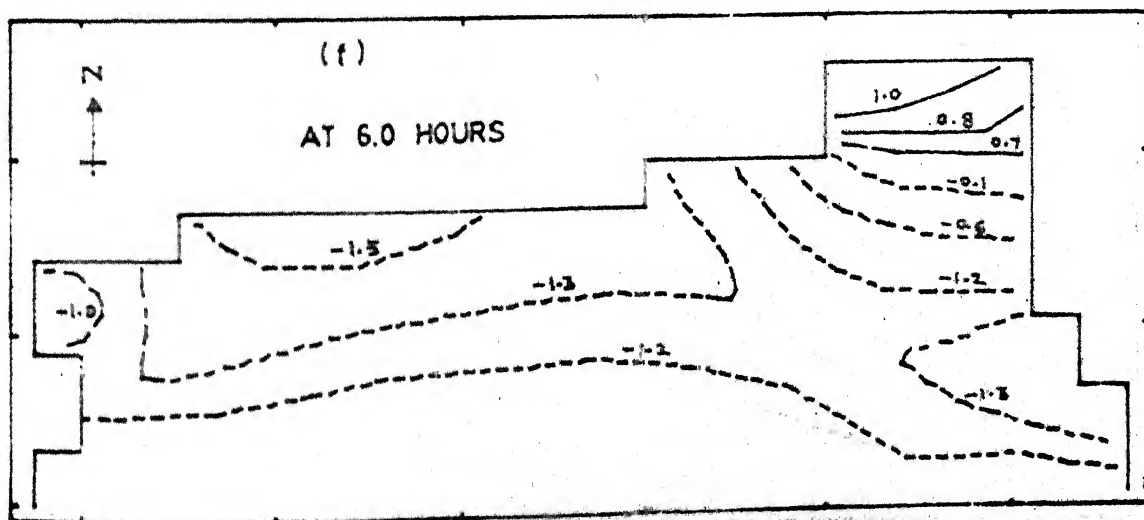
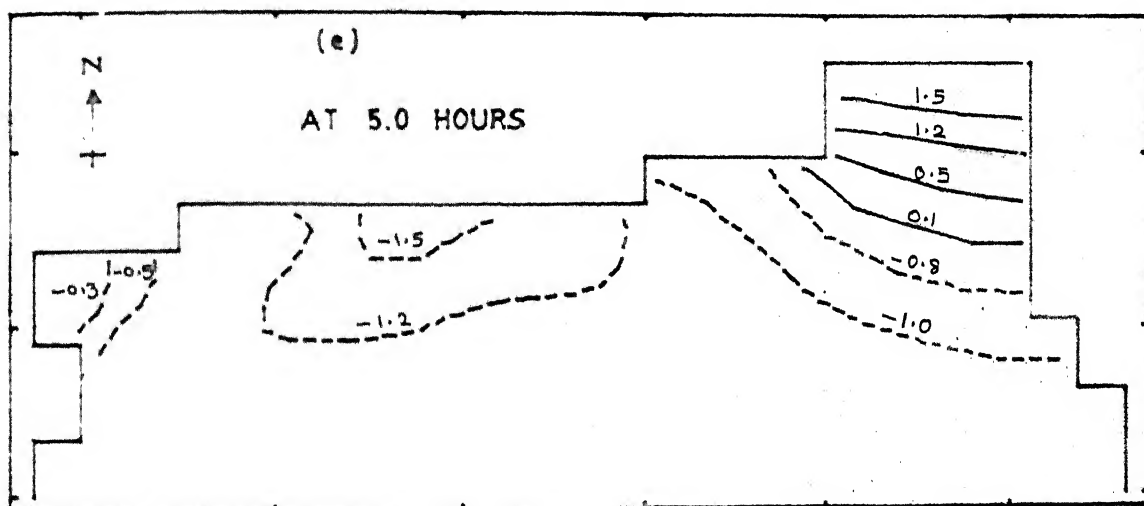
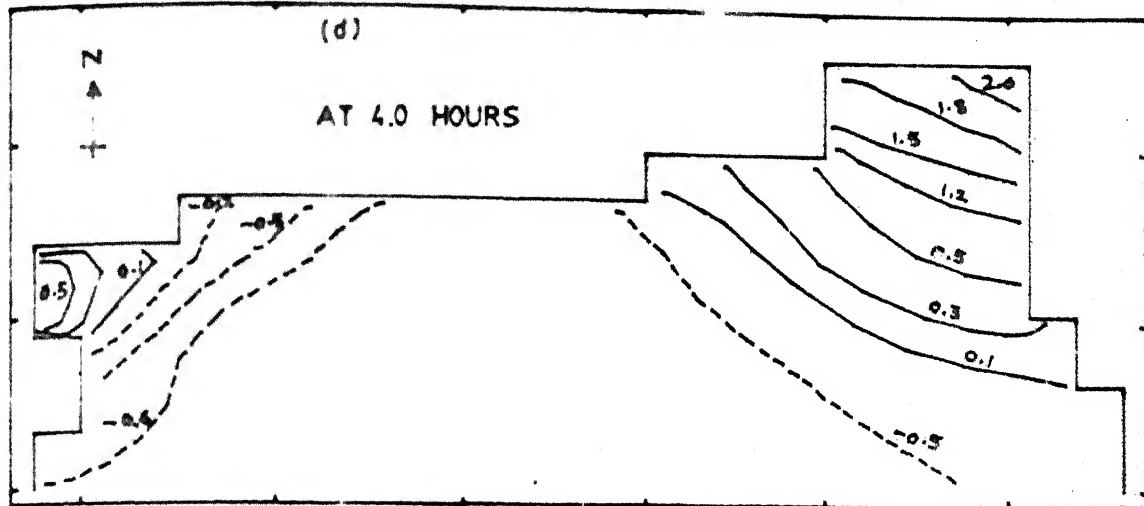


FIG.12. d,e,f

ELEVATION CONTOURS IN METERS
(AT LUNAR HOURS)

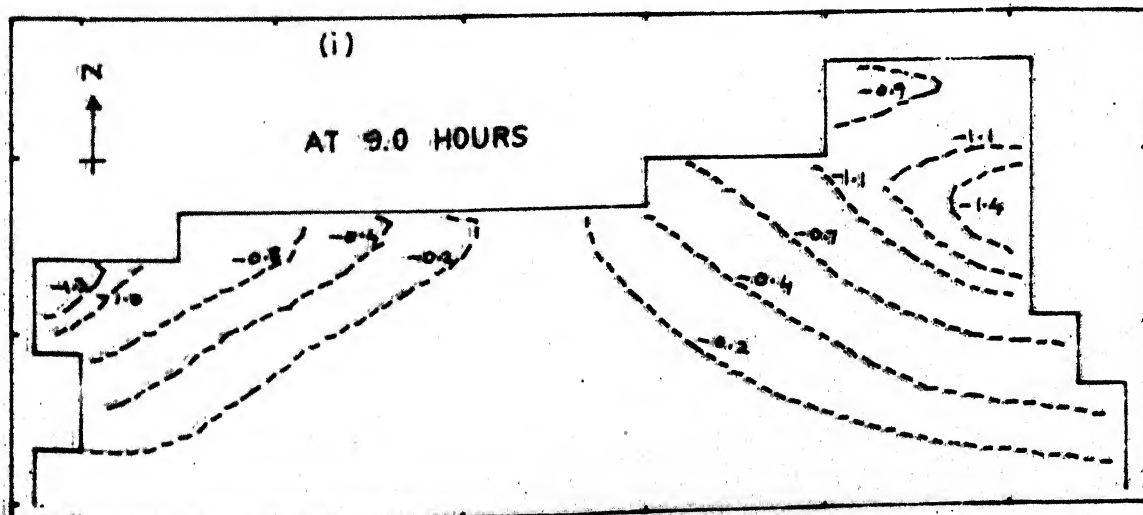
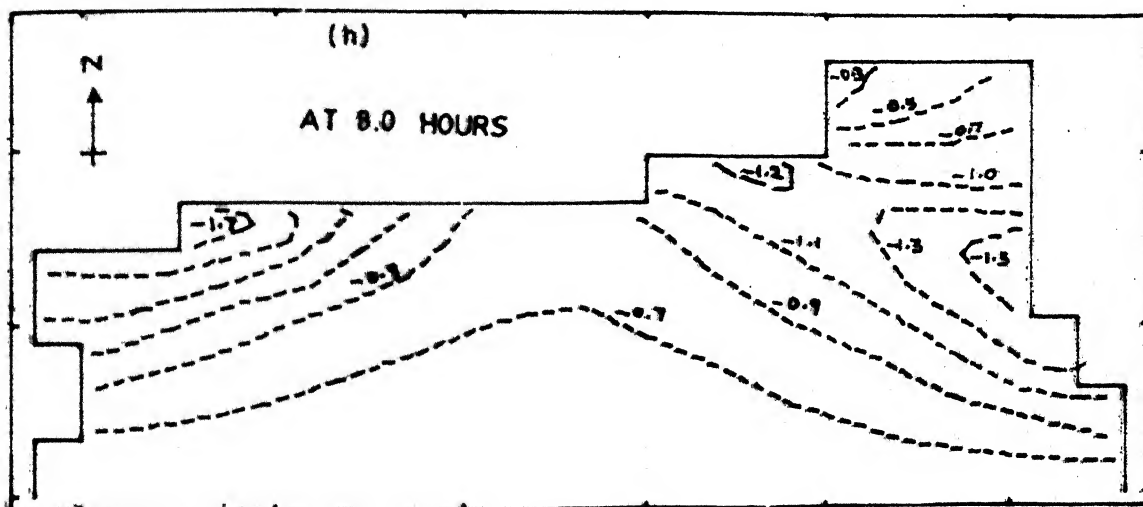
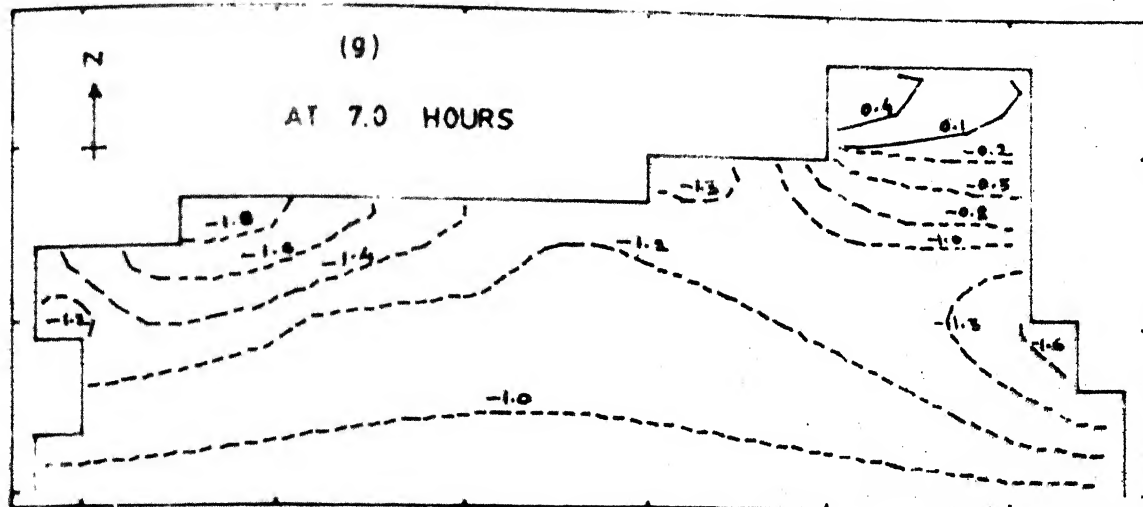


FIG. 12. g, h, i

ELEVATION CONTOURS IN METERS
(AT LUNAR HOURS)

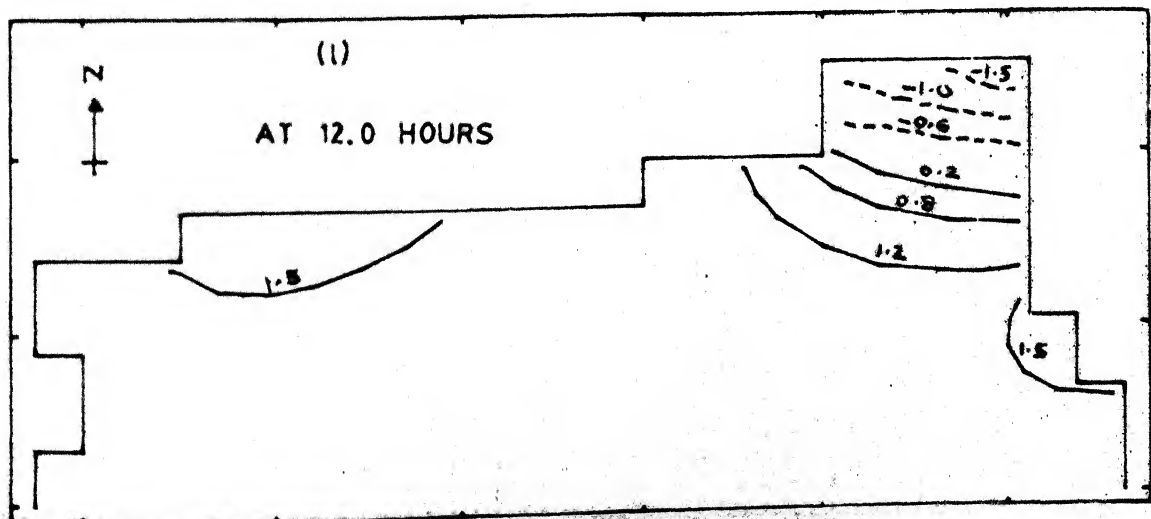
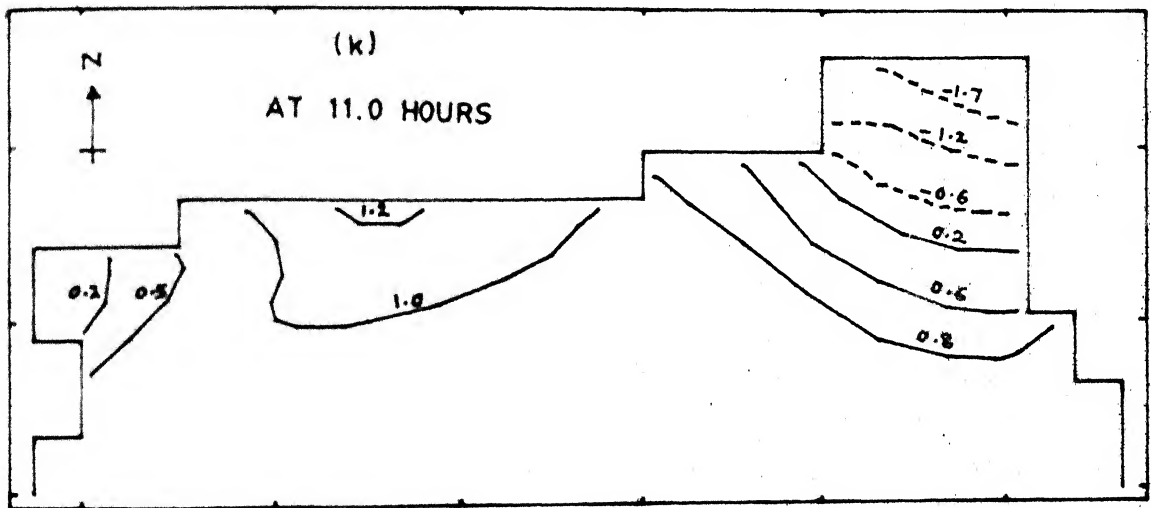
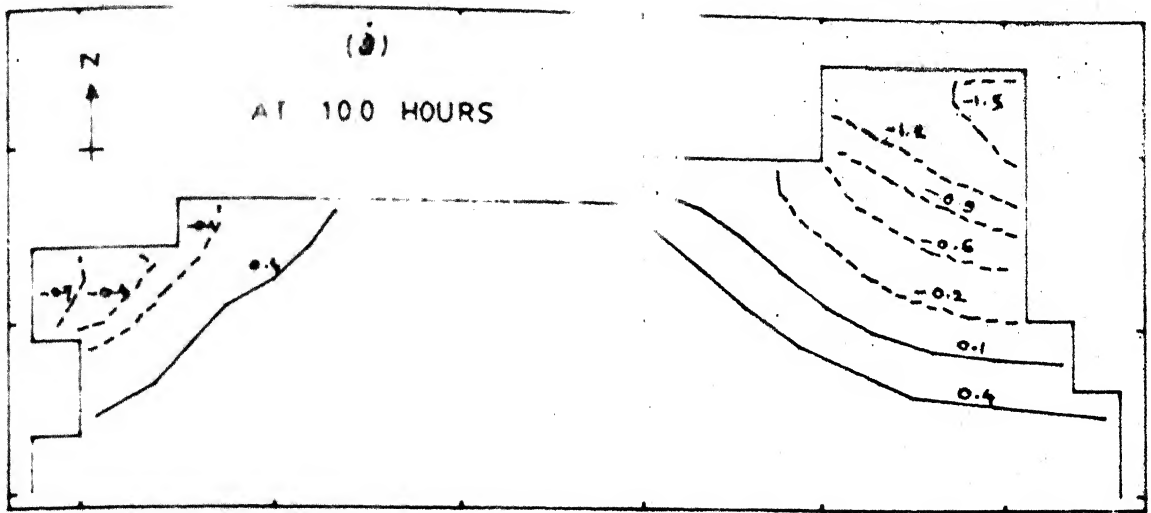


FIG.12.j,k,l

ELEVATION CONTOURS IN METERS
(AT LUNAR HOURS)

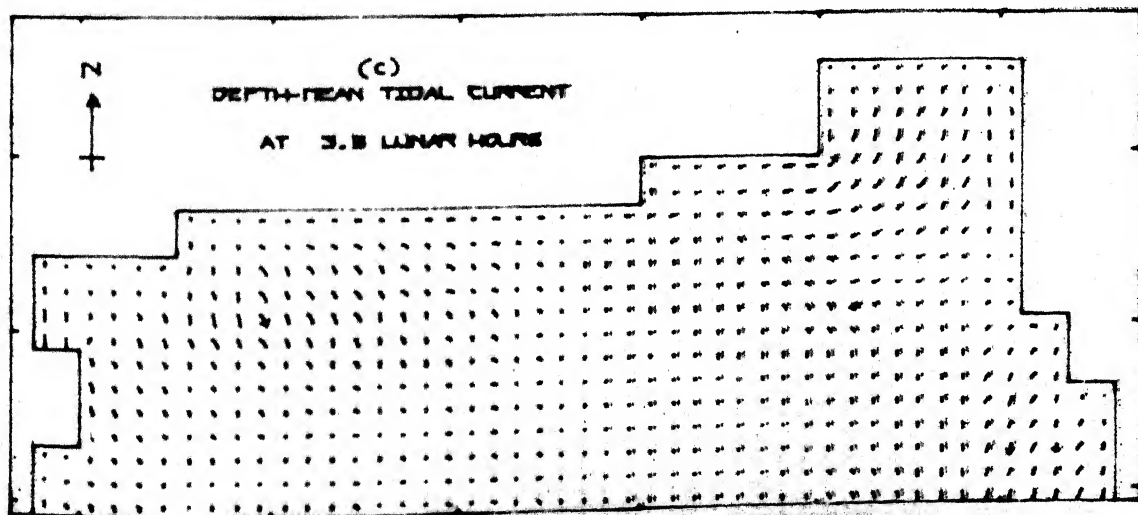
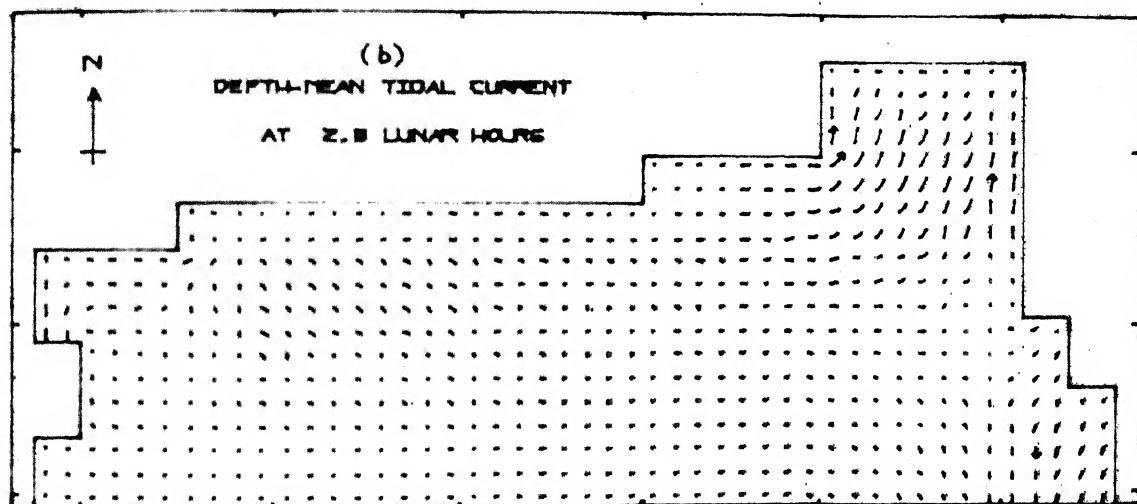
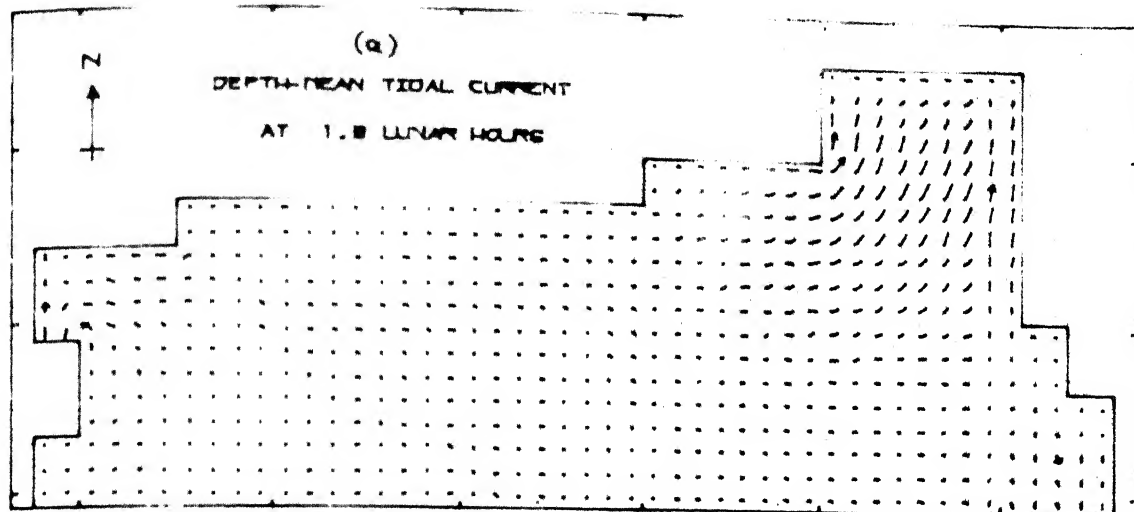
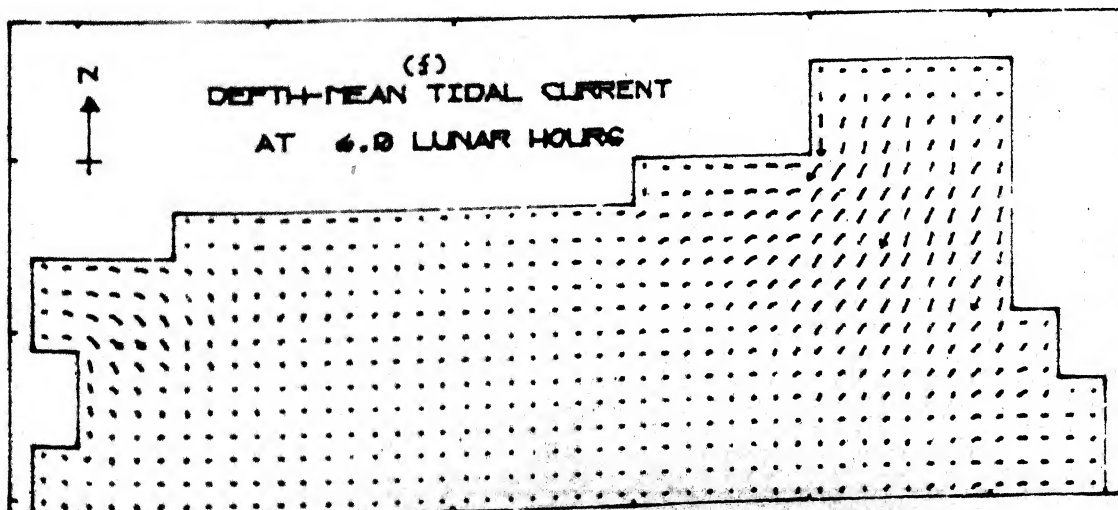
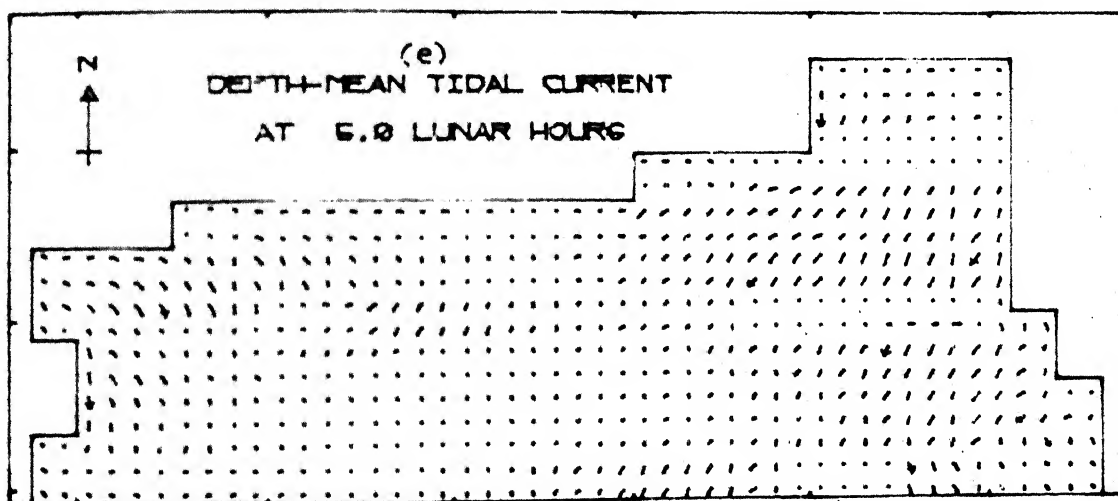
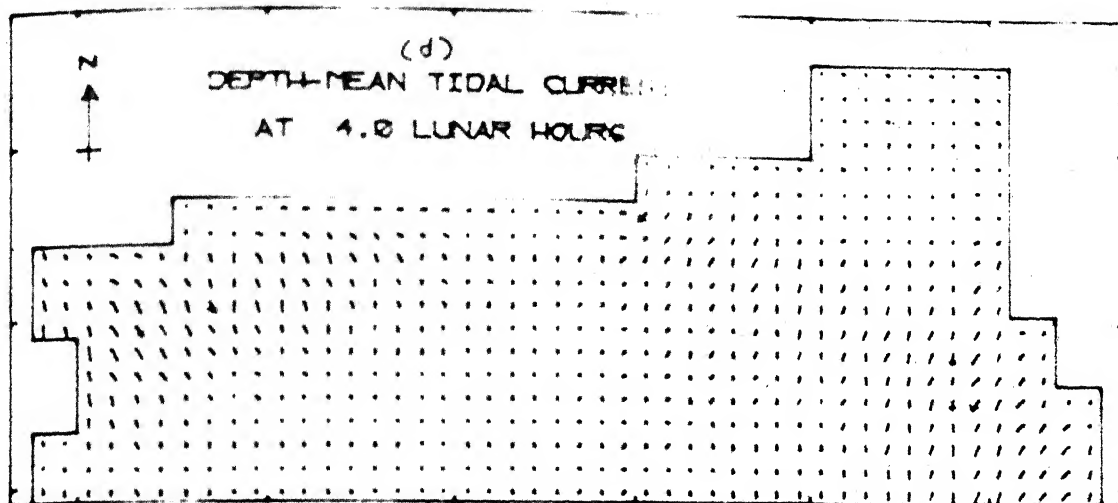


FIG.13.a,b,c

Current strength $\rightarrow = 2.0$ mt/sec



Current strength \rightarrow 2.0 mt/sec

FIG.13.d,e,f

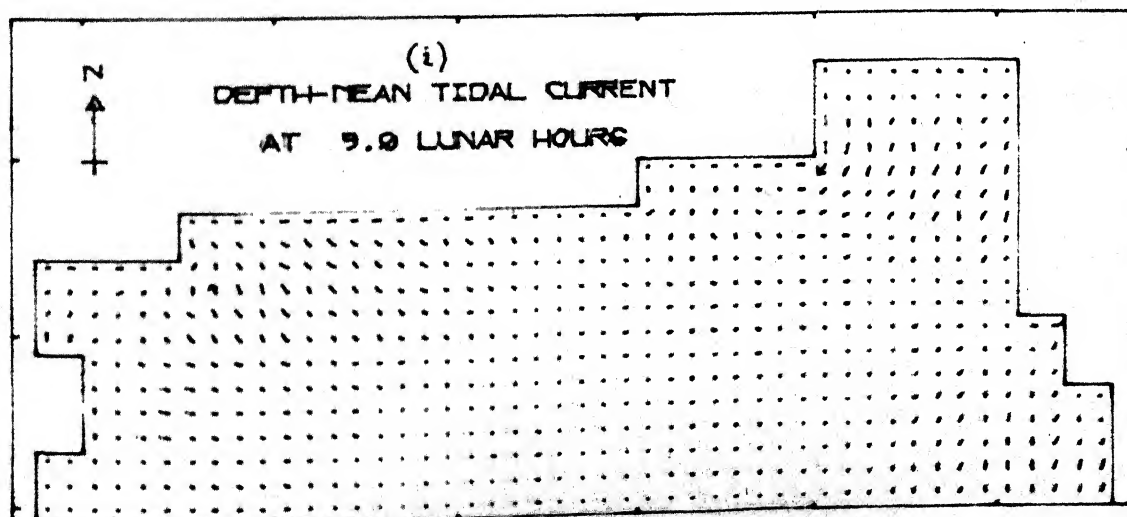
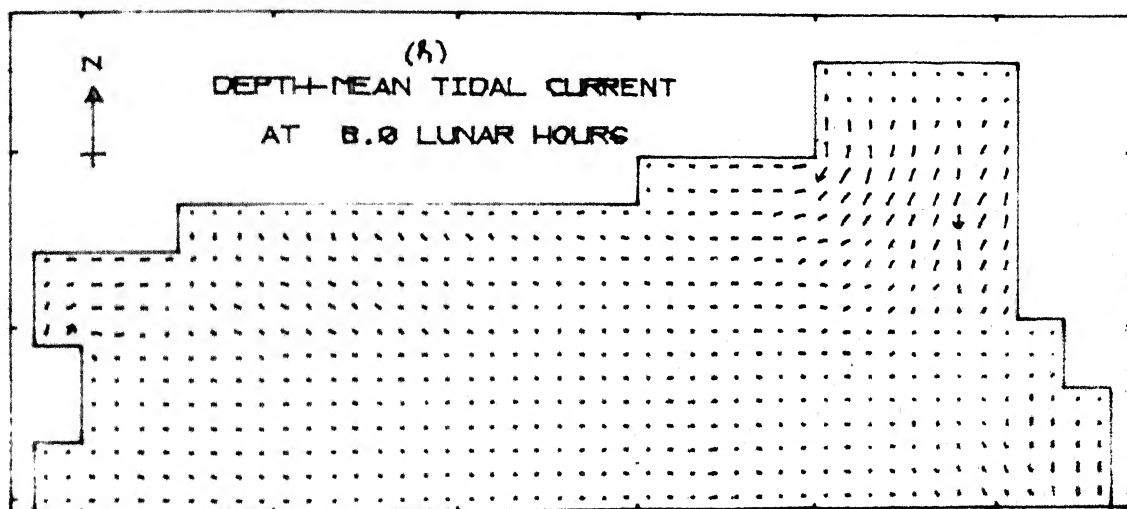
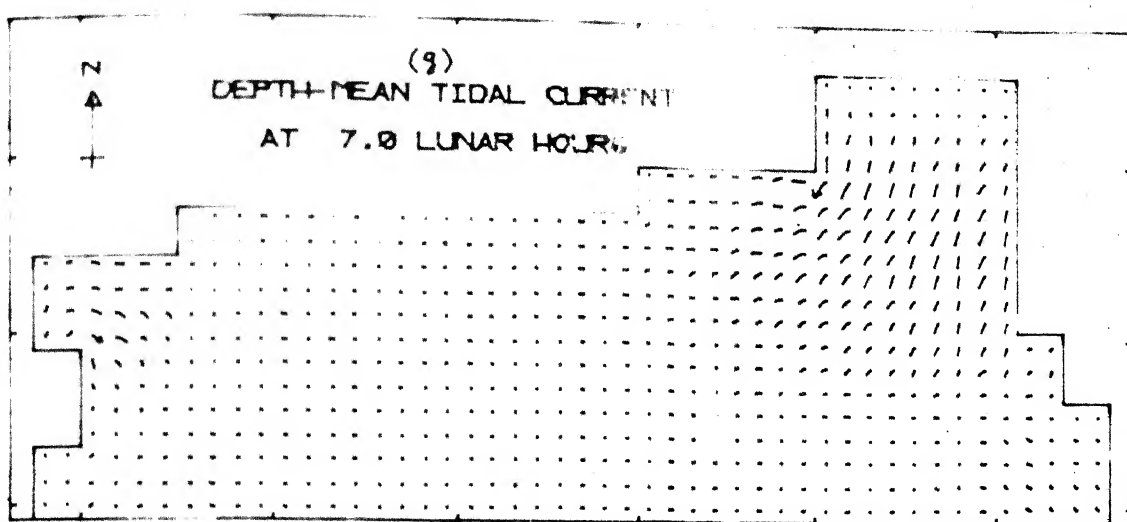


FIG. 13.g,h,i

Current strength $\rightarrow = 2.0$ m./sec

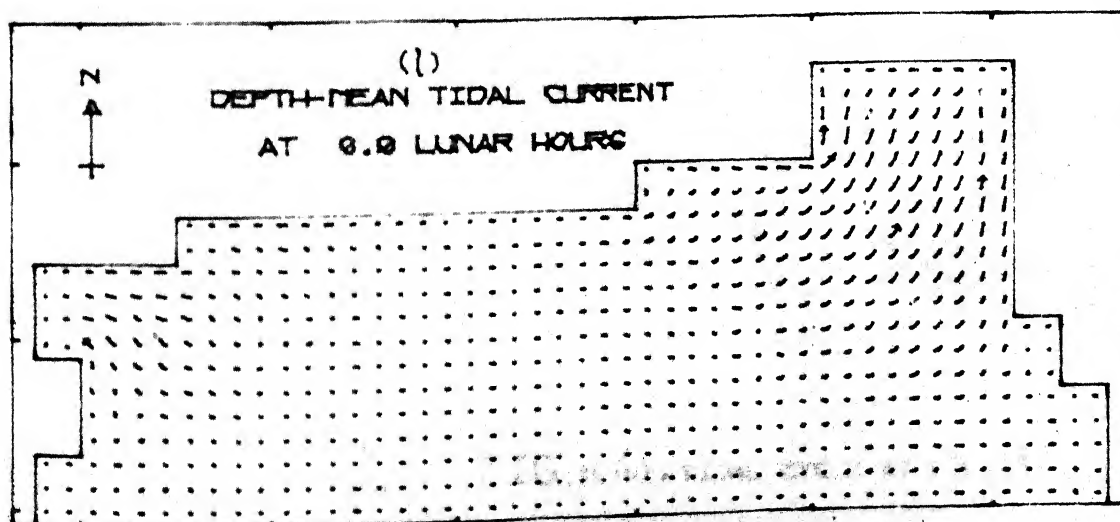
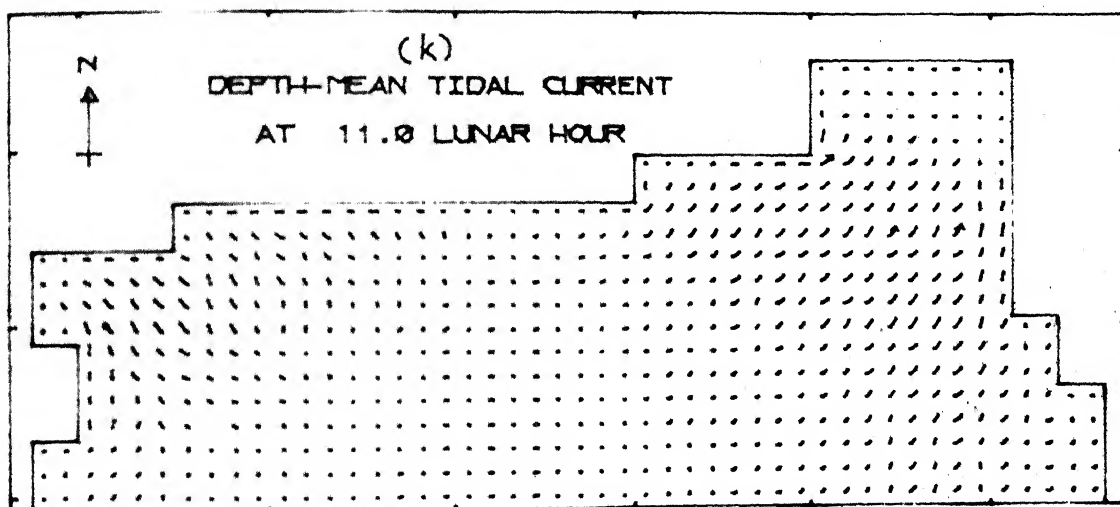
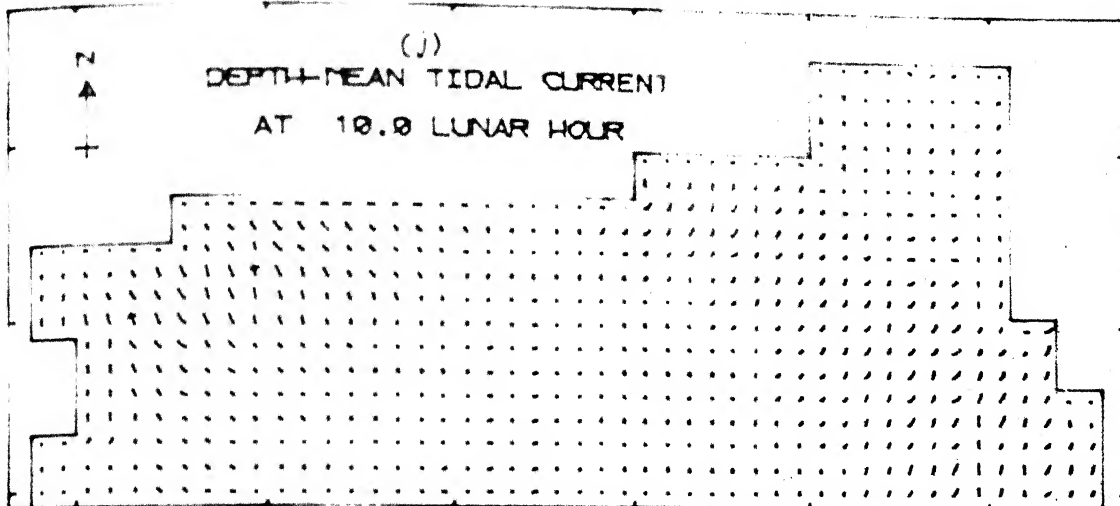
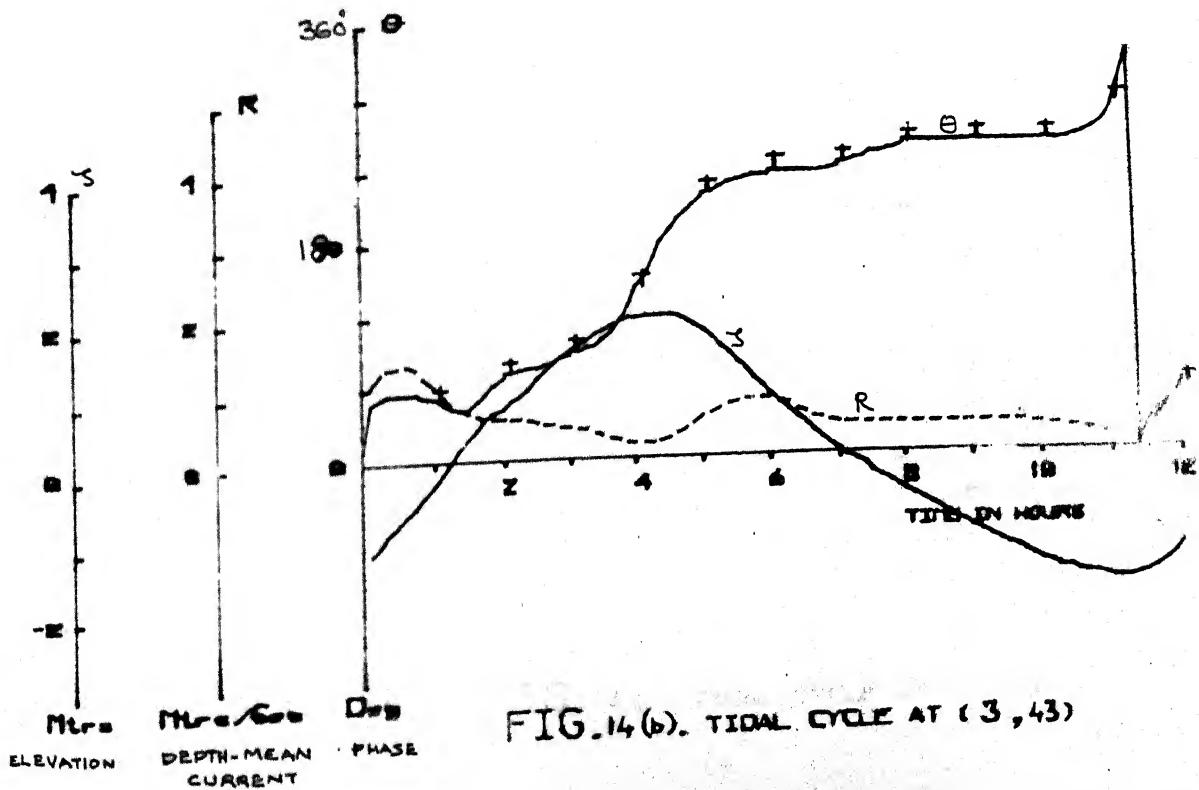
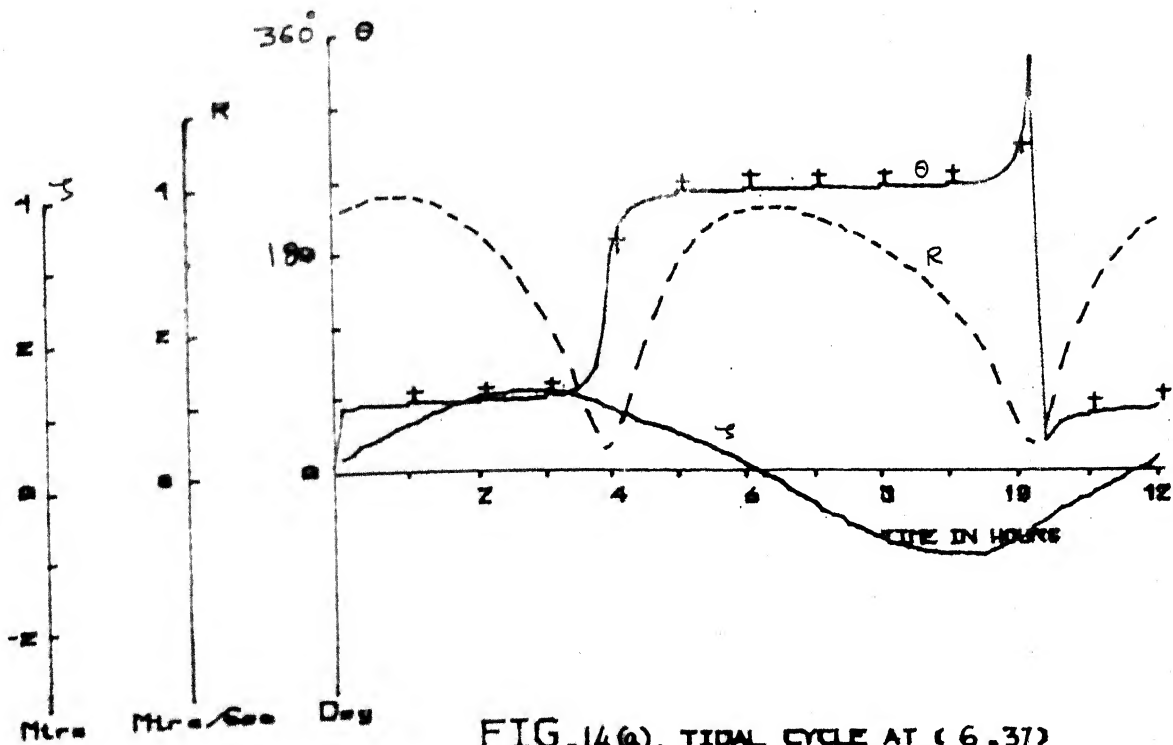


FIG.13.j,k,l

Current strength $\rightarrow = 2.0$ mt/sec



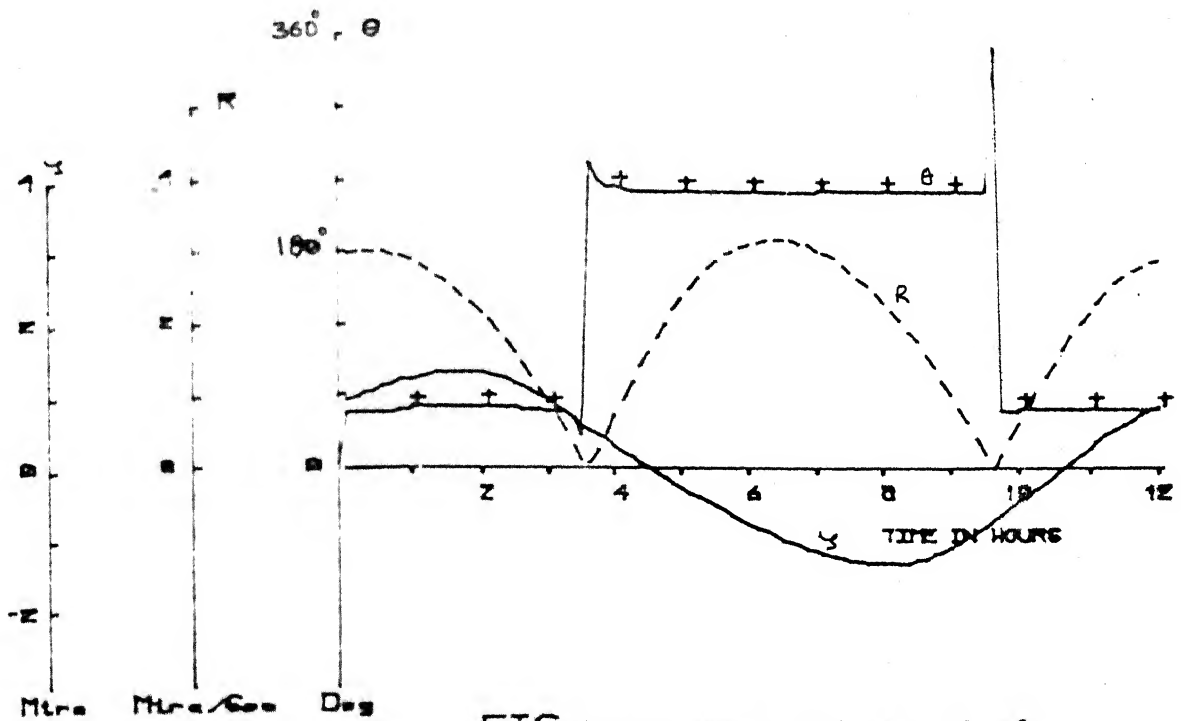


FIG.14(c). TIDAL CYCLE AT (9,38)

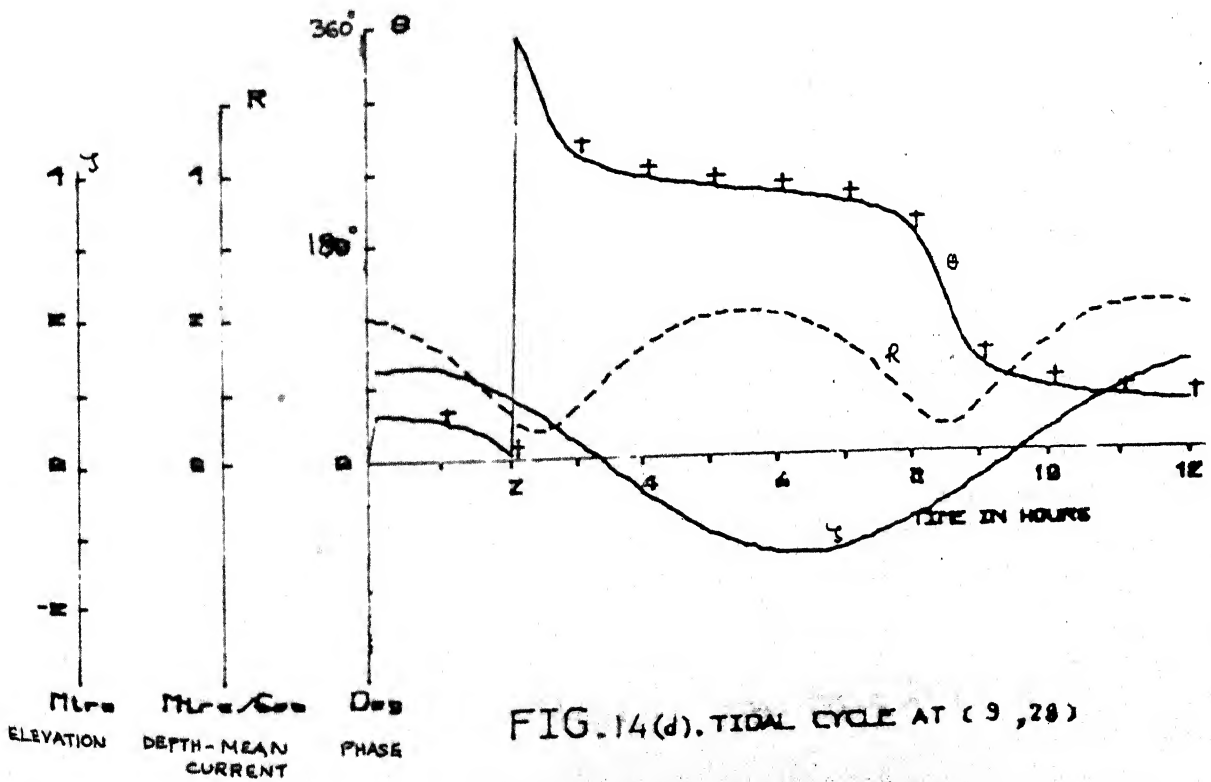
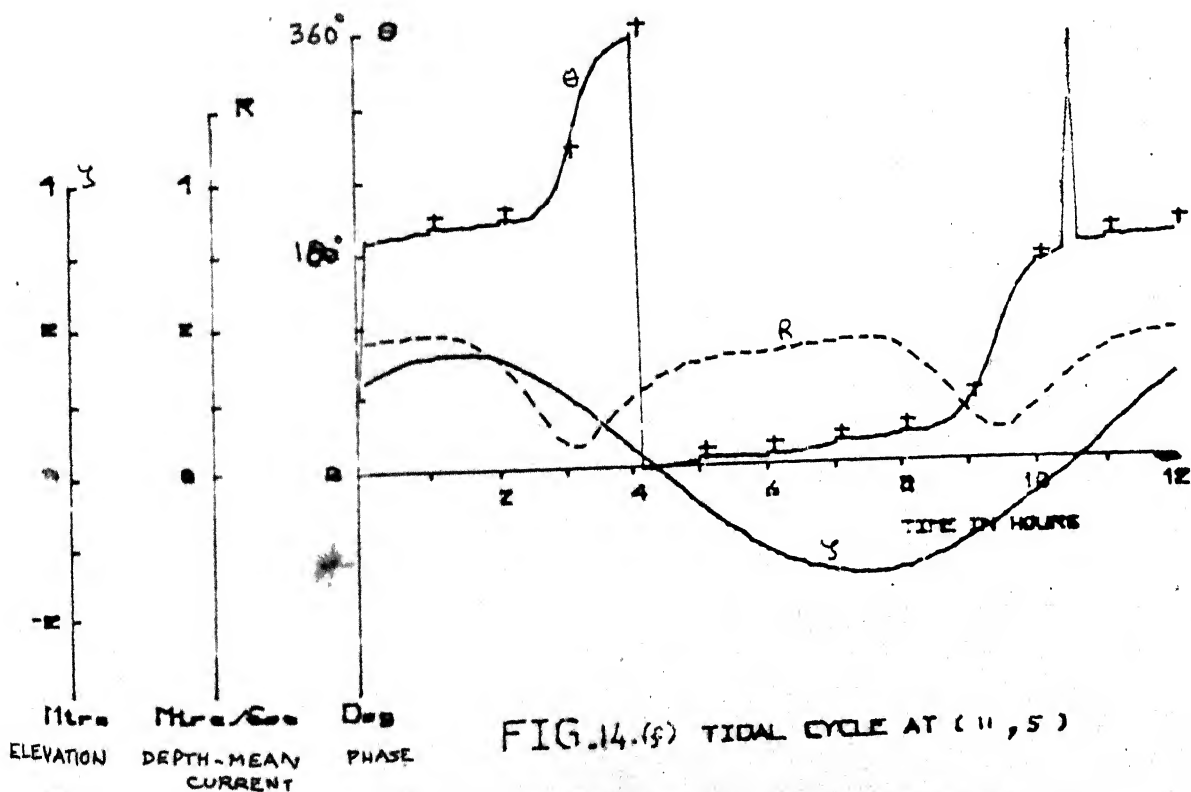
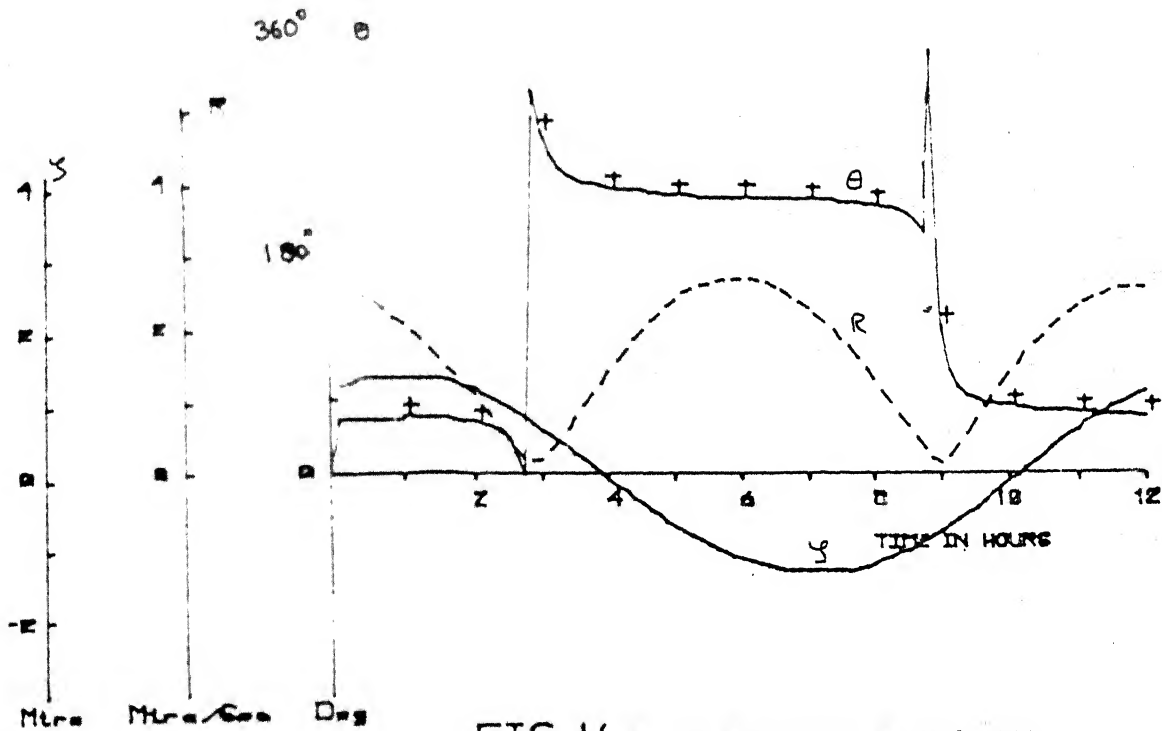
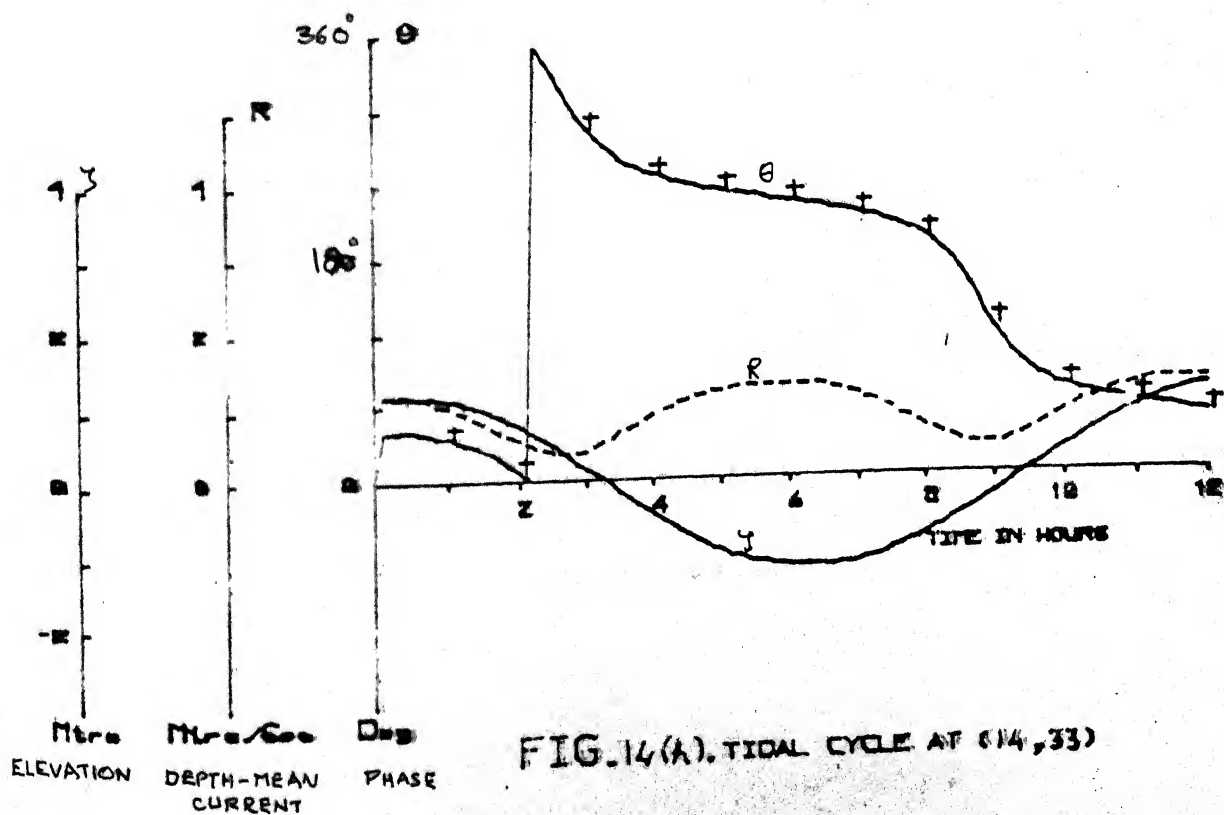
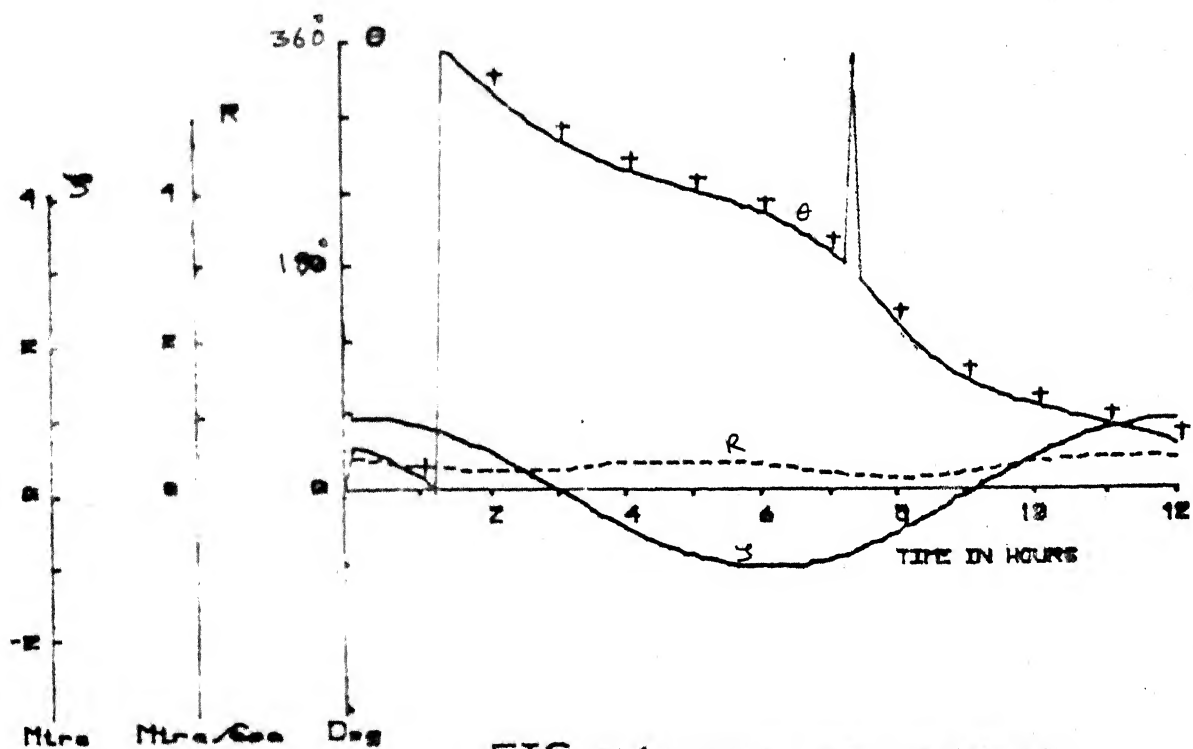


FIG.14(d). TIDAL CYCLE AT (9,28)





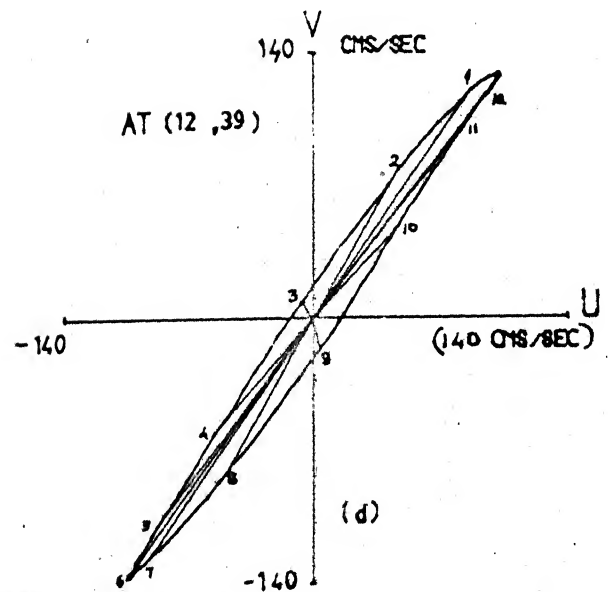
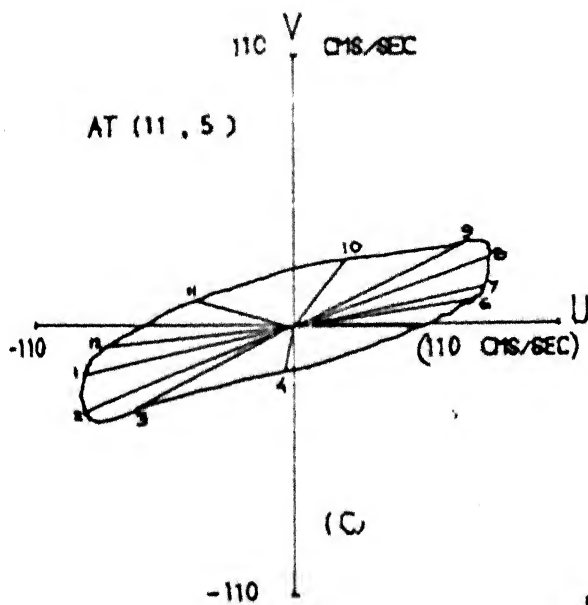
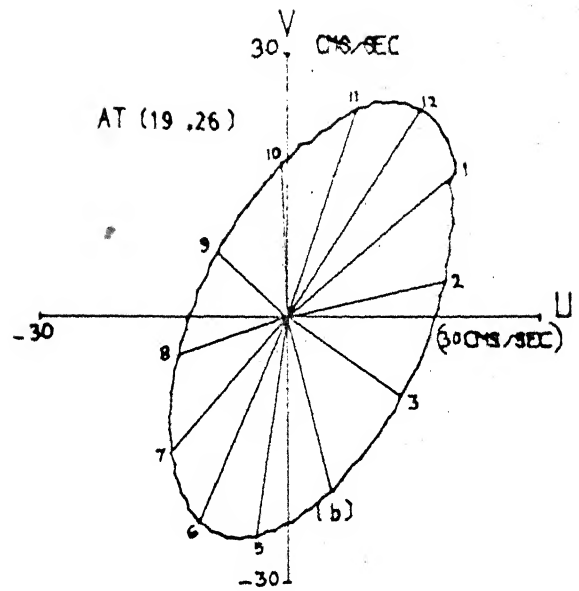
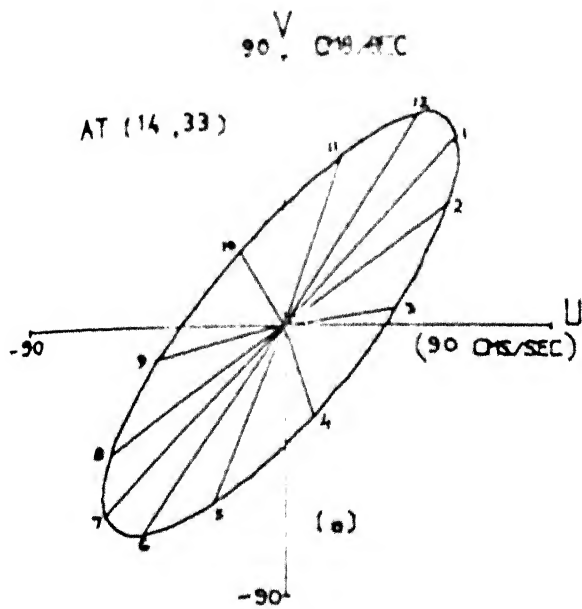


FIG.15. a,b,c,d
Depth mean current Ellipses
For the computed tide.

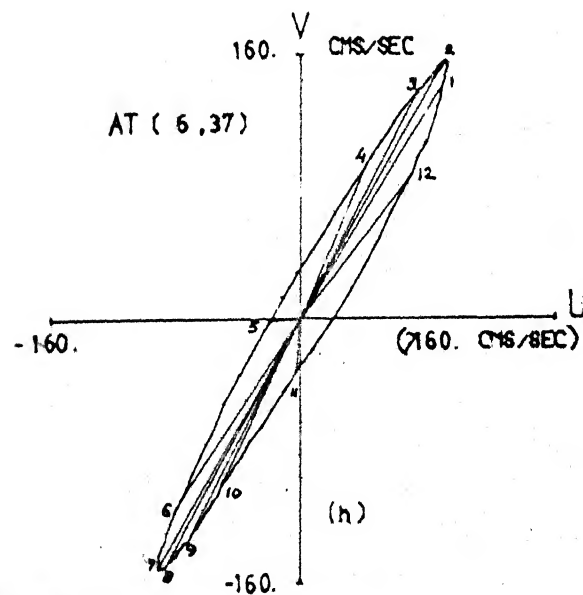
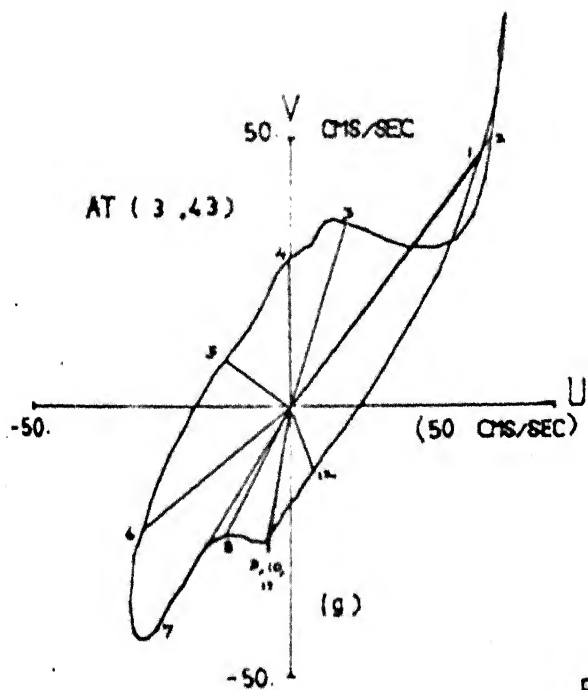
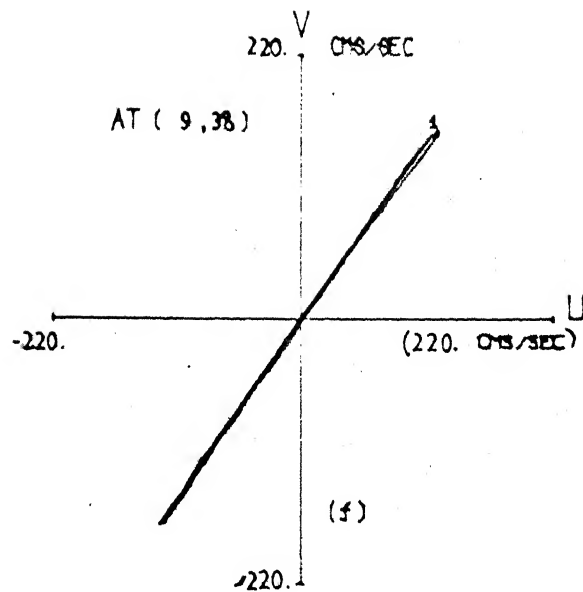
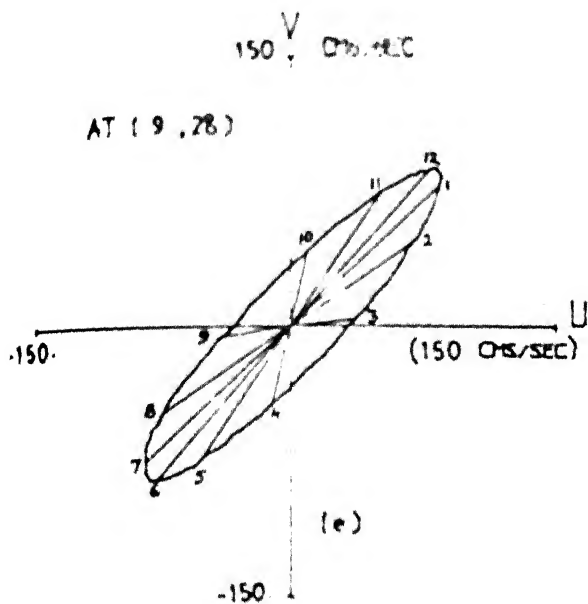
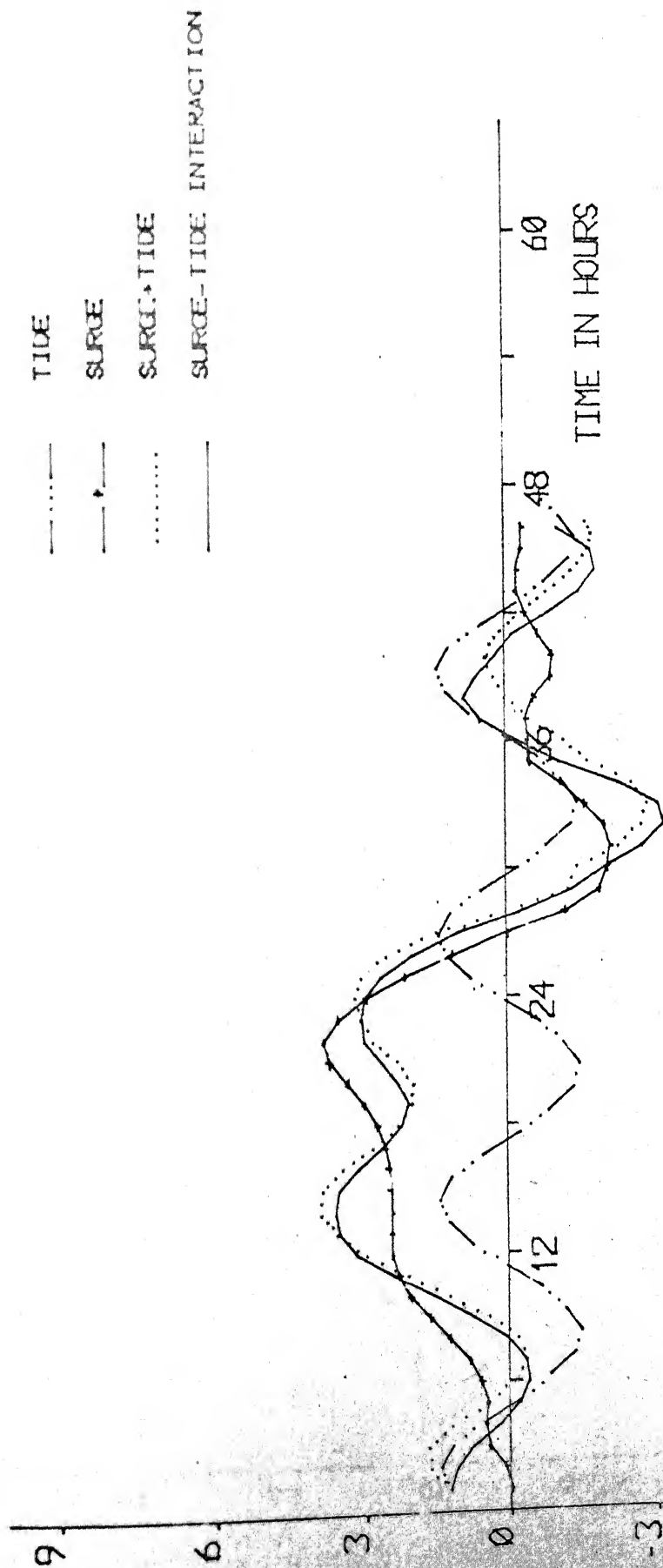


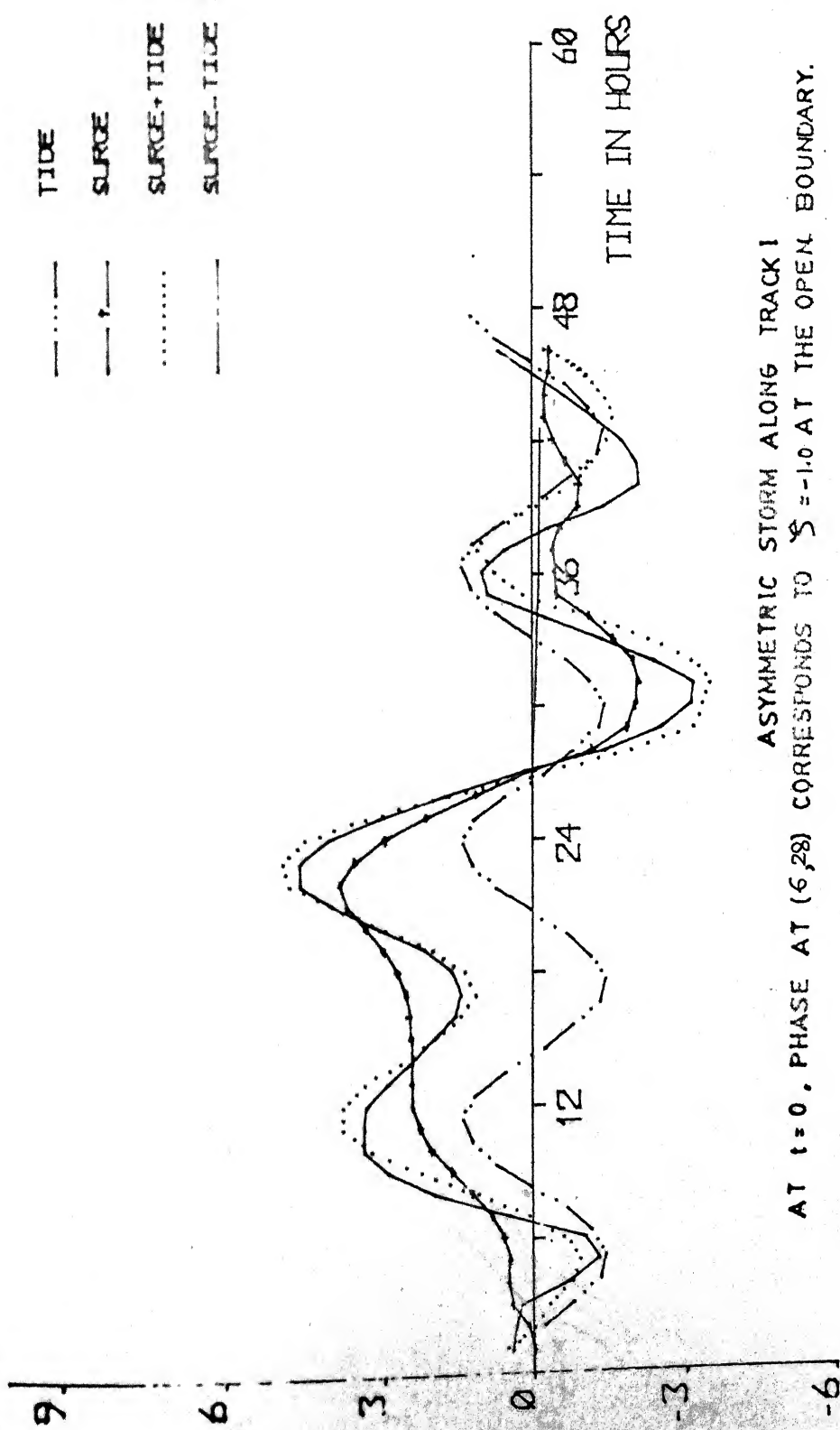
FIG.15. e,f,g,h
Depth mean current Ellipses
For the computed tide.



ASYMMETRIC STORM ALONG TRACK I
 AT $t=0$, PHASE AT (6,28) CORRESPONDS TO $S=0$ AT THE OPEN BOUNDARY.

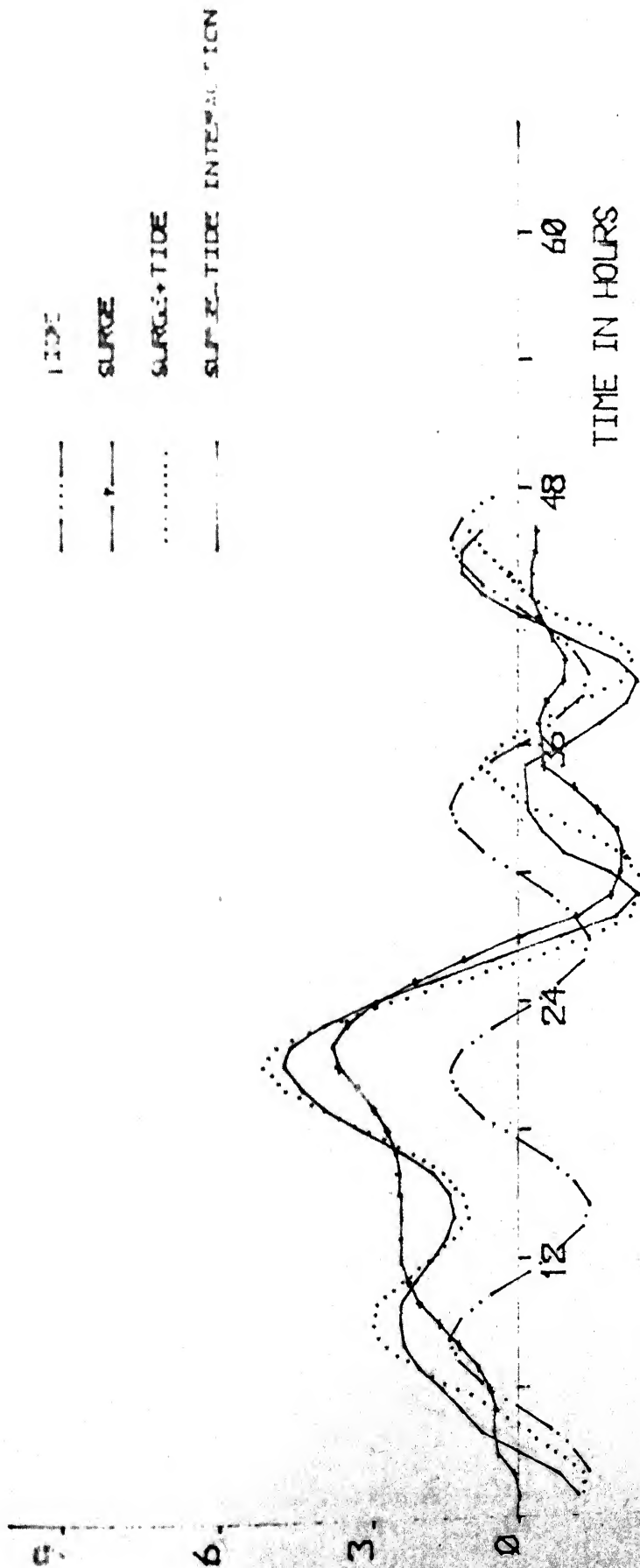
FIG. 16. (a) TIDE-SURGE INTERACTION AT (6,28)

Mtr 8



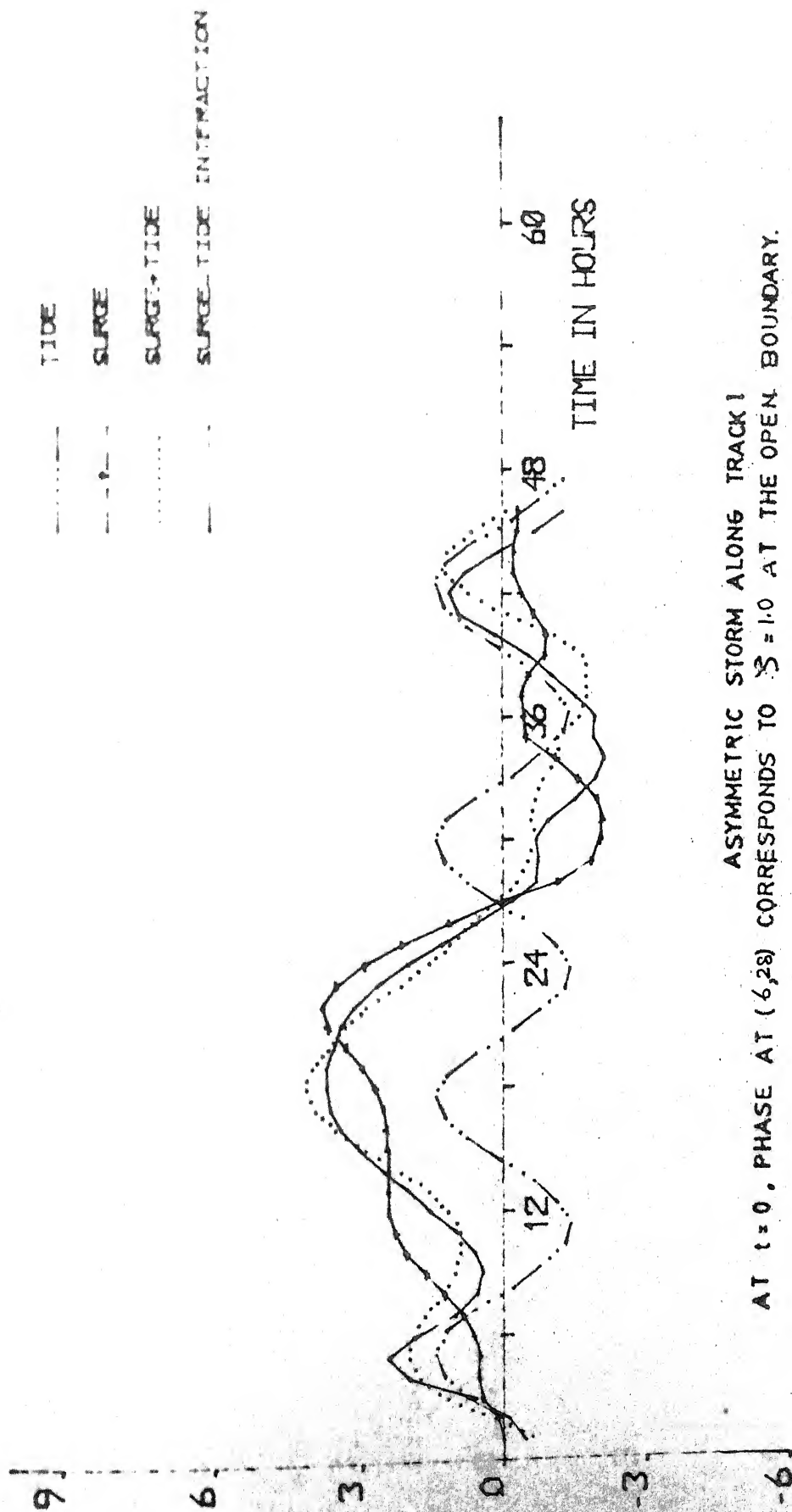
ASYMMETRIC STORM ALONG TRACK I
 AT $t=0$, PHASE AT (6,28) CORRESPONDS TO $S=-1.0$ AT THE OPEN BOUNDARY.

Mtrs
 FIG.16.(b) TIDE-SURGE INTERACTION AT (6,28)



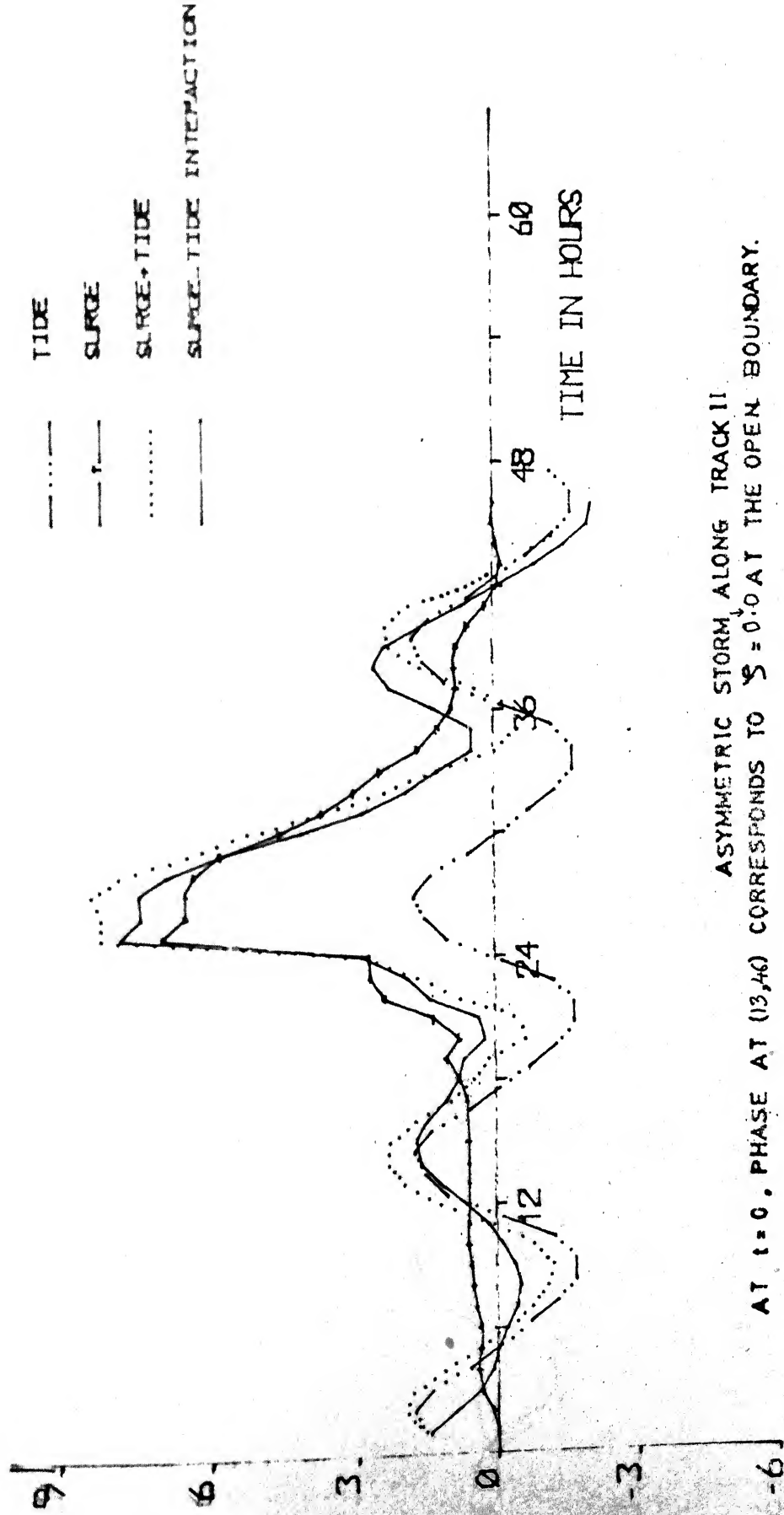
ASYMMETRIC STORM ALONG TRACK I
 AT $t=0$, PHASE AT (6,28) CORRESPONDS TO $S=0.0$ AT THE OPEN BOUNDARY.

Mtrs
 FIG. 16.(c). TIDE-SURGE INTERACTION AT (6,28)



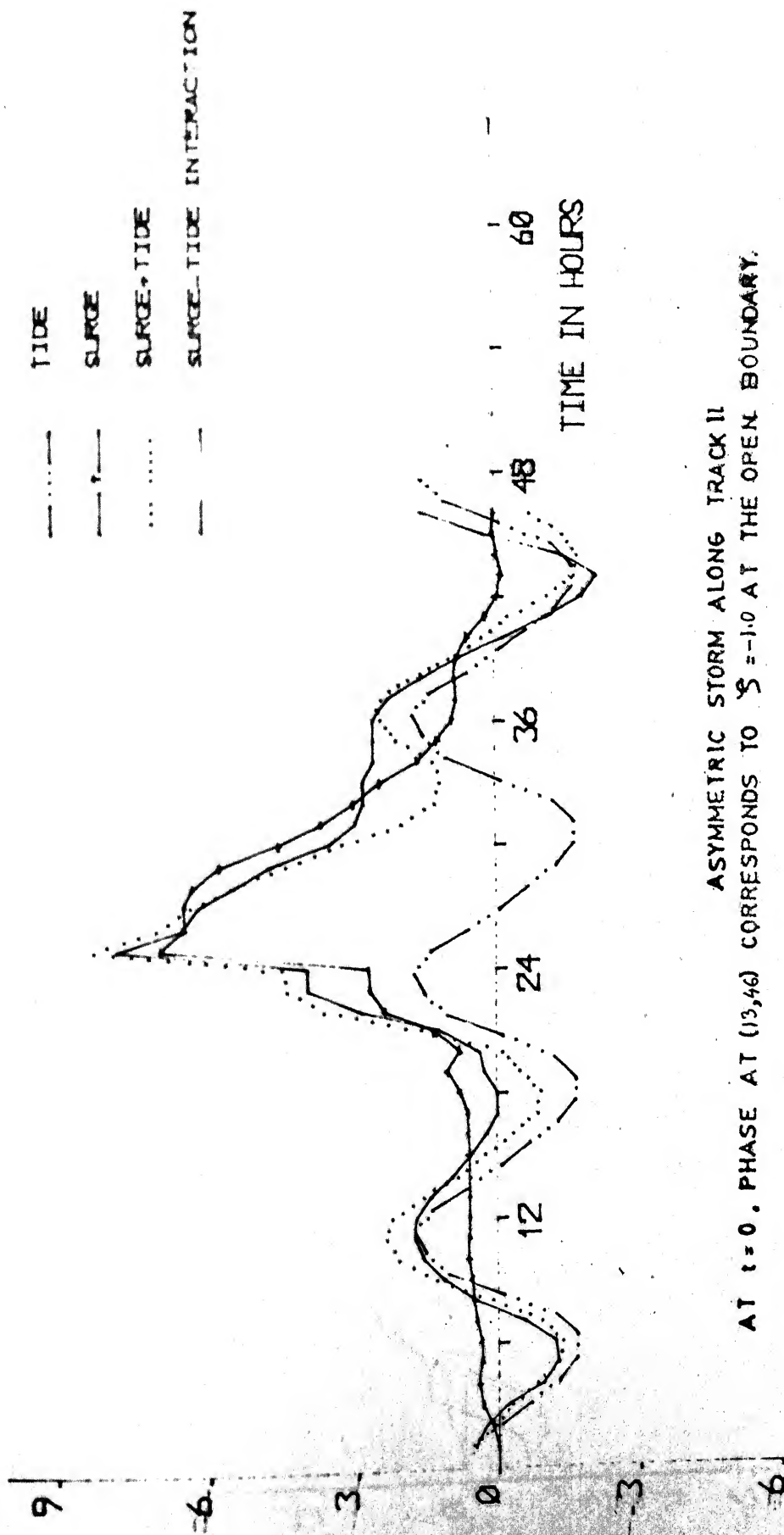
ASYMMETRIC STORM ALONG TRACK I
 AT $t=0$, PHASE AT (6,28) CORRESPONDS TO $S=1.0$ AT THE OPEN BOUNDARY.

FIG. 16.(d). TIDE-SURGE INTERACTION AT (6,28)



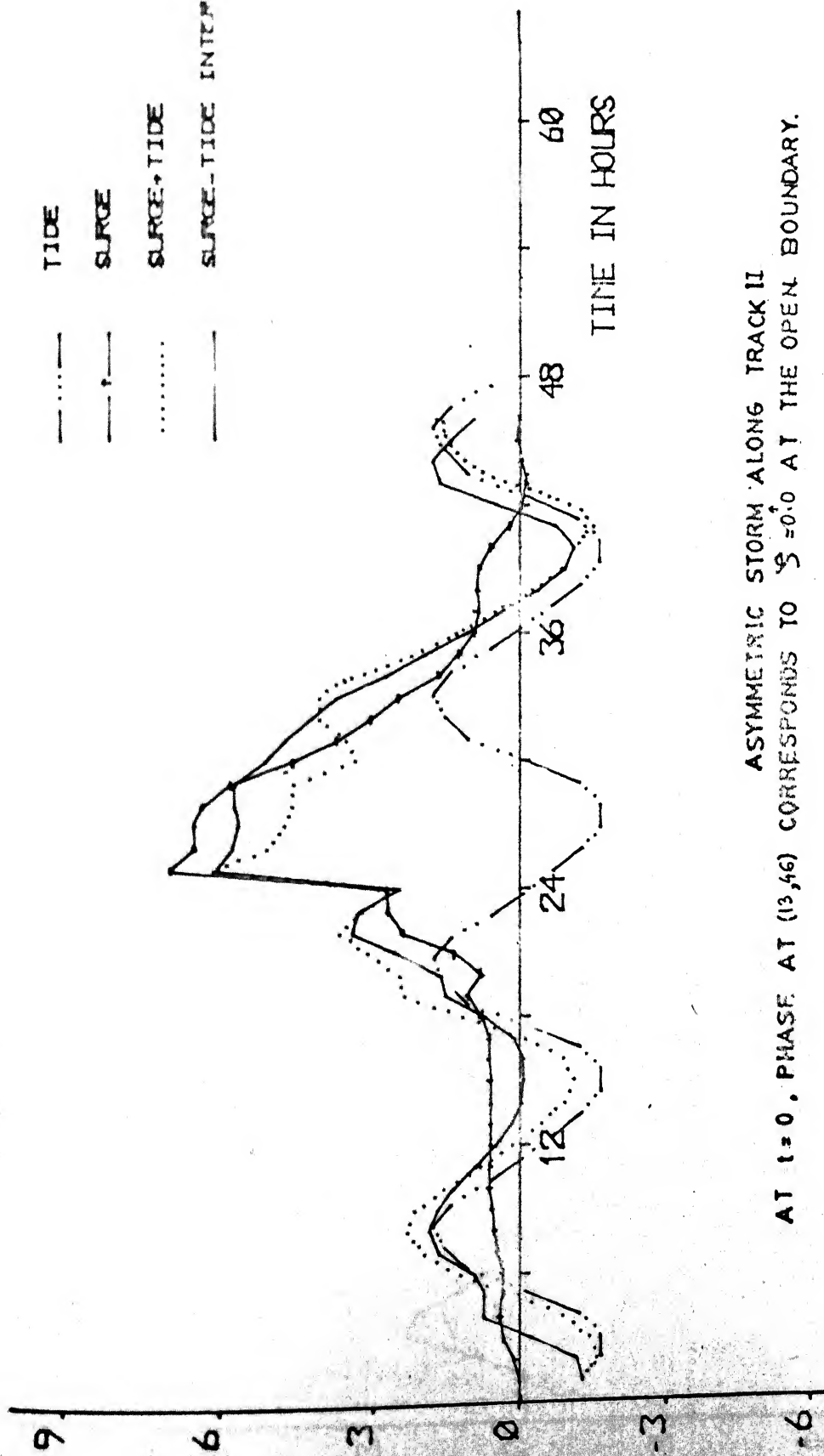
ASYMMETRIC STORM, ALONG TRACK II
 AT $t=0$, PHASE AT (13,40) CORRESPONDS TO $S=0.0$ AT THE OPEN BOUNDARY.

Mtrs
 FIG.17 (a). TIDE-SURGE INTERACTION AT (13,40)



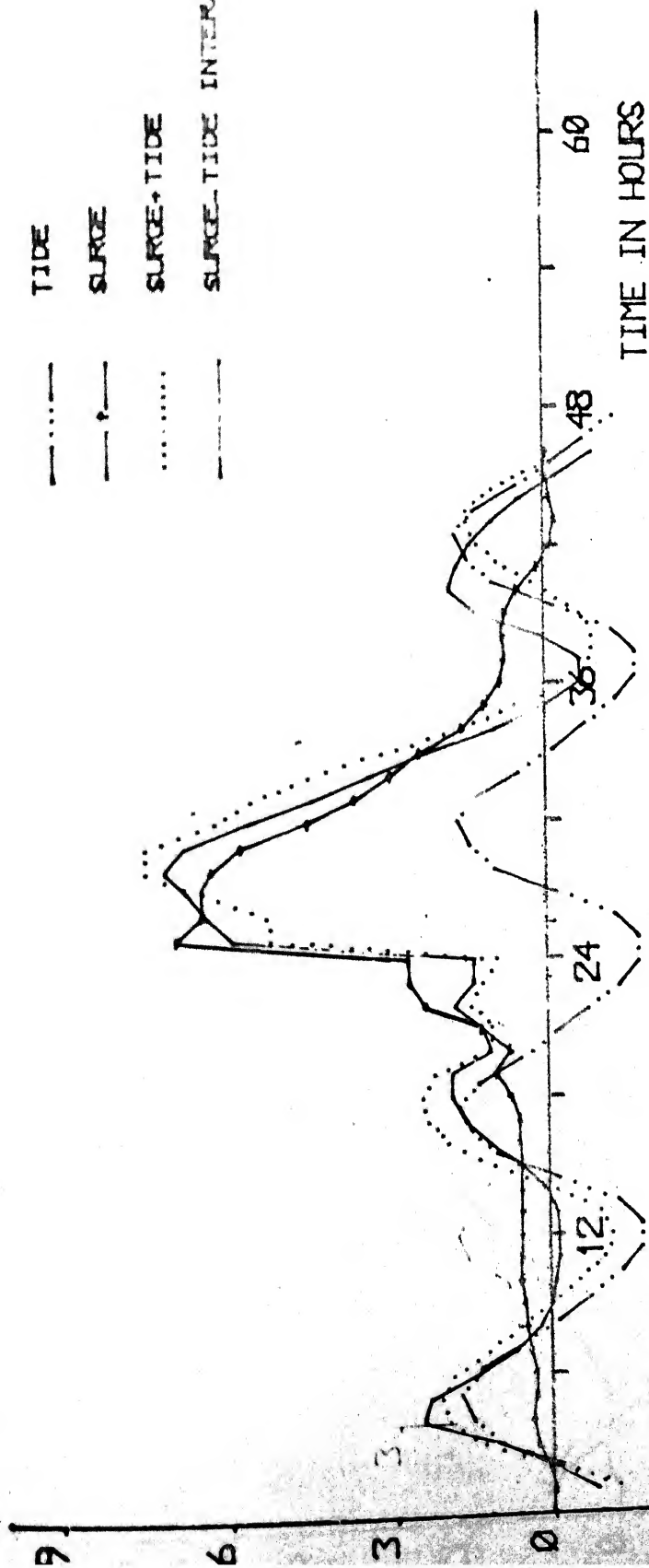
ASYMMETRIC STORM ALONG TRACK II
 AT $t=0$. PHASE AT (13,46) CORRESPONDS TO $S=-1.0$ AT THE OPEN BOUNDARY.

FIG. 17(b). TIDE-SURGE INTERACTION AT (13,46)



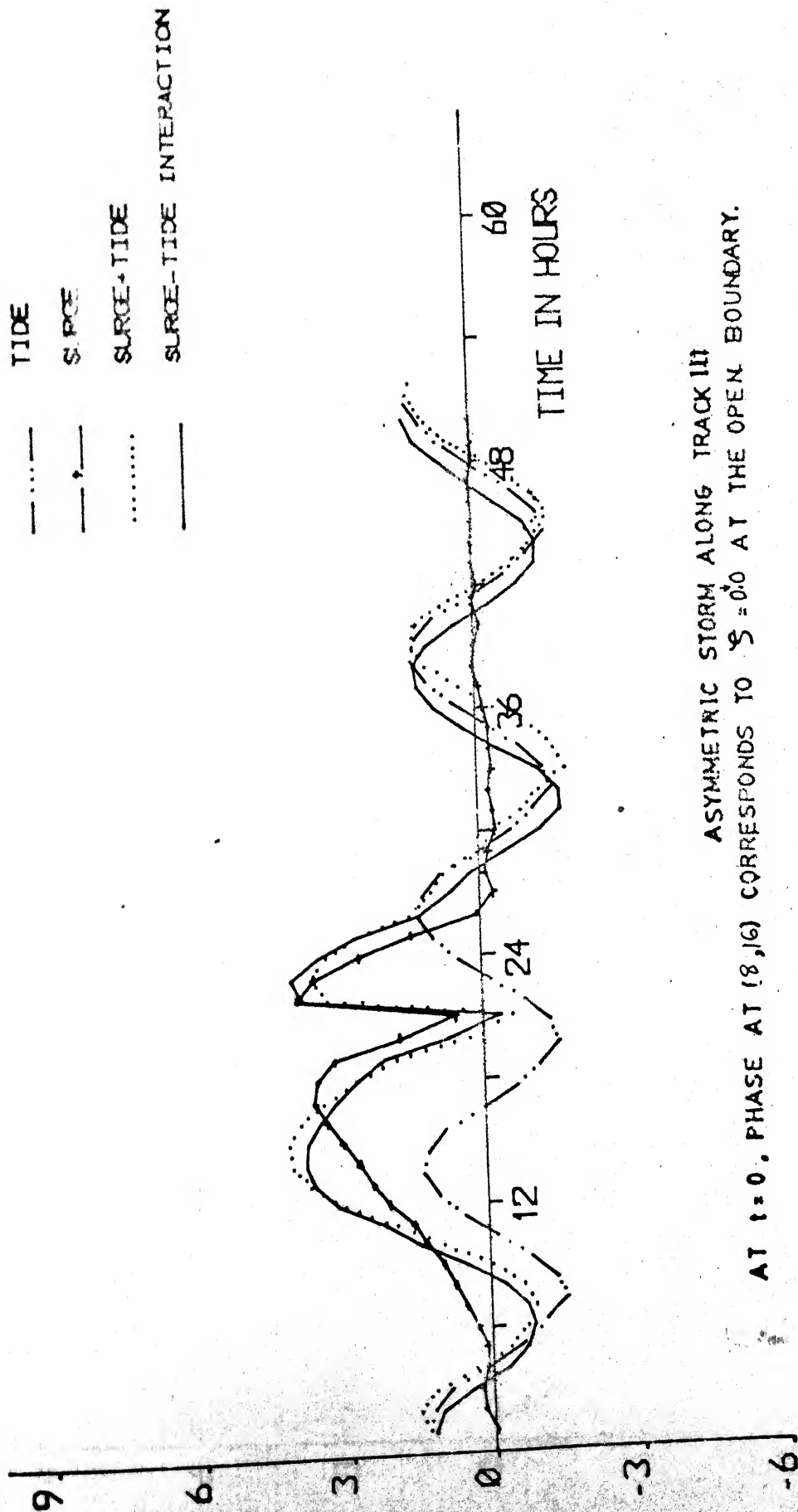
ASYMMETRIC STORM ALONG TRACK II
 AT $t=0$, PHASE AT (13,46) CORRESPONDS TO $S=0.0$ AT THE OPEN BOUNDARY.

Mtr s
 FIG. 17(c). TIDE-SURGE INTERACTION AT (13,46)



ASYMMETRIC STORM ALONG TRACK 11
 AT $t=0$, PHASE AT (13,46) CORRESPONDS TO $S=1.0$ AT THE OPEN BOUNDARY.

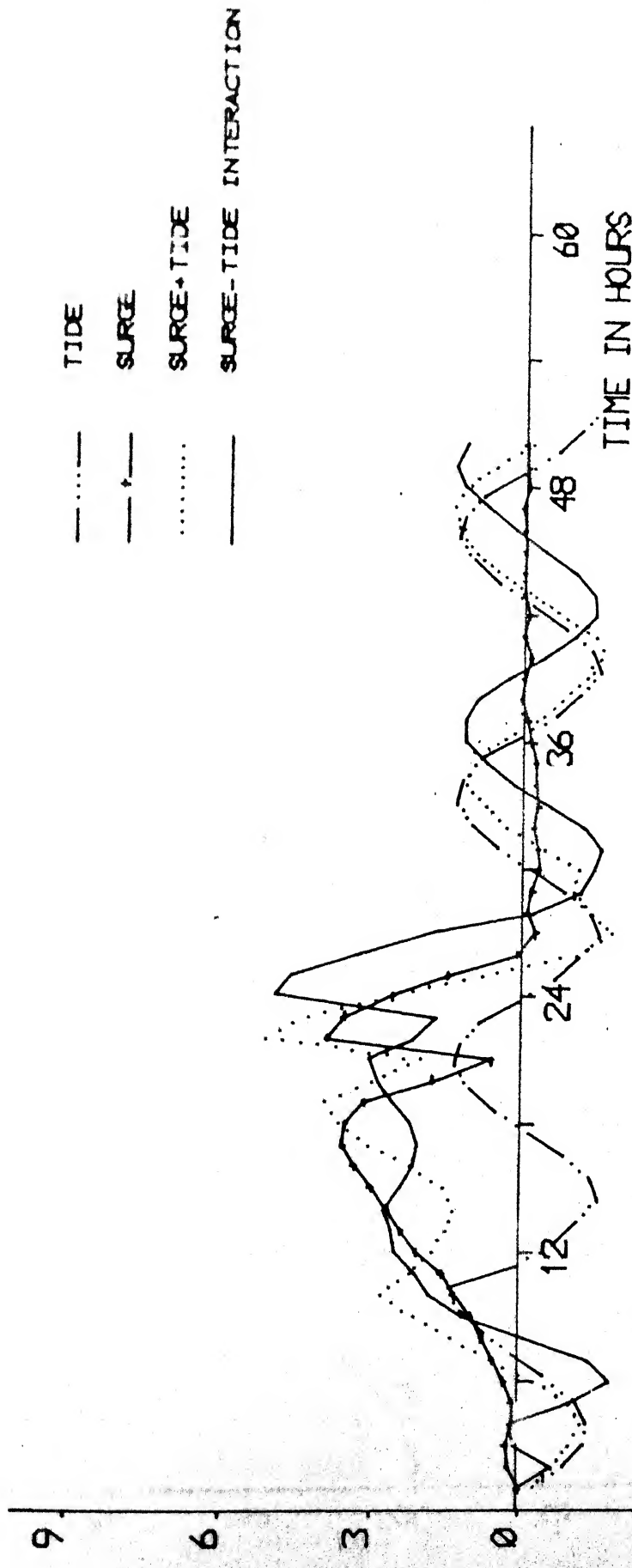
Mtr 6
 FIG. 17 (d). TIDE-SURGE INTERACTION AT (13,46)



ASYMMETRIC STORM ALONG TRACK III
 AT $t=0$, PHASE AT (8,16) CORRESPONDS TO $S=0.0$ AT THE OPEN BOUNDARY.

FIG. 18(a). TIDE-SURGE INTERACTION AT (8,16)

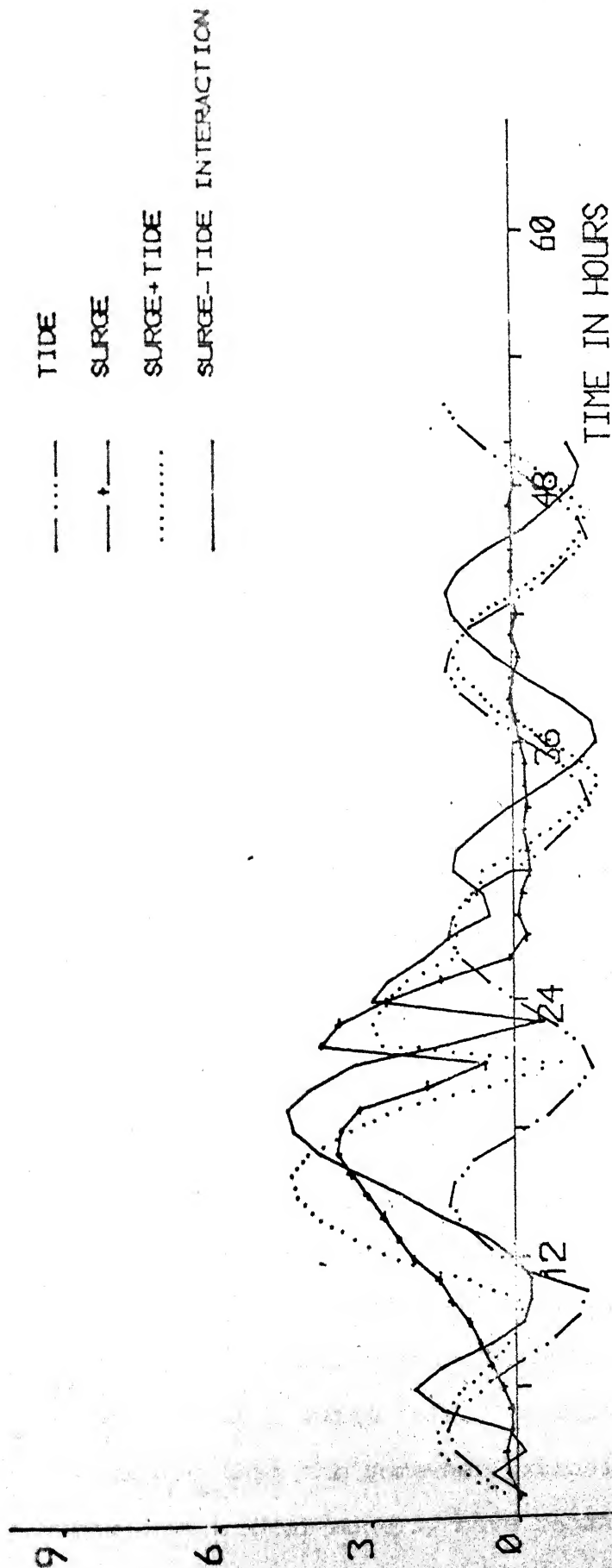
Mtrs



ASYMMETRIC STORM ALONG TRACK III
 AT $t=0$, PHASE AT (8,16) CORRESPONDS TO $S=-1.0$ AT THE OPEN BOUNDARY.

Mtrs

FIG.18 (b). TIDE-SURGE INTERACTION AT (8,16)



ASYMMETRIC STORM ALONG TRACK III
 AT $t=0$, PHASE AT (8,16) CORRESPONDS TO $S=1.0$ AT THE OPEN BOUNDARY.

FIG. 18_(d). TIDE-SURGE INTERACTION AT (8,16)

CHAPTER 3

NUMERICAL SIMULATION OF THREE-DIMENSIONAL SURGE USING A SPECTRAL MODEL

3.1 Introduction

In certain situations it will be useful and interesting to know the vertical structure of the ocean characteristics such as the ocean currents and the ocean thermocline. Though the vertically-averaged models are quite powerful in the studies dealing with the elevations and the depth-mean currents, the three-dimensional models are more realistic and provide very useful information regarding the vertical structure of the ocean, particularly when the ocean circulation is predominant in the vertical. In sections 0.2 and 0.4 we have mentioned some of the well known three-dimensional models. Many of these models are quite recent and there are relatively a few number of studies as compared to their two-dimensional counterparts. The reason is simple, of course. Many of the studies either do not require them or avoid them because of the expensive involvement. But in the studies of residual circulations, and other circulations these models play a vital role. Also, it can be seen from the literature that the somewhat extensive studies, using the three-dimensional models, have begun only in the 1970s.

Many of these models follow either the multilevel (or multi-layer) approach or the spectral approach. In the present work we consider the spectral model given by Heaps (1976) for the purpose of simulating the three-dimensional surge in the Bay of Bengal. This choice provides us some of the advantages of the spectral model over the multi-level model. The apparent advantages are, the easy and natural way of representing the bottom topography; the direct way of satisfying the dynamical conditions at the free surface and at the bottom; the determination of the currents at any desired level (as opposed to the determination of the currents at fixed levels only) and the achieving of sufficient accuracy in the determination of the vertical structure by increasing the number of eigen functions, and hence the number of terms in the summations. We consider the same kind of meteorological forcing as has been taken in Chapter 2, regarding the tracks and other storm parameters. However, only asymmetric storm will be considered because of the limited number of numerical experiments that can be carried out. As in the previous chapter, the storm forcing will be typical of a severe cyclonic storm in the Bay of Bengal.

As regards the simulation of surges for the region of the Bay of Bengal, to the best of the author's knowledge, only one significant study has been carried out with the help of a multi-level model (Johns et al. 1982(a)). The high-light of

the present investigation is the discussion on the vertical structure and the residual circulation patterns. However, a comparison of the results of the present work with the work of Johns et al. (1982) is not possible because of the entirely different features of the works. The only anchor is the set of few available observations for the region of the Bay of Bengal, where some kind of comparison can be made.

In the following section we briefly describe the numerical scheme and then proceed to the aspects of numerical experiments.

3.2 Numerical Scheme

In the present investigation we adopt the numerical scheme given by Sielecki and Wurtele (1970) for solving the system of equations (0.4.31), (0.4.32) and (0.4.34) with the appropriate initial and boundary conditions. The same scheme has also been considered by Heaps (1976) in his formulation to include the nonlinear terms. With the use of the staggered grid taken in Chapter 2, we have (for the variables $\zeta, \hat{u}_r, \hat{v}_r$)

$$\left. \begin{array}{l} \text{at } \zeta\text{-point } i : \zeta = \zeta_i, h = h_i \\ \text{at } u\text{-point } i : u = u_i, \hat{u}_r = \hat{u}_{r,i}, \lambda_r = \lambda_{r,i}^u, F_s = F_i ; \text{ and} \\ \text{at } v\text{-point } i : v = v_i, \hat{v}_r = \hat{v}_{r,i}, \lambda_r = \lambda_{r,i}^u, G_s = G_i \end{array} \right\} \quad (3.2.1)$$

Simple averaging yields estimates for total depth at u-point i:

$$d_i = (h_i + \zeta_i + h_{i+1} + \zeta_{i+1})/2 \quad (3.2.2)$$

Similarly the total depth at v-point i is given by

$$e_i = (h_i + \zeta_i + h_{i+m} + \zeta_{i+m})/2 \quad (3.2.3)$$

In the same way other averaged equantities are taken as follows:

$$\left. \begin{aligned} u \text{ at v-point } i : \tilde{u}_i &= (u_{i-1} + u_i + u_{i+m-1} + u_{i+m})/4 \\ v \text{ at u-point } i : \tilde{v}_i &= (v_{i-m} + v_{i-m+1} + v_i + v_{i+1})/4 \\ \hat{u}_r \text{ at v-point } i : \tilde{u}_{r,i} &= (\hat{u}_{r,i-1} + \hat{u}_{r,i} + \hat{u}_{r,i+m-1} + \hat{u}_{r,i+m})/4 \\ \hat{v}_r \text{ at u-point } i : \tilde{v}_{r,i} &= (\hat{v}_{r,i-m} + \hat{v}_{r,i-m+1} + \hat{v}_{r,i} + \hat{v}_{r,i+1})/4 \end{aligned} \right\} \quad (3.2.4)$$

Also, on the basis of the quadratic law for bottom friction we have

$$\left. \begin{aligned} \lambda_{r,i}^u &= \frac{k}{c} \alpha_r^2 \{ (u_i)_{-h}^2 + (v_i)_{-h}^2 \}^{1/2} / d_i \\ \lambda_{r,i}^v &= \frac{k}{c} \alpha_r^2 \{ (\tilde{u}_i)_{-h}^2 + (\tilde{v}_i)_{-h}^2 \}^{1/2} / e_i \end{aligned} \right\} \quad (3.2.5)$$

where from (0.4.33)

$$\left. \begin{aligned} (u_i)_{-h} &= \sum_{r=1}^M \Psi_r \hat{u}_{r,i} \cos \alpha_r \\ (v_i)_{-h} &= \sum_{r=1}^n \Psi_r \hat{v}_{r,i} \cos \alpha_r \end{aligned} \right\} \quad (3.2.6)$$

Introducing a time step τ and including the terms

$R_{u,r}$, $R_{v,r}$, $S_{u,r}$ and $S_{v,r}$, the proposed numerical scheme by Sielecki and Wurtele (1970) can be used to write equations (0.4.34), (0.4.31) and (0.4.32) respectively in the finite difference form as follows:

$$\frac{\zeta_i(t+\tau) - \zeta_i(t)}{\tau} = - \sum_{r=1}^M a_r \Psi_r \{ d_i(t) \hat{u}_{r,i}(t) - d_{i-1}(t) \hat{u}_{r,i-1}(t) + e_{i-m}(t) \hat{v}_{r,i-m}(t) - e_i(t) \hat{v}_{r,i}(t) \} / s \quad (3.2.7)$$

$$\begin{aligned} \frac{\hat{u}_{r,i}(t+\tau) - \hat{u}_{r,i}(t)}{\tau} = & - \lambda_{r,i}^u(t) \hat{u}_{r,i}(t+\tau) + f \hat{v}_{r,i}(t) \\ & - \frac{ga_r}{s} \{ \zeta_{i+1}(t+\tau) - \zeta_i(t+\tau) - \zeta'_{i+1}(t+\tau) + \zeta'_i(t+\tau) \} \\ & + \frac{F_i(t)}{\rho d_i(t)} + R_{u,r,i} - S_{u,r,i} \end{aligned} \quad (3.2.8)$$

$$\begin{aligned} \frac{\hat{v}_{r,i}(t+\tau) - \hat{v}_{r,i}(t)}{\tau} = & - \lambda_{r,i}^v(t) \hat{v}_{r,i}(t+\tau) - f \hat{u}_{r,i}(t+\tau) \\ & - \frac{ga_r}{s} \{ \zeta_i(t+\tau) - \zeta_{i+m}(t+\tau) - \zeta'_i(t+\tau) + \zeta'_{i+m}(t+\tau) \} \\ & + \frac{G_i(t)}{\rho e_i(t)} + R_{v,r,i} + S_{v,r,i} \end{aligned} \quad (3.2.9)$$

followed by a second step of the form

$$\begin{aligned}
\frac{\hat{u}_{r,i}^*(t+\tau) - \hat{u}_{r,i}(t)}{\tau} = & -\lambda_{r,i}^u \hat{u}_{r,i}^*(t+\tau) + f\tilde{v}_{r,i}(t+\tau) \\
& - \frac{ga_r}{s} \{ \zeta_{i+1}(t+\tau) - \zeta_i(t+\tau) - \zeta'_{i+1}(t+\tau) + \zeta'_i(t+\tau) \} \\
& + \frac{F_i(t)}{\rho d_i(t)} + R_{u,r,i} - S'_{u,r,i} \quad (3.2.10)
\end{aligned}$$

$$\begin{aligned}
\frac{\hat{v}_{r,i}^*(t+\tau) - \hat{v}_{r,i}(t)}{\tau} = & -\lambda_{r,i}^v(t) \hat{v}_{r,i}^*(t+\tau) - f\hat{u}_{r,i}^*(t+\tau) \\
& - \frac{ga_r}{s} \{ \zeta_i(t+\tau) - \zeta_{i+1}(t+\tau) - \zeta'_i(t+\tau) - \zeta'_{i+m}(t+\tau) \} \\
& + \frac{G_i(t)}{\rho e_i(t)} + R_{v,r,i} - S'_{v,r,i} \quad (3.2.11)
\end{aligned}$$

$$\text{where } \tilde{u}_{r,i}^* = (\hat{u}_{r,i-1}^* + \hat{u}_{r,i}^* + \hat{u}_{r,i+m-1}^* + \hat{u}_{r,i+m}^*)/4 \quad (3.2.12)$$

The quantities $\zeta_i(t+\tau)$, $\hat{u}_{r,i}^*(t+\tau)$, $\hat{v}_{r,i}^*(t+\tau)$ represent the final values of the fields at $t+\tau$ as deduced from those at time t using (3.2.7) to (3.2.11) in succession. In the equations (3.2.8) to (3.2.11), the finite-difference forms of the nonlinear terms $R_{u,r}$, $R_{v,r}$, $S_{u,r}$, $S_{v,r}$, $S'_{u,r}$ and $S'_{v,r}$ are

$$R_{u,r,i} = \frac{1}{d_i(t)} \left\{ \frac{\zeta_i(t+\tau) - \zeta_i(t)}{\tau} \right\} \{ -\hat{u}_{r,i}(t) + \sum_{j=1}^n (1 + \alpha_r b_{r,j}) \Psi_j \hat{u}_{j,i}(t) \} \quad (3.2.13)$$

$$R_{v,r,i} = \frac{1}{e_i(t)} \left\{ \frac{\zeta_i(t+\tau) - \zeta_i(t)}{\tau} \right\} \{ -\hat{v}_{r,i}(t) + \sum_{j=1}^n (1 + \alpha_r b_{r,j}) \Psi_j \hat{v}_{j,i}(t) \} \quad (3.2.14)$$

$$\begin{aligned} S_{u,r,i} = & \sum_j \sum_n \Psi_j \Psi_n \left[\frac{1}{2} \{ \eta \hat{u}_j(i-1, i, t) + \eta \hat{u}_j(i, i+1, t) \} \right. \\ & \delta \hat{u}_n(i+1, i-1, t) + \eta \hat{v}_j(i-m, i-m+1, t) \delta \hat{u}_n(i-m, i, t) \\ & \left. + \eta \hat{v}_j(i, i+1, t) \delta \hat{u}_n(i, i+m, t) \right] D_{r,j,n} \\ & + \frac{1}{4d_i(t)} \sum_j \sum_n \Psi_j \Psi_n \{ \eta \hat{u}_j(i-1, i, t) + \eta \hat{u}_j(i, i+1, t) \} \\ & \{ \Delta_i(t) + \Delta_{i+1}(t) \} \frac{\alpha_j}{\alpha_n} E_{r,j,n} \quad (3.2.15) \end{aligned}$$

$$\begin{aligned} S_{v,r,i} = & \sum_j \sum_n \Psi_j \Psi_n \left[\eta \hat{u}_j(i-1, i+m-1, t+\tau) \delta \hat{v}_n(i, i-1, t) \right. \\ & + \eta \hat{u}_j(i, i+m, t+\tau) \delta \hat{v}_n(i+1, i, t) \\ & \left. + \frac{1}{2} \{ \eta \hat{v}_j(i-m, i, t) + \eta \hat{v}_j(i, i+1, t) \} \delta \hat{v}_n(i-m, i+m, t) \right] D_{r,j,n} \\ & + \frac{1}{4e_i(t)} \sum_j \sum_n \Psi_j \Psi_n \{ \eta \hat{v}_j(i-m, i, t) + \eta \hat{v}_j(i, i+m, t) \} \\ & \{ \Delta_i(t) + \Delta_{i+m}(t) \} \frac{\alpha_j}{\alpha_n} E_{r,j,n} \quad (3.2.16) \end{aligned}$$

$$\begin{aligned} S'_{u,r,i} = & \sum_j \sum_n \Psi_j \Psi_n \left[\frac{1}{2} \{ \eta \hat{u}_j(i-1, i, t) + \eta \hat{u}_j(i, i+1, t) \} \right. \\ & \delta \hat{u}_n(i+1, i-1, t+\tau) + \eta \hat{v}_j(i-m, i-m+1, t) \delta \hat{u}_n(i-m, i, t+\tau) \\ & \left. + \eta \hat{v}_j(i, i+1, t) \delta \hat{u}_n(i, i+m, t+\tau) \right] D_{r,j,n} \end{aligned}$$

$$\begin{aligned}
& + \frac{1}{4d_i(t+\tau)} \sum_j \sum_n \Psi_j \Psi_n \{ \eta \hat{u}_j(i-1, i, t) + \eta \hat{u}_j(i, i+1, t) \} \\
& \{ \Delta_i(t+\tau) + \Delta_{i+1}(t+\tau) \} \frac{\alpha_j}{\alpha_n} E_{r,j,n} \quad (3.2.17)
\end{aligned}$$

$$\begin{aligned}
S'_{v,r,i} = & \sum_j \sum_n \Psi_j \Psi_n [\eta \hat{u}_j(i-1, i+m-1, t+\tau) \delta \hat{v}_n(i, i-1, t+\tau) \\
& + \eta \hat{u}_j(i, i+m, t+\tau) \delta \hat{v}_n(i+1, i, t+\tau) \\
& + \frac{1}{2} \{ \eta \hat{v}_j(i-m, i, t) + \eta \hat{v}_j(i, i+m, t) \} \delta \hat{v}_n(i-m, i+m, t+\tau)] D_{r,j,n} \\
& + \frac{1}{4e_i(t+\tau)} \sum_j \sum_n \Psi_j \Psi_n \{ \eta \hat{v}_j(i-m, i, t) + \eta \hat{v}_j(i, i+m, t) \} \\
& \{ \Delta_i(t+\tau) + \Delta_{i+m}(t+\tau) \} \frac{\alpha_j}{\alpha_n} E_{r,j,n} \quad (3.2.18)
\end{aligned}$$

where

$$\left. \begin{aligned}
\delta \hat{u}_n(p, q, t) &= \frac{\hat{u}_{n,p}(t) - \hat{u}_{n,q}(t)}{2s} \\
\delta \hat{v}_n(p, q, t) &= \frac{\hat{v}_{n,p}(t) - \hat{v}_{n,q}(t)}{2s} \\
\eta \hat{u}_j(p, q, t) &= \frac{\hat{u}_{j,p}(t) + \hat{u}_{j,q}(t)}{2} \\
\eta \hat{v}_j(p, q, t) &= \frac{\hat{v}_{j,p}(t) + \hat{v}_{j,q}(t)}{2}
\end{aligned} \right\} \quad (3.2.19)$$

and

$$\begin{aligned}
\Delta_i(t) = & \{ d_i(t) \hat{u}_{n,i}(t) - d_{i-1}(t) \hat{u}_{n,i-1}(t) + e_{i-m}(t) \hat{v}_{n,i-m}(t) \\
& - e_i(t) \hat{v}_{n,i}(t) \} / s \quad (3.2.20)
\end{aligned}$$

In all the above summations, the indices j and n are carried from 1 to M . The expressions for $B_{r,j}$, $D_{r,j,n}$ and $E_{r,jn}$ can be found from (0.4.65) to (0.4.69).

Applied successively, in the order stated, these relations may be used explicitly to advance from the fields of ζ_i , $\hat{u}_{r,i}$, $\hat{v}_{r,i}$ at time t to the corresponding fields at time $t+\tau$, thereby forming the basis of a marching technique for computing the quantities ζ_i , $\hat{u}_{r,i}$ and $\hat{v}_{r,i}$ through space and time.

Boundary Conditions

In the present three-dimensional model, we consider the surge without the tidal forcing. Owing to the limitation on the computer budget, the fresh establishment of the tidal regime (which is necessary) by means of the spectral model was not possible. Under this situation we specify the following appropriate boundary conditions.

At the coastal boundaries we set

$$\hat{u}_{r,i} = \hat{v}_{r,i} = 0 \quad \text{for } t \geq 0 \quad (3.2.21)$$

At the open boundary we set

$$\zeta_i = 0 \quad \text{for } t \geq 0, \quad (3.2.22)$$

$$\begin{aligned} \hat{v}_{1,i}(t) = & \frac{1}{h_{i1,i}^v a_{1,i}^v \psi_{1,i}^v} \left[\frac{s}{\tau} \{ \zeta_i(t+\tau) - \zeta_i(t) \} \right. \\ & + \sum_{r=1}^n \{ h_{r,i}^u a_{r,i}^u \psi_{r,i}^u \hat{u}_{r,i}(t) - h_{i-1}^u a_{r,i-1}^u \psi_{r,i-1}^u \hat{u}_{r,i-1}(t) \\ & \left. + h_{i-m}^v a_{r,i-m}^v \psi_{r,i-m}^v \hat{v}_{r,i-m}(t) \} \right] \quad t \geq 0 \quad (3.2.23) \end{aligned}$$

$$\text{and } \hat{v}_{n,i} = 0, \quad t \geq 0, \quad n=2,3,4,\dots \quad (3.2.24)$$

We set the initial values of u_i , v_i and ζ_i equal to zero, which correspond to the undisturbed sea. With the above initial and boundary conditions and with the specified storm forcing, we seek the response of the sea region through the numerical solutions. Knowing the values of $\hat{u}_{r,i}$, $\hat{v}_{r,i}$ and ζ_i the current structure is determined by the relations

$$\left. \begin{aligned} u_i &= \sum_{r=1}^M \psi_r \hat{u}_{r,i} \cos(\alpha_r \xi) \\ v_i &= \sum_{r=1}^M \psi_r \hat{v}_{r,i} \cos(\alpha_r \xi) \end{aligned} \right\} \quad (3.2.25)$$

The depth-averaged currents are given by

$$\left. \begin{aligned} u_i^{DA} &= \sum_{r=1}^M \psi_r \hat{u}_{r,i}^a \\ v_i^{DA} &= \sum_{r=1}^M \psi_r \hat{v}_{r,i}^a \end{aligned} \right\} \quad (3.2.26)$$

Setting $\xi = 0$ in (3.2.25) we obtain the currents near the

free-surface. Thus, the currents at the free surface are given by

$$\left. \begin{aligned} u_i^{FS} &= \sum_{r=1}^M \Psi_r \hat{u}_{r,i} \\ \text{and } v_i^{FS} &= \sum_{r=1}^M \Psi_r \hat{v}_{r,i} \end{aligned} \right\} \quad (3.2.27)$$

Similarly, setting $\xi = -1$ in (3.2.25) the bottom currents (which are required for the bottom stress parameterization) can be obtained.

3.3 Numerical Experiments

In the present investigation, the model shelf area, the asymmetric storm forcing and the tracks (Fig. 3(a), (b), (c) of Chapter 2) are kept the same as in the case of two-dimensional surge simulation (Chapter 2). The main features of the storm forcing are given in Table 2.1. Surge-tide interaction is kept out of the scope of the present chapter because the model requires the generation of a fresh tidal regime which should provide all the spectral modes at any required phase of the tidal cycle. The establishing of a fresh tidal regime requires a large computer budget and constrained by the limited resources the study is confined to the simulation of surge alone. As in the previous chapter a probe run is carried out to

extract first hand information regarding various aspects such as the location, time and magnitude of the maximum peak surge; the number of terms (modes) required for a reasonable convergence of solutions etc. The grid spacing is taken as in the case of two-dimensional surge (Chapter 2) and the corresponding time step of 2 minutes is taken to satisfy the overall stability criterion (2.3.4). The probe run is carried out with the asymmetric storm forcing along track I for a period 46 hours taking the landfall at 35th hour. With the results of Chapter 2 in view, regarding the weak role of the nonlinear advection in the model, the advection terms are included. The value of $\frac{K}{N}$ in the equation (0.4.54) is taken equal to 0.0307, which represents an average value for the present model. The first five modes are taken as significant modes and the remaining modes are neglected.

The results of the probe run have indicated the behaviour, regarding elevations, similar to that of the corresponding two-dimensional model. However, the elevations obtained in the spectral model are slightly higher in magnitude as compared to the elevations of the corresponding run of the two-dimensional model. The overall weak role of the nonlinear advection is also seen in the spectral model. This fact, as well as the prohibitively huge computer budget per run of the model has

compelled the model to drop the advection terms in the subsequent runs.

With the above considerations we have run the present model three times, with the storm forcing along the three chosen tracks. Based on the information from the probe runs the following plan has been envisaged for recording the results from the model executions.

1) For each run, corresponding to the storm forcing along the chosen track, three locations, namely, the location of maximum peak surge, the location of land fall and the location of a second maximum peak surge (same as those of the corresponding run of the two-dimensional model) have been selected for noting the hourly elevations. The coordinates of these locations for the runs for each track are given below

Table 3.1

Coordinates of the selected locations

| | Location of MPS | Location of LF | Location of second MPS |
|-----------|--------------------|-------------------|---------------------------|
| Track I | (2, 36) | (3, 43) | (6, 28) |
| Track II | (13, 46) | (3, 43) | (2, 36) |
| Track III | (8, 22) | (8, 16) | (6, 28) |

where we denote

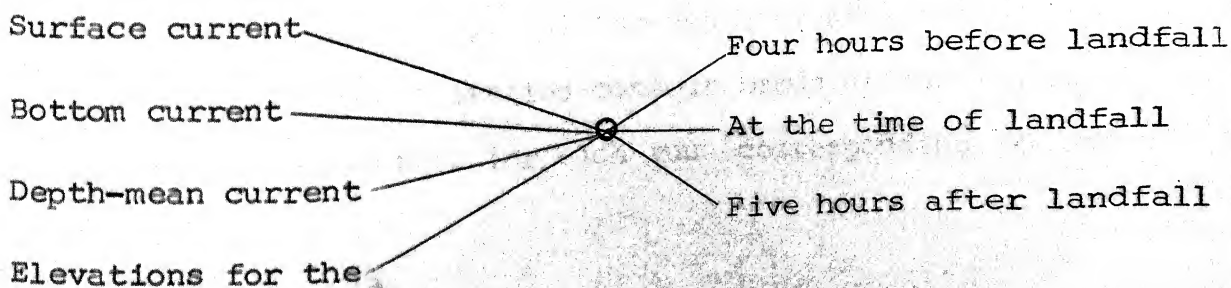
MPS : Maximum Peak Surge

LF : Land fall

2) Ten locations have been chosen to examine the current structure through the depth. At these locations the values of u, v and the roots of the equation (0.4.54) at hourly intervals are recorded for the first five eigen values (corresponding to the first five modes). With these values the current structure at any required level in the range between $\xi = -1$ (bottom) and $\xi = 0$ (free surface) can be determined using the equations (0.4.33). The selected locations include the locations mentioned in Table 3.1. These locations are shown in Fig. 18 whose coordinates are given below.

| | |
|------------|-------------|
| A1 (2, 36) | A6 (10, 16) |
| A2 (4, 40) | A7 (11, 20) |
| A3 (6, 28) | A8 (13, 24) |
| A4 (8, 16) | A9 (13, 46) |
| A5 (8, 20) | A10 (18, 6) |

For the purpose of presenting the current vectors and the elevation pattern for the entire shelf area under consideration, three time intervals have been chosen. These results, for each run, are presented at three instants of time which are given below



Finally the hourly maximum peak surge is noted to have a comparative look with respect to the corresponding hourly maximum (in space) peak surge of the two-dimensional model.

With this plan of noting the values, the runs of the model are executed with the duration of the storm forcing along each track as taken in the corresponding two-dimensional model. That is,

track I : 46 hours with the landfall at 35th hour
along track II : 46 hours with the landfall at 35th hour
track III : hours with the landfall at 26th hour.

Results and Discussion

All the runs of the spectral model have revealed slightly large magnitudes of the surge elevations as compared to the corresponding surge elevations of their two-dimensional counter parts. This is clearly shown in Figs. 1(a) through 1(c), 2(a) through 2(c) and 3(a) through 3(c). In most of the cases any significant difference in magnitudes of the corresponding elevations at any instant never exceeded 1 meter. Also, the corresponding evolution patterns of the elevation at a location remained almost the same in both the models. Figures 4(a) through 4(c), 5(a) through 5(c) and 6(a) through 6(c) show the elevation contour bands at the three selected instants of time for each run (corresponding to the

storm forcing along each track). Except for small difference in magnitudes, these contours are similar to the corresponding contours of the two-dimensional model. As in the case of two-dimensional model for track II, the landfall location in the present model has experienced negative surge around the hours of landfall. Fig. 7 shows a comparative behaviour of the elevation pattern due to storm forcing along tracks I and II at the point of landfall. Owing to the orientation of track II, the storm has, most of the time during its movement, produced off-shore winds at the point of landfall. On the other hand, the storm along track I has produced north-ward long-shore winds causing a positive surge at the same point of landfall. The evolution of the elevation patterns at the three selected locations (for each track) are shown in Figs. 8(a) through 8(c). These figures can be compared with the Figs. 8(a), (b), (c) of Chapter 2. Except for the excessive magnitudes of the elevations near the concave corner points, all the above results indicate a close similarity, to a large extent, in the elevation patterns of the depth-averaged model and the spectral model.

Unlike the elevation patterns, which present smoothly varying gross features, the ocean currents are difficult to conceive and analyze. This is particularly so, for the surface currents which quickly respond to the strong winds and for which no reliable observations are available. The

current meter readings very near to the surface are not available, even for the moderate wind conditions. Also, the attribution of the current structure is difficult (in the absence of observations) because the resulting current depends not only on the direct external forcing but also on the overall dynamics. Taking these limitations into account, the residual current patterns are presented for the region under consideration under the prevailing strong wind forcing.

The current vectors at the free surface, at the bottom, and the depth-mean current vectors for the numerical experiment with the storm forcing along track I, at the three chosen instants of time, are shown in Figs. 9(a) through 9(c); 10(a) through 10(c); and 11(a) through 11(c) respectively. The corresponding current vectors for the numerical experiment with the storm forcing along track II are shown in Figs. 12(a) through 12(c); 13(a) through 13(c); and 14(a) through 14(c) respectively. Similarly the corresponding current vectors for the numerical experiment with the storm forcing along track III are shown in Figs. 15(a) through 15(c); 16(a) through 16(c); and 17(a) through 17(c) respectively.

In all these figures we observe the horizontal circulation with an inflow at the central portion of the open boundary, and out flow side ways along the continental-shelf (shown as

'IN' and 'OUT' in the figures). This is expected because of the wide extent of the basin (comparable to the size of the storm), and the smaller depth of the basin as compared to the so called 'Ekman depth' ($E.E = \pi \sqrt{2A/f}$)
A is the coefficient
of vertical friction

for the region under consideration (see Appendix). This is found to be in agreement with the horizontal circulation pattern described by Welander (1961). Perhaps the comparable sizes of the bay and the storm (Harris 1957, 1959) might have resulted in this type of circulation. We observe the concentration of outgoing surface currents across the ends of the open boundary. In all the numerical experiments the strongest currents prevailed to the south-west of the storm centre and this strong residual circulation prevailed many hours after the storm crossed the coast.

Another major feature is the large magnitudes of the surface currents (more than 6 meters/sec. !?) in the core wind region during the development stage of the stationed cyclone (Figs. 22(c), (d) and 24(c), (d)). However, when the storm has started its movement these surface currents have shown a decreasing trend in magnitude. Long fetch of accelerating surface winds upto mature stage of the cyclone has produced stronger surface currents than the maximum winds of the developed cyclone. However, the persisting strong surface currents near the shelf ends of

the open boundary are believed due to the strengthening of the currents by the winds and bottom slope. Figures 25, 26, 27 (a to d) show that the bottom currents to a large extent have the same direction as that of the surface currents showing either (locally) weak or no vertical circulation in the region of study. However, at the present no reliable field observations are available regarding the wind driven currents for the region of the Bay of Bengal for a comparison of the present values. If one disregards the period of the developing stage of the cyclone, the present values (magnitudes) of the surface currents, when compared with the studies with similar storm forcing, are in agreeable range.

Figure 31(d) shows an abrupt oscillation of the v-component of the current in the surface layer during the landfall hours while there is a continuous change of the magnitude of the u-component from negative to positive during the same period. This fact and the presence of the coast towards the north are believed to be the cause for the swift accumulation of the water mass in the vicinity (particularly to the right) of the point of landfall. However, as anticipated in chapter 2, this oscillation is confined to the surface layer (top $\frac{1}{4}$ th). Except for this swift adjustment the overall variation in the elevation (or current) is smooth and it is believed that this kind of

oscillation is a very particular situation. In fact it has been verified with the help of the two-dimensional model, that no swift oscillation has occurred if we choose the track obliquely in either direction (passing through the same landfall point of track III).

Concluding Remarks

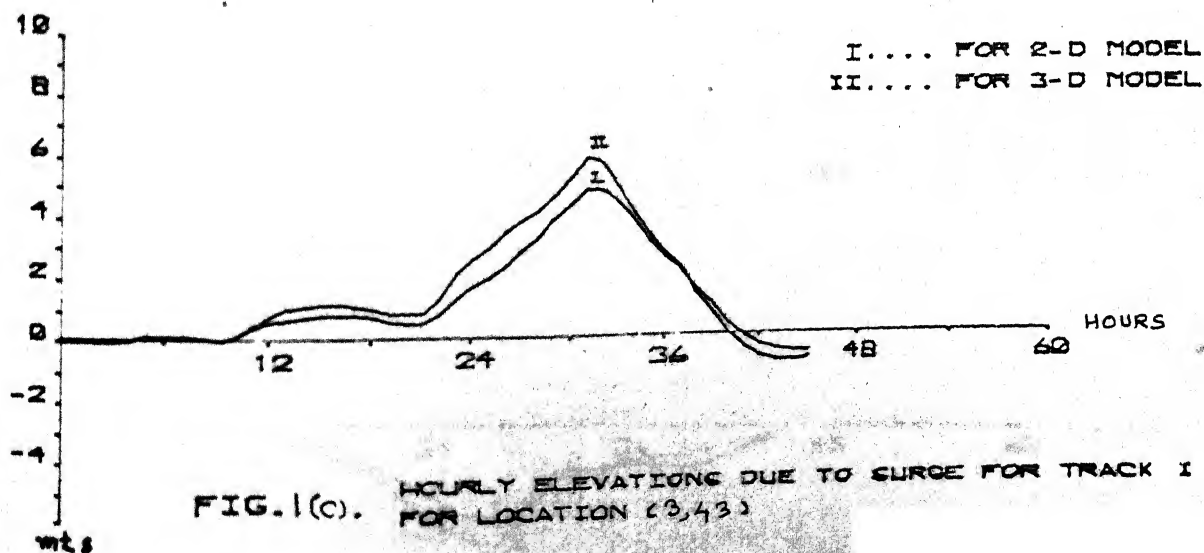
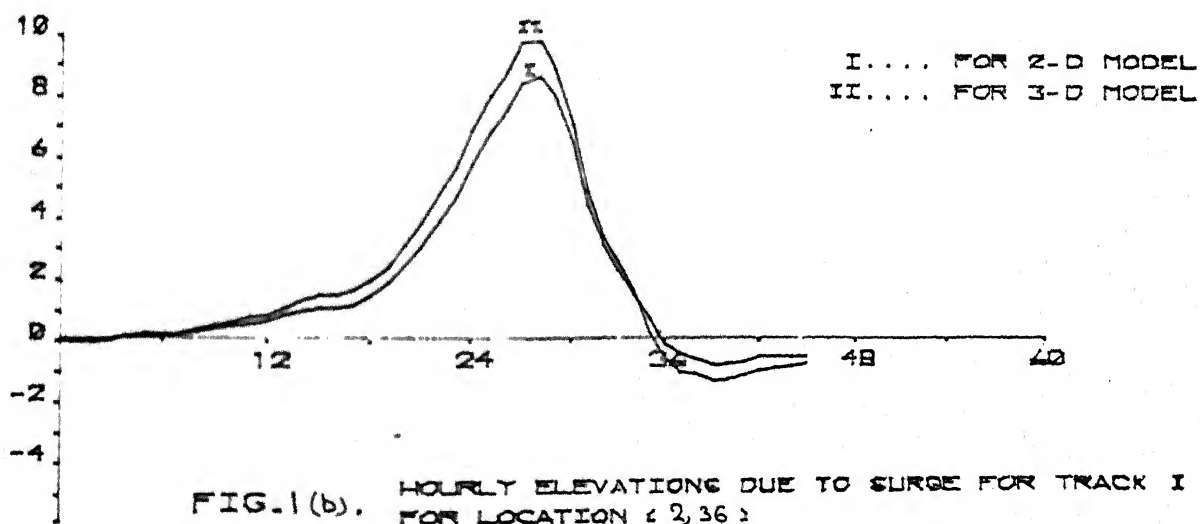
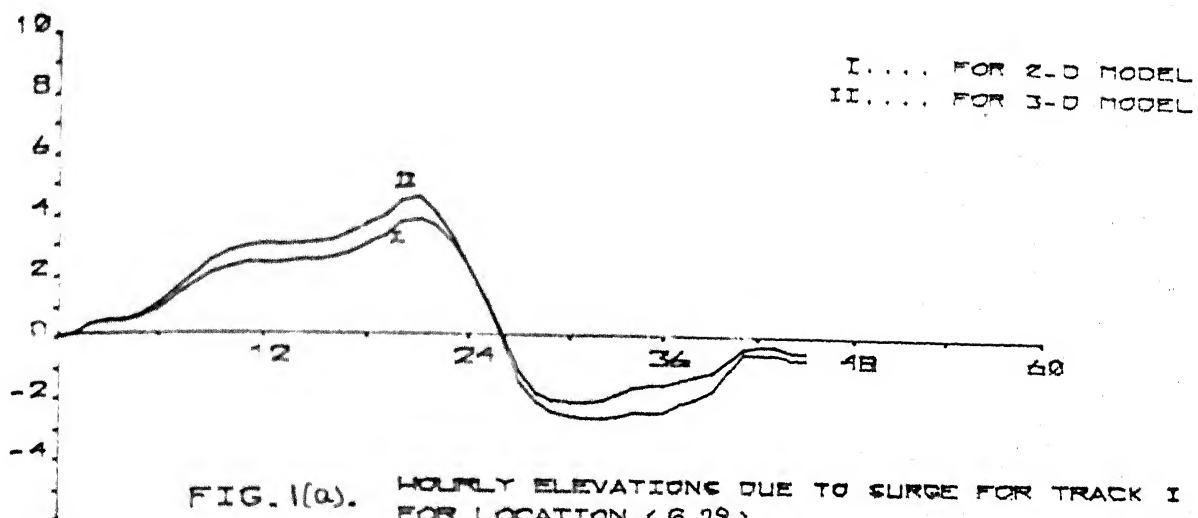
The numerical experiments in the present chapter have demonstrated the variety in the bay response to the storm forcing. From the limited number of results taken from the three numerical experiments (which has resulted in a paltry 61 figures!) the following conclusions are made.

1) Regarding elevations, both the models (Depth-averaged and spectral) have produced similar kind of response. However, the elevations obtained in the three-dimensional model have shown higher magnitudes (upto 10%) than the corresponding elevations of the two-dimensional model. It is assumed that the formulation of the bottom stress with the bottom current and the limited number of terms (modes) taken in the three-dimensional model might have resulted in this discrepancy.

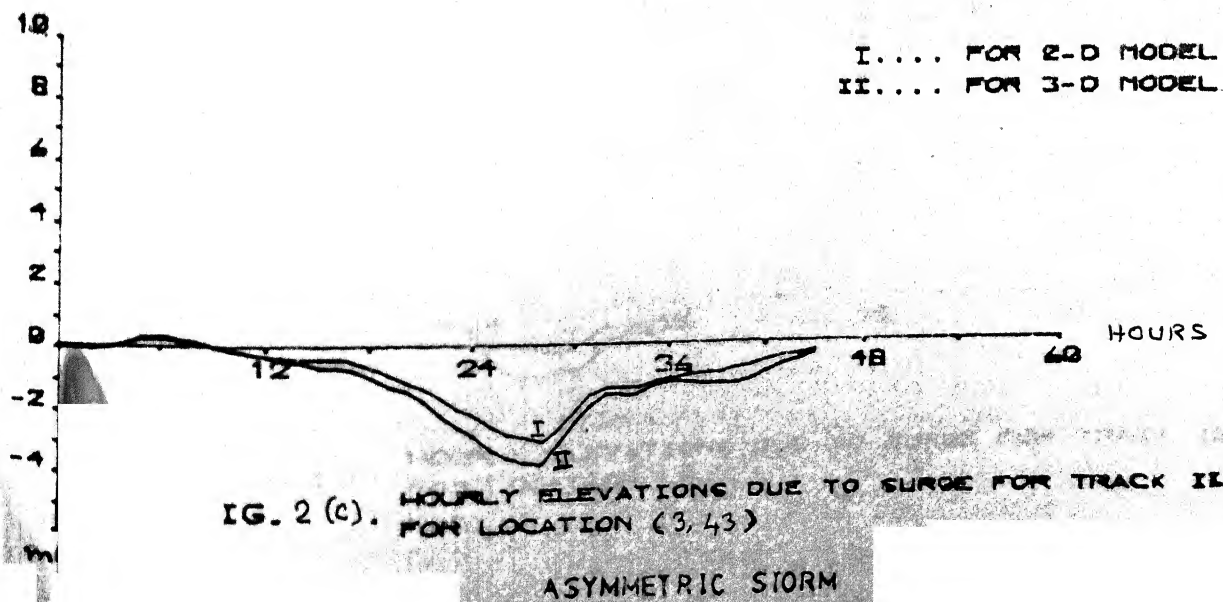
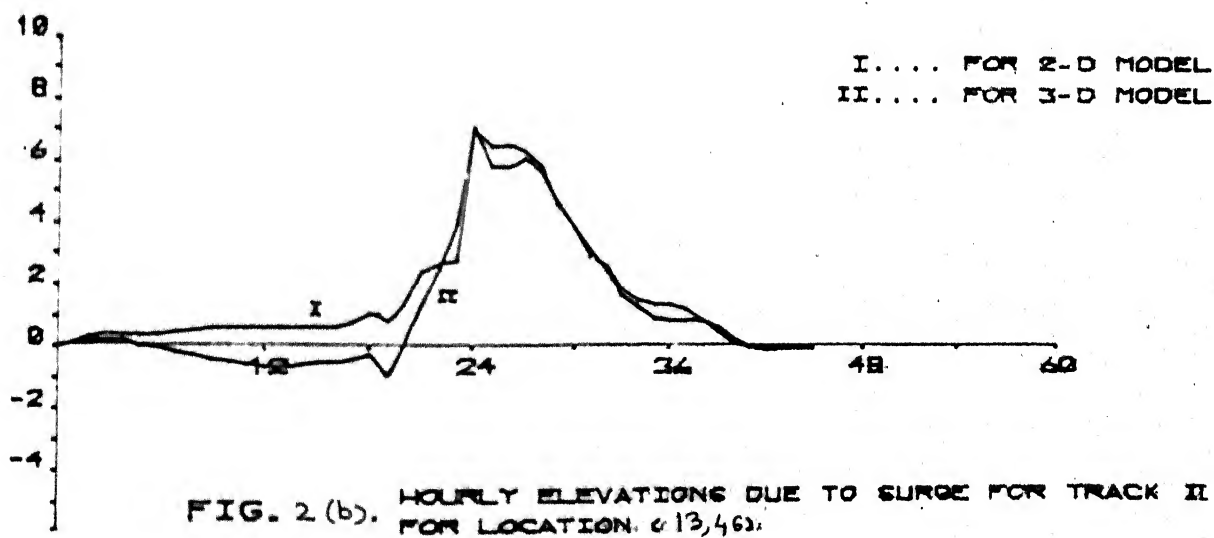
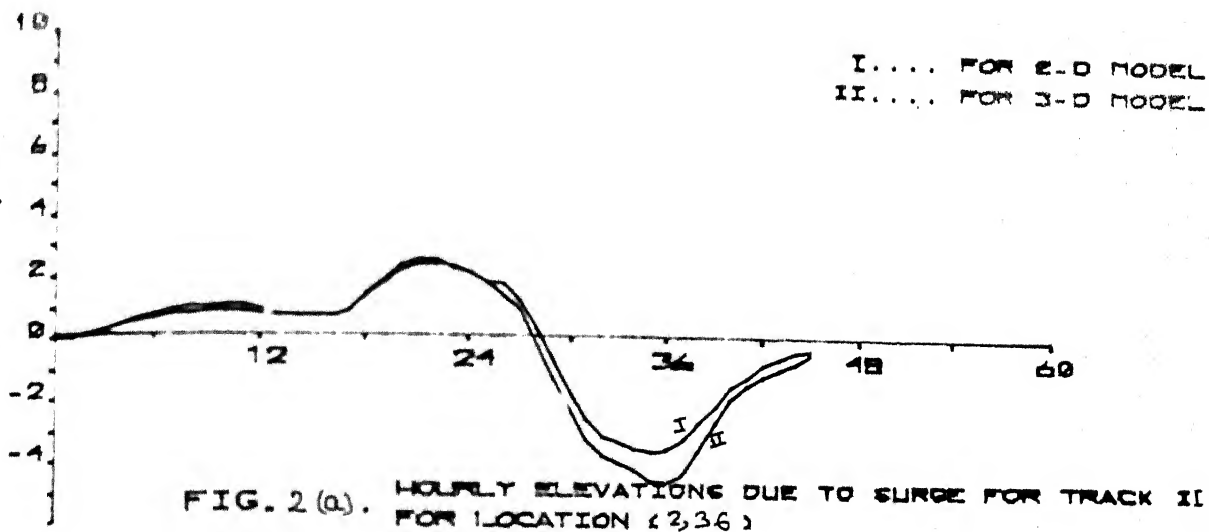
2) Under the strong storm forcing the bay has responded with a predominant horizontal circulation with an inflow near the central portion and the outflow sideways across the open boundary.

3) The model has shown strong surface current in the surface layer during the developing period of the cyclone. At some locations these currents have shown magnitudes in excess of the normally expected values. A varification of this was not possible at the present stage, due to non-availability of observational data.

4) The local, swift oscillation of the surface elevation due to the storm forcing along track III is explained in a better way as compared to the explanation given in the depth averaged model, showing the worthiness of the three-dimensional model in particular situations. It is also shown that the oscillation is a very particular case and is confined to the surface layer (resulting in quick damping). No swift oscillation has been observed in the numerical experiments with the storm forcing taken along the oblique tracks (either way) passing through the same point of landfall.



ASYMMETRIC STORM



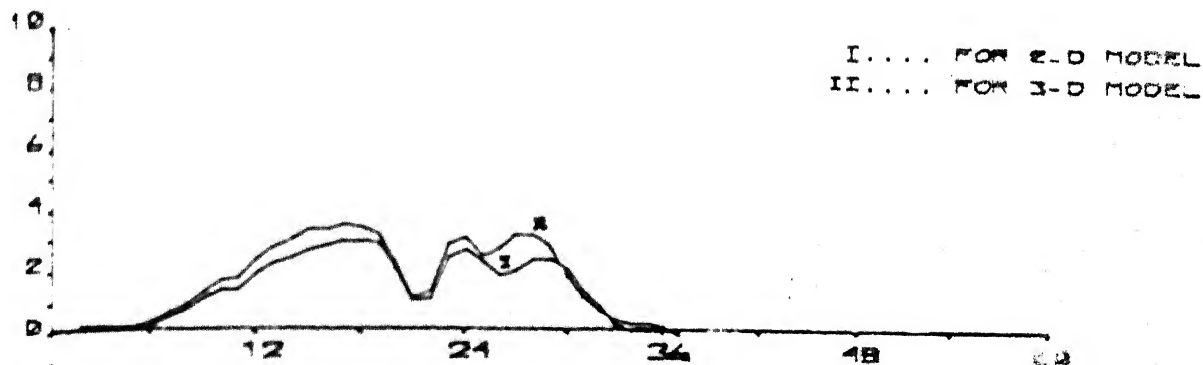


FIG. 3(a) HOURLY ELEVATIONS DUE TO SURGE FOR TRACK III
FOR LOCATION (6, 18)

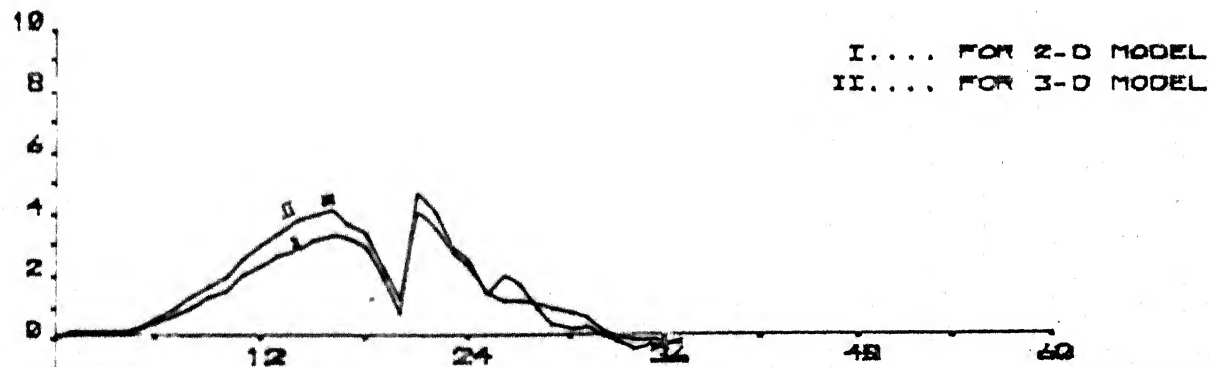


FIG. 3(b) HOURLY ELEVATIONS DUE TO SURGE FOR TRACK III
FOR LOCATION (8, 6)



FIG. 3(c) HOURLY ELEVATIONS DUE TO SURGE FOR TRACK III
FOR LOCATION (8, 20)

ASYMMETRIC STORM

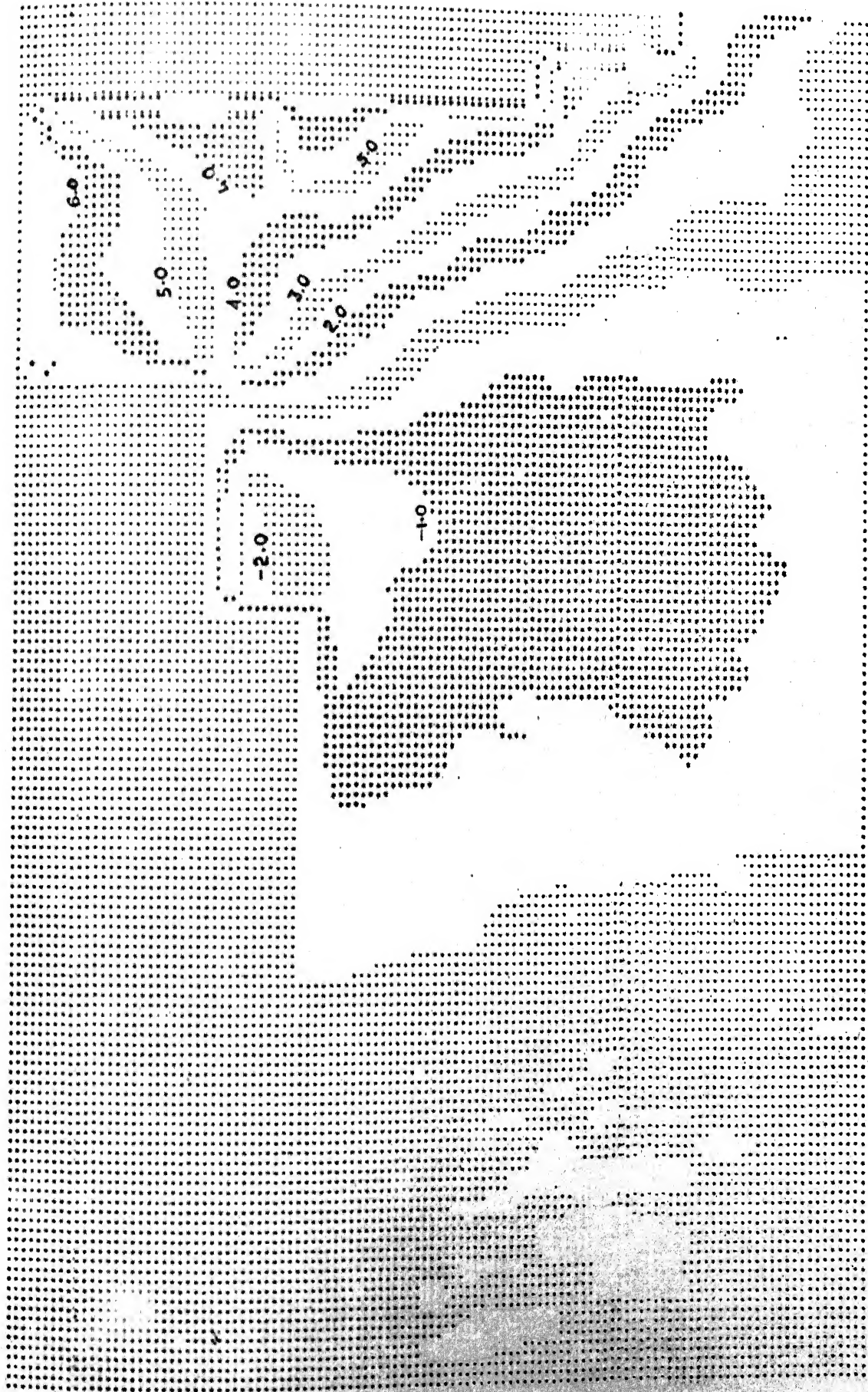


FIG. 4(a). ELEVATION CONTOUR BANDS IN METERS)
AT 29 HOURS
ASYMMETRIC STORM - TRACK I

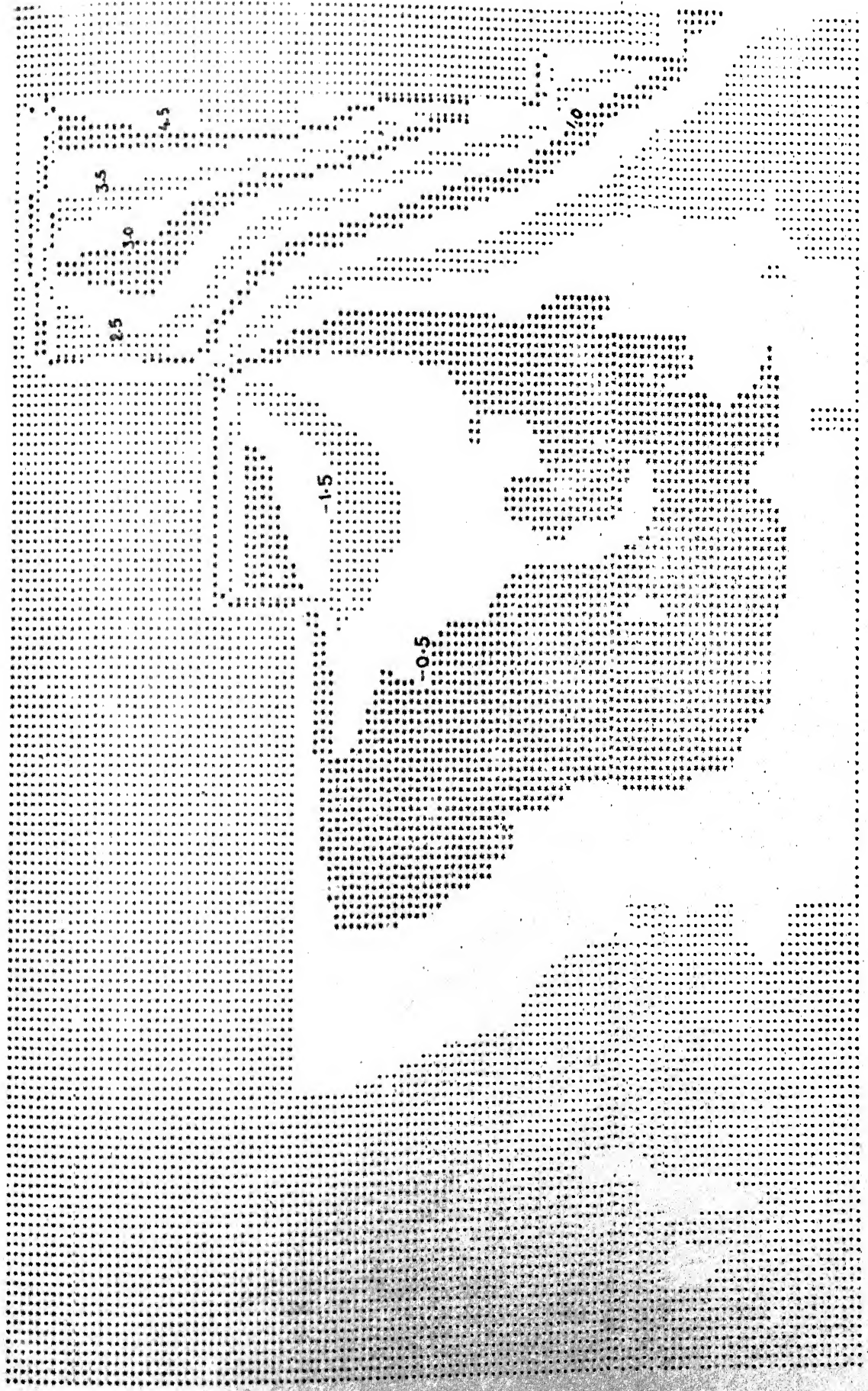


FIG. 4 (b). ELEVATION CONTOUR BANDS (IN METERS)
AT 35 HOURS
ASYMMETRIC STORM - TRACK I

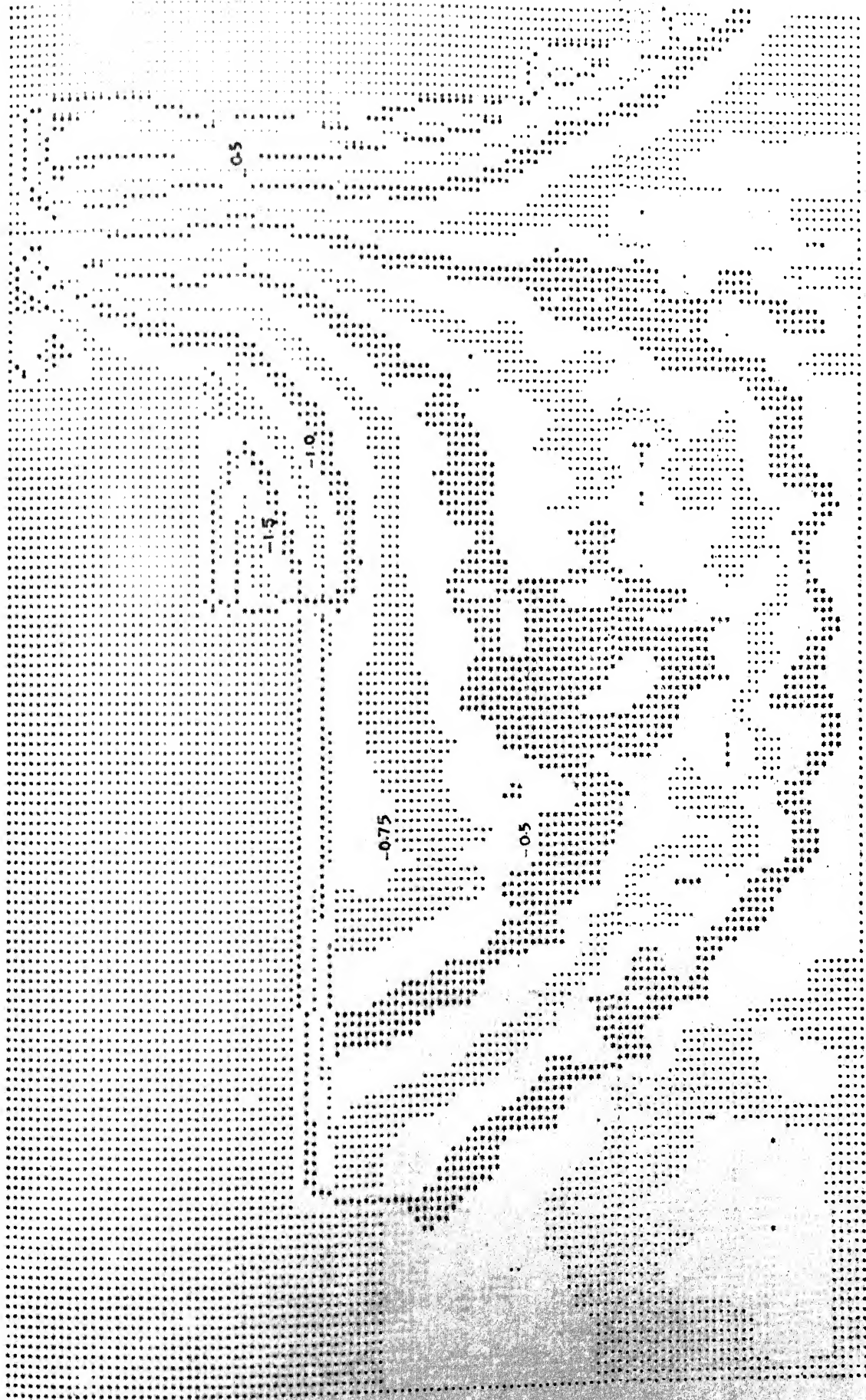


FIG. 4(c). ELEVATION CONTOUR BANDS (IN METERS) AT 40 HOURS
ASYMMETRIC STORM - TRACK I



FIG. 5 (a). ELEVATION CONTOUR BANDS IN METERS)
AT 29 HOURS
ASYMMETRIC STORM - TRACK II



FIG. 5 (b). ELEVATION CONTOUR BANDS (IN METERS)
AT 35 HOURS
ASYMMETRIC STORM - TRACK II

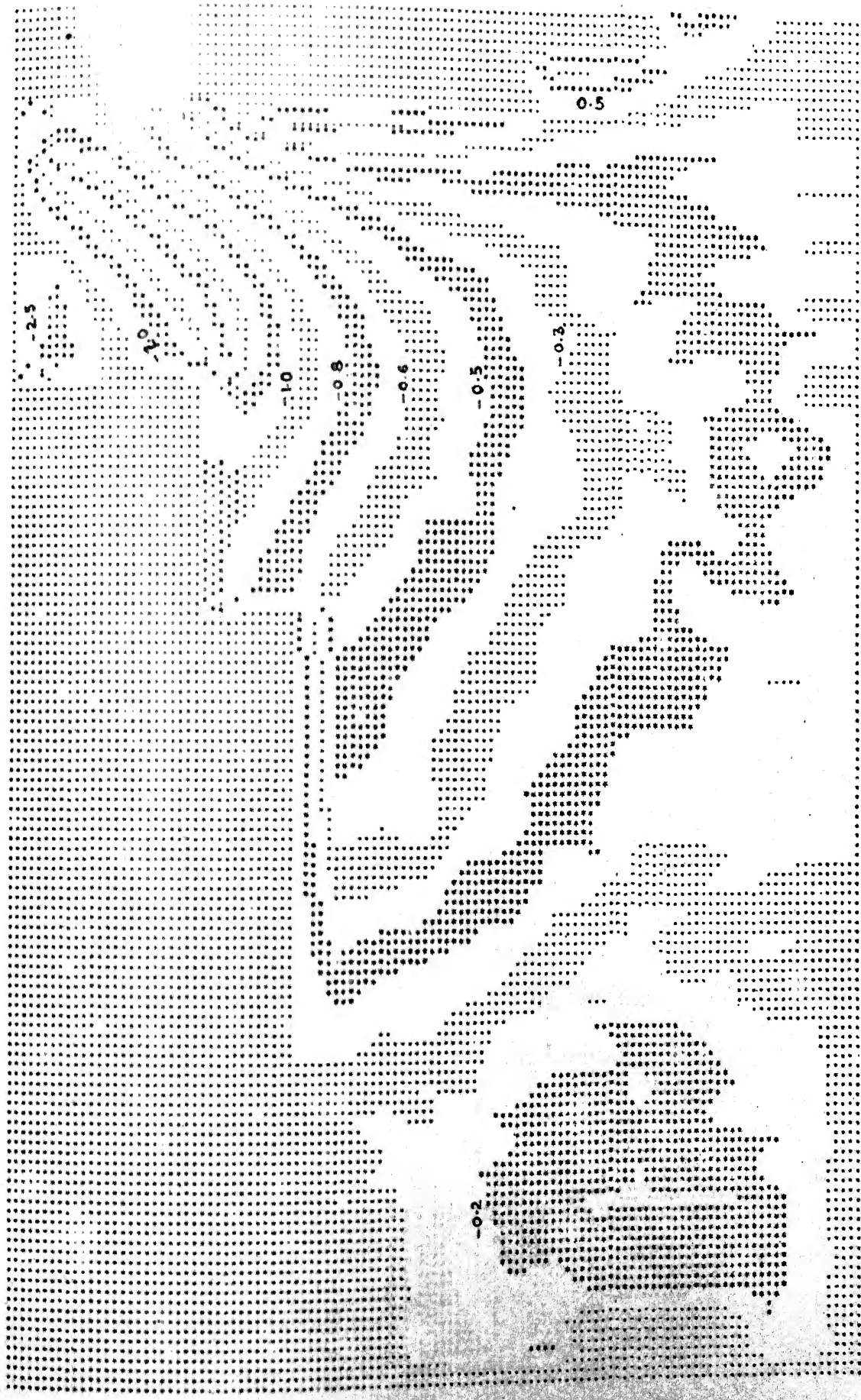


FIG. 5 (c). ELEVATION CONTOUR BANDS (IN METERS)
AT 40 HOURS
ASYMMETRIC STORM - TRACK II

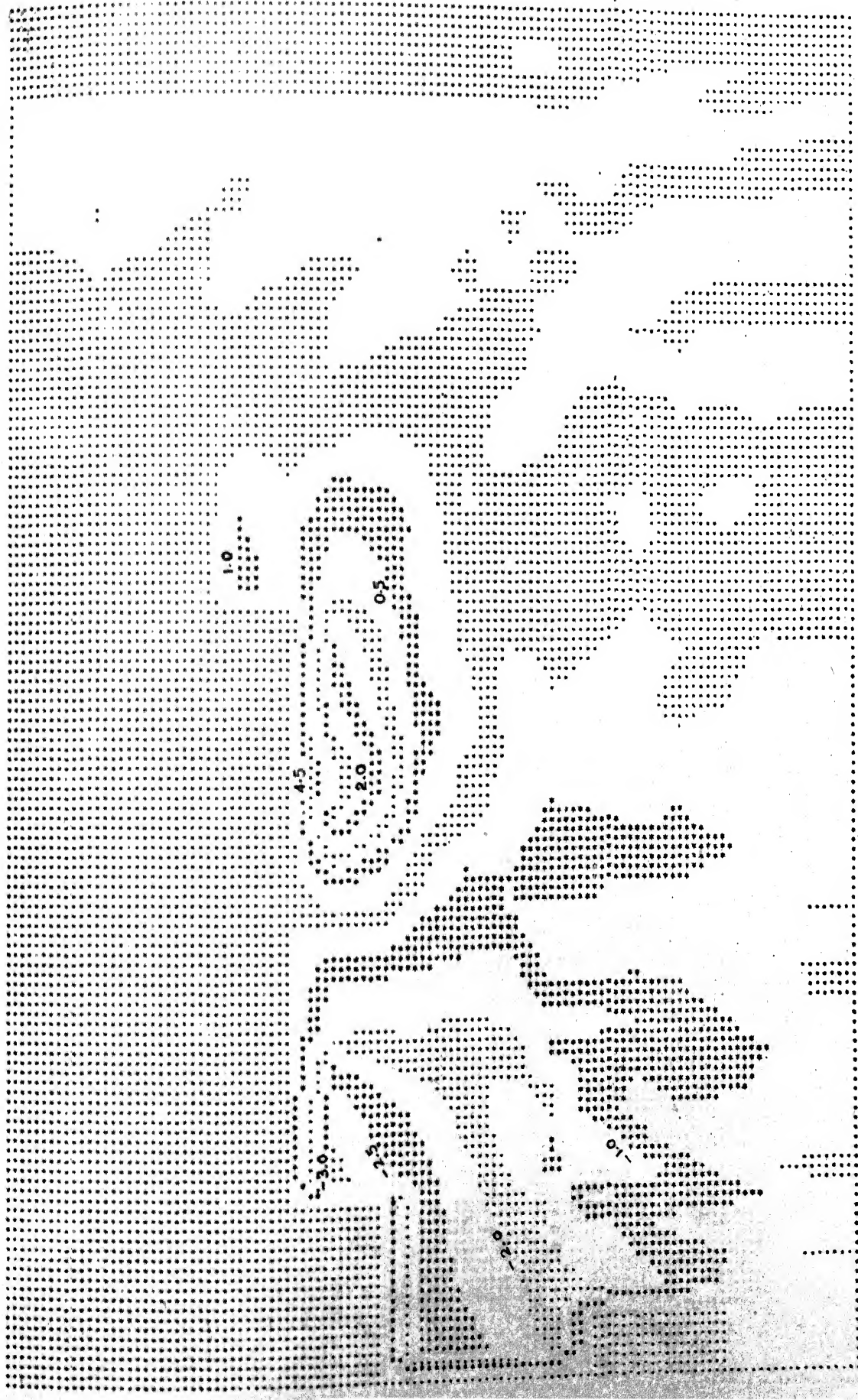


FIG. 6(a). ELEVATION CONTOUR BANDS (IN METERS)
AT 22 HOURS
ASYMMETRIC STORM - TRACK III

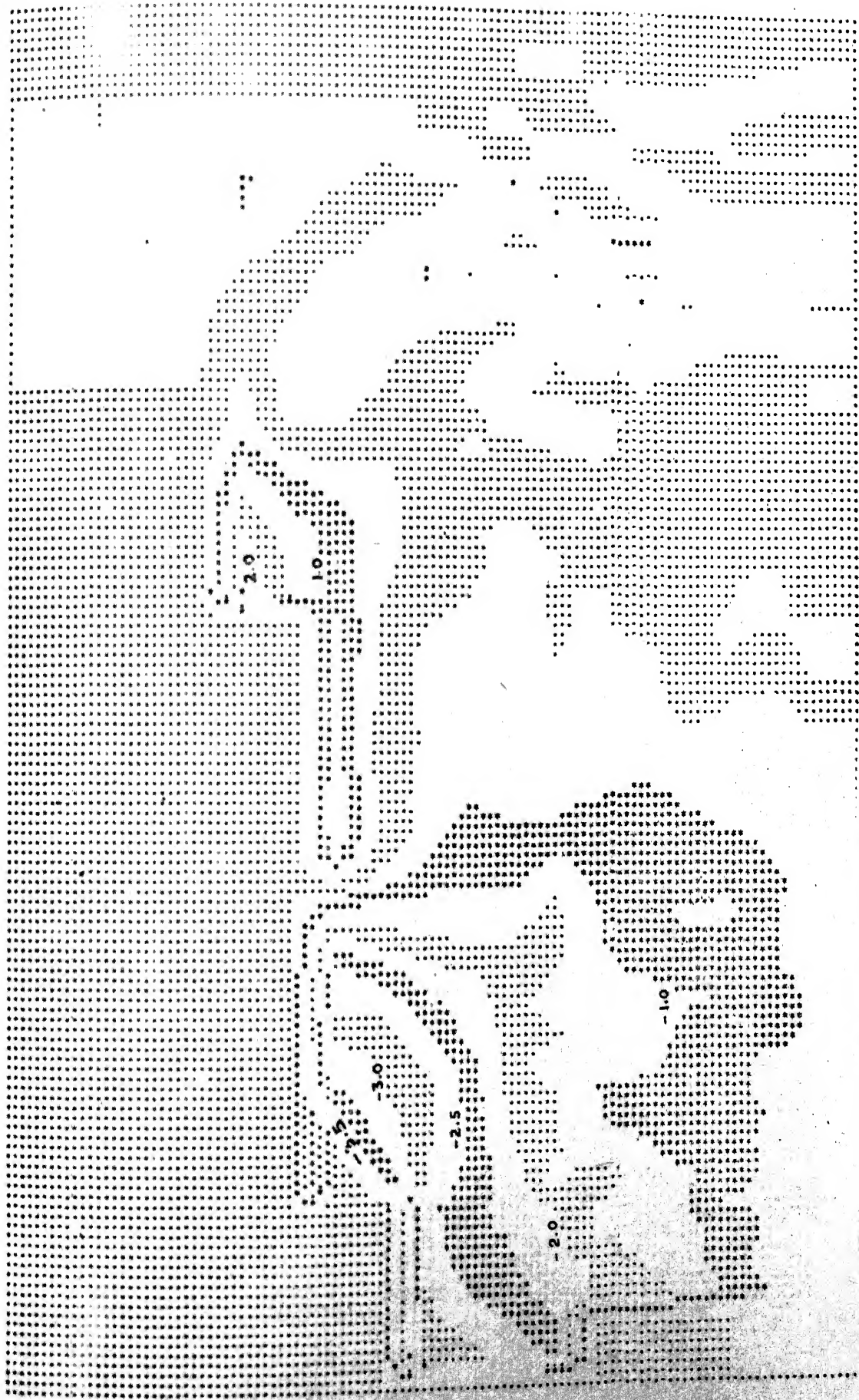


FIG. 6 (b) ELEVATION CONTOUR BANDS (IN METERS)
AT 26 HOURS
ASYMMETRIC STORM - TRACK III

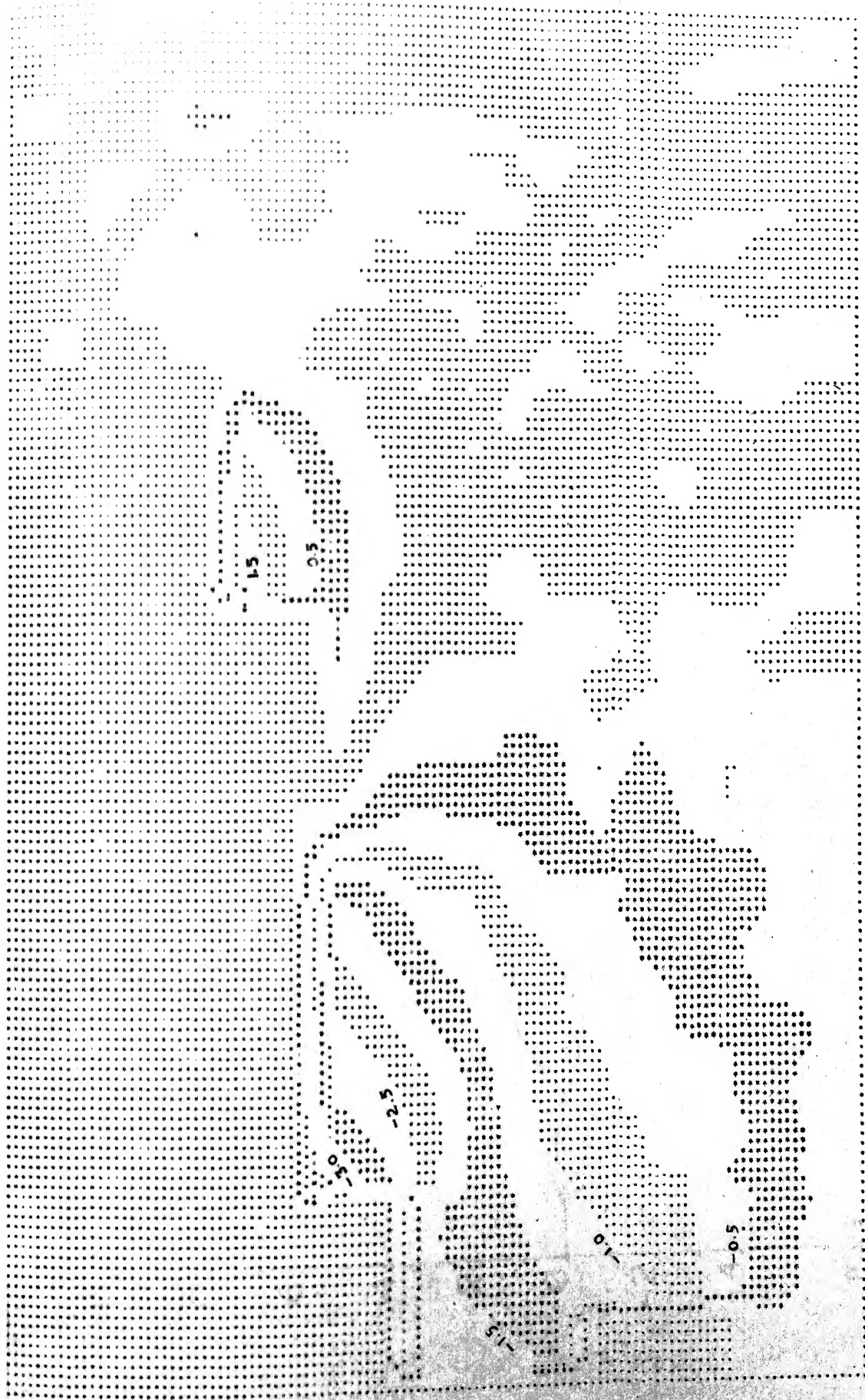
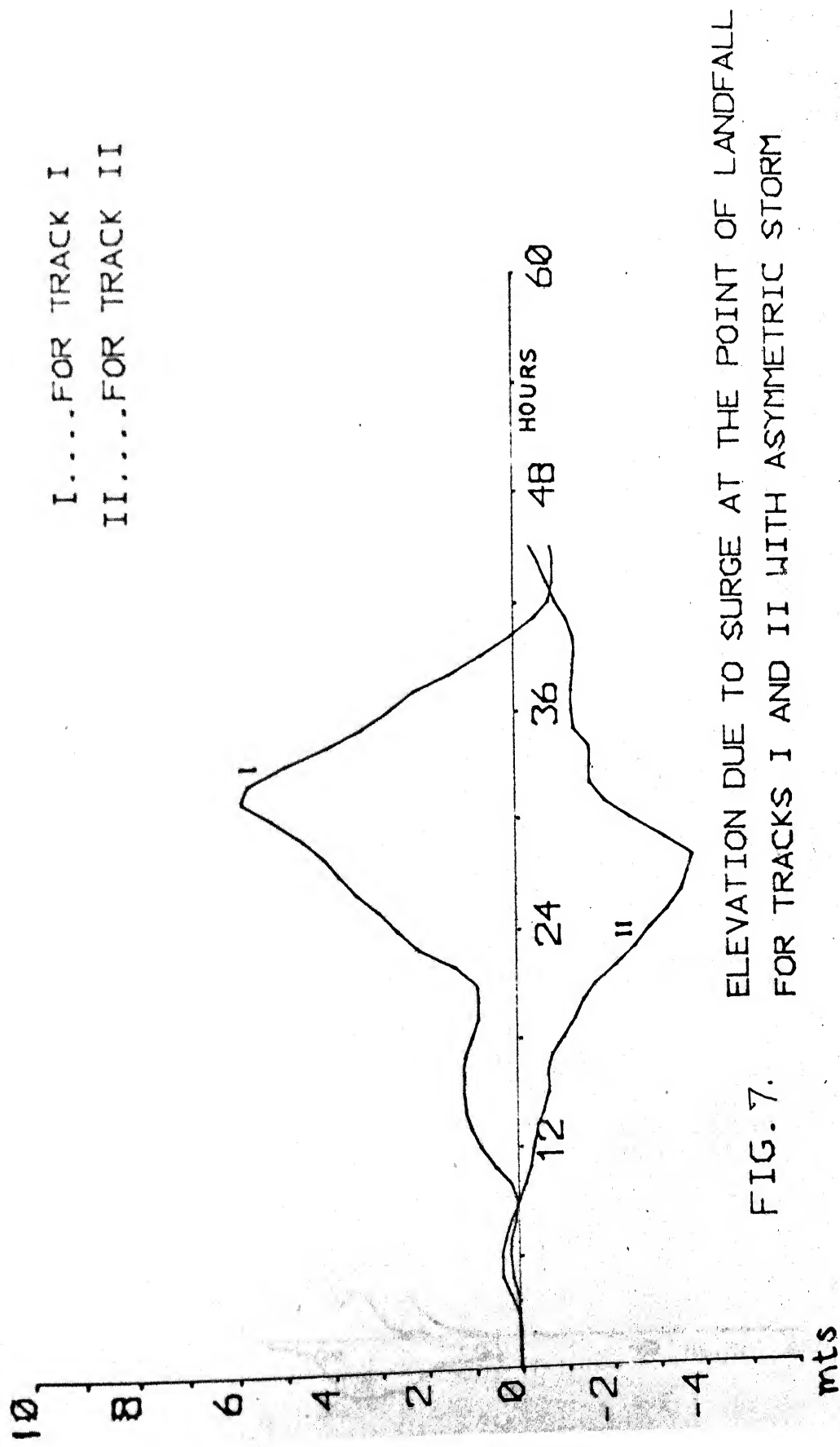
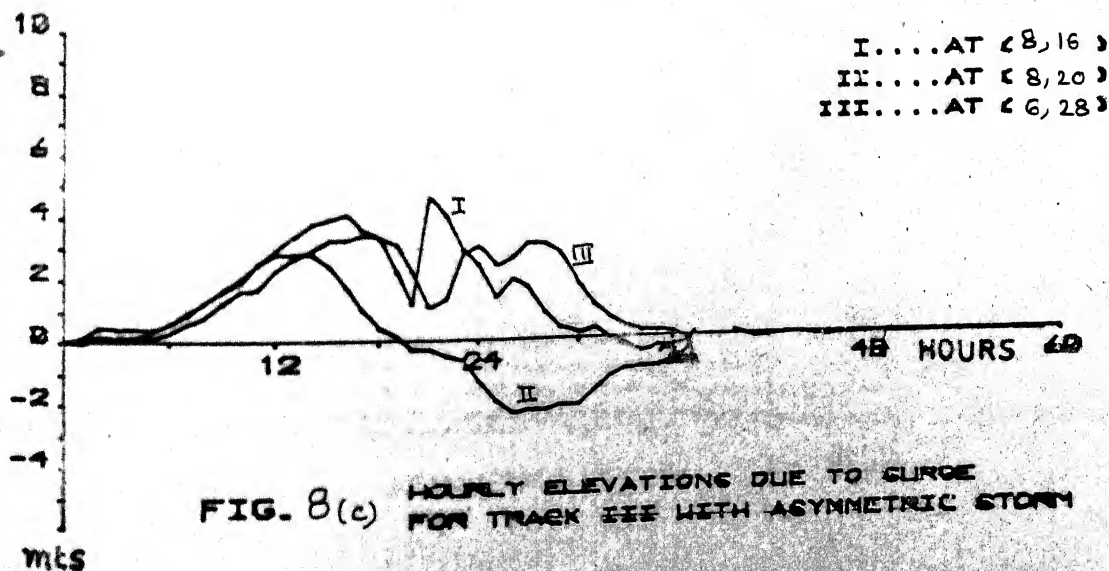
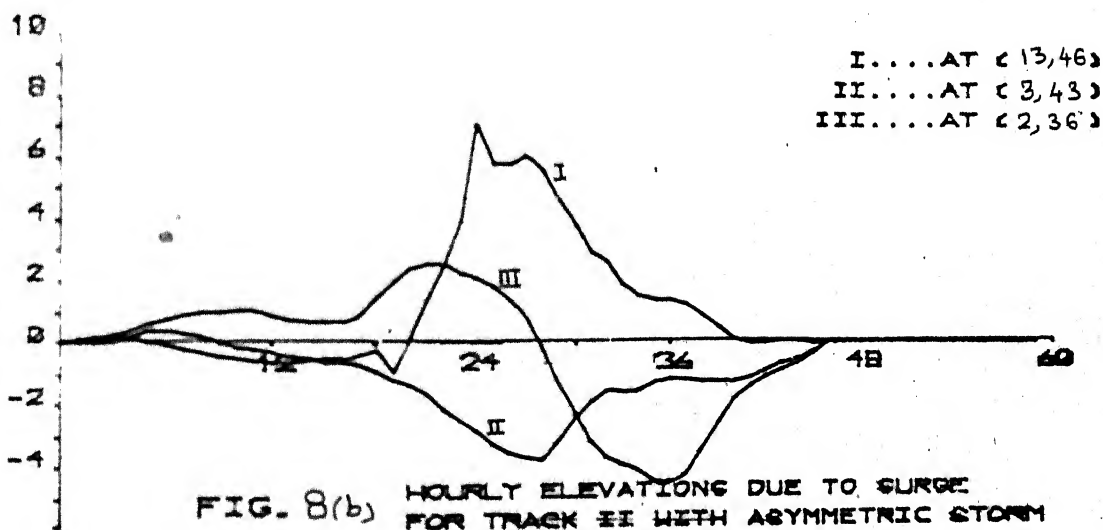
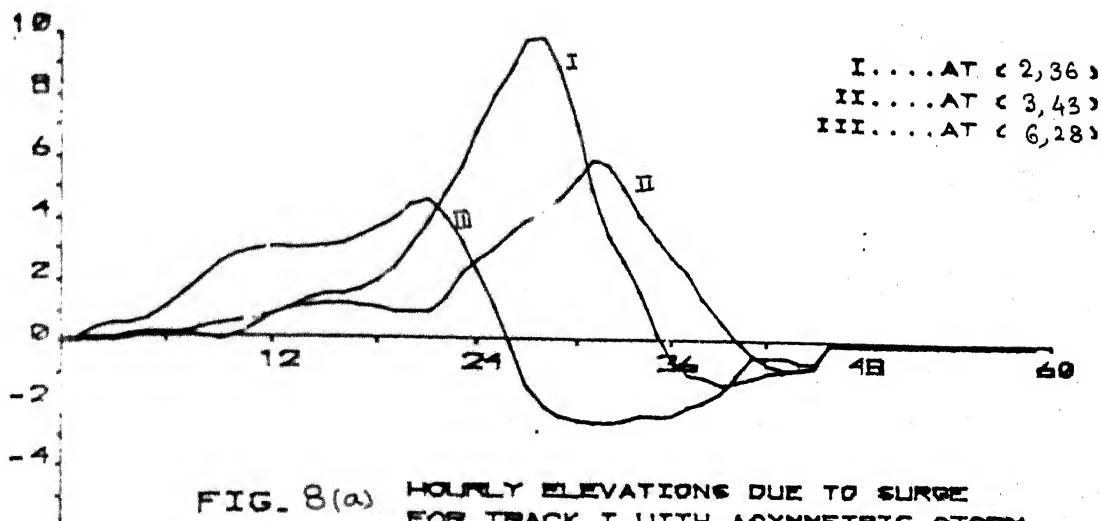


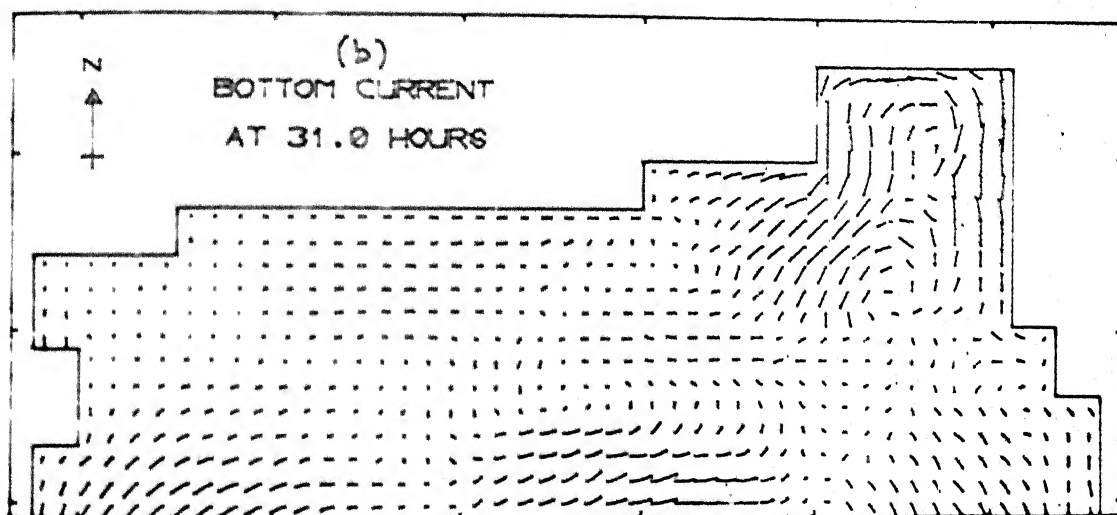
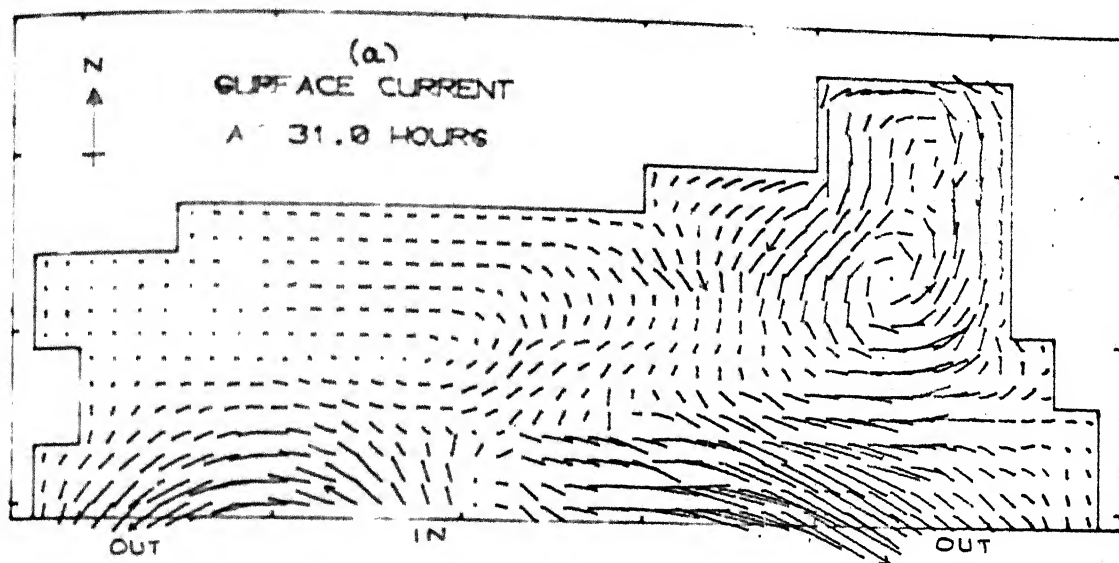
FIG. 6(c) ELEVATION CONTOUR BANDS (IN METERS)
AT 31 HOURS
ASYMMETRIC STORM - TRACK III



ELEVATION DUE TO SURGE AT THE POINT OF LANDFALL
FOR TRACKS I AND II WITH ASYMMETRIC STORM

FIG. 7.





CURRENT STRENGTH \longrightarrow 2.0 MT/SEC

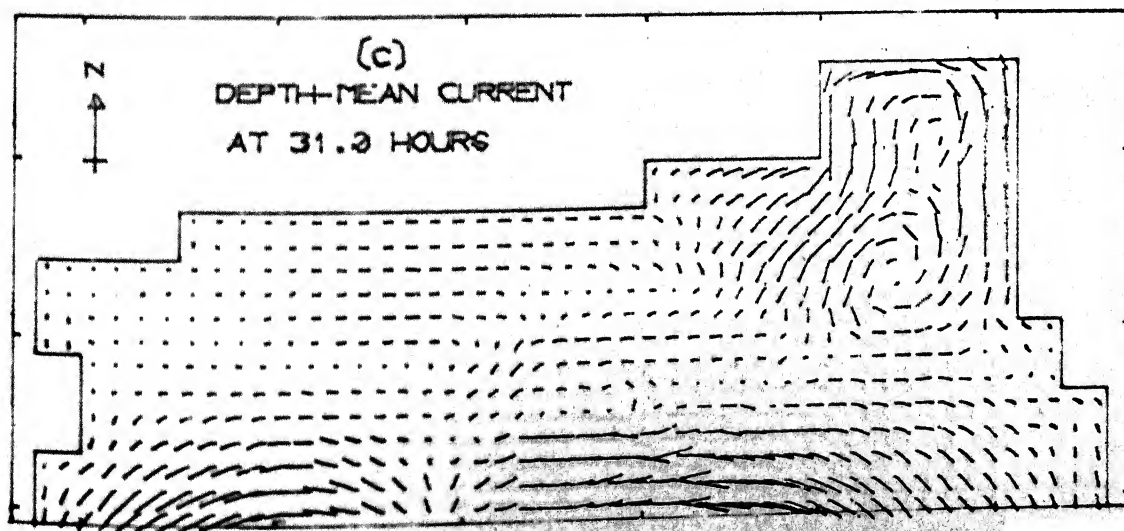
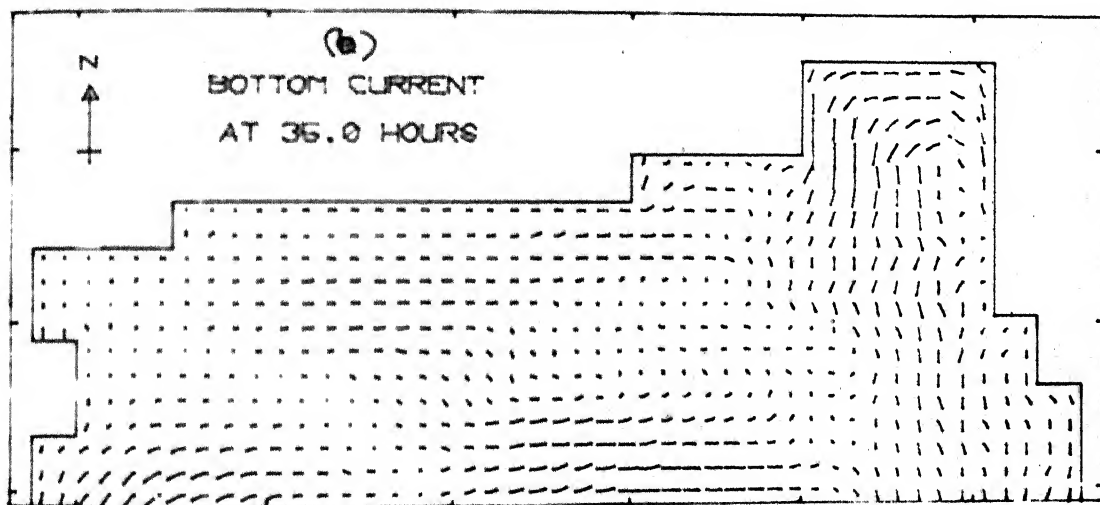
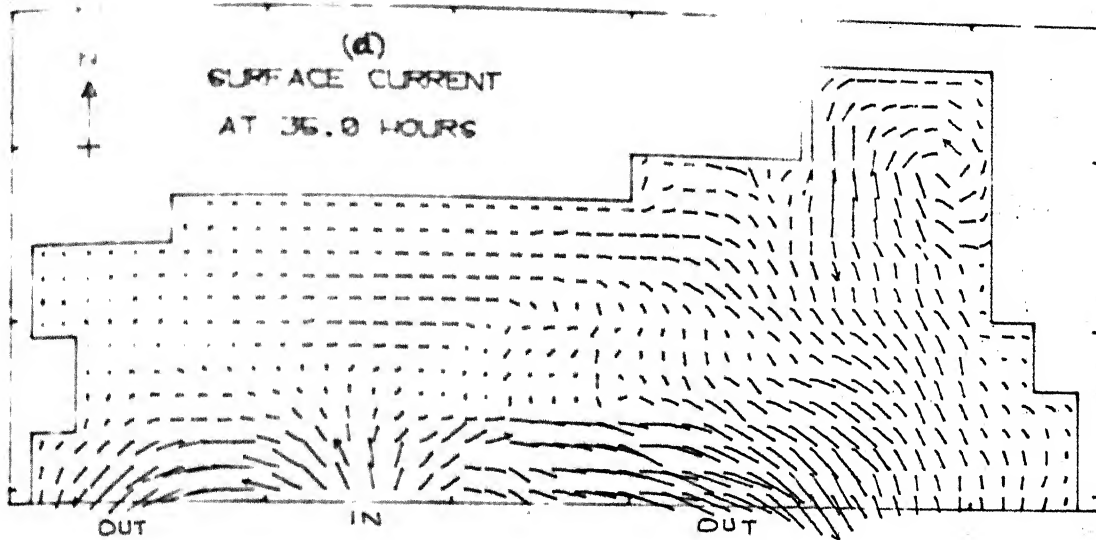


FIG. 9. a, b, c. ASYMMETRIC STORM ALONG TRACK :



CURRENT STRENGTH \longleftrightarrow 2.0 MT/SEC

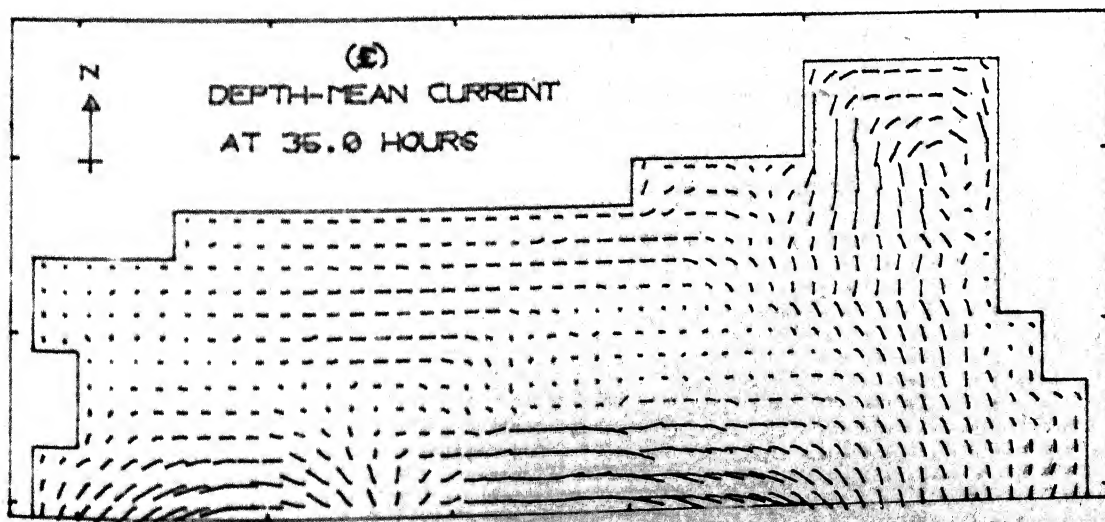
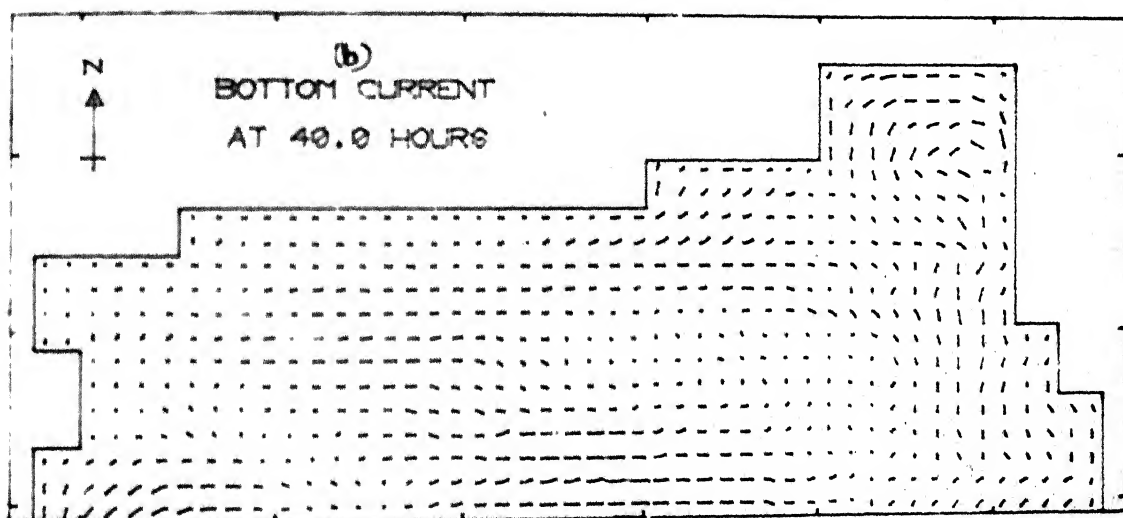
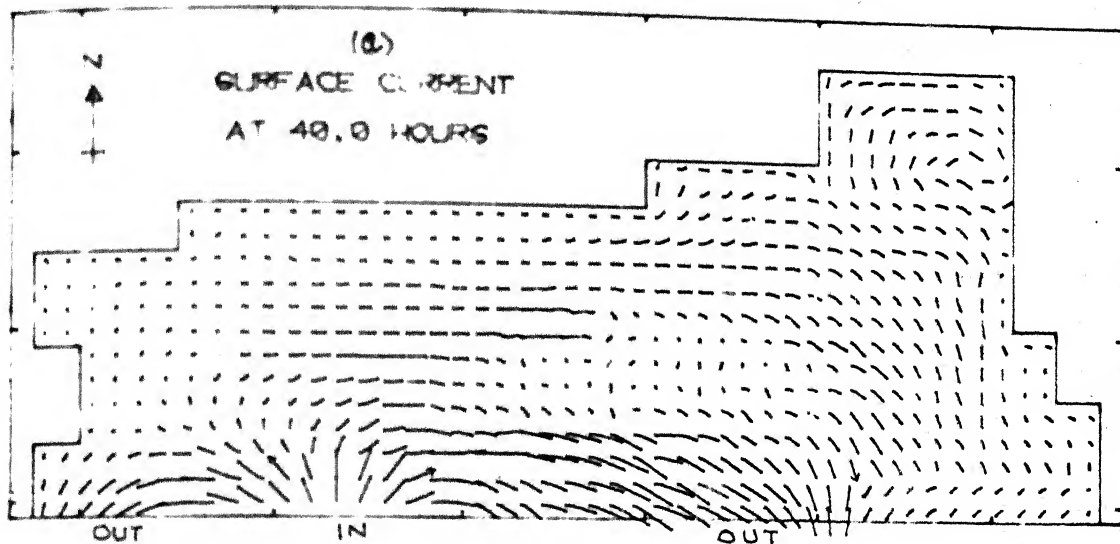


FIG. 10. a, b, c. ASYMMETRIC STORM ALONG TRACK 1



CURRENT STRENGTH \longrightarrow 2.0 MT/SEC

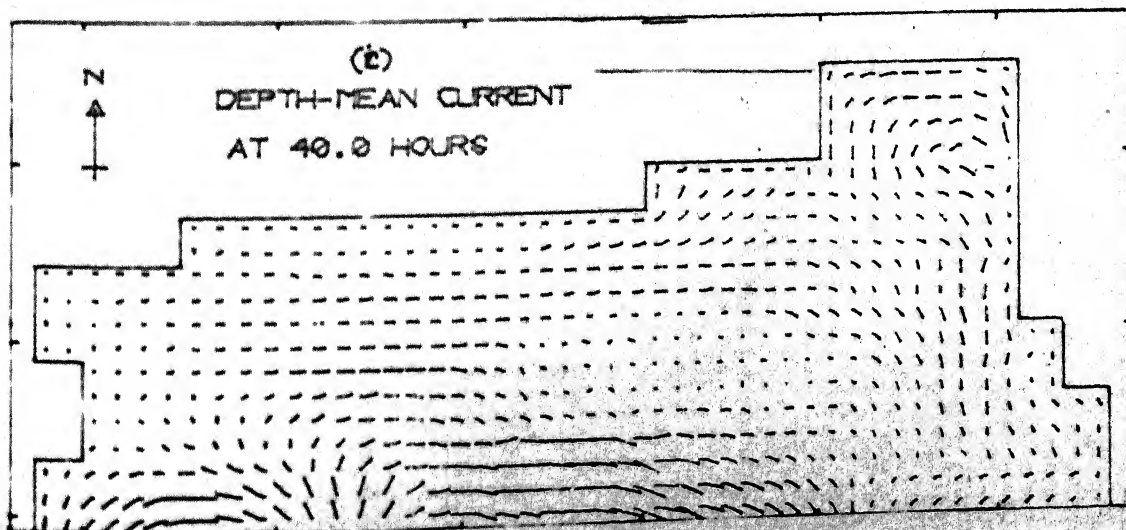
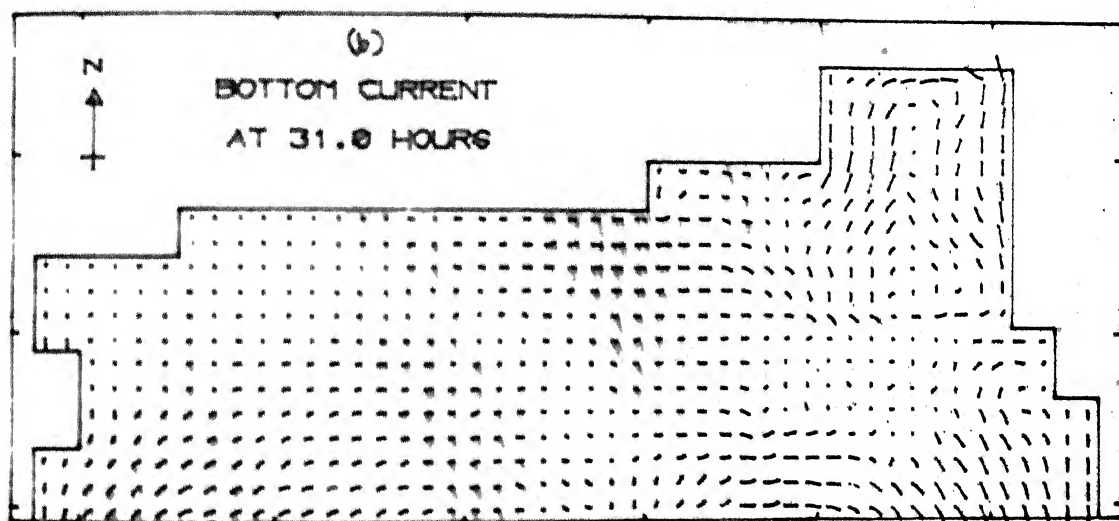
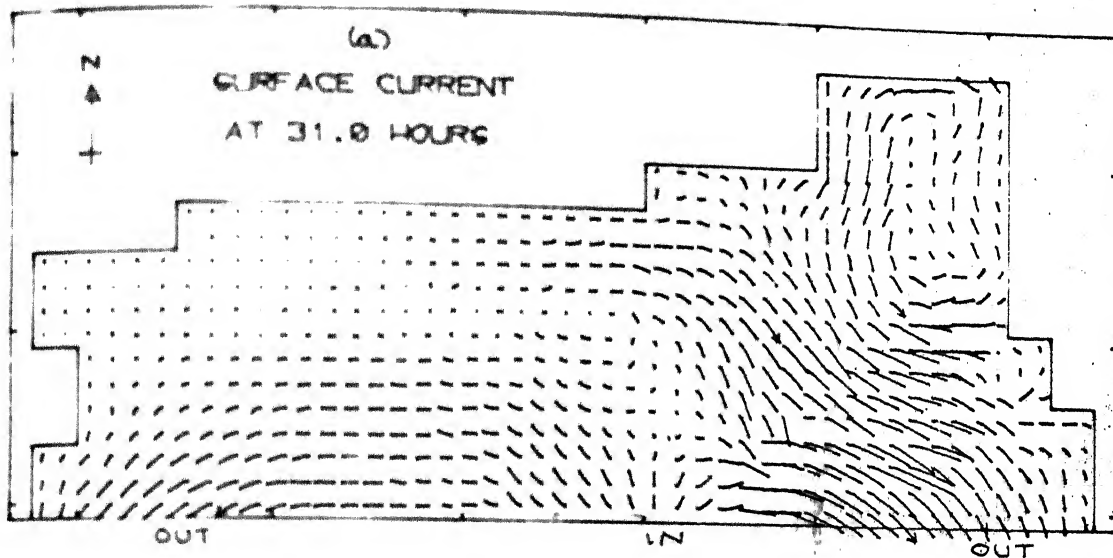


FIG. 11. (a), (b), (c). ASYMMETRIC STORM ALONG TRACK 1



CURRENT STRENGTH \longrightarrow 2.0 MT/SEC

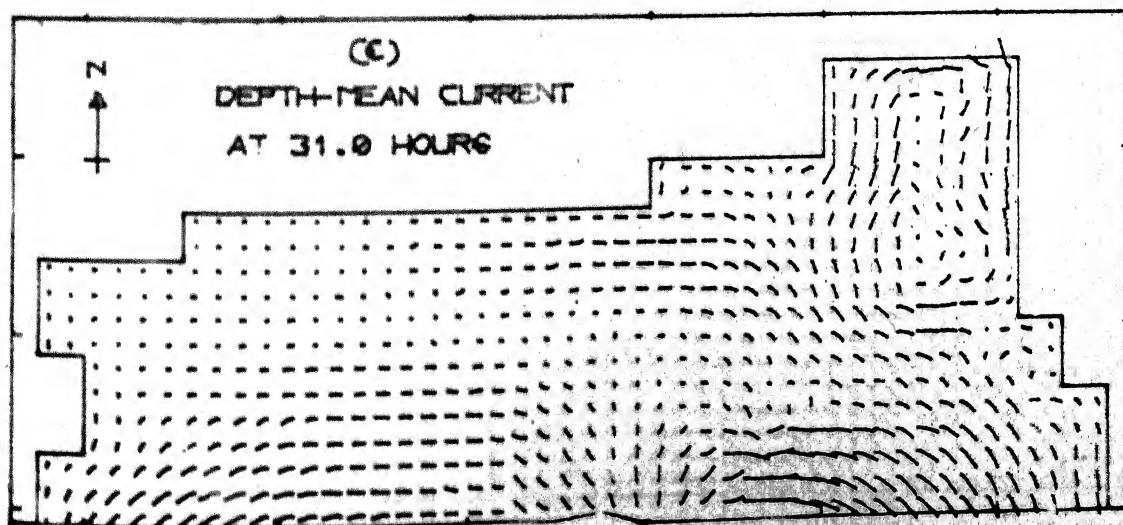
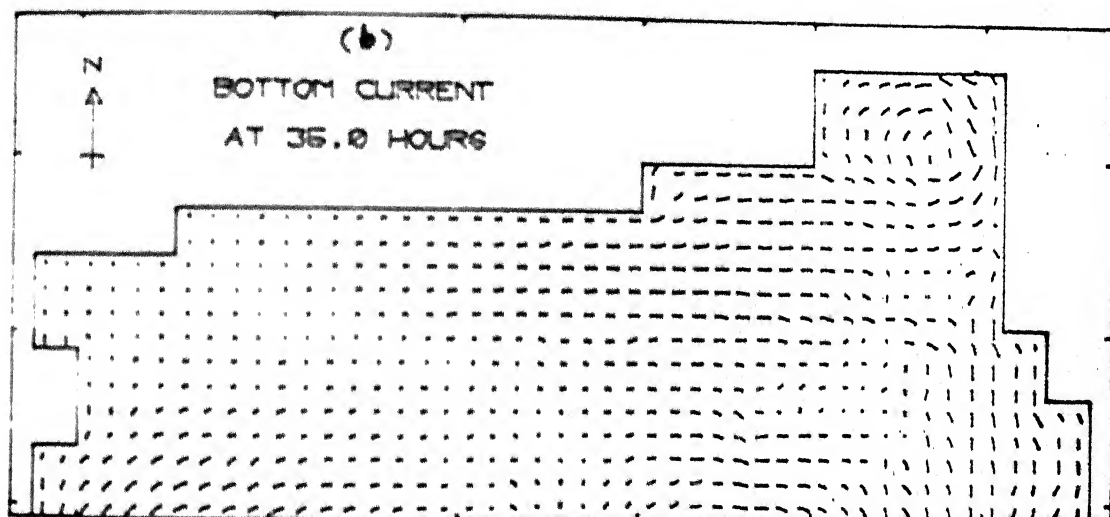
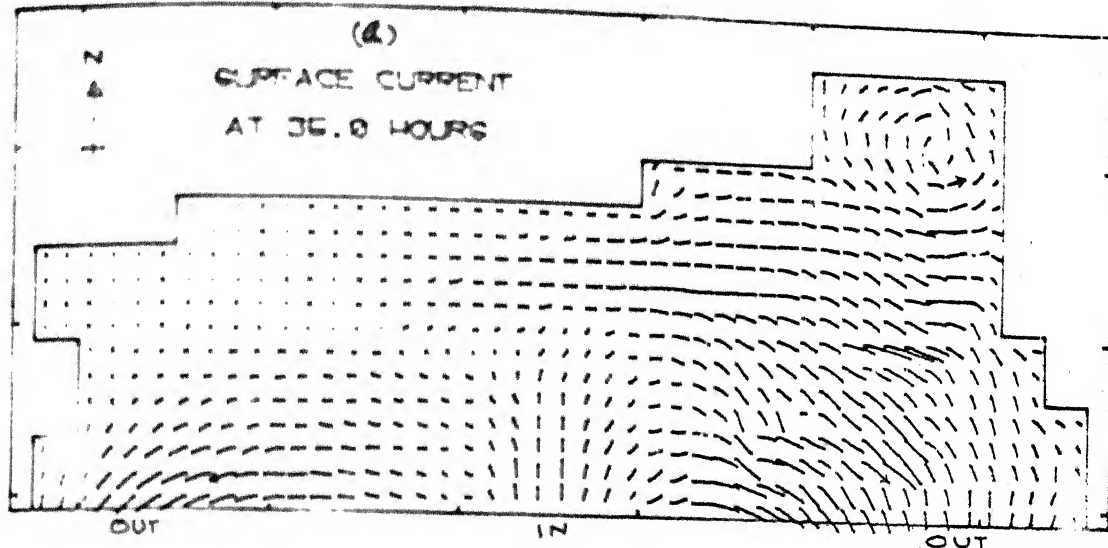
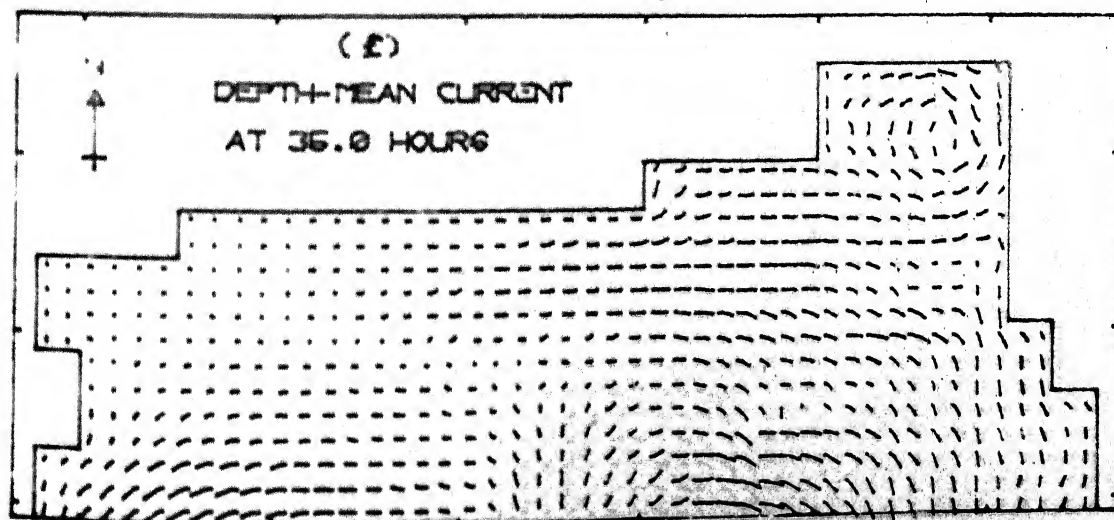


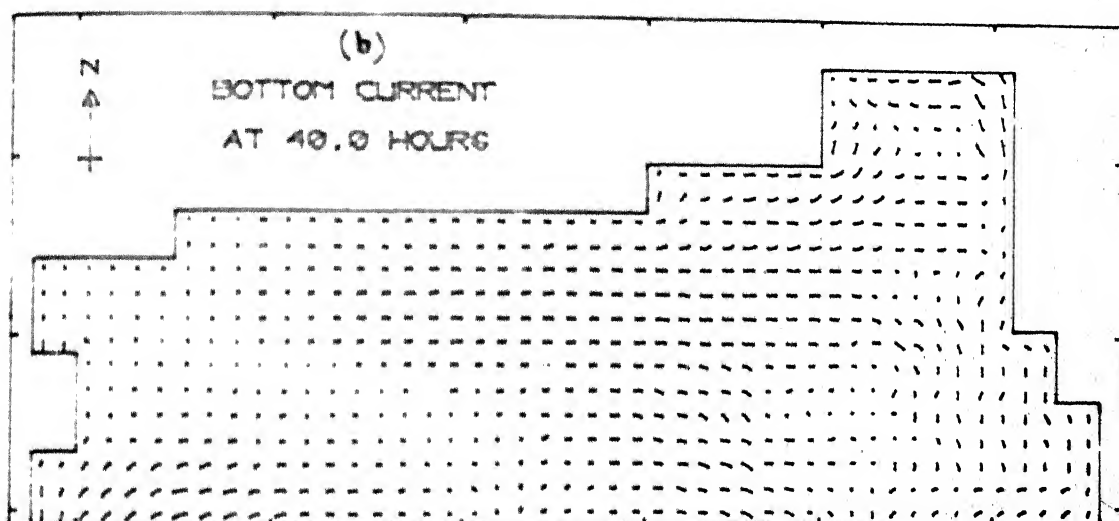
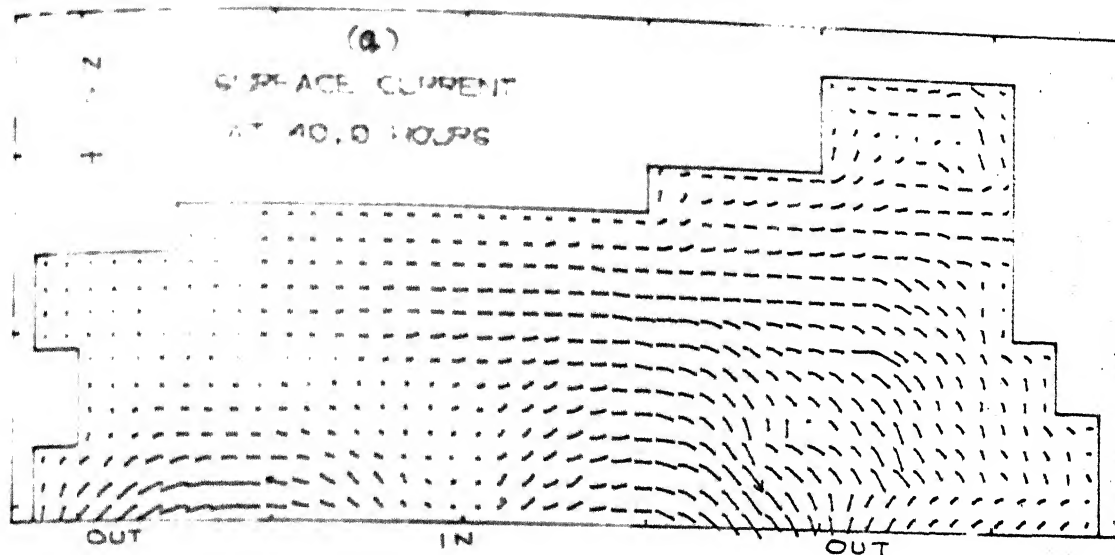
FIG. 12 (a), (b), (c). ASYMMETRIC STORM ALONG TRACK 11



CURRENT STRENGTH — 2.0 MT/SEC



FIGS. 13 a, b, c. ASYMMETRIC STORM ALONG TRACK II



CURRENT STRENGTH \longrightarrow 2.0 METERS / SEC

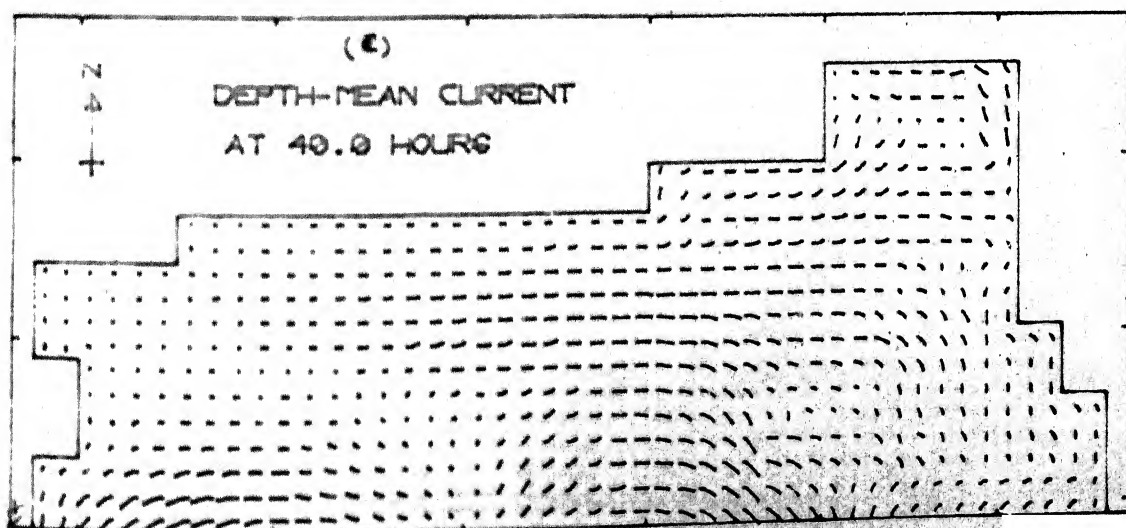
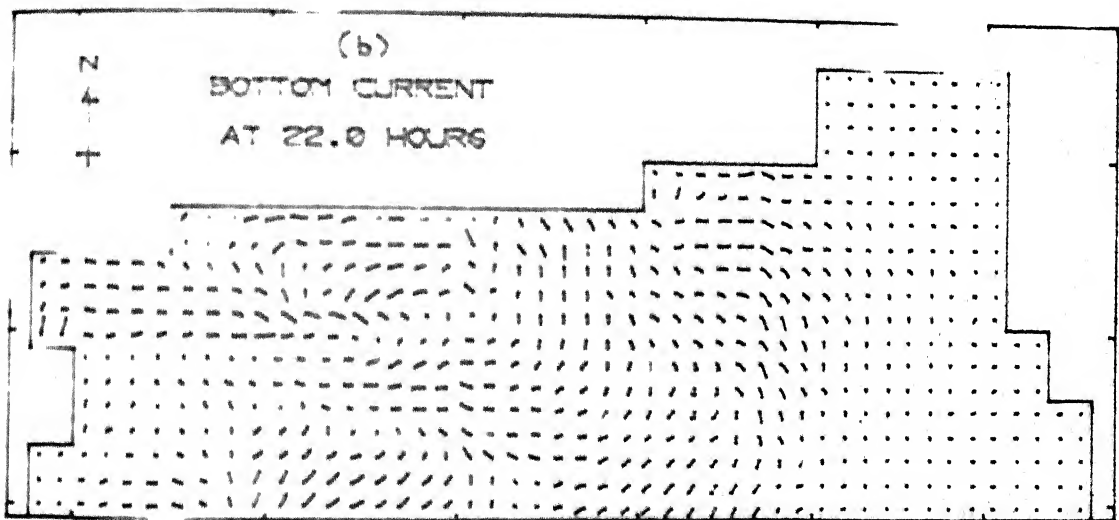
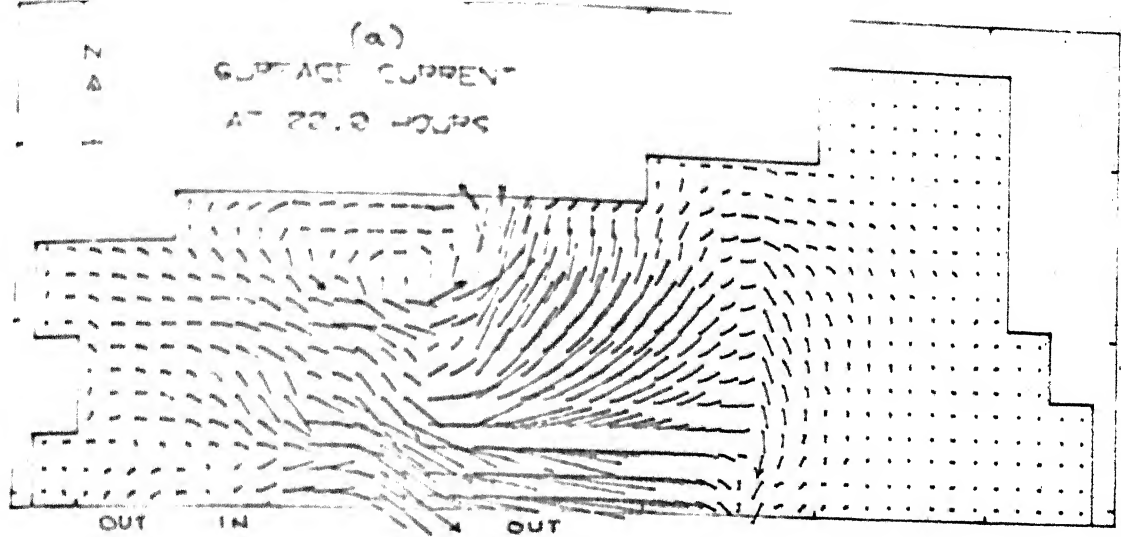


FIG. 14 a, b, c. ASYMMETRIC STORM ALONG TRACK II



CURRENT STRENGTH \longrightarrow 2.0 MT/ SEC

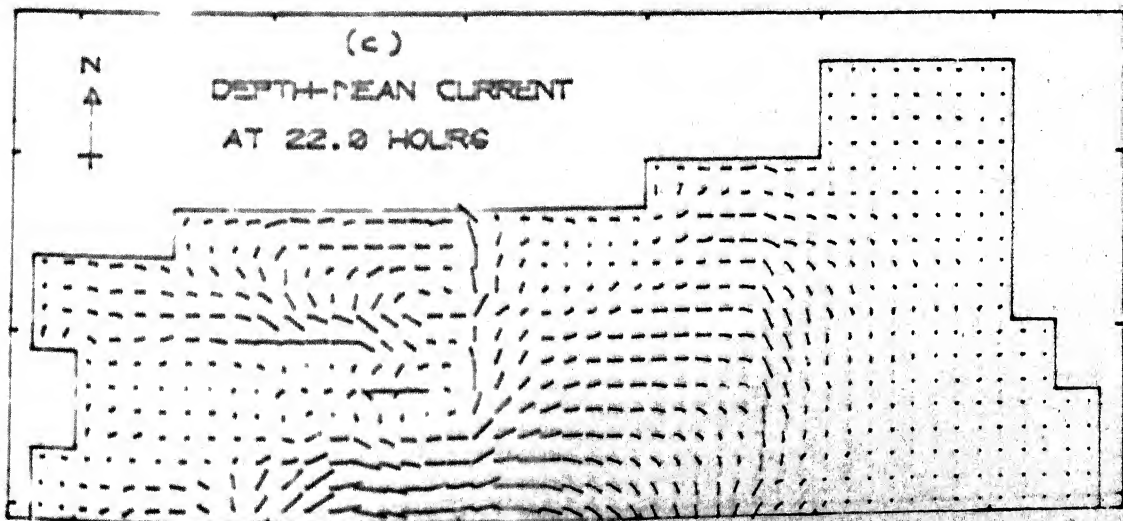
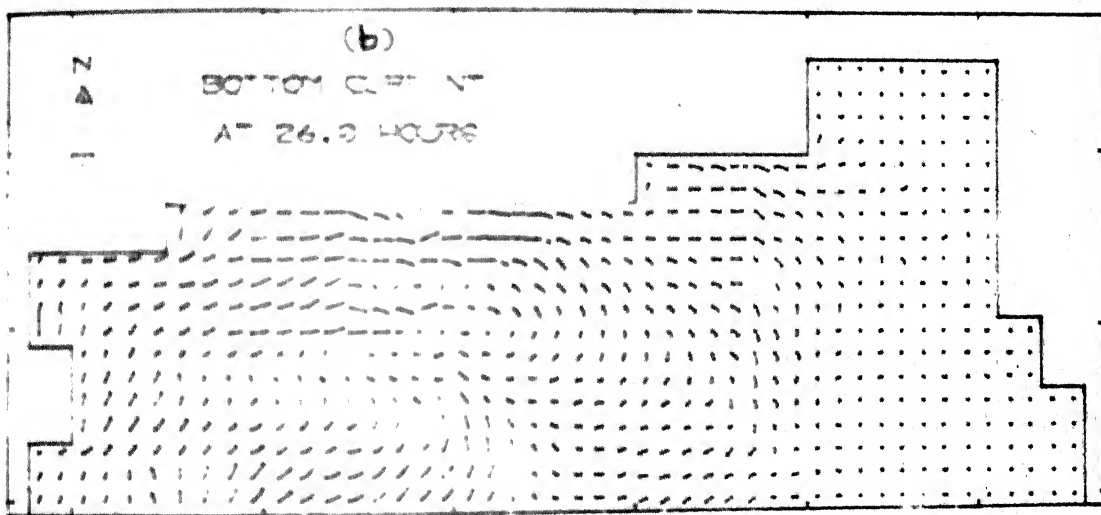
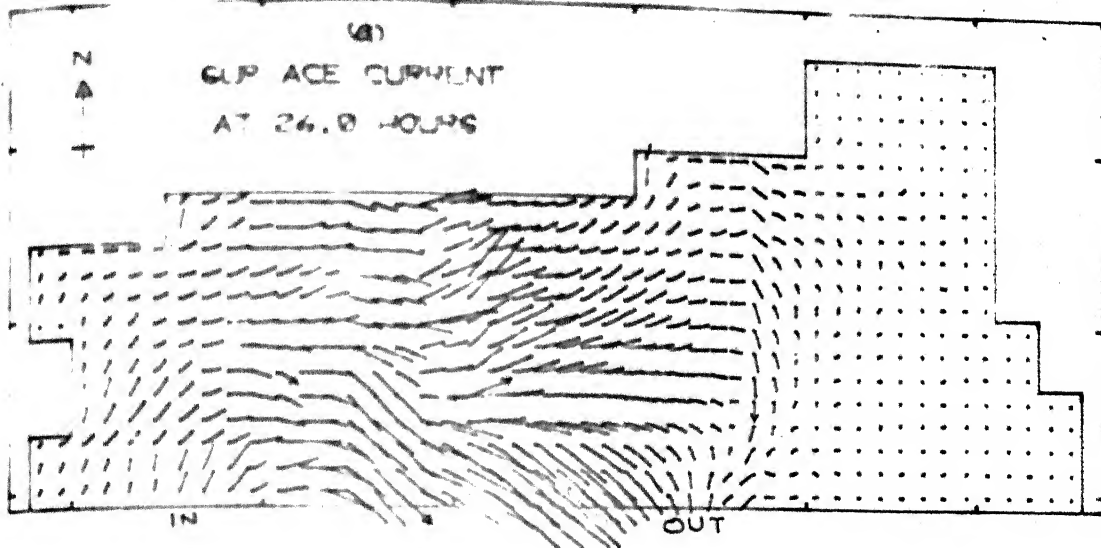


FIG. 15 a, b, c. ASYMMETRIC STORM ALONG TRACK



CURRENT STRENGTH — 2.0 MT/SEC

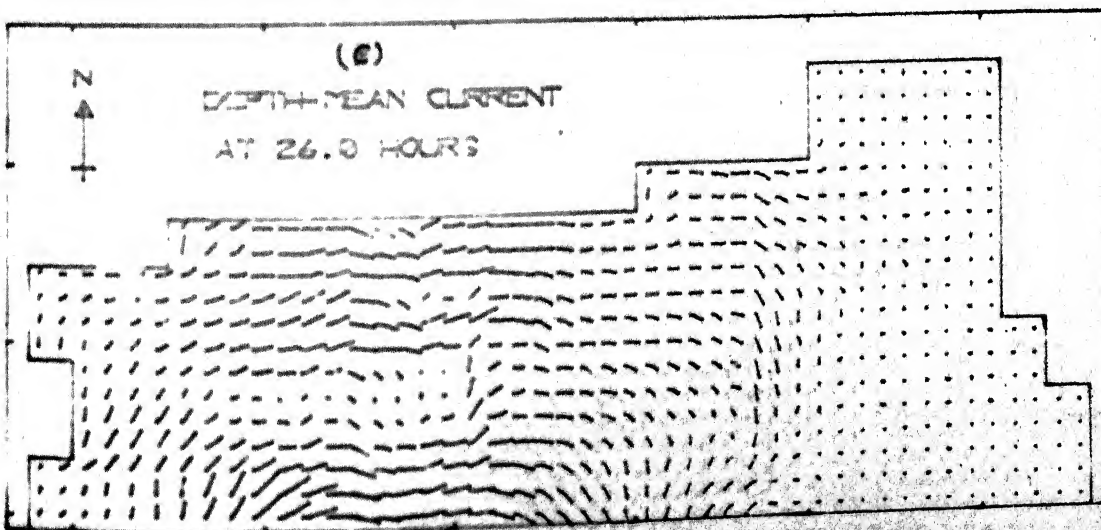
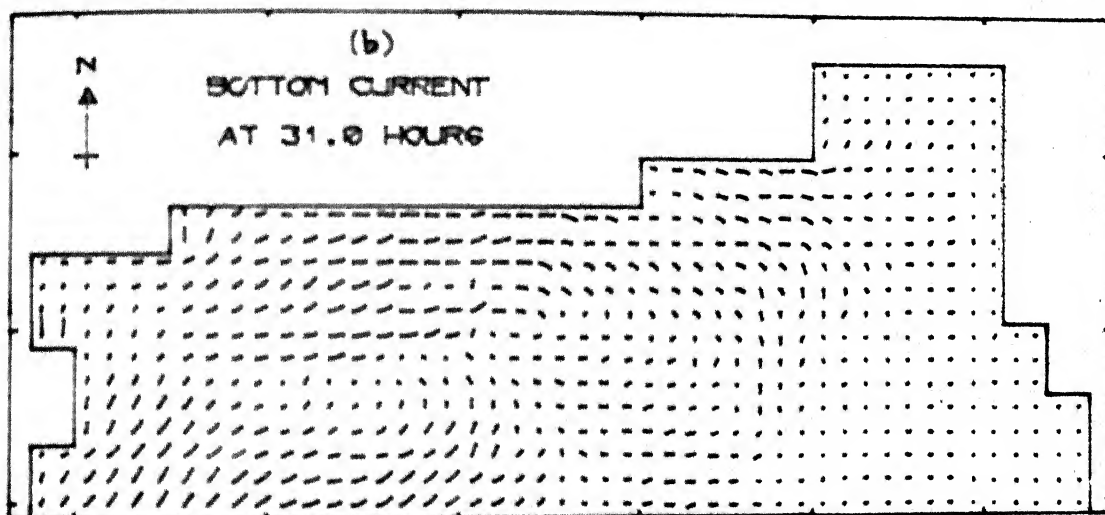
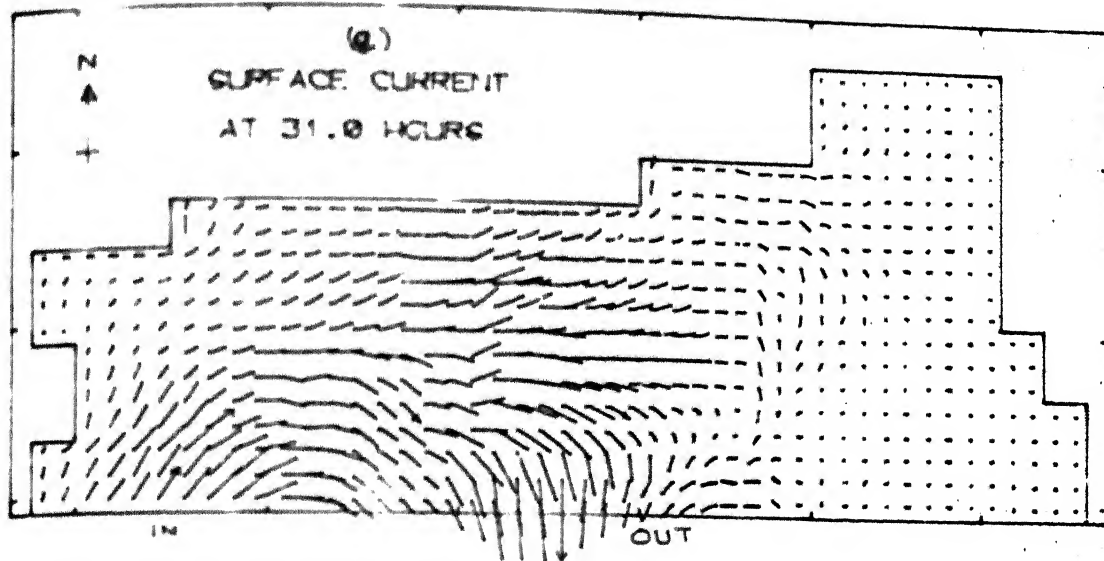


FIG. 16a,b,c. ASYMMETRIC STORM ALONG TRACK III



CURRENT STRENGTH \longrightarrow 2.0 MT/SEC

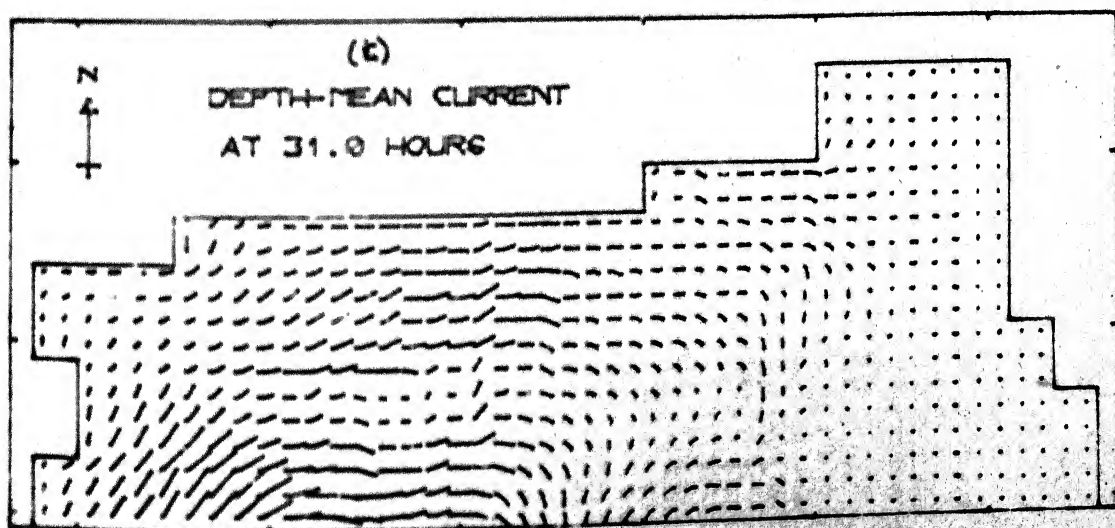


FIG. 17 a,b,c. ASYMMETRIC STORM ALONG TRACK III

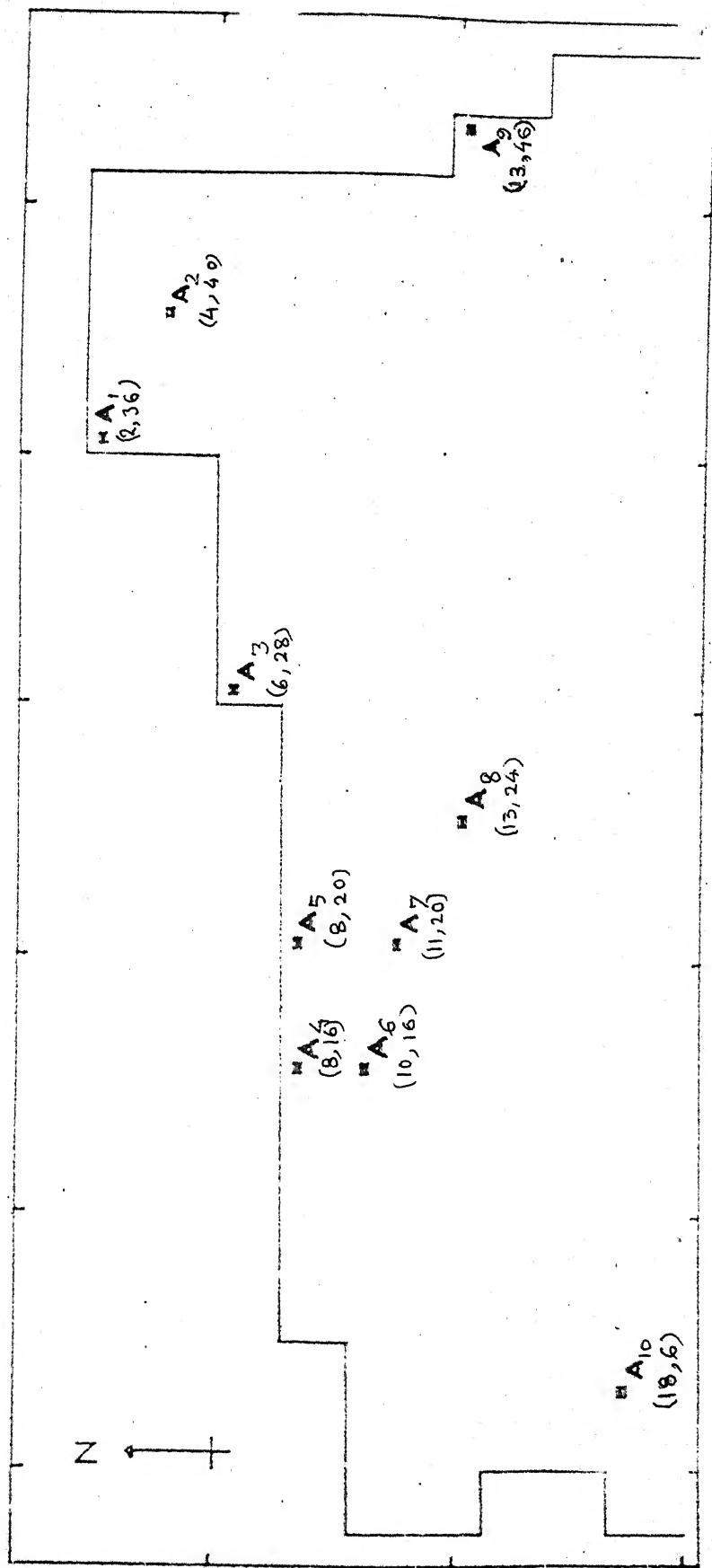
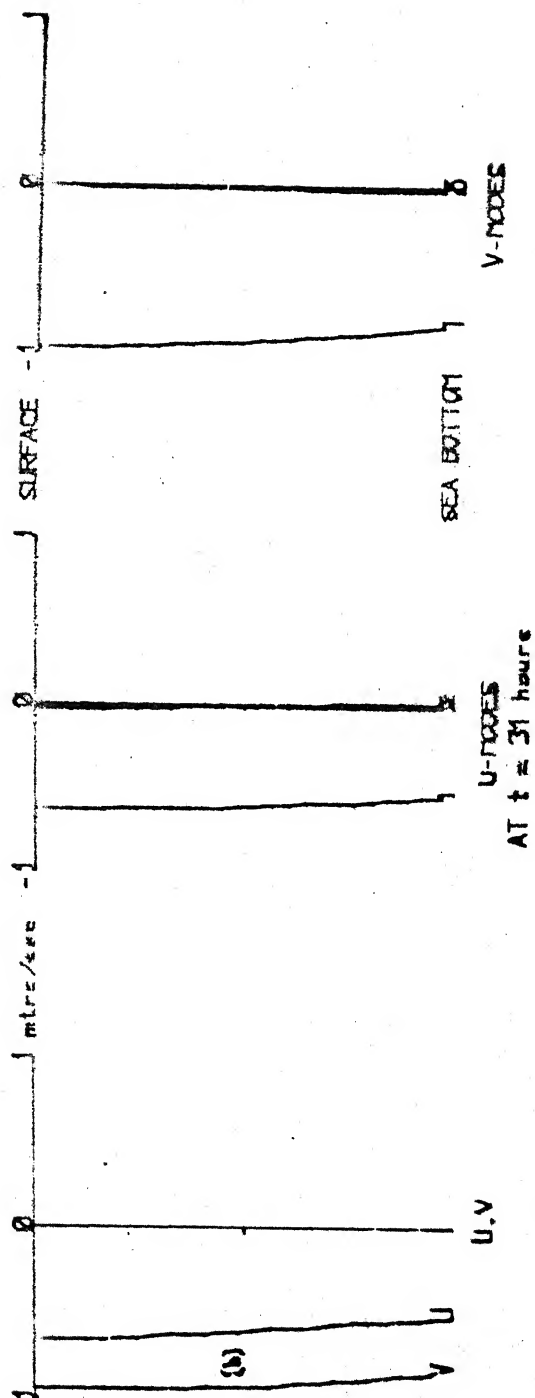
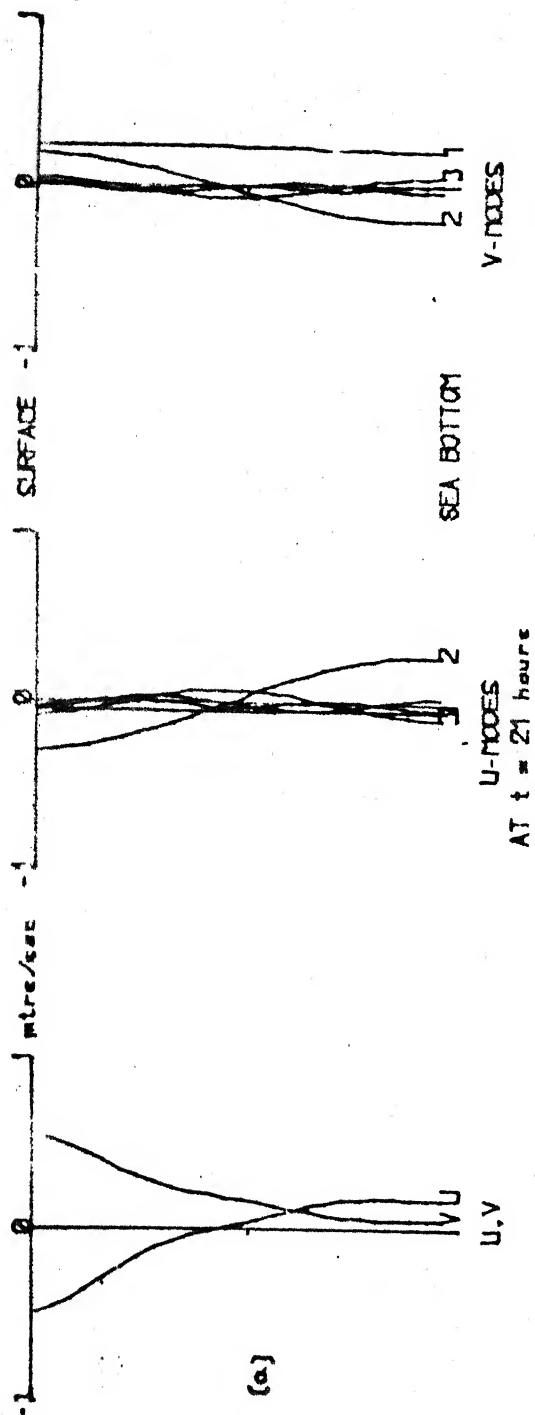


FIG. 18. SELECTED 10 LOCATIONS.



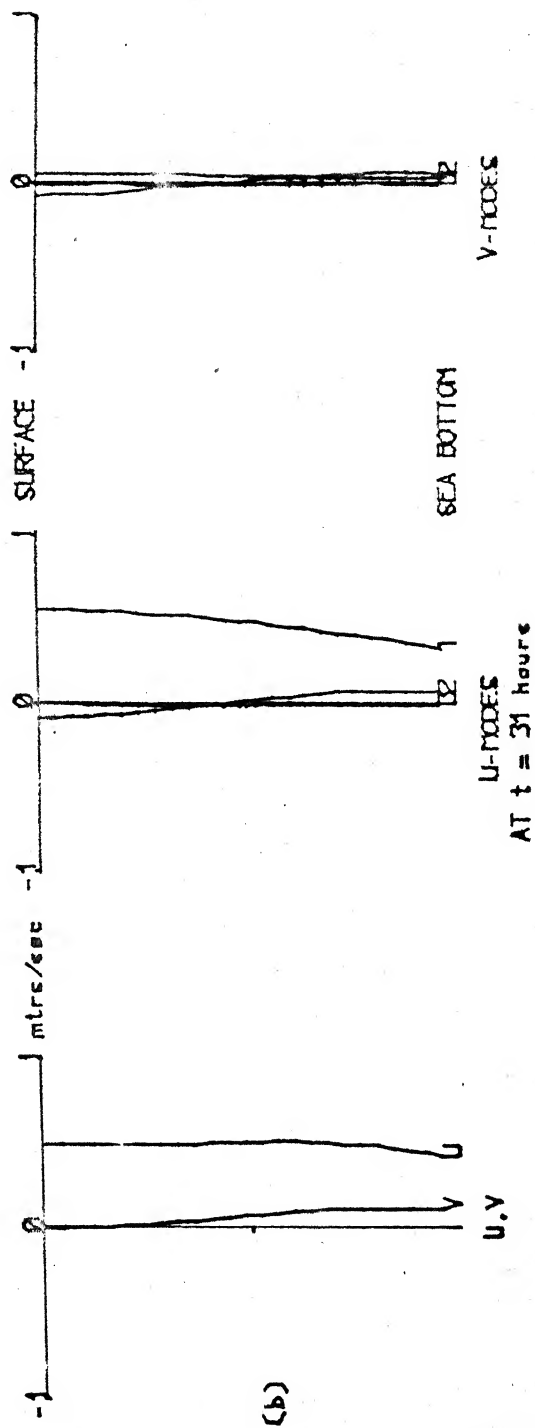
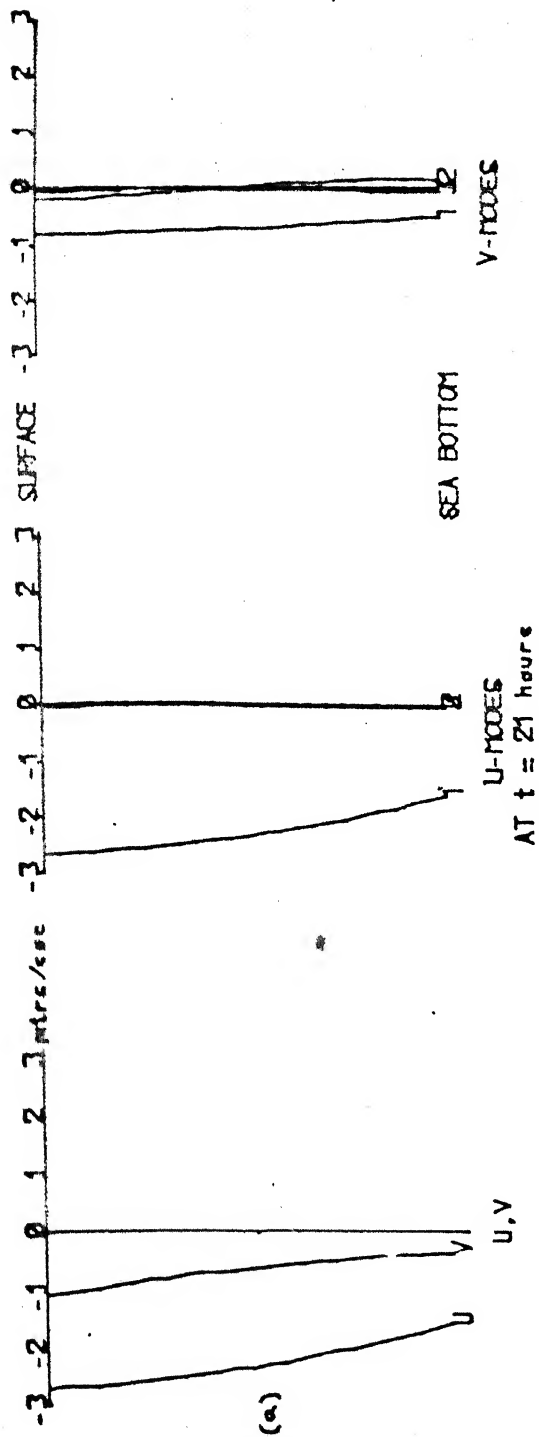


FIG. 20. a, b. VERTICAL PROFILES OF U, V AND THEIR MODAL CONTRIBUTIONS

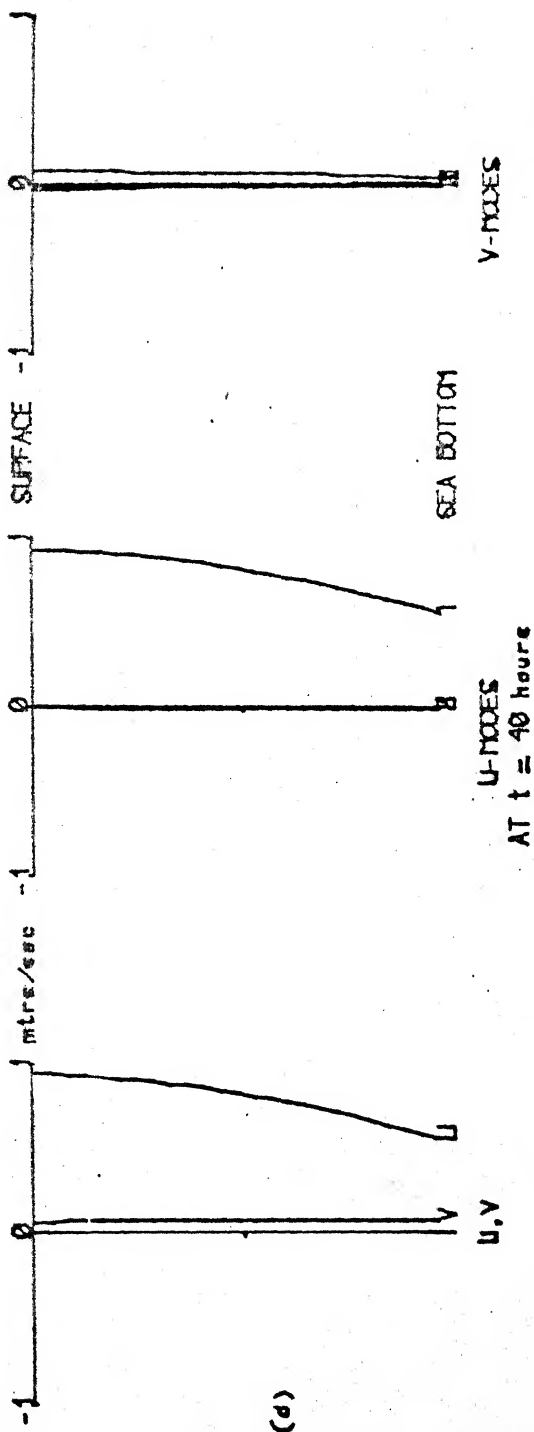
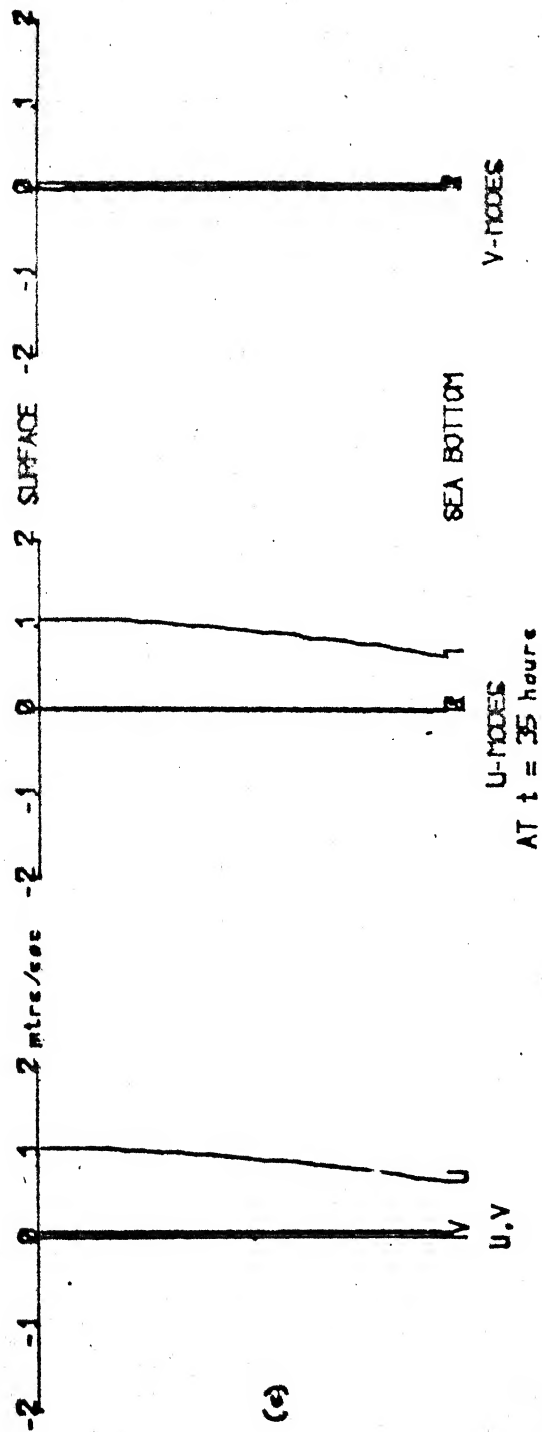


FIG. 20.c,d. VERTICAL PROFILES OF U, V AND THEIR MODAL CONTRIBUTIONS
ASYMMETRIC STORM - TRACK I - AT (11,20)

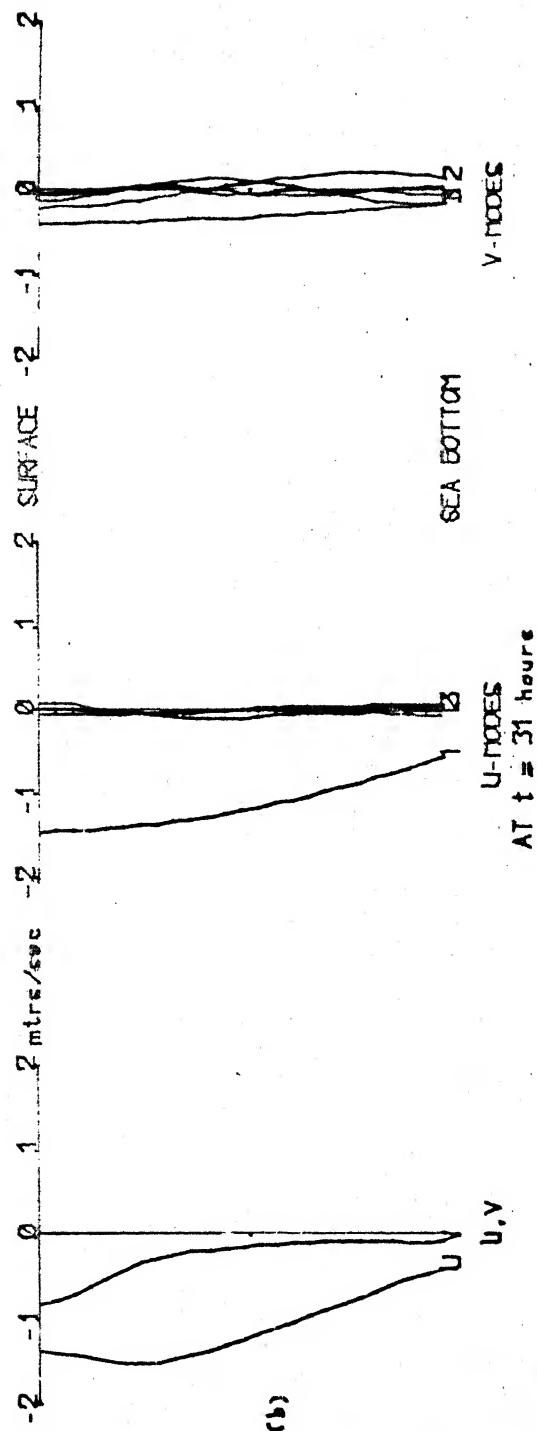
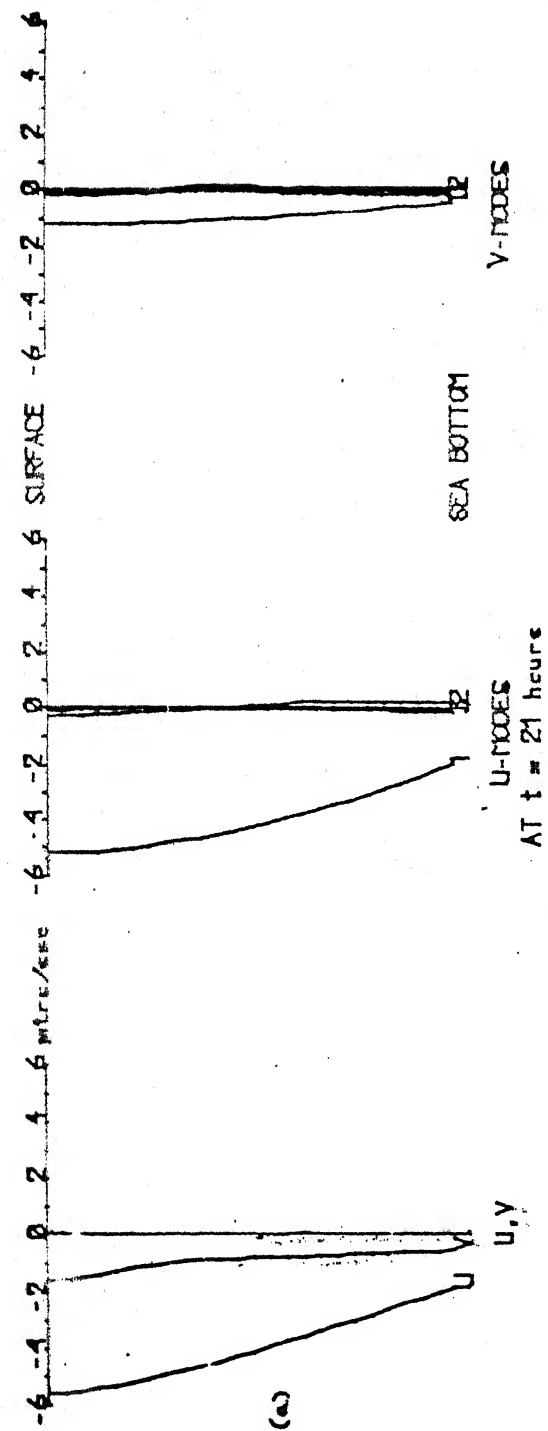


FIG. 21 a, b. VERTICAL PROFILES OF U , V AND THEIR MODAL CONTRIBUTIONS
ASYMMETRIC STORM - TRACK I - AT (13, 24)

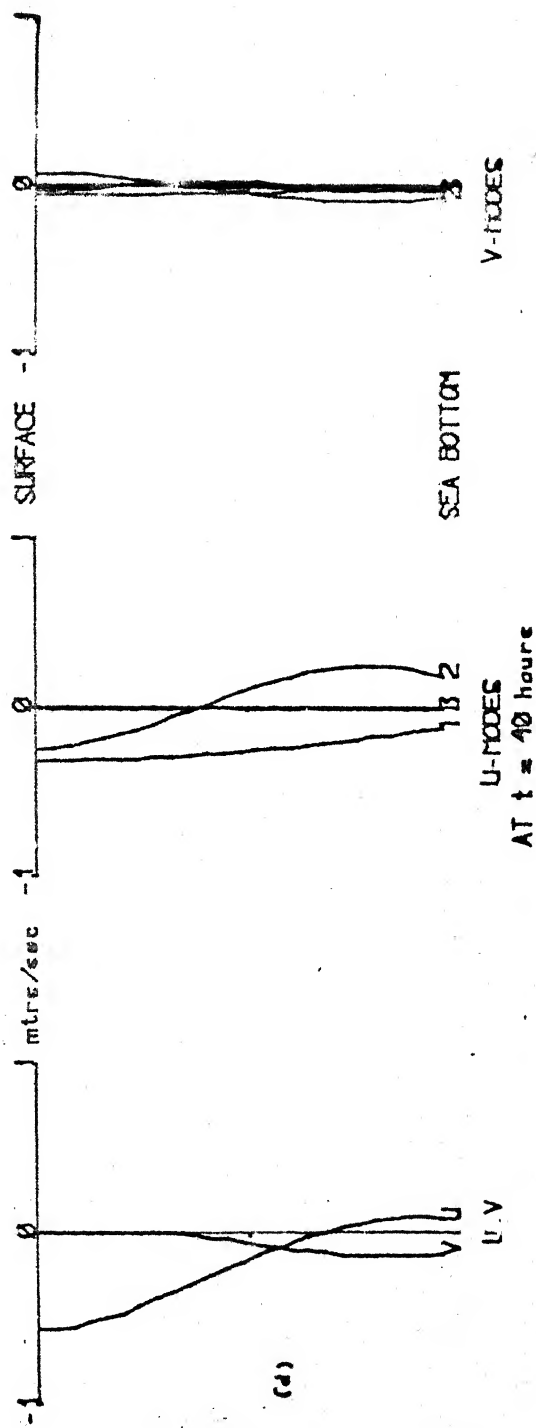
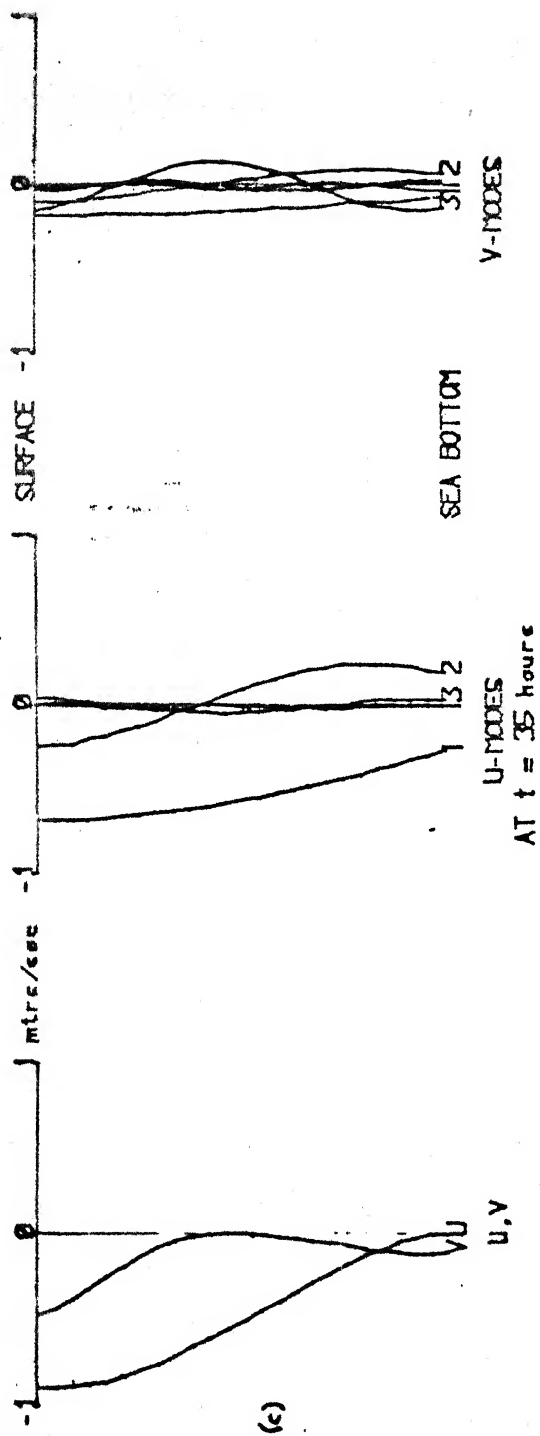


FIG. 21 c, d. VERTICAL PROFILES OF U, V AND THEIR MODAL CONTRIBUTIONS
ASYMMETRIC STORM - TRACK 1 - AT (13, 24)

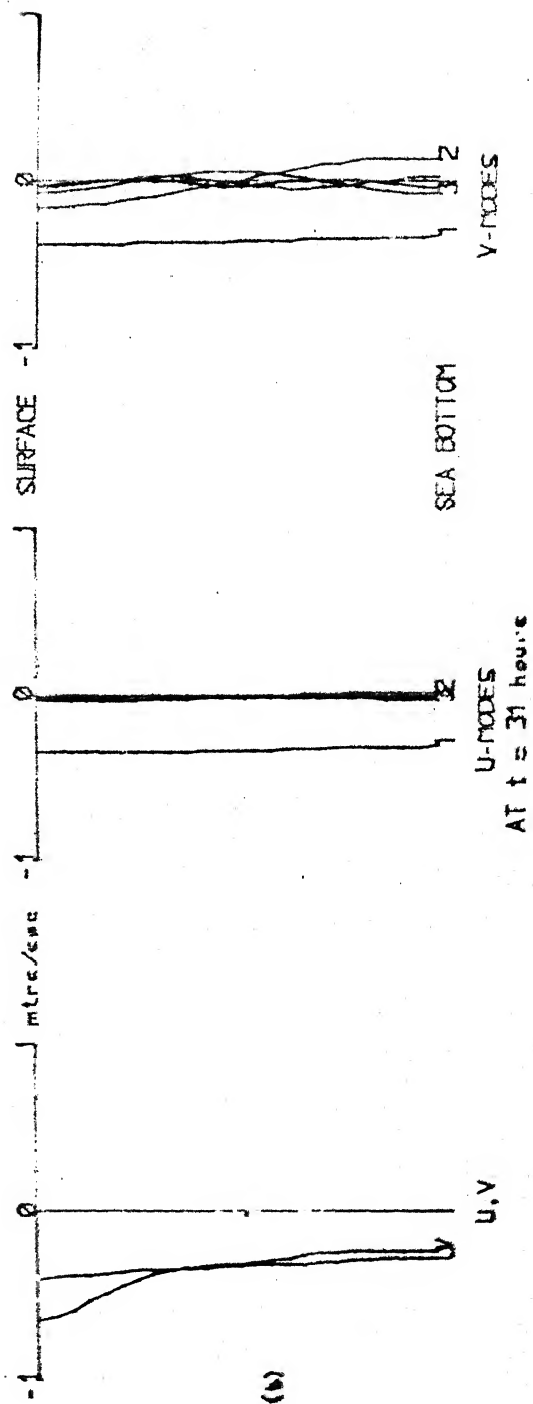
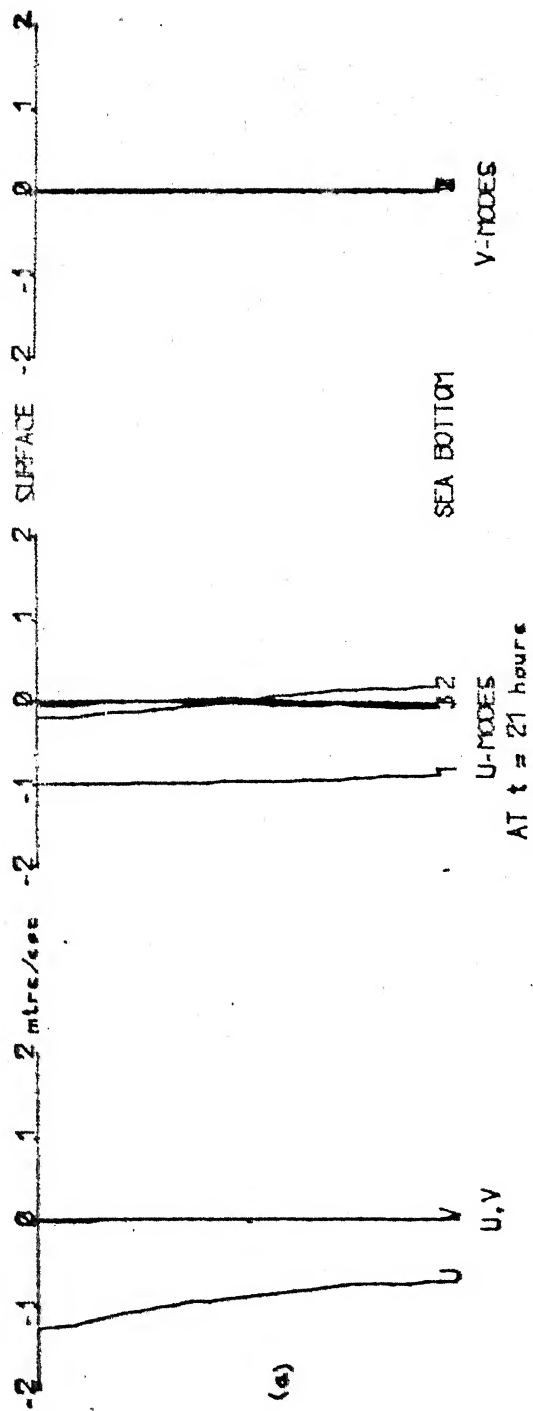


FIG. 22 a, b, VERTICAL PROFILES OF U, V AND THEIR MODAL CONTRIBUTIONS
ASYMMETRIC STORM - TRACK II - AT (4,40)

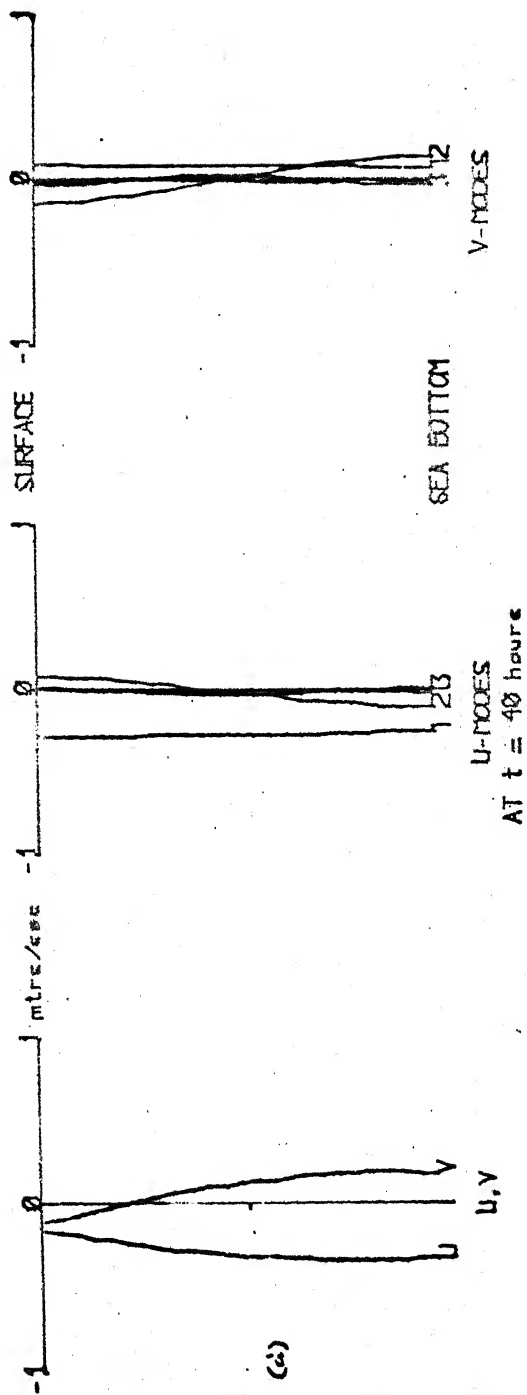
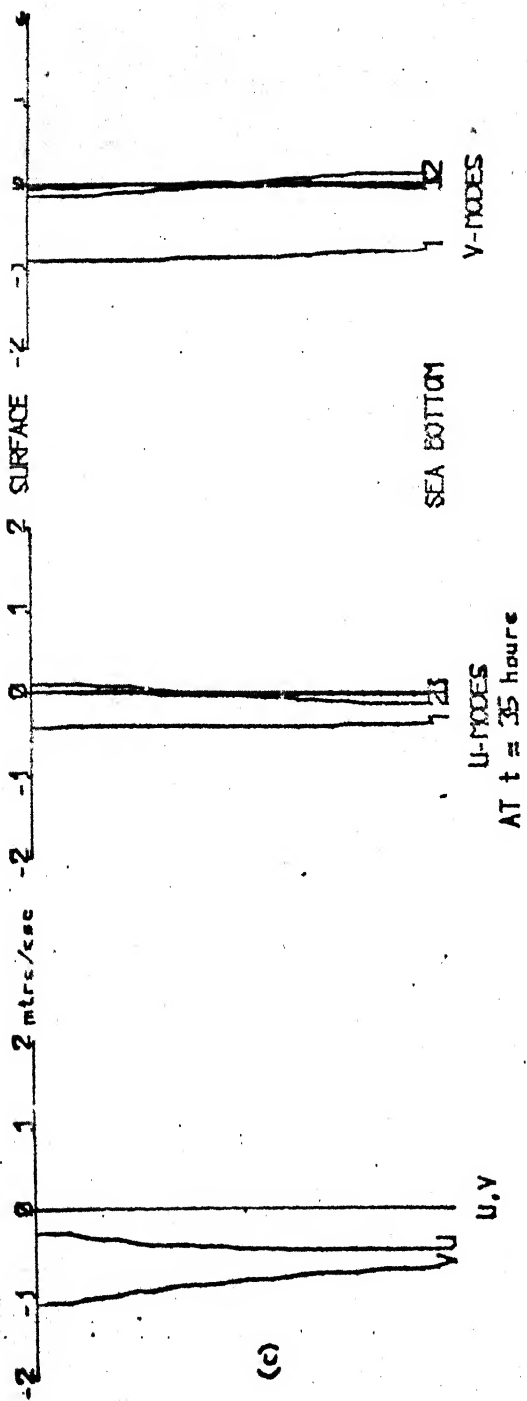


FIG. 22.c,d. VERTICAL PROFILES OF U, V AND THEIR MODAL CONTRIBUTIONS
ASYMMETRIC STORM - TRACK II - AT (4,40)

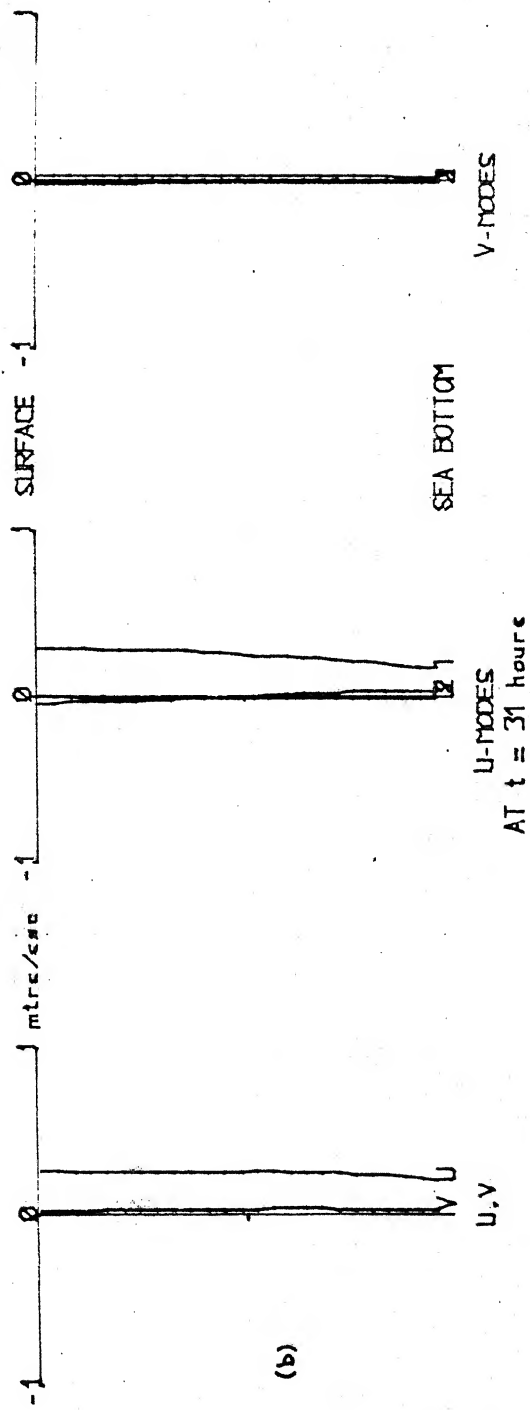
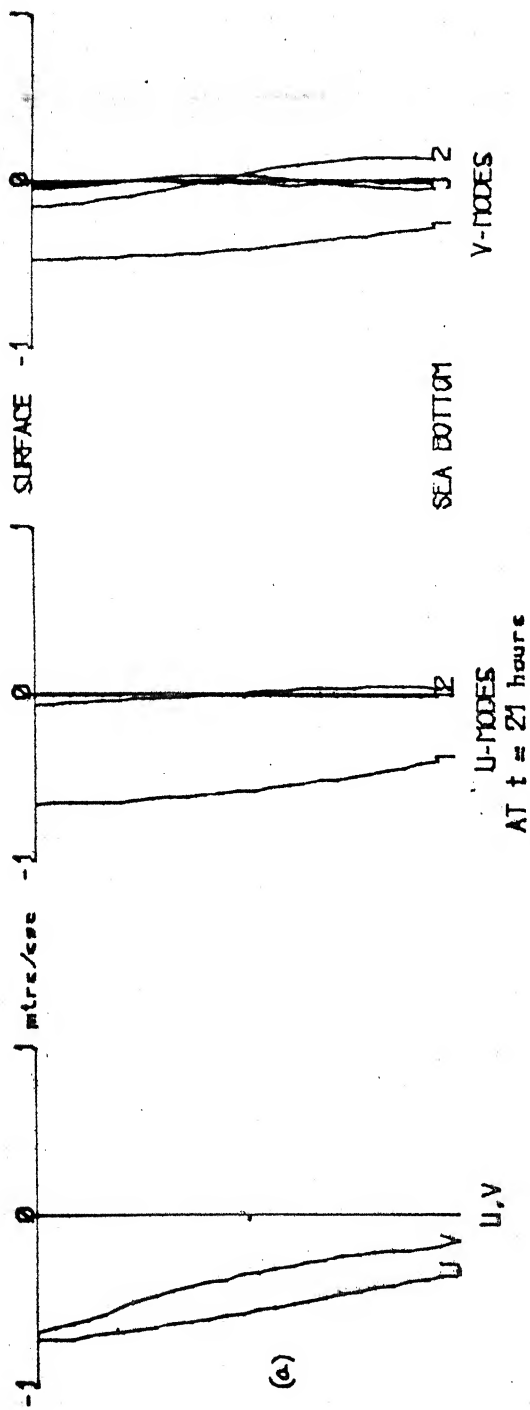


FIG. 23 a, b. VERTICAL PROFILES OF U, V AND THEIR MODAL CONTRIBUTIONS
ASYMMETRIC STORM - TRACK II - AT (11, 20)

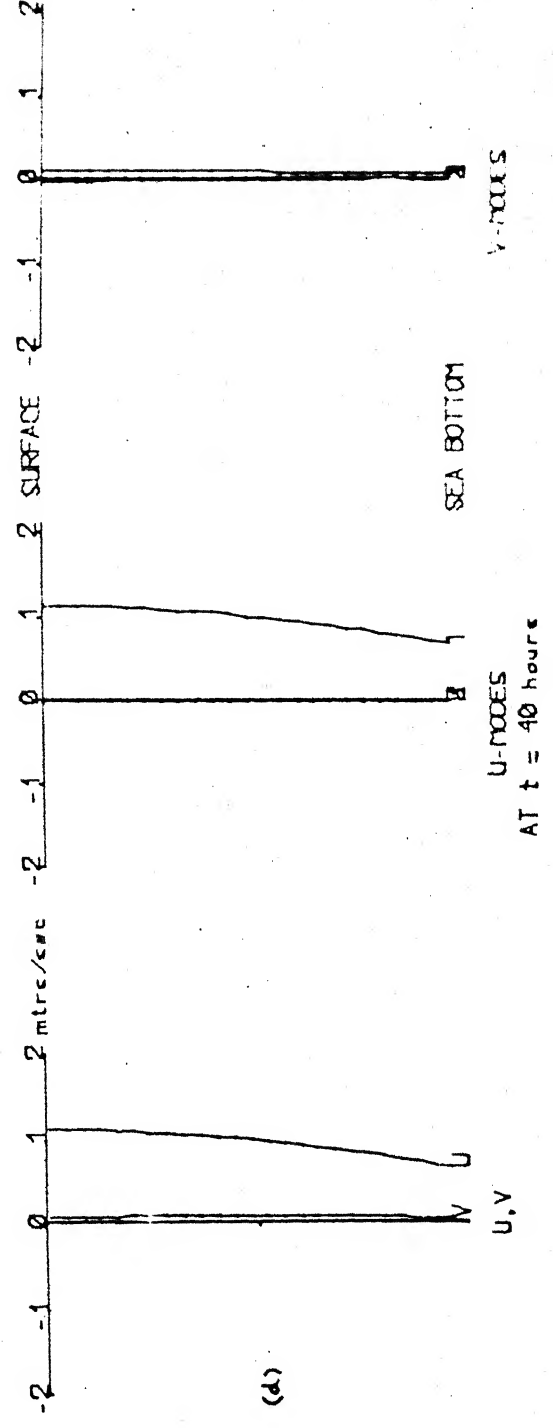
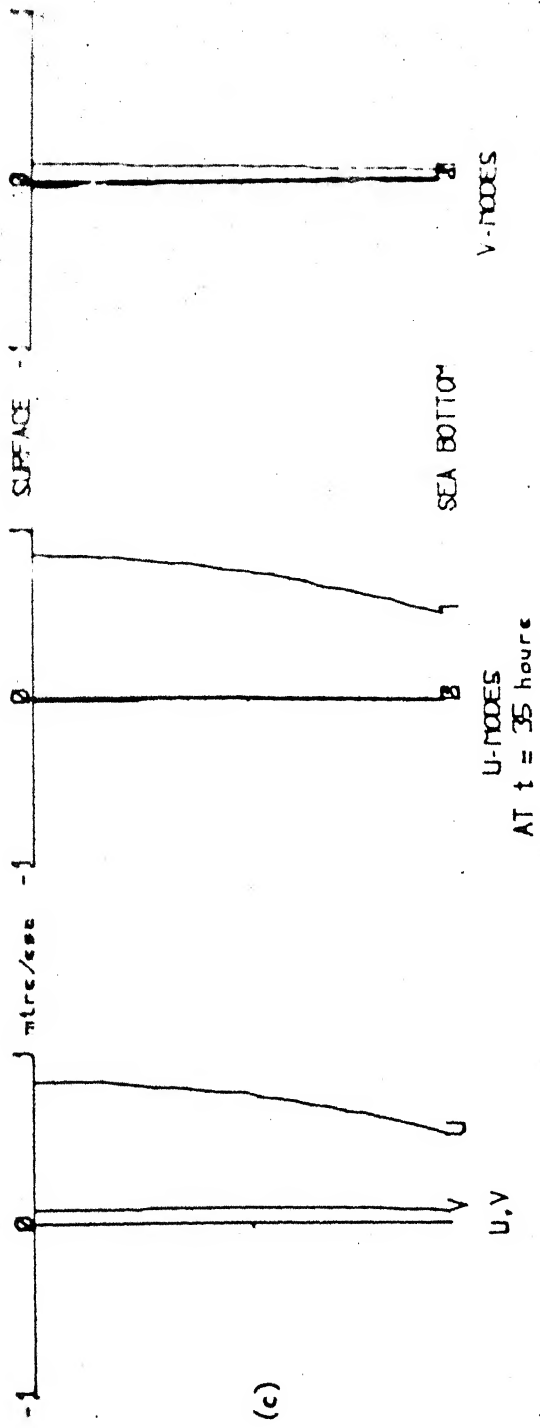


FIG. 23 c,d. VERTICAL PROFILES OF U, V AND THEIR MODAL CONTRIBUTIONS
ASYMMETRIC STORM - TRACK II - AT (11,20)

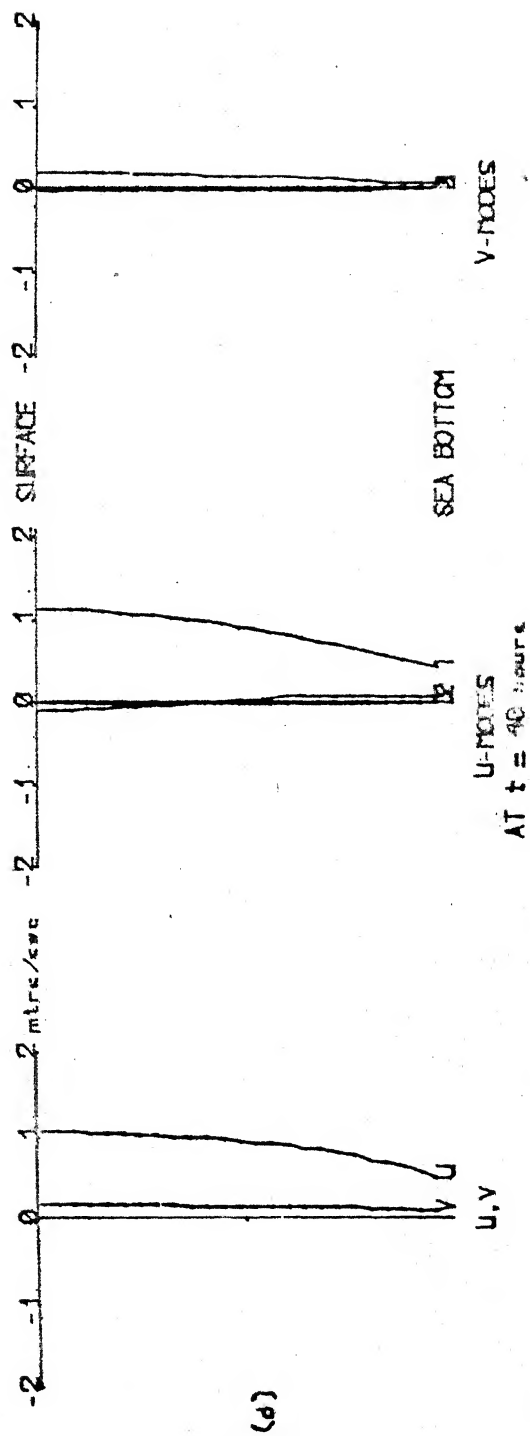
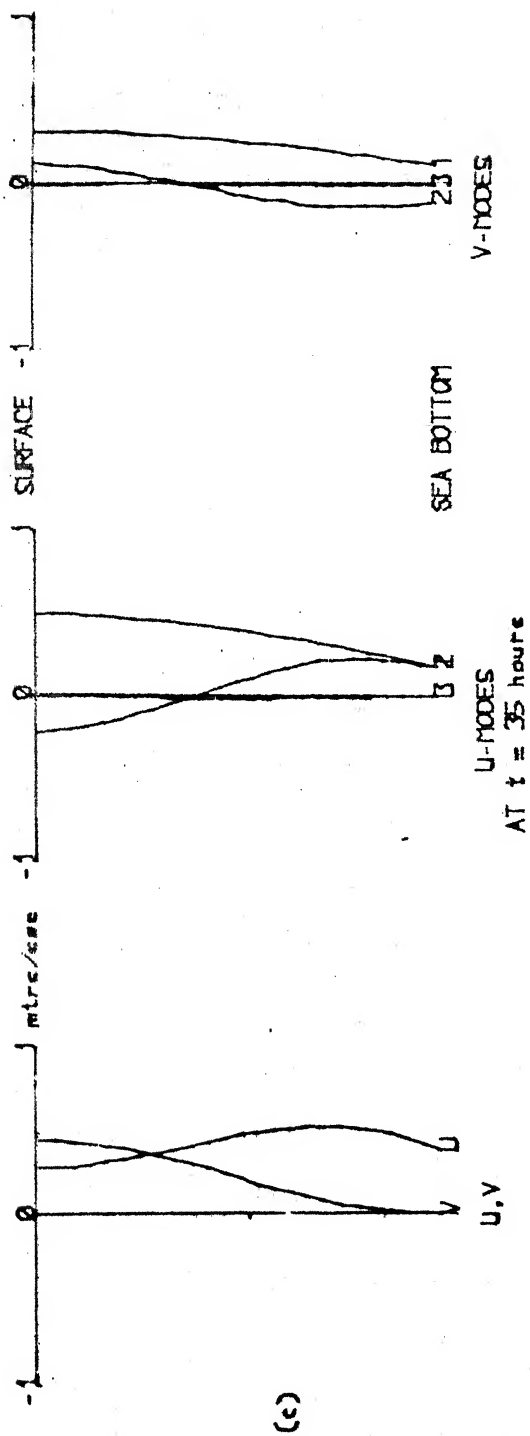


FIG. 24 c,d, VERTICAL PROFILES OF U, V AND THEIR MODAL CONTRIBUTIONS
ASYMMETRIC STORM - TRACK II - AT (13,24)

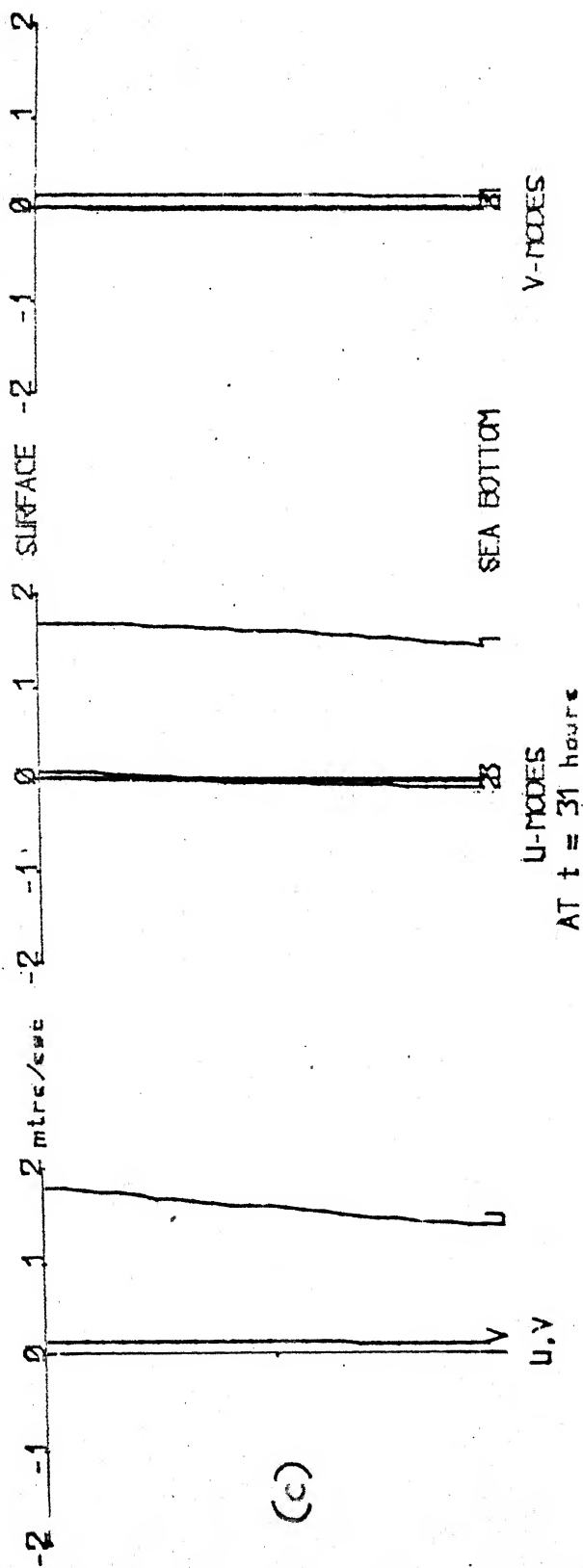


FIG. 25 (c) VERTICAL PROFILES OF U, V AND THEIR MODAL CONTRIBUTIONS
ASYMMETRIC STORM - TRACK III - AT (8, 16)

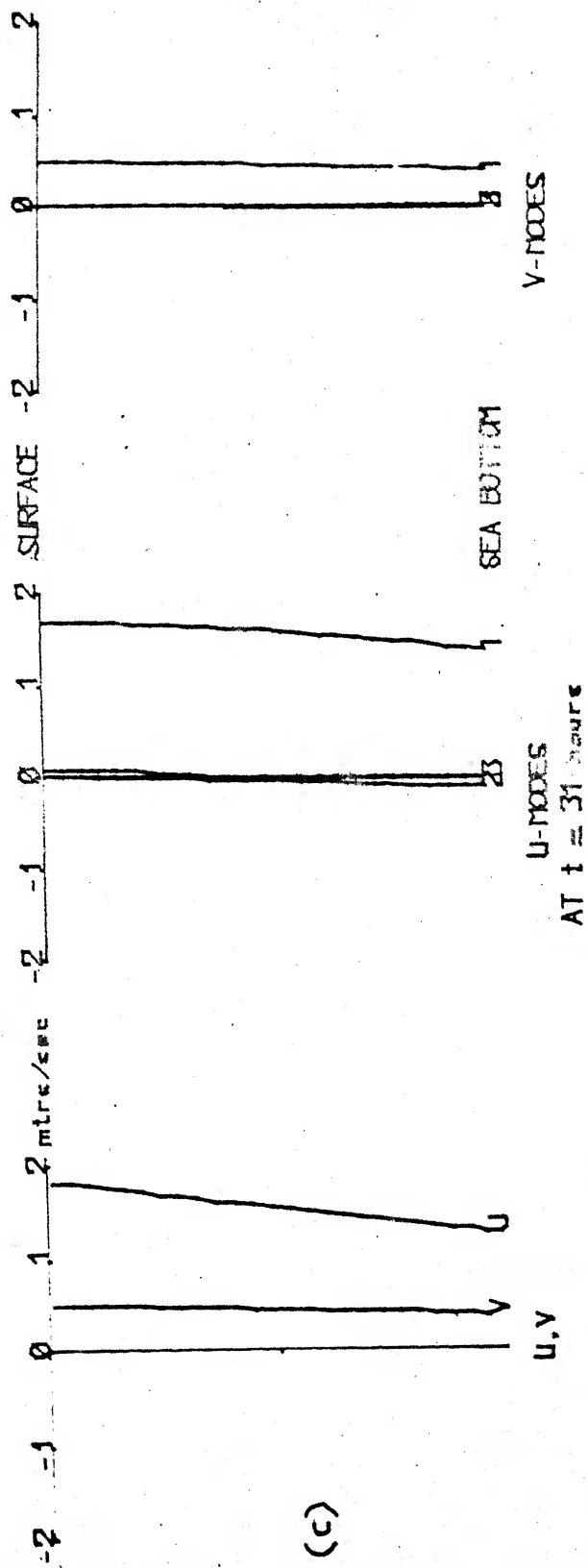


FIG. 26 (c). VERTICAL PROFILES OF U, V AND THEIR MODAL CONTRIBUTIONS
ASYMMETRIC STORM - TRACK III - AT (10, 16)

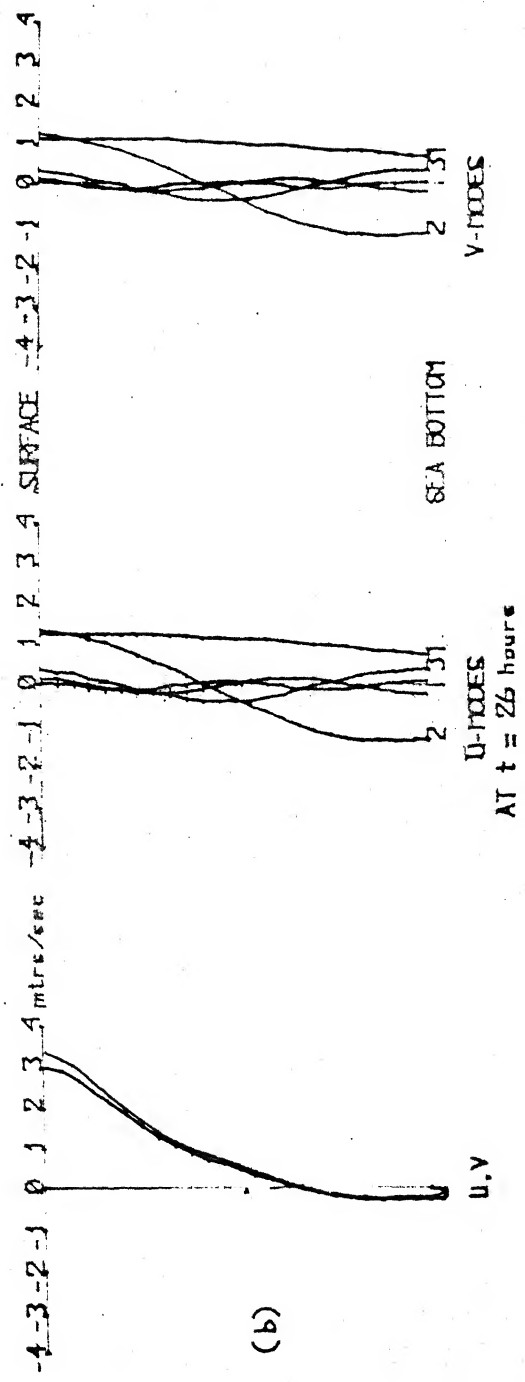
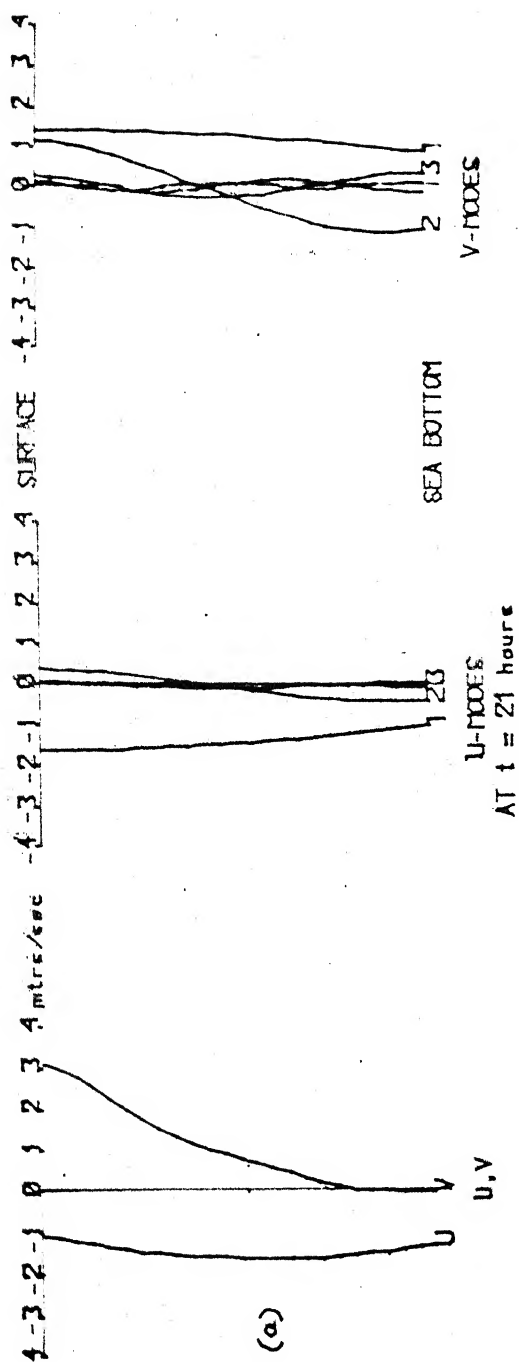


FIG. 27 a, b. VERTICAL PROFILES OF U , V AND THEIR MODAL CONTRIBUTIONS
ASYMMETRIC STORM - TRACK II - AT (11, 20)

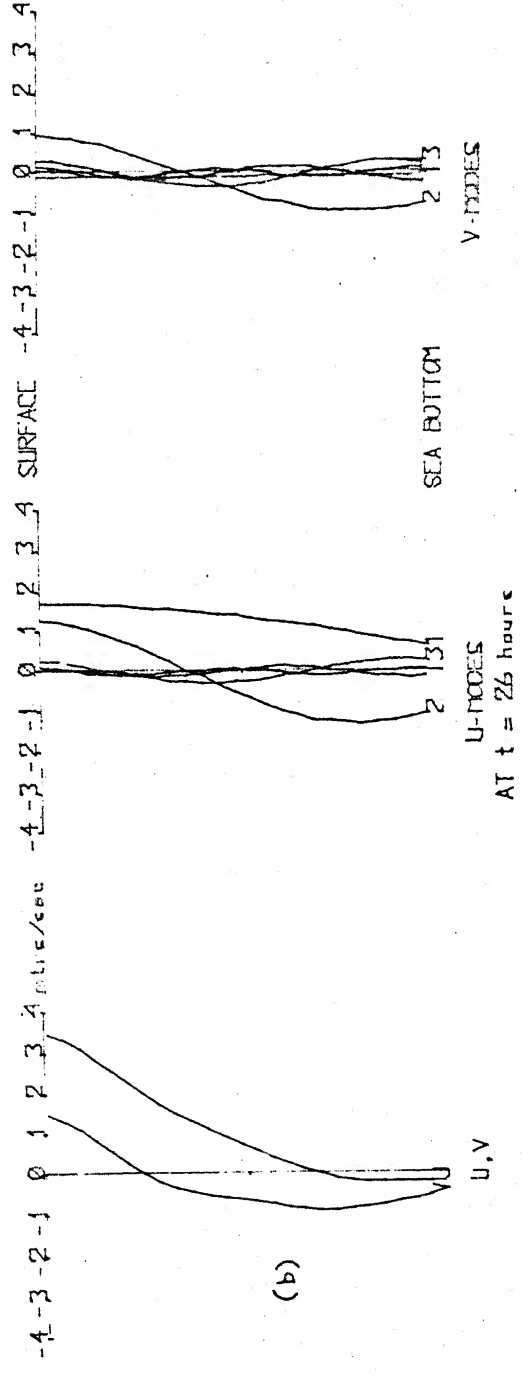
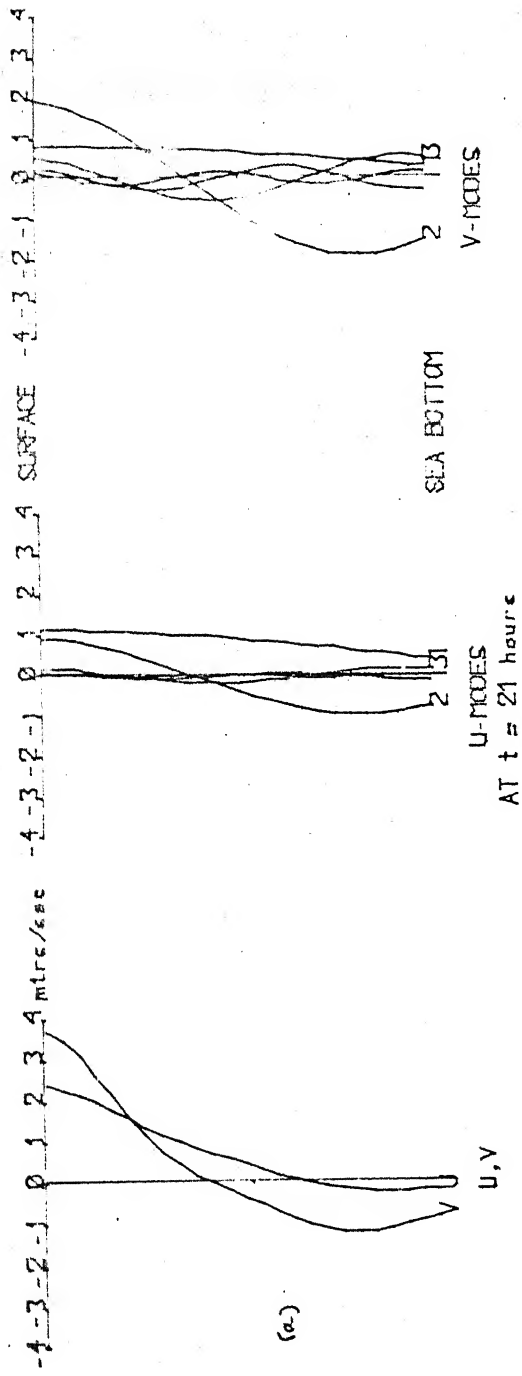


FIG. 28 a, b, VERTICAL PROFILES OF U, V AND THEIR MODAL CONTRIBUTIONS ASYMMETRIC STORM - TRACK III - AT (13, 24)

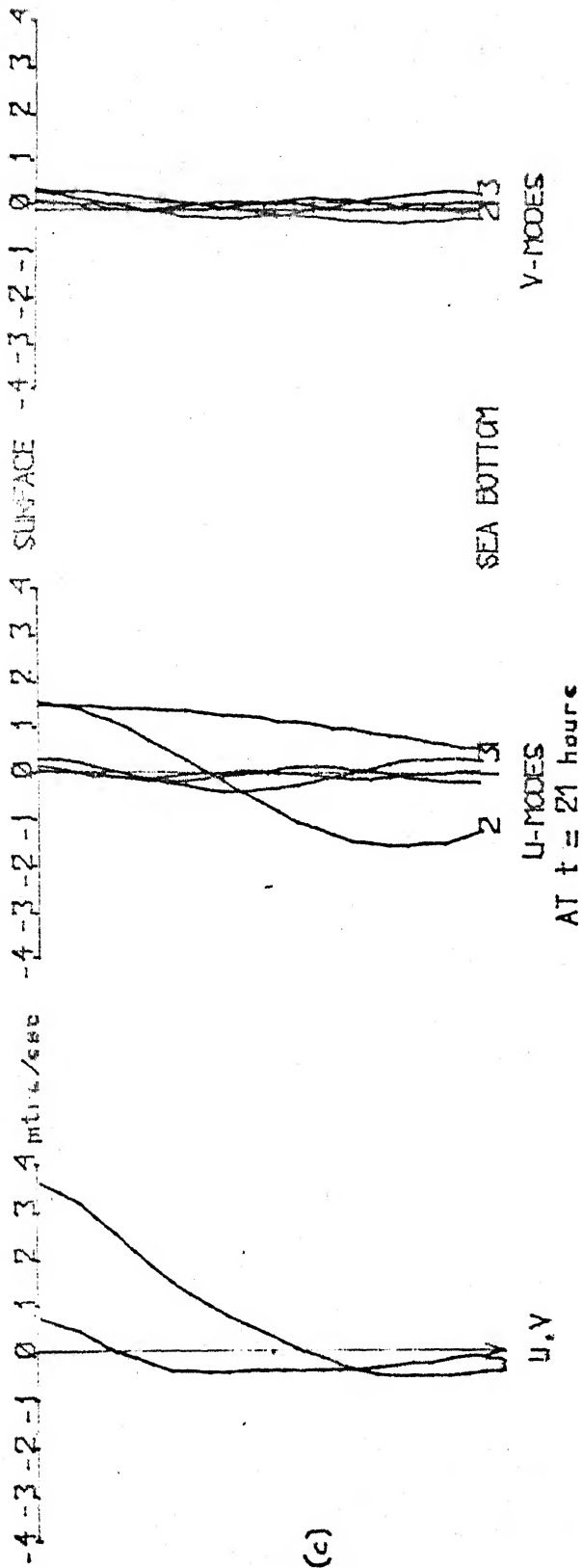


FIG. 28 c. VERTICAL PROFILES OF U, V AND THEIR MODAL CONTRIBUTIONS
ASYMMETRIC STORM - TRACK III - AT (13, 24)

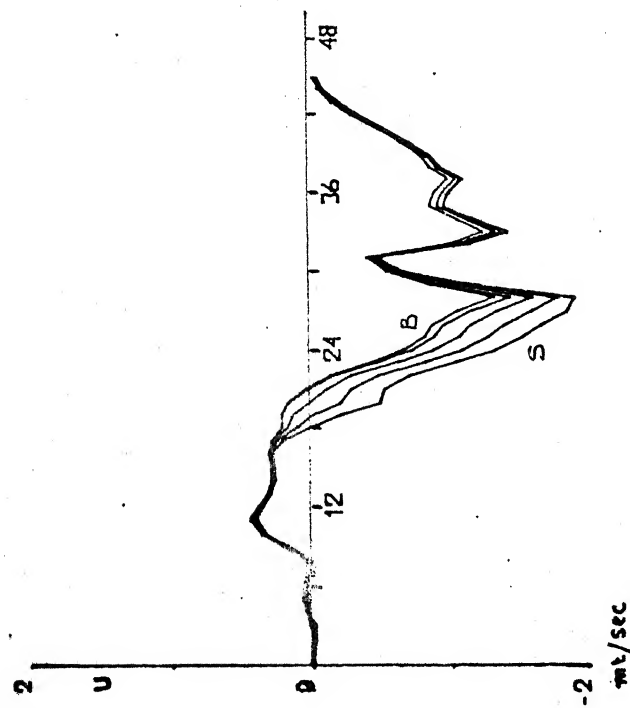


FIG. 29 a. HOURLY VALUES OF U, V AT 5 LEVELS - AT (4,40)

(a)

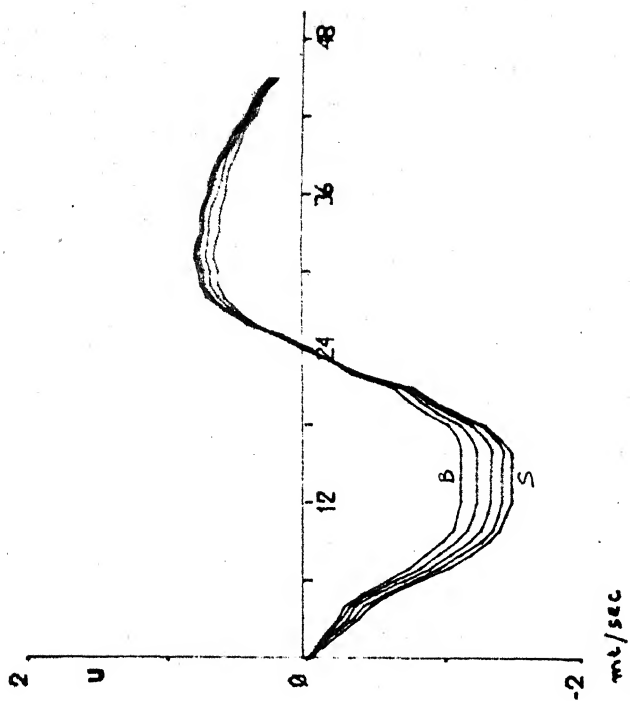
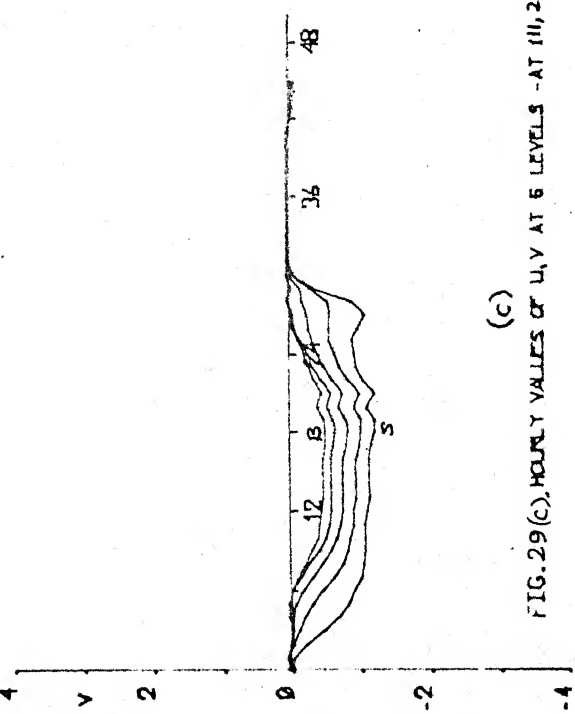
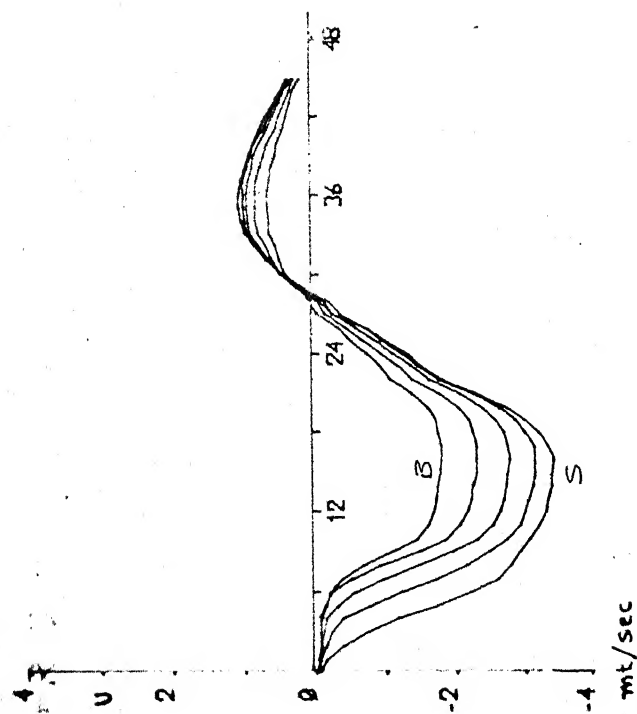


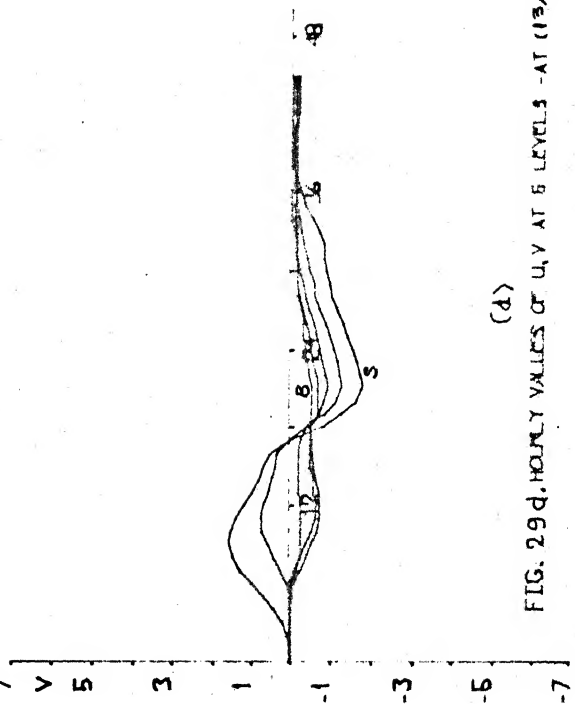
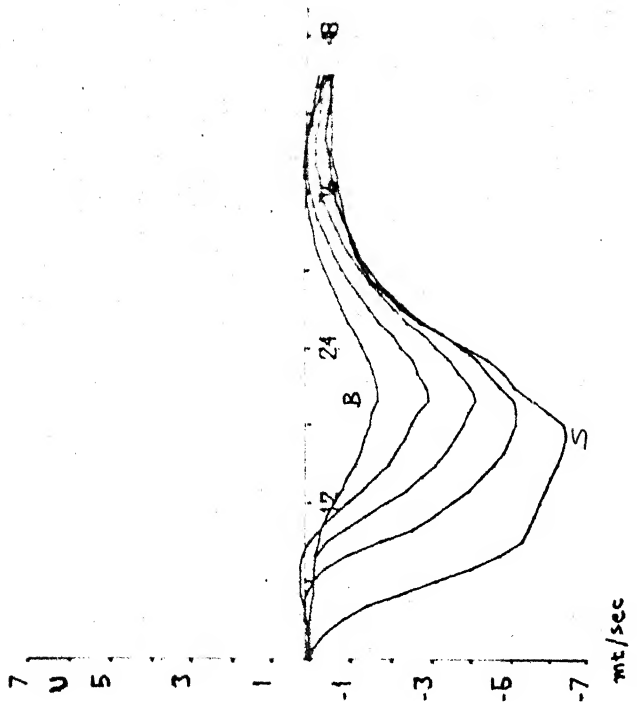
FIG. 29 b. HOURLY VALUES OF U, V AT 5 LEVELS - AT (10,16)

(b)



(c)

FIG. 29(c), HOURLY VALUES OF U, V AT 5 LEVELS - AT (11, 20)



(d)

FIG. 29(d), HOURLY VALUES OF U, V AT 5 LEVELS - AT (13, 24)

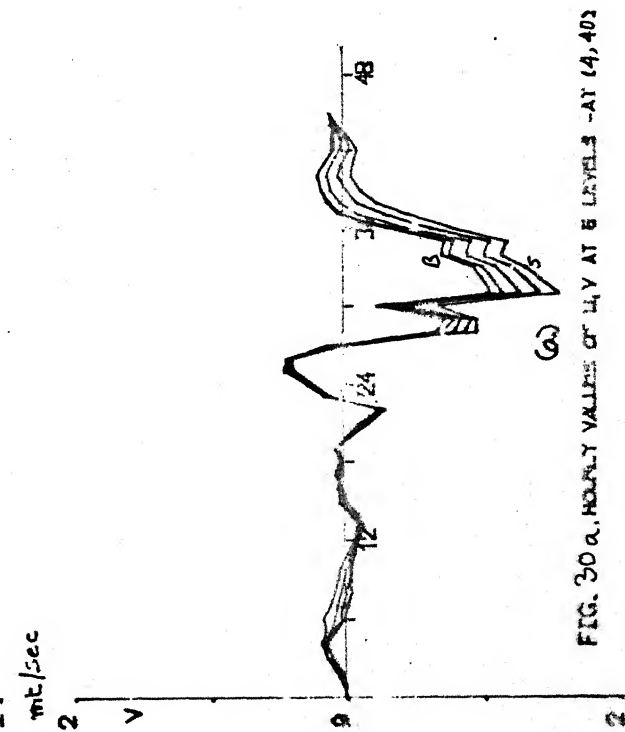
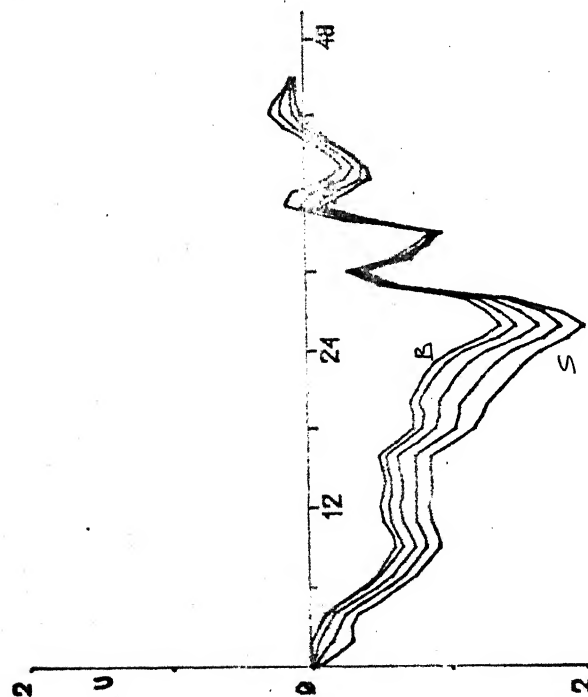
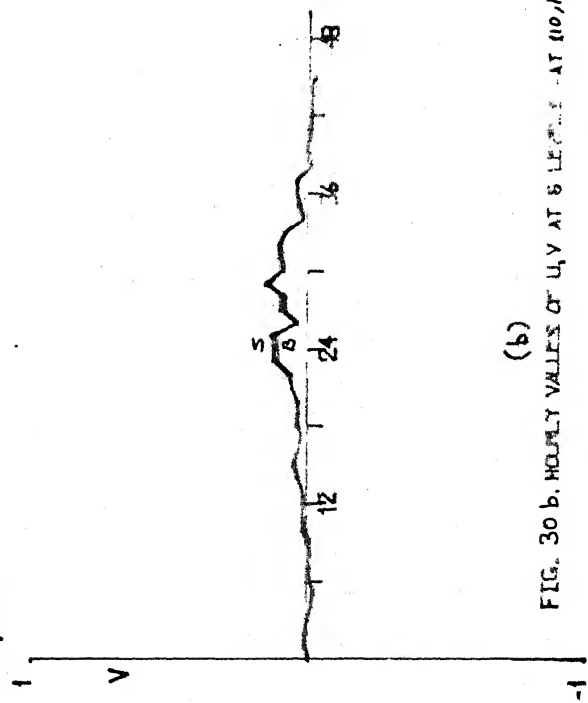
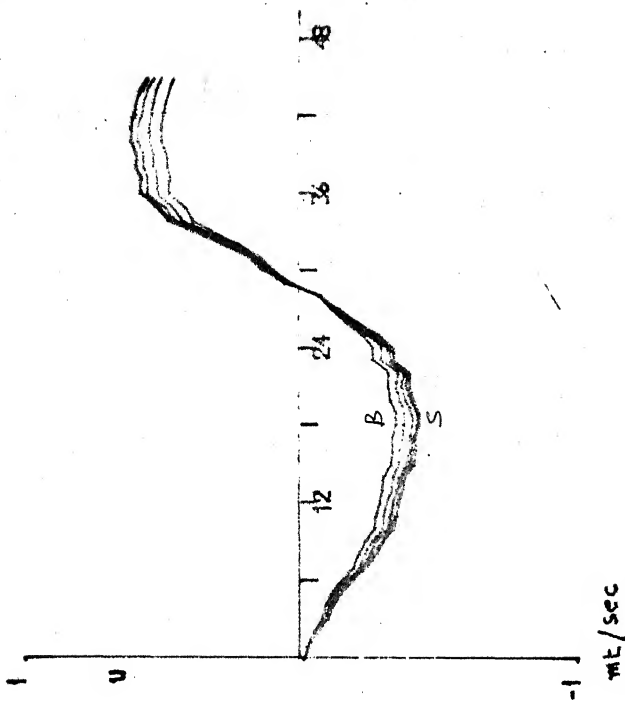
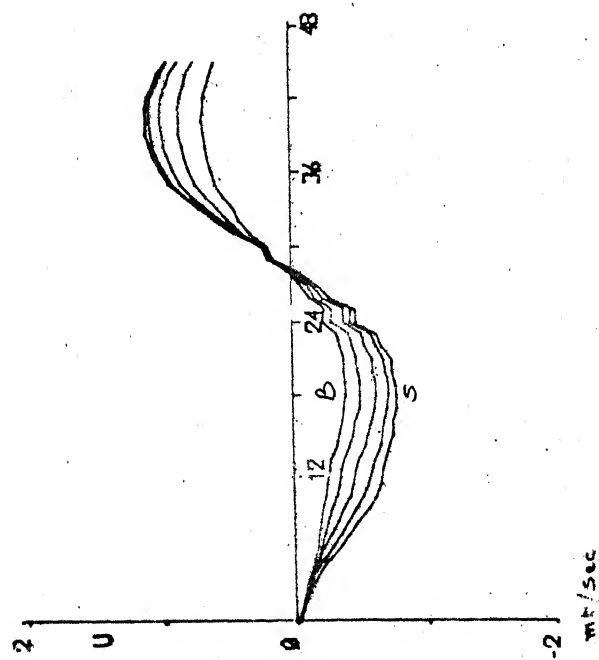


FIG. 30 a. HOURLY VALUES OF U, V AT 6 LEVELS - AT (4, 40)



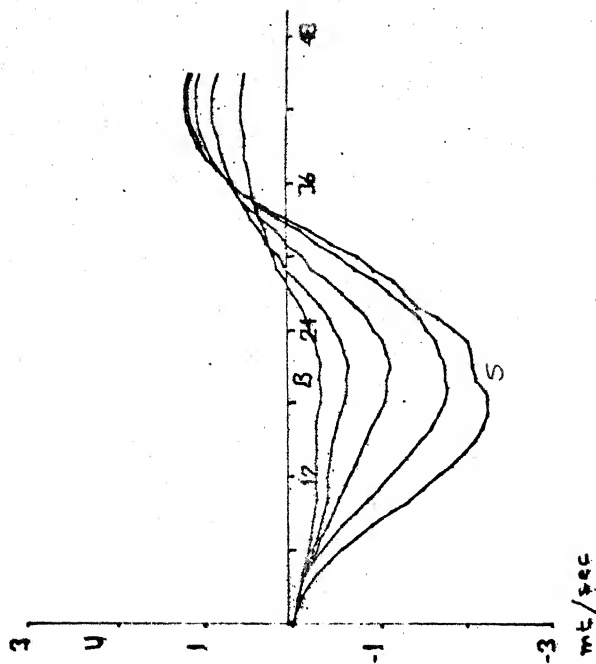
(b)

FIG. 30 b. HOURLY VALUES OF U, V AT 6 LEVELS - AT (10, 16)



(c)

FIG. 30 c. HOURLY VALUES OF U, V AT 6 LEVELS - AT (11, 20)



(d)

FIG. 30 d. HOURLY VALUES OF U, V AT 6 LEVELS - AT (13, 20)

ASYMMETRIC STORM TRACK II
S: SURFACE; B: BOTTOM

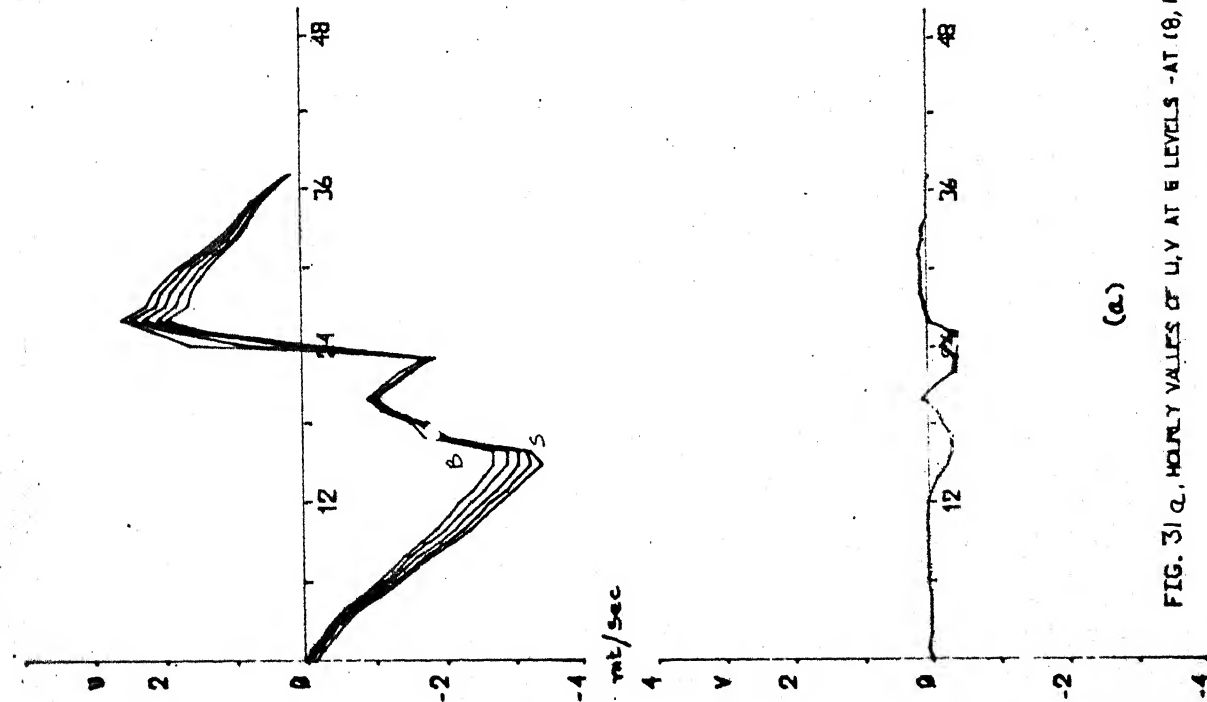


FIG. 3(a) HOURLY VALUES OF U, V AT 6 LEVELS - AT (8, 16)

(a)

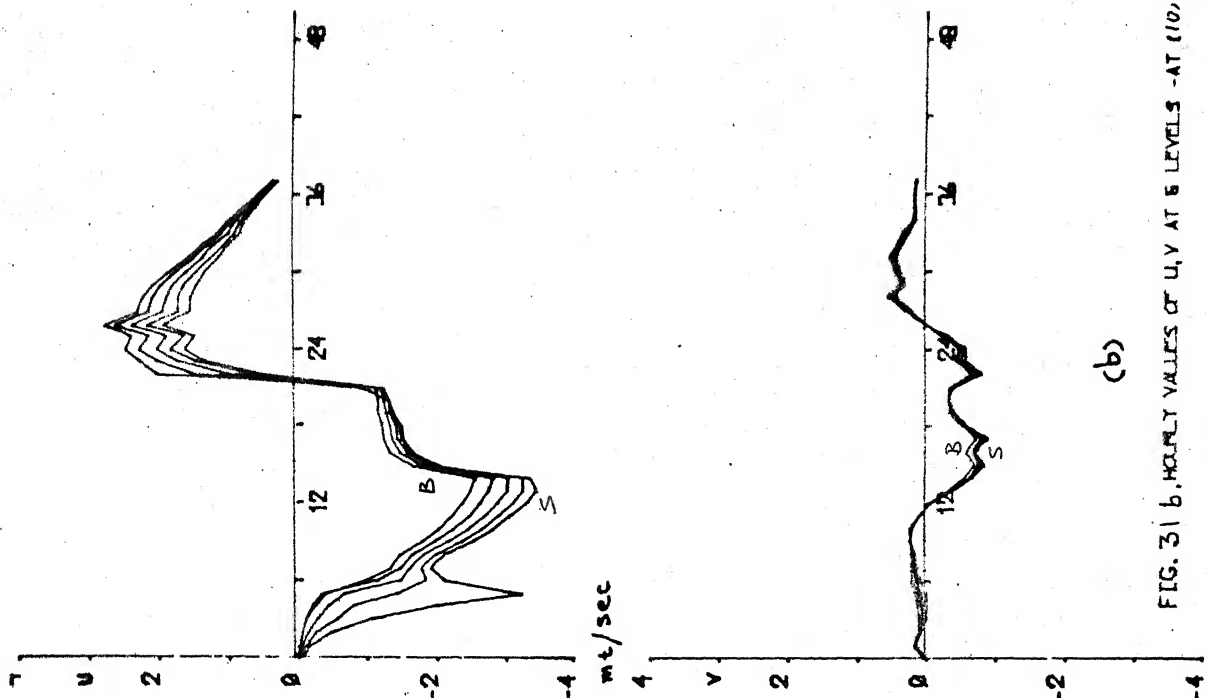
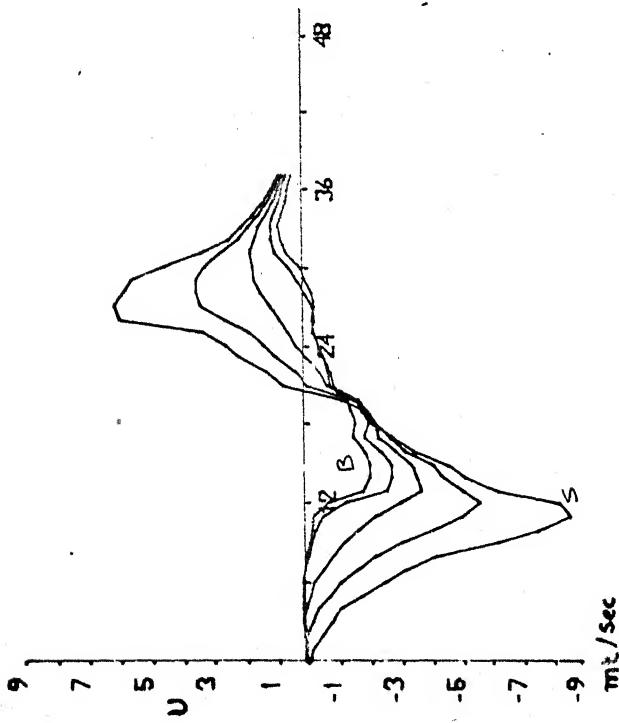


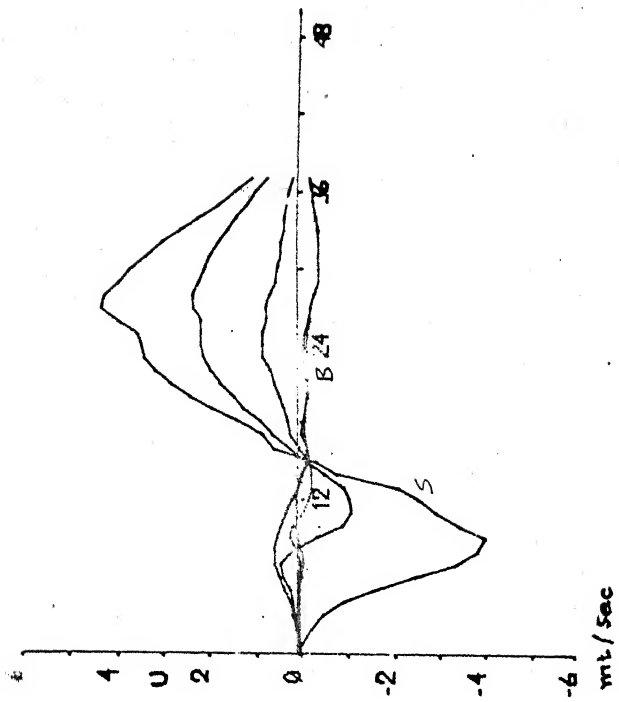
FIG. 3(b) HOURLY VALUES OF U, V AT 6 LEVELS - AT (10, 16)

(b)



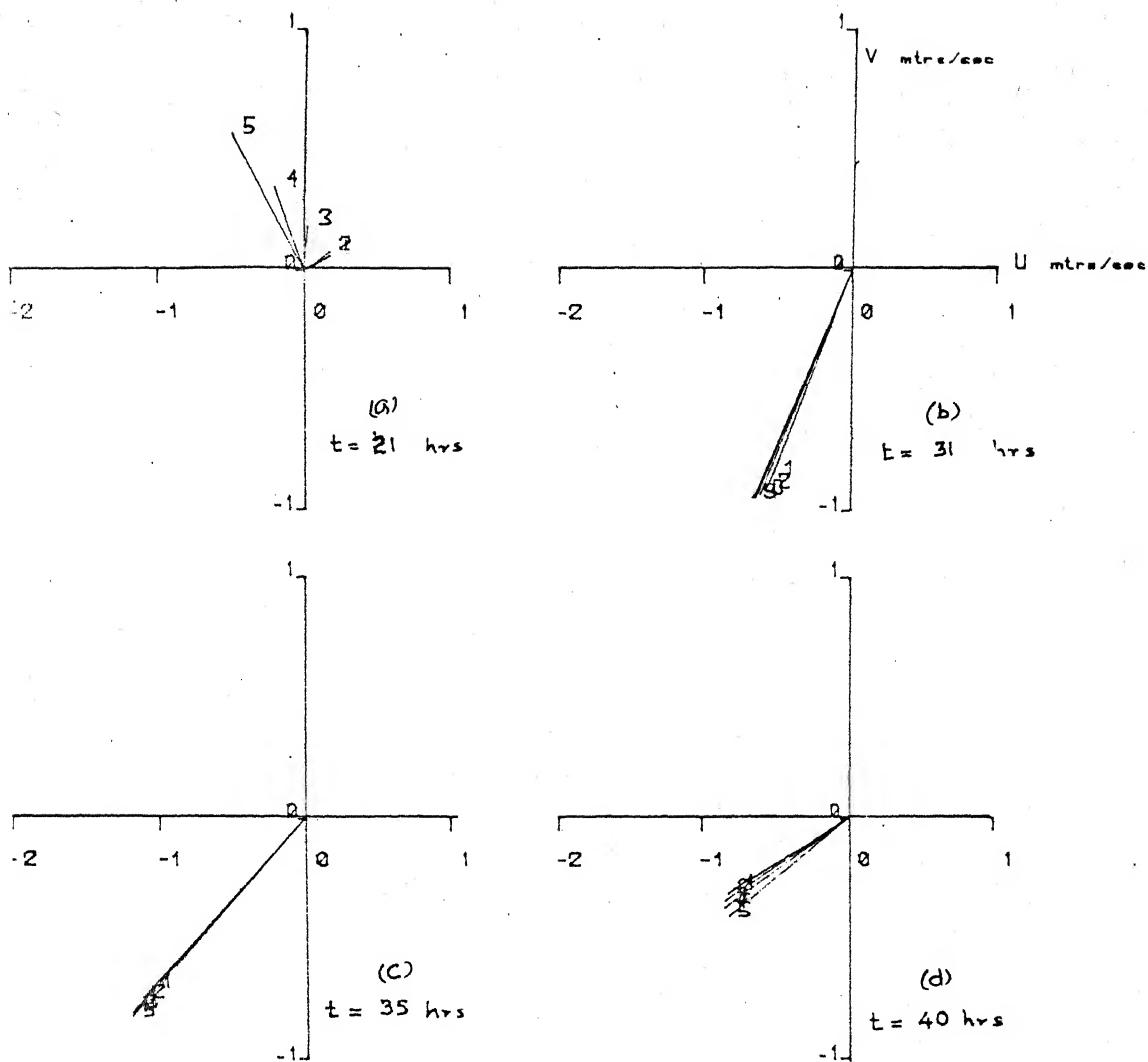
(c)

FIG. 31 c. HOURLY VALUES OF U, V AT 6 LEVELS - AT (11, 20)



(d)

FIG. 31 d. HOURLY VALUES OF U, V AT 6 LEVELS - AT (13, 24)

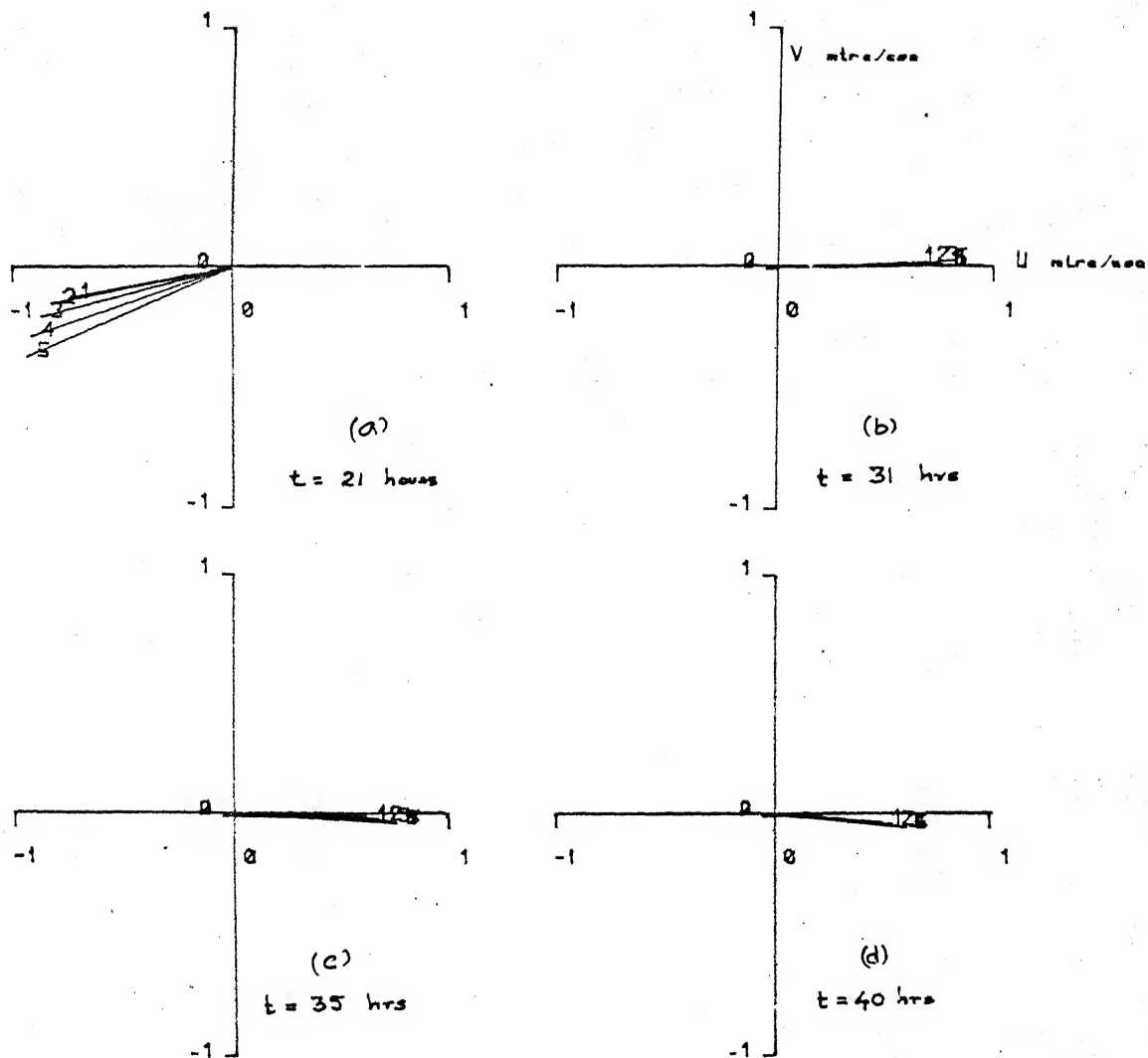


AT (4,40)

FIG. 32 a, b, c, d. CURRENTS AT 5 LEVELS ($\xi = -1.0, -0.75, -0.5, -0.25, 0.0$)

LEVEL 1: ($\xi = -1.0$): BOTTOM

ASYMMETRIC STORM ALONG TRACK I

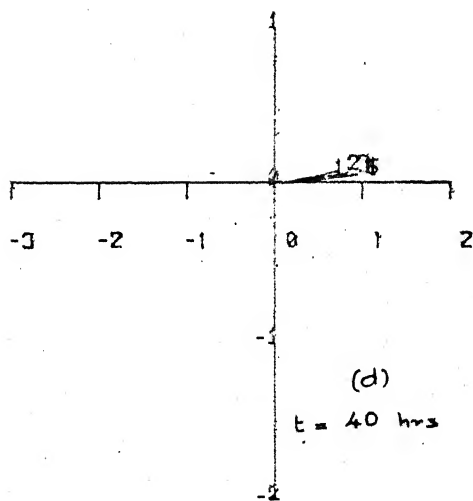
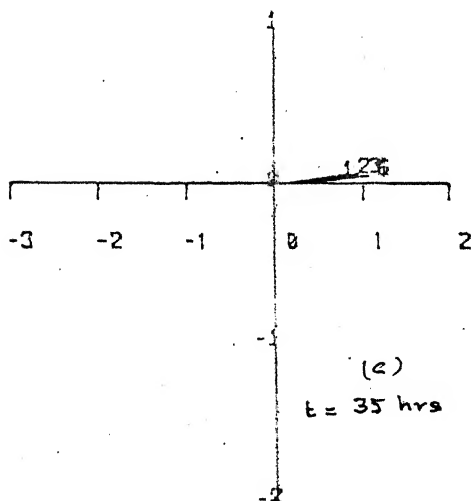
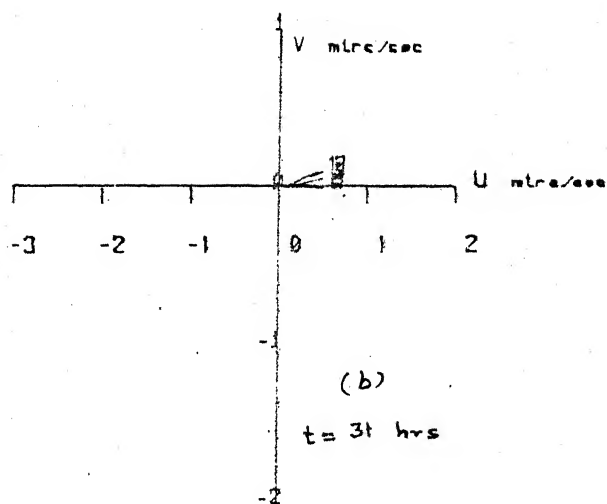
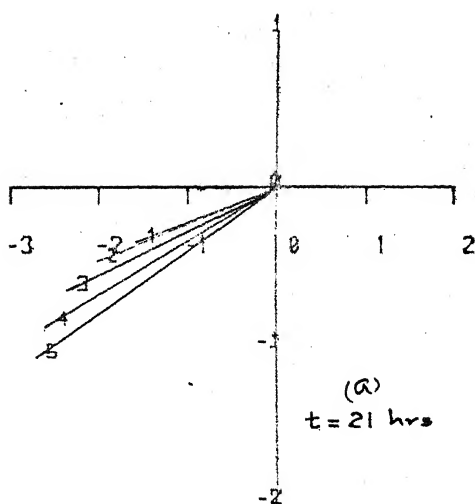


AT (10, 16)

FIG. 33 a, b, c, d. CURRENTS AT 5 LEVELS ($\xi = -1.0, -0.75, -0.5, -0.25, 0.0$)

LEVEL 1: ($\xi = -1.0$): BOTTOM

ASYMMETRIC STORM ALONG TRACK J

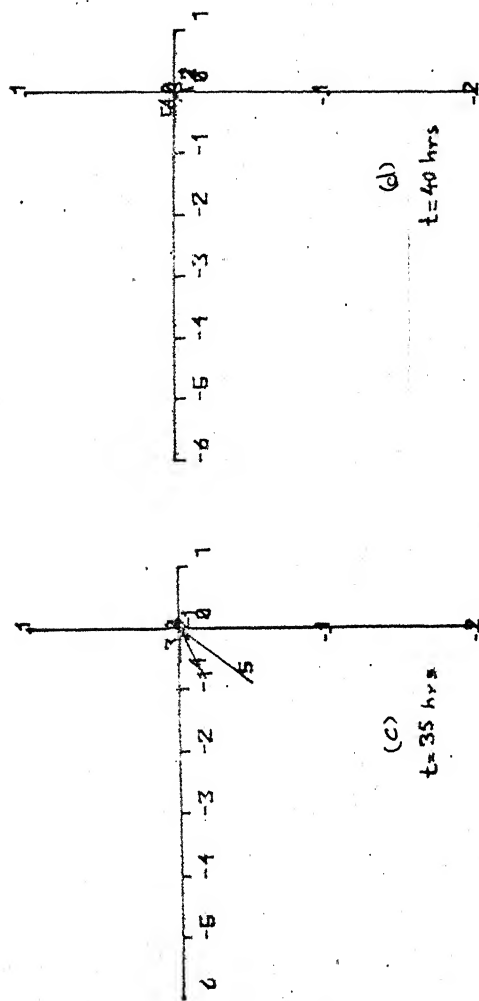
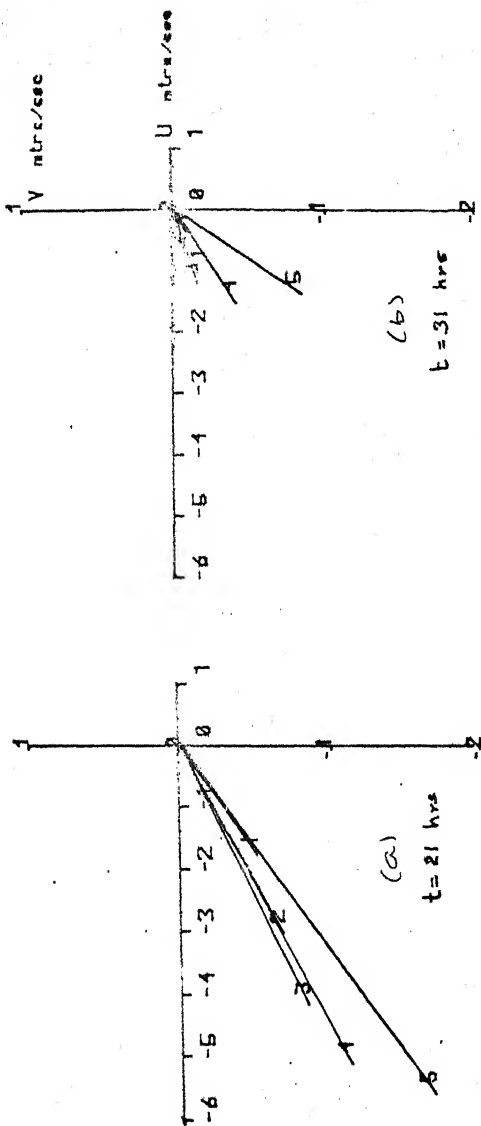


AT (11, 20)

FIG. 34 a, b, c, d. CURRENTS AT 5 LEVELS ($\xi = -1.0, -0.75, -0.5, -0.25, 0.0$)

LEVEL 1: ($\xi = -1.0$): BOTTOM

ASYMMETRIC STORM ALONG TRACK 1

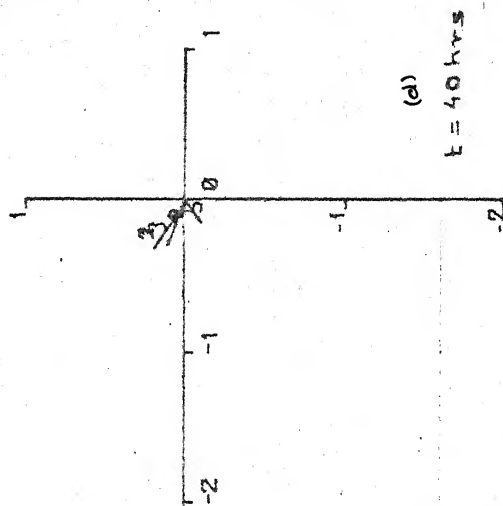
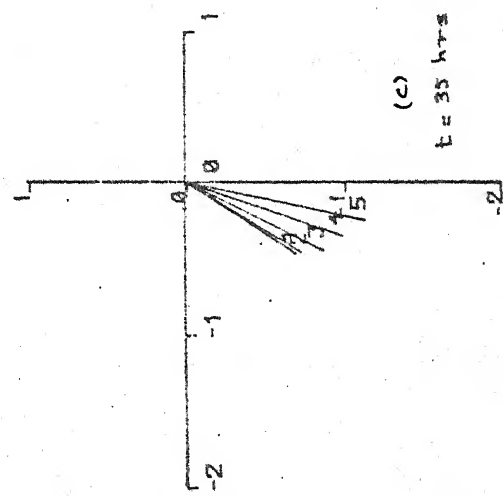
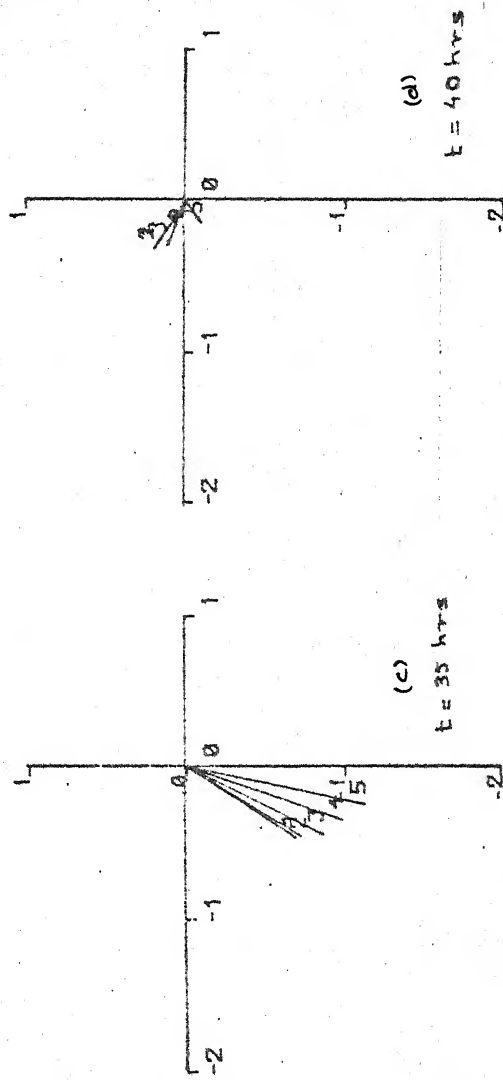
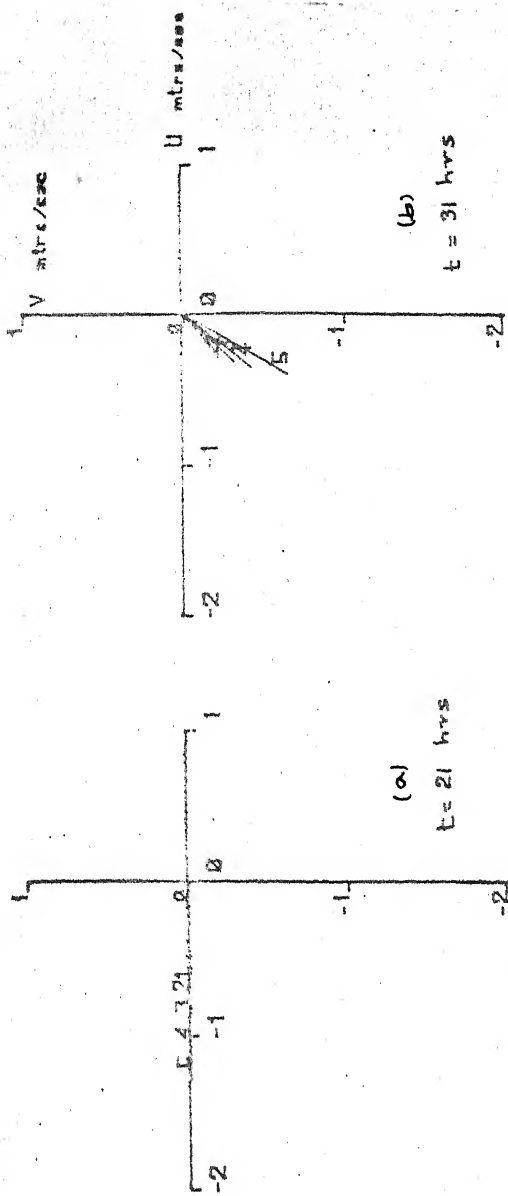


AT (13,24)

FIG. 35 a, b, c, d. CURRENTS AT 5 LEVELS ($\xi = -1.0, -0.75, -0.5, -0.25, 0.0$)

LEVEL 1: ($\xi = -1.0$): BOTTOM

ASYMMETRIC STORM ALONG TRACK 1

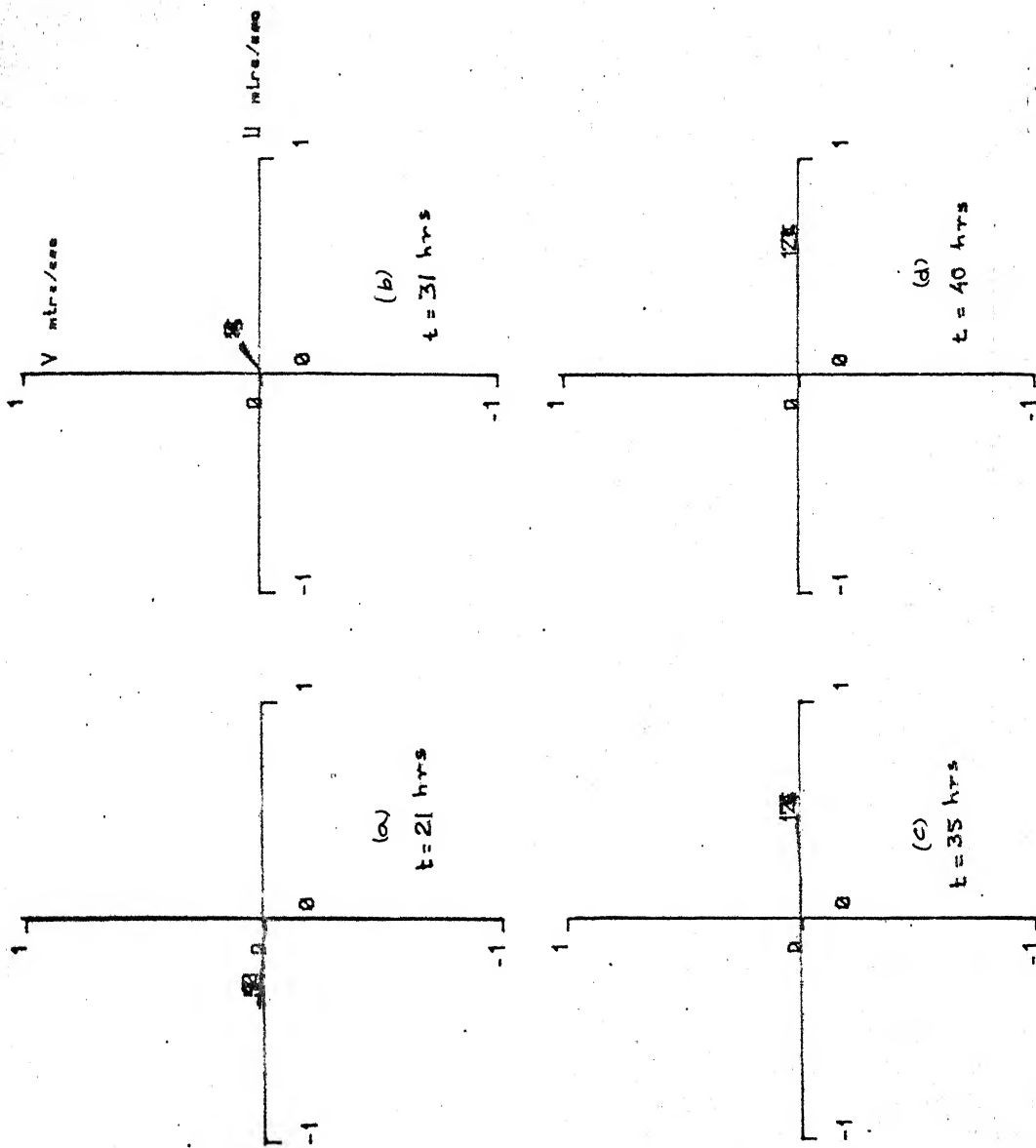


AT (4.40)

FIG. 36 a, b, c, d. CURRENTS AT 5 LEVELS ($\bar{y} = -1.0, -0.75, -0.5, -0.25, 0.0$)

LEVEL 1: ($\bar{y} = -1.0$); BOTTOM

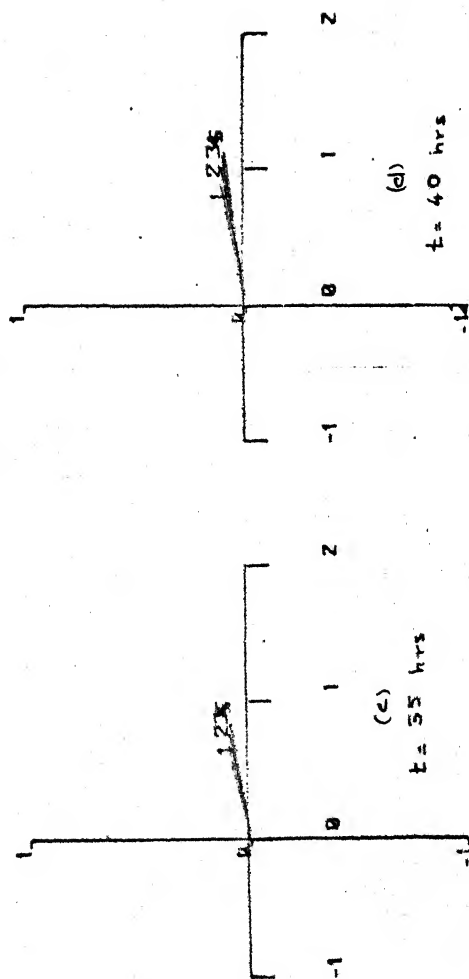
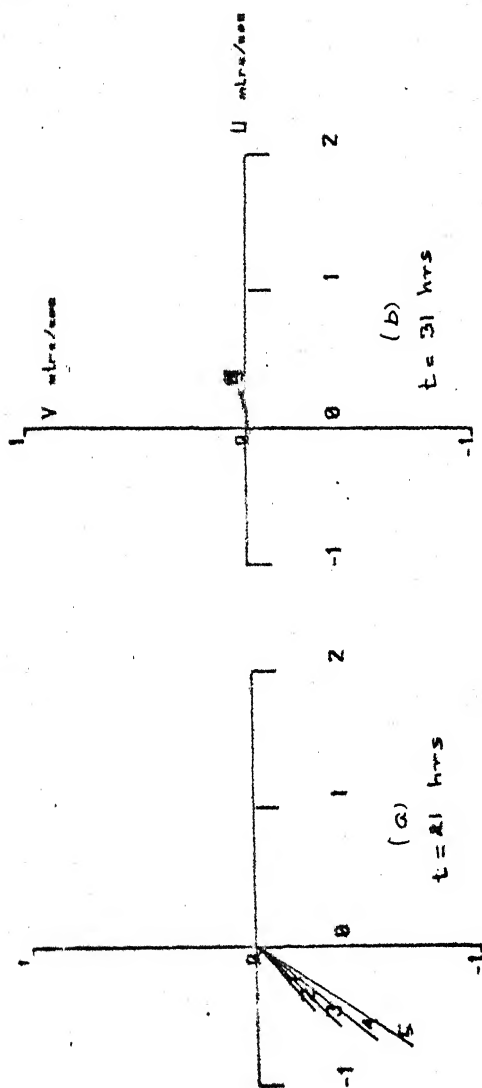
ASYMMETRIC STORM ALONG TRACK II



AT (10, 16)

FIG. 37 a, b, c, d. CURRENTS AT 5 LEVELS ($\chi = -1.0, -0.75, -0.5, 0.25, 0.0$)
LEVEL 1: ($\chi = 1.0$): BOTTOM

ASYMMETRIC STORM ALONG TRACK II

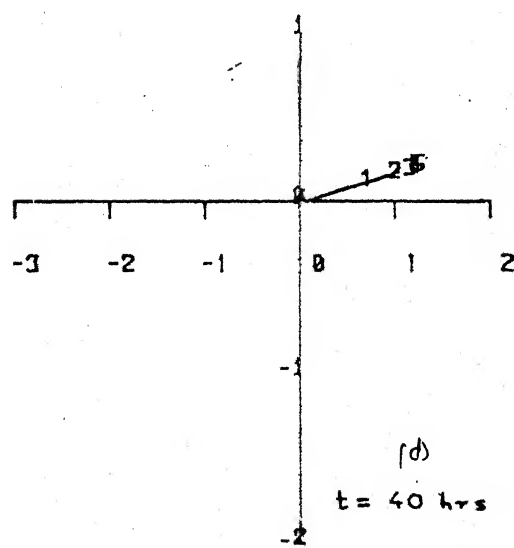
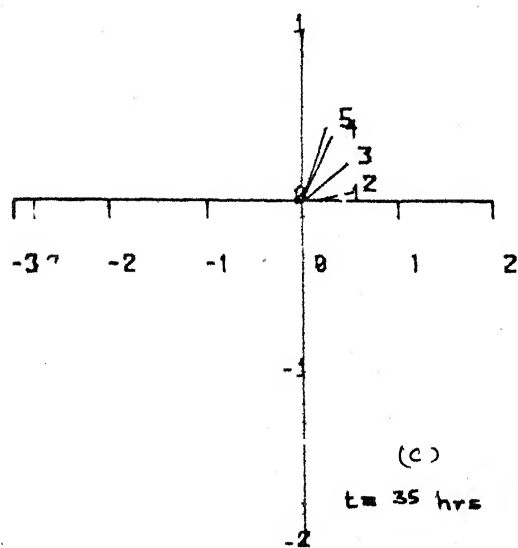
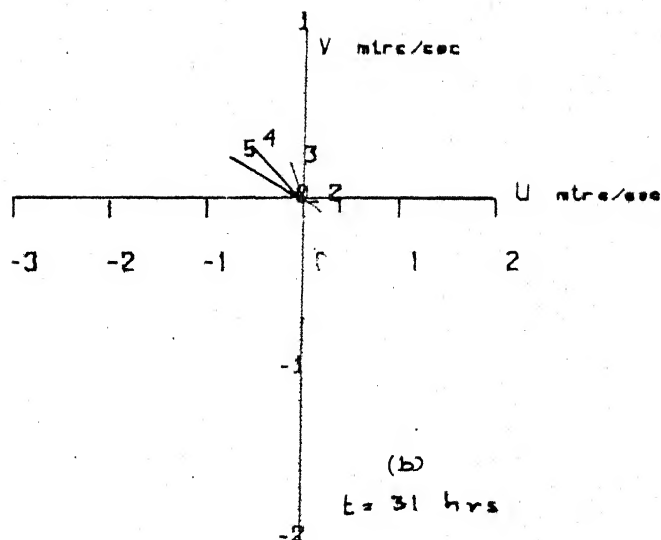
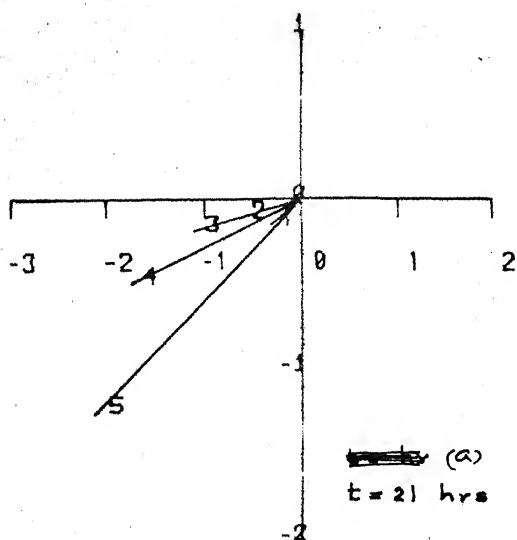


AT (11, 20)

FIG. 38. a, b, c, d. CURRENTS AT 5 LEVELS ($\lambda = 1.0, -0.75, -0.5, -0.25, 0.0$)

LEVEL 1: ($\lambda = 1.0$) : BOTTOM

ASYMMETRIC STORM ALONG TRACK II

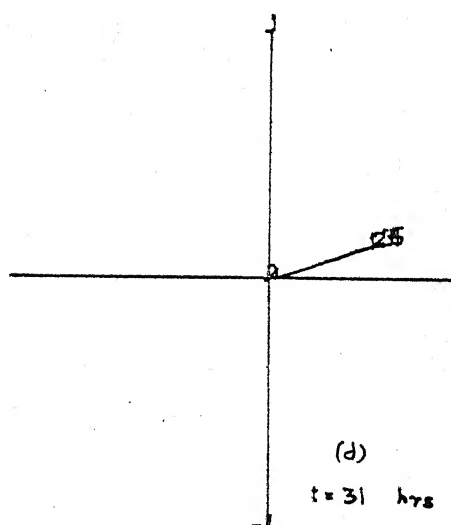
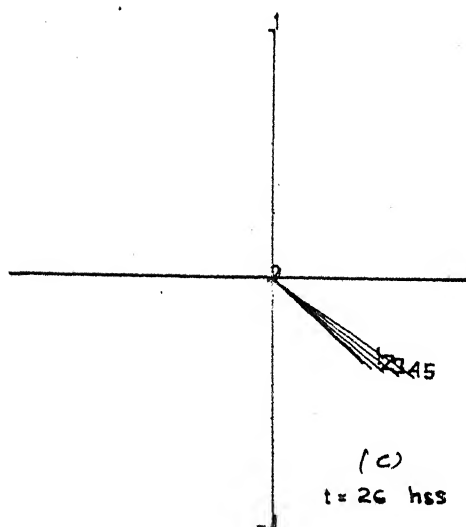
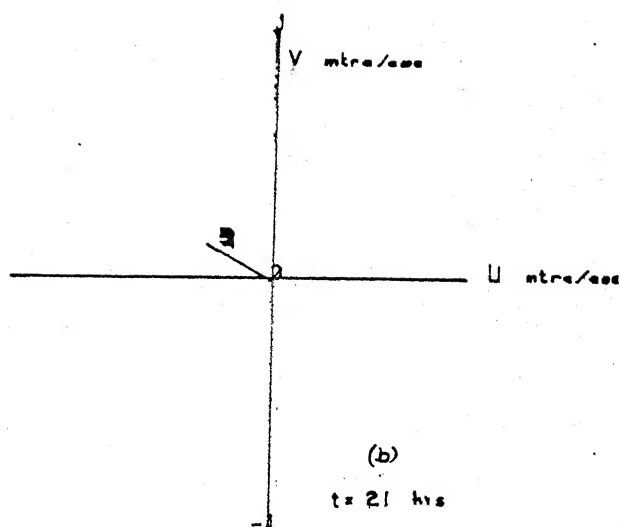
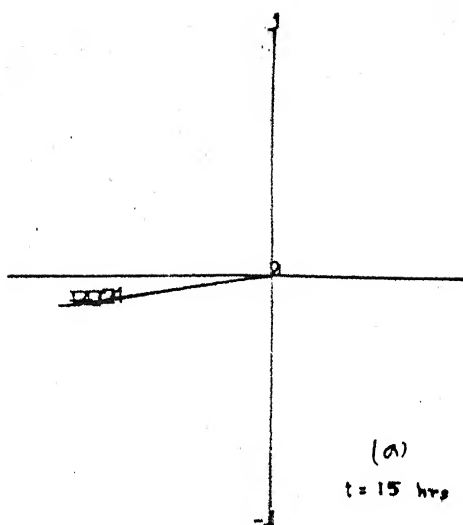


AT (13, 24)

FIG. 39 a, b, c, d. CURRENTS AT 5 LEVELS (ξ 1.0, -0.75, -0.5, -0.25, 0.0)

LEVEL 1: (ξ = 1.0): BOTTOM

ASYMMETRIC STORM ALONG TRACK III

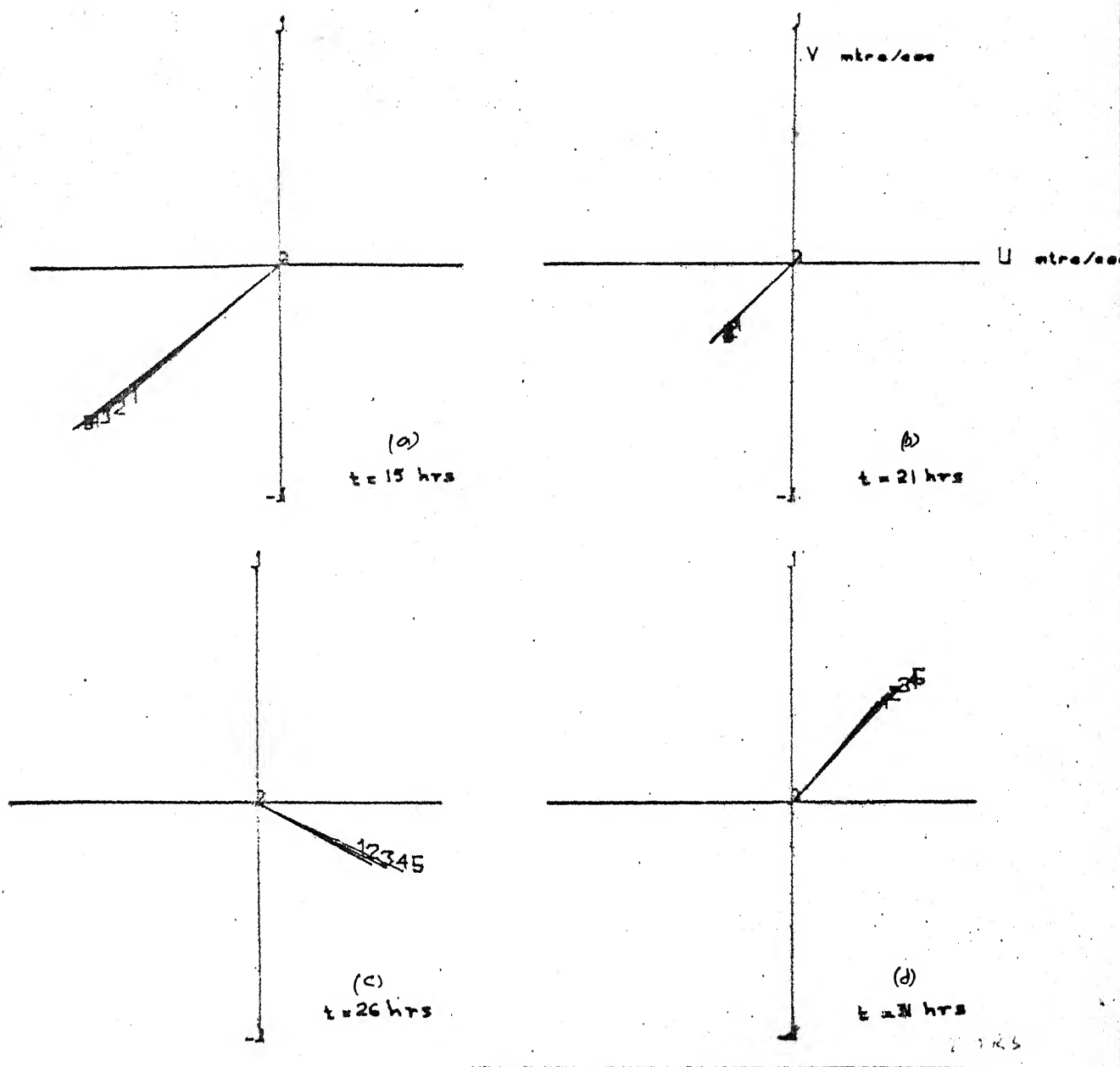


AT (8.16)

FIG. 40 a, b, c, d. CURRENTS AT 5 LEVELS ($\xi = -1.0, -0.75, -0.5, -0.25, 0.0$)

LEVEL 1: ($\xi = -1.0$): BOTTOM

ASYMMETRIC STORM ALONG TRACK III

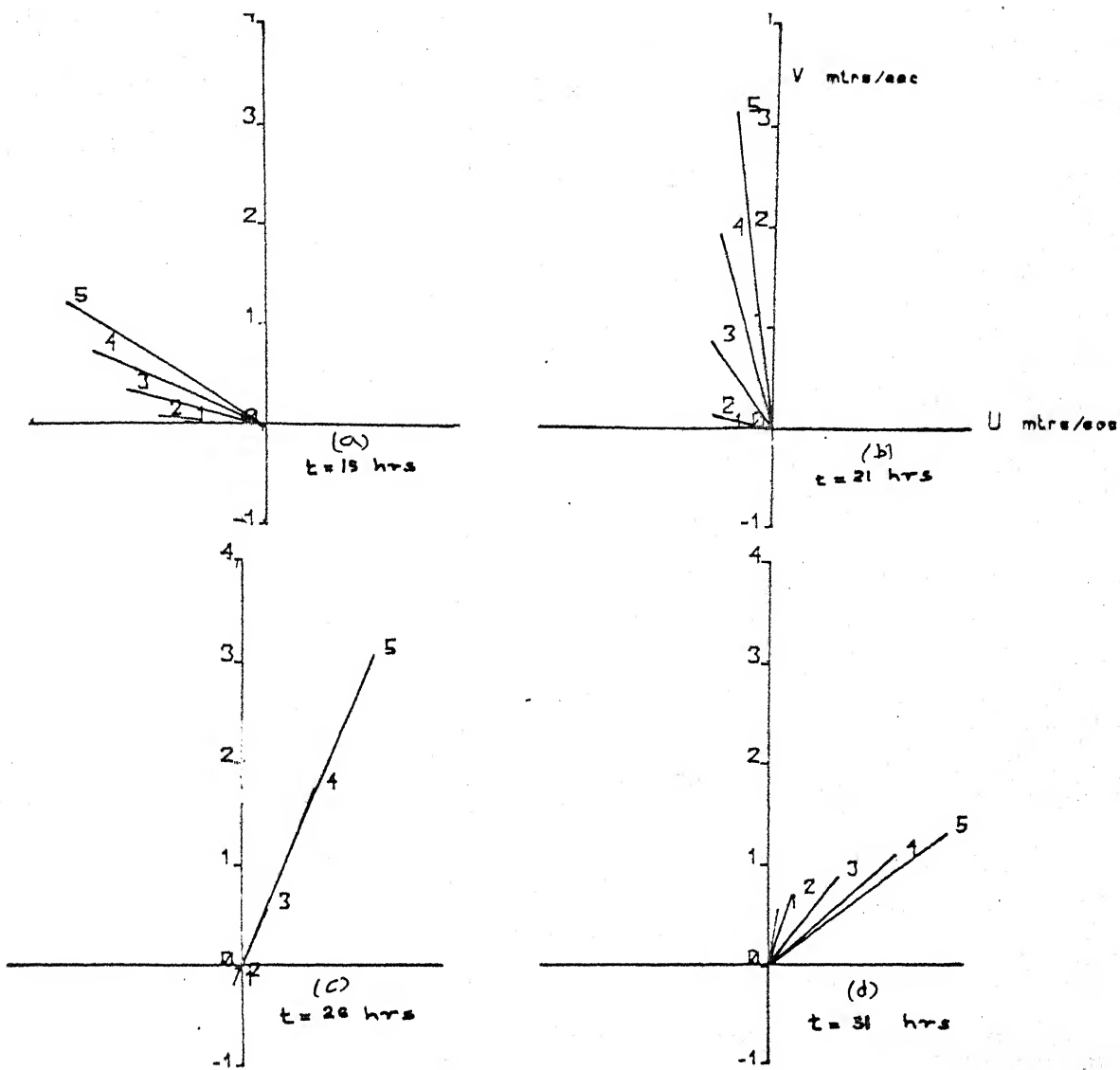


AT (11, 20)

FIG. 41 a, b, c, d. CURRENTS AT 5 LEVELS ($\xi = -1.0, -0.75, -0.5, -0.25, 0.0$)

LEVEL 1: ($\xi = -1.0$): BOTTOM

ASYMMETRIC STORM ALONG TRACK 11



A¹ (13, 24)

FIG. 42. a, b, c, d. CURRENTS AT 5 LEVELS ($\xi = -1.0, -0.75, -0.5, -0.25, 0.0$)

LEVEL 1: ($\xi = -1.0$): BOTTOM

ASYMMETRIC STORM ALONG TRACK III

CHAPTER 4

A CRITICAL REVIEW AND SOME SUGGESTIONS

We conclude the present dissertation with a critical review of the work carried out in Chapters 1,2 and 3. Some suggestions will be made regarding the improvement of the present work and the inclusion of new aspects such as the coastal upwelling and the thermal structure of the Bay of Bengal as a response to the translating cyclones and the large scale wind circulations such as the monsoons.

In the present dissertation an attempt has been made to study some details of the dynamics of tides and surges in the Bay of Bengal through numerical experiments. The study has been carried out in two stages. In the first stage (Chapter 1), the distribution of M_2 -tide is determined for the region of the Bay of Bengal (from 10°N to 20°N) using the tidal theorem enunciated by Proudman (1925). The availability of the limited number of coastal-station observations (harmonic constants) made the present study to rely much on numerical experimentation through matching of the obtained distribution and the harmonic constants at the coastal stations. The recent acquisition of some additional tide gauges (to be set up along the coast) would help

further investigation regarding the determination of the open-sea tides for the region of the Bay of Bengal. The co-tidal map obtained in the present work (Chapter 1), for the region of the Bay of Bengal, is reasonably close to the observations and agrees with the trends indicated by the co-tidal chart in the work of Pekeris and Accad (1969).

In the second stage (Chapters 2 and 3) surges, tides and their interaction are studied with the help of a vertically averaged model (Chapter 2) given by Flather and Heaps (1975), and a spectral model regarding the three-dimensional surge (Chapter 3) given by Heaps (1976). The moving coastal boundaries are not incorporated in the formulation of the surge problem, and as a result the magnitudes of the elevations (and currents) are found to be in excess of the observed values. At the present stage a comparison of the results of the present work, regarding elevations and currents, with the field observations could not be made because no adequate and reliable field data is available for the region of the Bay of Bengal. The recent acquisition of the research vessel ('Sagar Kanya' by the National Institute of Oceanography at Goa, India), the geosynchronous satellite (INSAT 1B) and the setting up of additional tide gauges along the coast etc., would, perhaps, provide a base for the field data for the future investigations.

Owing to the nature of the shelf area at the head Bay of Bengal, many complex types of motion are possible. Some of these are the swift, local oscillations obtained in the numerical experiments with track III (Chapters 2 and 3) and the entirely different behaviour of the surge at the same point of landfall due to storms along different tracks. The models used in Chapters 2 and 3 have shown a relatively weak response regarding the nonlinear advection and the interaction between the tide and the surge. These nonlinear physical processes are believed to be stronger at smaller scales (of space and time) and hence require a greater resolution regarding the grid spacing, particularly in the shallow areas. The inclusion of further shallow areas such as the river mouths and the nearby Islands in the model area is necessary for the actual surge prediction.

The tidal regime established in Chapter 2 has produced tidal oscillations which are remarkably close (regarding the amplitudes) to the observed tides near the coastal stations. But the depth-mean current (as indicated by the current ellipses) has shown some complexity with the rotation of the current vector in the clockwise direction at some locations. At the present a justification of this is not possible due to lack of adequate field observations for the region under study. This task is left for a future investigation.

The depth-averaged model as well as the spectral model of the present work have shown remarkable similarity regarding the elevation patterns and the depth-mean current structure. An interesting result is the horizontal circulation under the strong meteorological forcing where the storm has the horizontal extent comparable with that of the shelf at the head Bay of Bengal. The present investigation has considered only the strong meteorological forcing typical of severe Cyclonic storms in the Bay of Bengal. It will be interesting to study the circulation patterns under moderate, large-scale wind conditions such as the monsoon winds. The baroclinic response and the coastal upwelling have to be taken up in the future investigations extending the scope and purview of the present models.

The present study also points out the need for adequate field observations for a comparison of the theoretical and observational studies. For instance, the numerical experiments of Chapter 3 indicated a strong surface currents during the developing (intensification) stage of the cyclonic storm (even during movement) and a verification of this aspect is not possible owing to the nonavailability of the pertinent information regarding the surface currents. Excepting the surface currents at some locations the overall current structure through the depth are within the physically possible (or observed) range.

With the results of the present work in view, the following problems are suggested for future investigations:

i) the role of the large submarine canyon (the Ganges Canyon) in the dynamics of tides and surges in the Bay of Bengal,

ii) the barotropic and the baroclinic response of the Bay of Bengal to the translating cyclones. In the recent studies it is observed that the development and the movement of cyclones are sensitive to the changes in the sea surface temperatures. As a part of air-sea interaction, it will be interesting to study this aspect in which the thermal structure of the ocean and the storm (and its movement) interact with each other. This study helps the prediction of the course of the storm movement and hence the prediction of the surge. With this view, consideration should be given to the large-area model (which we have discarded in Chapter 2) in which the entire course of the storm movement can be incorporated.

iii) circulation over the shelf and the coastal upwelling due to cyclonic storms and large scale wind conditions such as the monsoons.

In spite of the inclusion of the aspects such as the real bathymetry, the asymmetric storm forcing, the

nonlinear advection, the tide-surge interaction and the three-dimensional current structure, the present work has achieved the objectives in a limited way. What has been achieved in the present investigation is short of a tiny droplet. The droplet is showing the abundance of the ocean.

APPENDIX

Ekman Depth for the Region of Bay of Bengal

Wind effects penetrate to some considerable depth below the ocean surface, determined in part by the stability of the water column. The usual limit for wind effects (such as drift currents) is taken to be the depth at which the current arrow is exactly opposite to the surface-current arrow. At that depth, the current speed is about 4 percent of this surface current. Under a strong wind, wind-drift currents have been observed to extend to depths of about 100 meters. The depth of the Ekman Layer is given by

$$E.D. = \pi \sqrt{2A/f},$$

where A is the coefficient of vertical friction and f is the coriolis parameter. In the present investigation we take the value of $f = 0.5 \times 10^{-4}$ which corresponds to the latitude $20^{\circ}N$ and $A = 0.075 \text{ m}^2\text{s}^{-1}$ an average value for the Bay of Bengal. Thus the Ekman depth for the region under consideration is 172 meters. Also we see that in most part of the region under study we have the depth of the basis less than this 'Ekman Depth'.

BIBLIOGRAPHY

1. Airy, G.B. (1845)
Tides and Waves
Encyclopadia Metropolitana, London.
2. Ali, A. (1980)
The dynamics effects of barometric forcing on
storm surges in the Bay of Bengal.
Mausam (formerly Indian J. Met. Hydrol and
Geophysics), 31, 4, 517-522.
3. Banks, J.E. (1974)
A Mathematical Model of a River-Shallow sea
System used to investigate Tide, Surge and
their interaction in the Thames-Southern North
sea region.
Phil. Trans. Roy. Soc. (London), 275, 567-609.
4. Bretschneider, C.L., Collins, J.I. and Pick, G.S. (1966)
Theory, measurements and data collection: state of t
the art.
Natl. Eng. Sci. Company Tech. Rept. SN-134-14.
5. Bretschneider, C.L. and Pick, G.S (1966)
Bibliography on storm surge
Natl. Eng. Sci. Company Tech. Rept. SN-134-12.
Ref. Contract Nonr-4177(OO).
6. Bretschneider, C.L. (1967)
Storm Surges,
Adv. in Hydrosience, 4, 341-418.
7. Cartwright, D.E. (1968)
A unified analysis of Tides and Surges round
North and East Britain.
Phil. Trans. Roy. Soc., 263(A), 1-55.
8. Cartwright, D.E. (1977)
Ocean Tides
Reports on progress in Physics, 40, 665-708.
9. Cartwright, D.E. (1980)
The Historical Development of Tidal Science and
the Liverpool Tidal Institute.
Oceanography: The past, eds. Sears and
Marriman, Springer-Verlag, pp. 240-251.

10. Chang, S.W. and Anthes, R.A. (1978)
Numerical Simulations of the oceans Nonlinear, Baroclinic Response to Translating Hurricanes.
J. Phy. Oceano, V. 8, No. 3, 468-480.
11. Charnock, H. and Crease, J. (1957)
North Sea Surges.
Sci. Prog. (London), 45, 494-511.
12. Crease, J. (1956)
Long Waves on a rotating earth in the presence of a semi-infinite boundary.
J. Fluid Mechanics, 1.
13. Croweley, W.P. (1970)
A Numerical model for viscous, free surface, barotropic wind driven ocean circulations.
J. Comp. Phys., 5, 139-168.
14. Das, P.K. (1972)
Prediction Model for storm surges in the Bay of Bengal.
Nature, 239, 211-213.
15. Das, P.K., Sinha, M.C., and Bala Subrahmanyam, V. (1974)
Storm Surges in the Bay of Bengal.
Quart. J. Roy. Metro. Soc., 100, 437-449.
16. Das, P.K., (1981)
Storm Surges in Bay of Bengal.
Proc. Indian Acad. Sci. (Engg. Sci.), Vol. 4, Pt. 3, 269-276.
17. Davies, A.M. (1977a)
The Numerical solution of the three-dimensional hydrodynamic equations using a B-spline representation of the vertical current profile, in Bottom Turbulence. Proc. of the 8th Lie'ge colloquium on ocean Hydrodynamics, pp. 1-25, ed. Nihoul, J.C.J., Elsevier, Amsterdam (Elsevier Oceanography Series 19).
18. Davies, A.M. (1977b)
Three dimensional model with depth-varying eddy viscosity in Bottom Turbulence.
Proc. of the 8th Lie'ge colloquium on ocean Hydrodynamics, pp. 27-48, ed. Nihoul, J.C.J., Elsevier, Amsterdam (Elsevier Oceanography Series, 19).
19. Davies, A.M. (1981)
Three-dimensional modelling of surges.
Floods due to high winds and tides
(Peregrine ed.), Academic Press, 45-74.

20. Doodson, A.T. (1956)
Tides and Storm Surges in a long uniform Gulf.
Proc. Roy. Soc. (Lond.) A 237, 325-343.
21. Doodson, A.T. (1958)
Oceanic Tides.
Adv. in Geophysics, 5, 117-152.
22. Dronkers, J.J. (1964)
Tidal computations in Rivers and Coastal waters.
North-Holland Pub. Co. Amsterdam, p. 518.
23. Dronkers, J.J. (1975)
Tidal Theory and computations.
Adv. in Hydroscience, 10, 145-230.
24. Dube, S.K., Sinha, P.C. and Rao, A.D. (1982).
The effect of coastal geometry on the location of
peak surge.
Mausam, 33, 445-450.
25. Dunn, G.E. and Miller, B.I. (1964)
Atlantic Hurricanes.
Louisiana State Univ. Press, p. 377.
26. Durance, J.A. (1976)
A three-dimensional numerical model of tidal motion
in shallow sea.
Mem. Soc. R. Sci. Liege, 10, 125-132.
27. Fairbairn, L.A. (1954)
The Semi-Diurnal Tides along the equator in the
Indian Ocean.
Phil. Trans. Roy. Soc. (Lond.) A-247, 191-212.
28. Flather, R.A., and Heaps, N.S. (1975)
Tidal computations in Morecambe Bay.
Geophy. J. Roy. Astr. Soc., 42, 489-517.
29. Flierl, G.R. and Robinson, A.R. (1972)
Deadly Surges in the Bay of Bengal: Dynamics and
storm-tide tables.
Nature, 239, 213-215.
30. Forristall, G.Z. (1974)
3-D structure of storm generated currents.
J. Geophy. Res., 79(18), 2721-2729.
31. Goldsbrough, G.R. (1952)
A theory of North sea storm surges.
M.N.R. Astr. Soc. Geophys. Suppl., 6, 365-371.

32. Groen, P. and Groves, G.W. (1962)
 Surges
 The Sea-Vol. 1, edtr. M.N. Hill, Wiley-Interscience
 N.Y. pp. 611-646.
33. Hansen, W. (1956)
 Theorie Zur Errechnung des Wasserstomdes und der
 Stromungen in Randmeeren nebst Auwendungen.
 Tellus No.:8.
34. Harris, D.L. (1957)
 The hurricane surge,
 Proc. 6th conf. coastal Engg. Council Wave Research,
 Berkeley, California.
35. Harris, D.L. (1959)
 An interium hurricane surge forecasting guide.
 Natl. Hurricane Research Project Report No. 32,
 U.S. Weather Bureau.
36. Heaps, N.S., (1965)
 Storm Surges on a continental shelf.
 Phil. trans. R. Soc., (A) 257, 351-383.
37. Heaps, N.S. and Ramsbottom, A.E. (1966)
 Wind effects on the water in a narrow two-layered
 lake.
 Phil. Trans. Roy. Soc. (Lond.), 259(A), 391-430.
38. Heaps, N.S. (1967)
 Storm surges.
 Oceanogr. Mar. Biol. Ann. Rev., 5, 11-47.
39. Heaps, N.S. (1969)
 A two-dimensional numerical sea model.
 Phil. trans. Roy. Soc. (Lond.) 265(A), 93-137.
40. Heaps, N.S. (1971)
 On the numerical solution of the three-dimensional
 hydrodynamical equations for tides and storm surges.
 Mem. Soc. Roy. des. Sci. de Lie'ge, II, 143-180.
41. Heaps, N.S. (1973)
 Three dimensional numerical model of the Irish sea.
 Geophys. J.R. astr. Soc., 35, 99-120.
42. Heaps, N.S. (1974)
 Development of a 3-dimensional numerical model of
 the Irish sea.
 Rapp. P.V. Reun, cons. int., 167, 147-162.

43. Heaps, N.S. and Jones, J.E. (1975)
Storm surge computations for the Irish sea using a
3-dimensional numerical model.
Mem. Soc. Roy. des Sci de Li'ege, VII, 289-333.
44. Heaps, N.S. (1976)
On formulating a non-linear numerical model in
3-dimension for tides and storm surges.
Computing methods in Appl. Sci. Lect. Notes in
Physics, 58, 368-87.
45. Heaps, N.S. and Jones, J.E. (1977)
Density currents in the Irish sea.
Geophy. J. Roy. Astro. Soc. 51, 393-430.
46. Heaps, N.S. (1981)
Three-dimensional model for tides and surges with
vertical eddy viscosity prescribed in two layers-I,
Mathematical formulation.
Geophys. J.R. astr. Soc., 64, 291-302.
47. Heaps, N.S. and Jones, J.E. (1981)
Three dimensional model for tides and surges with
vertical eddy viscosity prescribed in two layers-II
Irish sea with bed friction layer.
Geophys. J.R. astro. Soc., 64, 303-320.
48. Hendershott, M.C. and Munk, W. (1970)
Tides.
Ann. Rev. Fluid Mech., 2, 205-224.
49. Hendershott, M.C. (1972)
The effects of solid-earth deformation on global
ocean tides.
Geophys. J. Roy. Astr. Soc. 29, 380.
50. Hendershott, M.C. (1973)
Ocean tides.
Eos Trans., AGU, 54, 76.
51. Hendershott, M.C. (1977)
Numerical models of ocean tides.
The sea, 6, 47.
52. Jelesnianski, C.P. (1965)
A numerical calculation of storm tides induced by a
tropical storm impinging on a continental shelf.
Month. Wea. Rev., 93, 343-358.
53. Jelesnianski, C.P. (1966)
Numerical calculation of storm surges without
bottom stress.
Mon. Wea. Rev., 94, 379-394.

54. Jelesnianski, C.P. (1970)
 Bottom stress time-history in linearised equations
 of motion for storm surges.
 Mon. Wea. Rev., 98, 462-478.
55. Jelesnianski, C.P. (1972)
 SPLASH I, landfall storms.
 NOAA, Tech. Mem. NWS TDL-46, Washington, 52pp.
56. Jelesnianski, C.P. (1976)
 A sheared coordinate system for storm surge equations
 of motion with a mildly curved coast NOAA Tech. Mem.
 NWS TDL-61.
 Techniques development laboratory, Silver Spring
 MD, 52pp.
57. Johns, B. and Ali, A. (1980)
 The numerical modelling of storm surges in the
 Bay of Bengal.
 Quart. J. Roy. Met. Soc. 106, 1-18.
58. Johns, B. (1981a)
 Numerical simulation of storm surges in the
 Bay of Bengal.
 Proc. Conf. Monsoon dynamics, New Delhi, December 5-9,
 1977, Camb. Univ. Press.
59. Johns, B., Dube, S.K., Mohanty, U.C. and Sinha, P.C. (1981b)
 Numerical simulation of the surge generated by the
 1977 Andhra Cyclone.
 Quart. J.R. Met. Soc., 107, 919-934.
60. Johns, B., Sinha, P.C., Dube, S.K., Mohanty, U.C. and
 Rao, A.D. (1982)
 Simulation of storm surges using a 3-dimensional
 numerical model: An application to the 1977
 Andhra cyclone.
 Communicated manuscript.
61. Kajiuura, K. (1959)
 A theoretical and empirical study of storms induced
 water level anomalies,
 Tech. Report. Ref. 59-23F, Dept. Ocean-Met., Texas
 A. and M. College, College station, Texas.
62. Kramer, M.P. (1955)
 Annotated Bibliography on strom surges.
 Meteo. Abstracts Bibliography, 6(1), 370-392.

63. Lauwerier, H.A. (1955)
The motion of a shallow sea under influence of a non-stationary wind.
Math. centre Report T.W. 31, Amsterdam.
64. Lax, P. and Wendroff, B. (1960)
Systems of conservation laws.
Comm. Pure. appl. Math., 9, 217-237.
65. Leblond, P.H. and Mysak, L.A. (1979).
Ocean Waves: A survey of some recent results.
SIAM Review, 21(3), 289.
66. Leendertse, J.J. (1967)
Aspects of a computational model for long period water-wave propagation.
The Rand corporation, Santa Monica, Calif.,
RM-5294-PR.
67. Lick, W. (1976)
Numerical modelling of lake currents.
Ann. Rev. Earth and Planetary Sciences, 4, 49-74.
68. Liu, S.K. and Leendertse, J.J. (1978)
Multidimensional numerical modelling of estuaries and coastal seas.
Adv. Hyd. Sci., 11, 95-164.
69. Masch, F.D., Narayanam, M. and Brandes, R. (1971)
A short-term conservative transport model for shallow estuaries.
Tech. Rep. Hyd. 12-7104, Univ. of Texas, Austin.
70. Miyazaki, M. (1965)
A numerical computation of storm surges of hurricane carla 1961 on the gulf of Mexico.
Oceanogr. Mag., 17, 109-140.
71. Mooley, D.A. (1980)
Severe cyclonic storms in the Bay of Bengal, 1877-1977
Mon. Wea. Rev., 108, 1647-55.
72. Nihoul, J.C.J. and Rood, F.C. (1976)
Hydrodynamic models of the North sea, A comparative assessment.
Mem. Soc. R. Sci. Liège, 10, 61-96.
73. Nihoul, J.C.J. (1977)
Three-dimensional model of tides and storm surges in a shallow well-mixed continental sea.
Dynamics of Atmospheres and oceans, 2, 29-47.

74. Pekeris, C.L. and Accad, Y. (1969)
Solution of Laplace's equations for the M_2 tide
in the world oceans.
Phil. Trans. Roy. Soc., A-265, 413-436.
75. Platzman, G.W. (1958)
A numerical computation of the surge of 26 June 1954
on lake Michigan.
Geophysics, Vol. 6, pp. 407-438.
76. Platzman, G.W. (1971)
Ocean tides and related waves.
Lect. Appl. Math. (Amer. Math. Soc. Providence R.I.)
14, 1971.
77. Prandle, D. (1975)
Storm surges in the southern North sea and river
Thames.
Proc. Roy. Soc., 344 (A), 509-539.
78. Prandle, D. and Wolf, J. (1978)
The interaction of surge and tide in the North sea
and river Thames.
Geophy. J. Roy. Astr. Soc., 55, 203-216.
79. Proudman, J. (1925)
A theorem in tidal dynamics.
Phil. Mag., 49, 570-579.
80. Proudman, J. (1940)
The effect of coastal friction on tides.
Mon. Not. R. Astr. Soc., Geophys. Suppl.
81. Proudman, J. (1953)
Dynamical oceanography, London, Methuen, p. 230.
82. Proudman, J. (1955a).
The propagation of tide and surge in an Estuary.
Proc. Roy. Soc. (Lond.) 231 (A), 8-24.
83. Proudman, J. (1955b)
The effect of friction on a progressive wave of
tide and surge in an Estuary.
Proc. Roy. Soc. (Lond.), 233(A), 407-418.
84. Reid, R.O. (1956)
Dynamic storm-tide potential.
Tech. Report 127-1, Ref. 56-37, Dept. Ocean, Met.,
Texas A. and M. College, College, Station, Texas.

85. Reid, R.O. (1957)
Modification of the quadratic bottom-stress law
for turbulent channel flow in the presence of
surface wind stress.
U.S. Tech., Mem., Beach, Eros., 93, 41.
86. Reid, R.O. and Bodine, B.R. (1968)
Numerical model for storm surges in Galveston Bay.
J. Waterways and Harbors division, Proc., ASCE, 94,
33-57.
87. Reid, R.O., Vastano, A.C., Whitaker, R.E. and
Wanstrath, J.J. (1977)
Experiments on storm surge simulation
The sea (ed. Goldberg et al.), 6, (Wiley Intersci.
Pub.), 145-168.
88. Robert, K.V. and Wiess, N.O. (1966)
Convective difference schemes.
Maths. Comput., 20, 272-299.
89. Rossiter, J.R. (1959)
A method of extracting storm surges from tidal
records.
Deut. Hydrograph, Z.12, pp. 117-127.
90. Sielecki, A. and Wurtele, M.G. (1970)
The Numerical integration of the nonlinear shallow
water equations with sloping boundaries.
J. Comp. Phy., 6, 219-236.
91. Simons, T.J. (1974)
Verification of numerical models of lake Ontario:
Part I circulation in spring and early summer.
J. Phy. Oceanogr., 4, 507.
92. Sinha, M.C. (1981)
Mausam, 32, 4.
93. Schwiderski, E.W. (1980)
On charting global ocean tides.
Reviews of geophysics and space physics, 18, 1,
243-268.
94. Weenink, M.P.H. (1958)
A theory and method of calculation of wind effects
on sea levels in a partly enclosed sea, with special
application to the South coast of the North sea.
Proc. Koninkl. Nederl. Akad. Wetensch, 73.

95. Welander, P. (1957)
Wind action on a shallow sea: Some generalization
of Ekman's theory.
Tellus, 9, 45-52.
96. Welander, P. (1961)
Numerical prediction of storm surges.
Adv. in Geophysics, 8, 315-79.
97. Wilson, B.W. (1959)
The prediction of hurricane storm tides in New York
Bay.
Tech. Report, 65-2, Ref. 5S-IF, Texas A. and M.
College, College Station, Texas.
98. World Meteorological Organization report on marine
science affairs (1978), No. 13.
Present techniques of tropical storm surge
prediction, pp. 87.
99. Wunsch, C. (1967)
The long-period tides.
Rev. Geophy., 5, 447-475.
100. Wunsch, C. (1972)
Bermuda sea level in relation to tides, weather
and baroclinic fluctuations.
Rev. Geophy and space phy., 10, 1-49.
101. Wunsch, C. (1975)
Internal tides in the ocean.
Rev. Geophy and space phy., 13, 167-182.
102. Wurtelle, M.G., Pagle, J. and Sielecki, A. (1971)
The use of open boundary conditions with storm
surges equations.
Mon. Wea. Rev., 99, 537-44.

DATE SLIP

This book is to be returned on
the date last stamped.

This image shows a blank sheet of white paper with horizontal ruling lines. A single vertical line runs down the center of the page, creating two equal-width columns. There are 20 horizontal lines in total, evenly spaced across the entire width of the page. The lines are thin and black. The paper appears slightly aged or off-white.